Magnetic Field Analysis, Modelling and Vibration Control in Bridge Configured Winding Induction Machines

A

Thesis submitted

for the award of the degree of

DOCTOR OF PHILOSOPHY

By

GAURAV KUMAR

DEPARTMENT OF MECHANICAL ENGINEERING

INDIAN INSTITUTE OF TECHNOLOGY GUWAHATI

GUWAHATI - 781 039, ASSAM, INDIA

August 2019

Certificate

This is to certify that the thesis entitled "**Magnetic Field Analysis, Modelling and Vibration Control in Bridge Configured Winding Induction Machines**", submitted by **GAURAV KUMAR** (126103028), a research scholar in the *Department of Mechanical Engineering, Indian Institute of Technology Guwahati*, for the award of the degree of **Doctor of Philosophy**, is a record of an original research work carried out by him under our supervision and guidance. The thesis has fulfilled all requirements as per the regulations of the institute and in our opinion has reached the standard needed for submission. The results embodied in this thesis have not been submitted to any other University or Institute for the award of any degree or diploma.

Dated:

Guwahati.

Dr. Karuna Kalita
Associate Professor
Deptartment of Mechanical Engineering
Indian Institute of Technology Guwahati
Guwahati - 781 039, Assam, India.

.

Dr. Atanu Banerjee
Associate Professor
Deptartment of Mechanical Engineering
Indian Institute of Technology Guwahati
Guwahati - 781 039, Assam, India.

To

My Grandfather

Late Shri Chandreshwar Prasad Singh

&

My Parents

Shri Sudhir Kumar Singh and Mrs. Manju Singh

Acknowledgements

This thesis would not have been possible without the immense help, support and guidance of several people in various measures. I would like to convey my acknowledgment to all of them.

I would like to express my special thanks of sincere gratitude to my supervisors Dr. Karuna Kalita and Dr. Atanu Banerjee, who gave me the opportunity to work on this interesting project on the topic "Magnetic Field analysis, modelling and vibration control in bridge configured winding induction machine". Without them, it would have not been possible for me to give a structured and concrete form to my research study. Their encouragement helped in boosting my confidence level. My supervisors ensured that the best in me was brought out by ensuring that my commitment and dedication towards my research work was not compromised at any point of time. I could not have achieved the desired outcome if they had not given me the full freedom to use the laboratory and its valuable instruments during the research study.

I sincerely thank Dr. Kari Tammi, Associate professor, Department of Mechanical Engineering, Aalto University, for his valuable suggestions on my research work, which helped me a lot in staying focused. His time to time guidance has helped me to get clarity on my subject of research. The regular skype meetings conducted by him for over two years has helped in solving my doubts and queries to a significant extent.

I would also like to thank Dr. Praveen Kumar, Professor Department of Electronics and Electrical Engineering, IIT Guwahati and Dr. Jenni Pippuri, senior scientist VTT, Finland for always extending their help in problem-solving and discussion.

I extend my gratitude to my doctoral committee members Prof. R. Tiwari, Prof. D. Chakraborty, and Prof. H. B. Nemade for their valuable feedback and suggestions on my work. I want to thank faculty members and the office staffs of the Department of Mechanical Engineering, IIT Guwahati, for their assistance in carrying out this research work.

I am thankful to my past Lab mates and fellow Ph.D. students Shivarama Krishnan Natesan, Firdausa Ahmed and Kamal Basumatary for their help and support in my Ph.D. journey. I would also like to thank Paban Bujor Barua, Dr. Ankit Dalal and Kashyap for having good technical discussion and help during my Ph.D. journey. I would like to thank Dr. Dheeraj, Dr. Sandeep and Umesh for helping me for the correction of the Ph.D. thesis.

Last but not least I must thank my wife who extended all kinds of support without any complaints.

Gaurav Kumar

Abstract

Technological advancement in rotating machines demands integration of electrical motors or generators in high speed flexible rotors operating at a wide range of speeds. These machines present great rotordynamic challenges and at the same time they also present great opportunities through the ability to achieve transverse actuation (in two independent directions) without any significant sacrifice. These opportunities can be tapped by developing electrical machines which can produce controllable transverse force for active vibration control and also for fully levitating the rotor. The use of controllable transverse force for vibration reduction may lead to the high operating life of mechanical components.

Bridge configured winding scheme is a specialized winding scheme which can be used to generate transverse force efficiently in an electrical machine with a low power requirement along with its primary function as a motor or generator. This winding configuration consists of two power supplies and they are isolated from each other. One of the power supply is responsible for the torque production and the other is responsible for the transverse force production. However, the nature of the magnetic fields and the method of producing controllable transverse forces especially in an induction machine with bridge configured winding are not fully understood.

This thesis characterizes the presence of magnetic field components in a four pole bridge configured winding and proposes a bridge supply scheme which can be used for the generation of controllable transverse force of any desired frequency.

The presence of eccentricity in parallel winding configuration electrical machines adds up an additional frequency component of the unbalanced magnetic pull in comparison with the series winding electrical machines. The bridge configured winding is also a parallel winding configuration and a detailed investigation of the generation of unbalanced magnetic pull is important to understand the phenomena of generation of the additional components of vibration. This thesis investigates the generation of unbalanced magnetic pull in a series

and parallel winding configuration electrical machine by analyzing the air gap magnetic field. For this purpose an electrical machine with series and parallel winding configurations has been modelled and analysed using COMSOL MULTIPHYSICS®.

The force generation in bridge configured winding is directly related to the currents flowing across the bridge points. A coupled magnetic field and electric circuit model is developed in the MATLAB® environment to analyze the behavior of bridge currents for static eccentricity, dynamic eccentricity and also combined both static and dynamic eccentricities.

A single or three phase of bridge supply leads to the generation of the force of multiple frequencies in a bridge configured winding electrical machine. A supply sequence is proposed based on the analysis of bridge configured winding orientation with respect to main and bridge supply which can be used for the generation of the force of particular frequency component.

Furthermore, the magnetic field and electric circuit equation model is coupled with the rotordynamic equation of the rotor bearing system to analyze the vibration patterns at different eccentricity conditions as well as at proposed bridge supply conditions. In addition to this, a simulation model is developed in MATLAB/SIMULINK® to demonstrate levitation, and multiple frequency vibration suppression in a four pole bridge configured winding electrical machine using PID and convergent control algorithm.

Two experimental setups having induction machines with bridge configured winding have been developed to verify the results obtained from the numerical analyses.

Contents

List of Figures

List of Tables

List of Acronyms

AC	Alternating Current
AMB	Active magnetic bearing
BCW	Bridge configured winding
DC	Direct current
DOF	Degree of freedom
EMF	Electromotive Force
FEM	Finite element method
FFT	Fast fourier transform
LTI	Linear time invariant
UMP	Unbalanced magnetic pull

List of Symbols

$\vec{A}$	Magnetic vector potential
B	Magnetic flux density
$\underline{\hat{B}}_1$	Space vector representation of two pole magnetic field
$\underline{\hat{B}}_3$	Space vector representation of six pole magnetic field
$\mathbf{B_{static}}$, $\mathbf{B_{dynamic}}$, $\mathbf{B_{mixed}}$	Pulsating component of magnetic field in a parallel winding four pole electrical machine in static, dynamic and mixed eccentricity conditions respectively
$\mathbf{b_{static}}$, $\mathbf{b_{dynamic}}$, $\mathbf{b_{mixed}}$	Magnetic field in a series winding four pole electrical machine in static, dynamic and mixed eccentricity conditions respectively
$\mathbf{b_{st}}$, $\mathbf{b_{dy}}$, $\mathbf{b_{mi}}$	Resultant magnetic field in a parallel winding four pole electrical machine in static, dynamic and mixed eccentricity conditions respectively
$[C_r]_{n\times n}$	Global matrix for induced emf due to the rotor bars
$\{d\}$	Rotor vibration vector
d_r	Outer diameter of rotor
E	Electric field intensity
F_{ss_x}, F_{sd_x}, F_{sm_x}	Force generated due to static, dynamic and mixed eccentricity conditions respectively, in a series winding electrical machine, along x axis
F_{ss_y}, F_{sd_y}, F_{sm_y}	Force generated due to static, dynamic and mixed eccentricity conditions respectively, in a series winding electrical machine, along y axis
F_{ps_x}, F_{pd_x}, F_{pm_x}	Force generated due to static, dynamic and mixed eccentricity conditions respectively, in a parallel winding electrical machine, along x axis
F_{ps_y}, F_{pd_y}, F_{pm_y}	Force generated due to static, dynamic and mixed eccentricity conditions respectively, in a parallel winding electrical machine, along y axis

f_1	Stator supply frequency
f_ε	Rotor rotational frequency
f_{bridge}	Force due to bridge supply
$\{f_{unb}\}$	Mass unbalance force vector
$\{f_{mag}\}$	Magnetic force vector
$[G]$	Gyroscopic couple
I_s	Stator coil current
i_A, i_B, i_C	Three phase currents of the stator
i_1, i_2, i_3	Coil currents in the parallel paths of the stator winding
$\{I_s\}_{u\times 1}$	Stator circuit current vector
$\{I_r\}_{v\times 1}$	Rotor bar current vector
$\overrightarrow{J}$	Current density
$\mid J \mid$	Jacobian
$[K_m]$	Stiffness matrix of the rotor
$[K]_{n\times n}$	Global magnetic stiffness matrix
$\overrightarrow{k}$	Unit vector parallel to z axis
$k_n^e, c_r, p_s, p_r, q_r, q_s$	Elemental matrix in natural coordinate system
$k_c^e, c_r^e, p_s^e, p_r^e, q_r^e, q_s^e$	Elemental matrix in cartesian coordinate system
L_{es}	End winding inductance of the stator coil
l_r	Axial length of the rotor
l	Length of the rotor bar
$[M]$	Mass matrix of the rotor
μ	Permeability
$\{N\}$	Shape function
n	Number of nodes
ν	Magnetic reluctivity
n_0	No. of turns in the stator winding

p	No. of pole pair
$[P_r]_{n\times v}$	Global matrix for the rotor conductor excitations
$[P_s]_{n\times z}$	Global matrix for the stator coil excitations
$Q_1 \dots Q_{12}$	Global matrix of the induced emf for the stator circuit equation for coil groups $W_1 \dots W_{12}$
$[Q_s]_{u\times n}$	Global matrix of the induced emf for the stator circuit equation
$[Q_s]_{v\times n}$	Global matrix of the induced emf for the rotor circuit equation
R	Stator coil resistance
$[R_r]_{v\times v}$	Rotor bar resistance matrix
$[R_s]_{u\times u}$	Stator coil resistance matrix
S_s	Cross sectional area of the stator coil
σ_r	Electrical conductivity of the rotor bar
$[T]_{z\times u}$	Transformation matrix for the transformation of phase currents to the coil side currents
t	Time
u	Number of stator circuit current
$\{U_r\}_{v\times 1}$	Rotor bar voltage vector
$\{U_s\}_{u\times 1}$	Stator coil voltage vector
V	Electric Scalar potential
V_A, V_B, V_C	Three phase voltages of the stator
V_{Ab}, V_{Bb}, V_{Cb}	Bridge supply voltages across the bridge terminals
v	Number of rotor conductors
x, y	Cartesian coordinates
ξ, η	Natural coordinate system

z	Number of coil sides

1 Introduction

Contents

1.1 Background

An electrical machine is an integral component of industry. It is widely used in various applications viz., pumps, compressors, elevators and many other rotating machines. Among all types of electrical machines, the induction machine is one of the most common types of electrical machines used across the world. It is widely used because it is cheap and robust in nature and also it requires low maintenance. Generally, an induction machine consists of a stator, squirrel cage rotor and bearings. The rotor of the motor is supported by two bearings through a shaft. Figure 1.1 shows these three main components of an induction machine. The orientation of rotor position with respect to the stator of the electrical machine brings additional dynamics in the machine. An eccentric position of the rotor makes air gap magentic field asymmetric which results in generation of unbalanced magnetic pull (UMP). The generation of UMP may lead to wear and tear of bearing. The study shows that 40-50 % of motor failure occurs due to bearing failure [1]. There are various ways to control the generation of UMP in an electrical machine. The bridge configured winding (BCW) is one of the effective winding configurations due to its capability to generate and control UMP in an electrical machine. The present work is all about study of UMP in a bridge configured winding induction machine as a whole and bridge configured winding configuration in particular to understand the generation of desirable UMP in a bridge configured winding electrical machine.

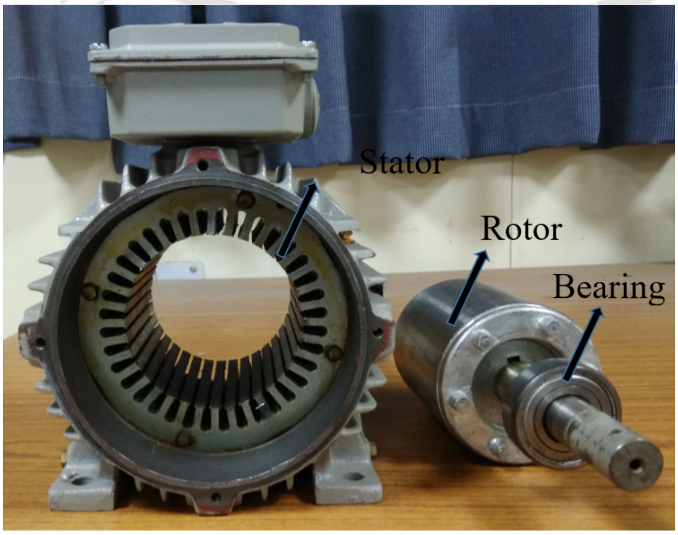

Figure 1.1: An electrical machine.

1.1.1 Unbalanced magnetic pull

An asymmetric airgap magnetic field is the reason behind the generation of unbalanced magnetic pull. There are various factors which leads to asymmetry in the air gap magnetic field. Bearing faults and eccentricity faults are among common faults in an electrical machine which leads to unbalanced magnetic pull generation. Due to manufacturing tolerances, rotor eccentricity is inherently present in any electrical machine. A rotor is said to be eccentric, if the rotor center is having some offset with respect to stator center of an electrical machine. Generally, three types of eccentricity exists in an electrical machine, viz., static eccentricity, dynamic eccentricity and mixed eccentricity. A rotor is said to be in static eccentricity condition when it rotates about its own axis but not about the axis of the stator. Figure 1.2(a) represents static eccentricity condition in an electrical machine. The rotor centre A is offset to the stator centre O and the rotor rotates about the axis passing through the rotor centre A. A rotor is said to be in dynamic eccentricity condition when it rotates about its own axis and the rotor whirls about the stator centre axis. Figure 1.2(b) represents dynamic eccentricity condition in an electrical machine. The rotor centre A is offset to the stator centre O and the rotor whirls about the axis passing through the stator centre O and rotates about the axis passing through the rotor centre A. The combination of static and dynamic eccentricity condition is called mixed eccentricity condition. A rotor is said to be in mixed eccentricity condition if the rotor whirls about any other axis but not the axis of the stator centre and rotates about its own axis. Figure 1.2(c) represents mixed eccentricity condition, the rotor rotates about the axis passing through the point A and whirls about the axis passing through the point B but not the axis passing through the point O.

An eccentric rotor generates additional $p \pm 1$ pole pair of magnetic fields where p is the pole pair of the fundamental component of the magnetic field. The interaction of p pole pair of magnetic field with $p \pm 1$ pole pair of magnetic field leads to generation of unbalanced magnetic pull in an eccentric rotor electrical machine. For example in a four pole electrical machine an eccentric rotor induces additional two pole and six pole components of the magnetic field. Figure 1.3 shows a simplified representation of interaction of fundamental four pole component of magnetic field and additional two pole component of the magnetic field in a four pole electrical machine which leads to generation of UMP . The nature of rotation of eccentricity induced magnetic field is dependent on the type of eccentricity present in the system. Different type of eccentricity condition leads to generation of different components of harmonics of UMP.

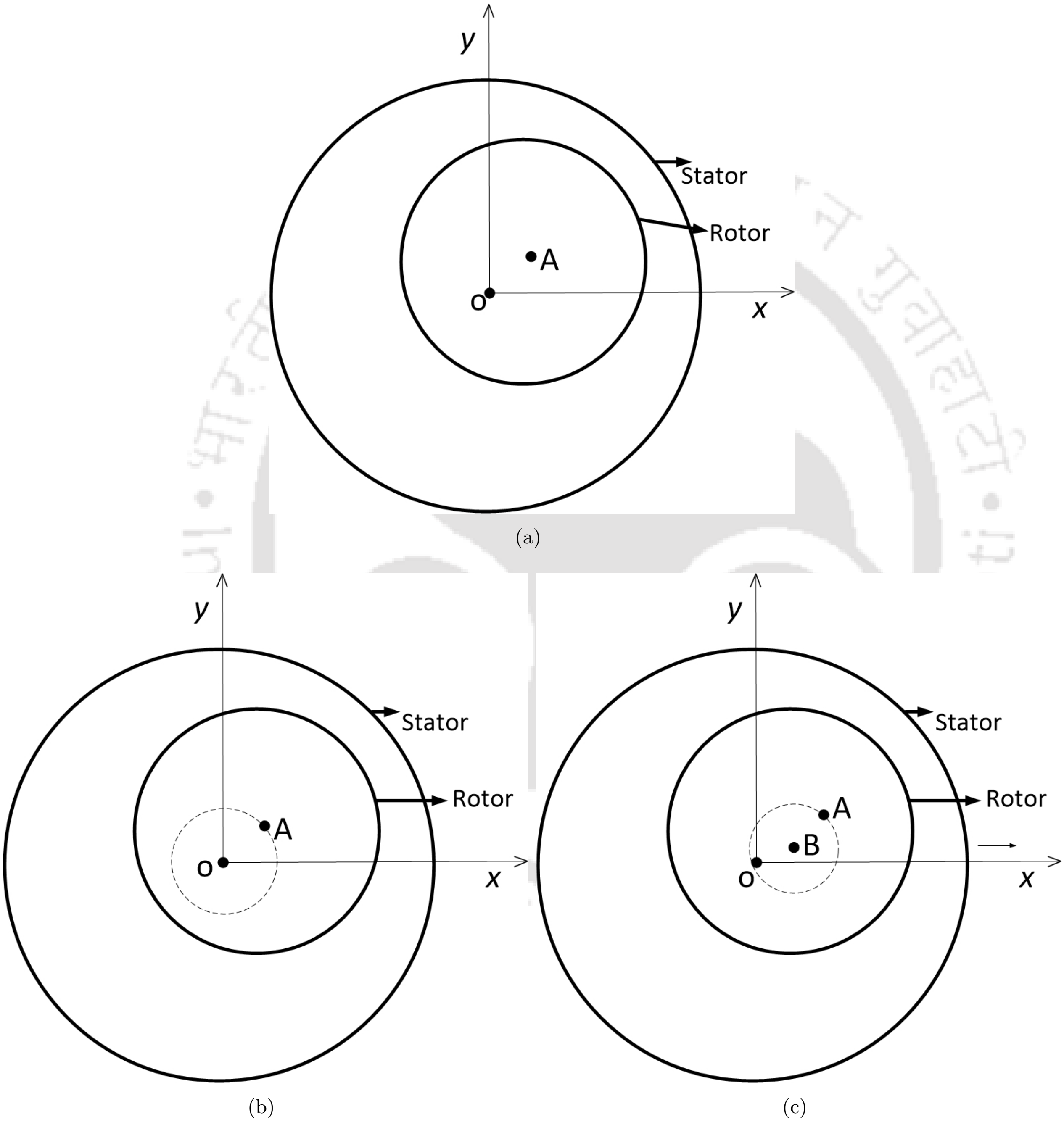

Figure 1.2: Various types of eccentricity conditions (a) static eccentricity, (b) dynamic eccentricity, (c) mixed eccentricity.

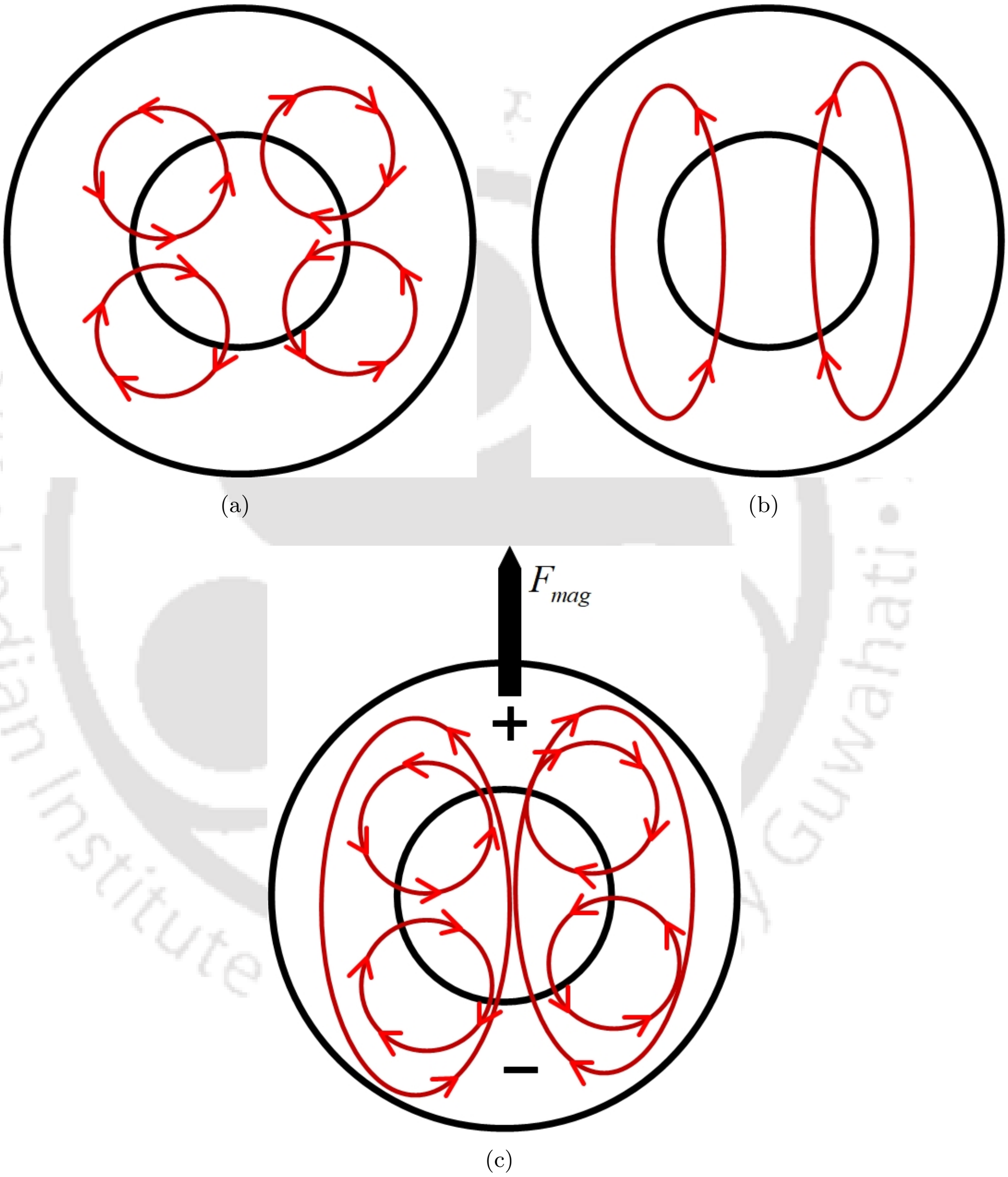

Figure 1.3: Magnetic field components in an eccentric rotor electrical machine (a) four pole magnetic field, (b) two pole magnetic field, (c) interaction of four pole and two pole magnetic field.

1.1.2 Bridge configured winding

UMP is undesirable if it is present due to certain faults such as eccentricity in an electrical machine. However, UMP can become desirable if it can be produced in required direction as per the requirement to counteract undesirable UMP. The current trends in all rotating machines are; (i) integration of an electrical motor or generator into the overall machine on a relatively longer shaft and, (ii) demand of higher power densities than ever before for better economies and efficiency. Combined, these two features mean that there is an ever-increasing opportunity to exploit the capability of electrical motors or generators to exert controllable transverse forces (or UMP) on the rotor. These transverse forces can be used for the multiple purposes such as vibration control, offsetting deflections due to external loads, alleviating bearing loads, enabling intelligent condition monitoring and development of bearingless machines.

The research group of Arkkio [2,3] and Chiba [4] have exploited the capability of electrical motors and generators to exert controllable transverse forces on the rotor and to generate bearing forces for bearing-less application. Both of these groups have achieved this by deploying two sets of stator winding, one for the torque production and other for the transverse force production. Khoo [5] introduced a stator winding called bridge configured winding, where a single set of winding has been used for the torque and transverse force production. Bridge configured winding is a single set, double layer winding scheme which can accommodate two different voltage or current supply sources which are isolated from each other [5]. The single set of winding configuration is advantageous in the sense that the same coils are used for the torque production and transverse force generation. Whereas in dual set of winding scheme the stator slots accomodate two different winding connection which effects the torque producing capability of the machine. Figure 1.4 represents the winding diagram of an induction machine with 36 stator slots and Figure 1.5 shows the circuit connection diagram of a single phase of bridge configured winding. V_A and V_{bA} are the two different supply sources isolated from each other and termed as main supply and bridge supply respectively. The main supply of the winding is used for the torque producing component of the magnetic field (p pole pair magnetic field), whereas the bridge supply of the winding is used for the production of an additional component of the magnetic field of a pole pair difference ($p \pm 1$ pole pair magnetic field) with respect to the torque producing component of the magnetic field. The bridge configured winding is a double layer winding having two parallel paths. Coils $(a1 - a3)$, $(aa4 - aa6)$ and $(aa1 - aa3)$, $(a4 - a6)$ form two parallel paths of the winding, $A - A_1 - B$ and $A - A_2 - B$ respectively. The coil group $a1 - a3$, $a4 - a6$, $aa1 - aa3$ and $aa4 - aa6$ has been termed as W1, W2, W3 and W4 respectively. The main supply voltage source V_a produces the current i_a which gets divided in both of the parallel path and a current $i_1 = i_a/2$ flows through it. A bridge supply voltage connected between the parallel path of the winding across point A_1 and A_2 generates a current i_{ba} which gets divided in upper $(A_2 - A - A_1)$ and lower $(A_2 - B - A_1)$ circuit of the winding and a current $i_2 = i_{ba}/2$ flows through it. It can be seen in Figure 1.5 that the bridge supply current i_2 flows in the same direction to the main supply current i_1 in coil groups W1 and W2, whereas it flows in opposite direction to that of the main supply current in coil groups W3 and W4. This addition and subtraction of currents lead to generation of asymmetry in the magnetic field which with a proper control can produce a controlled UMP. The flow of current i_1 through the coil groups W1, W2, W3 and W4 generates a four pole magnetic field whereas the flow of current i_2 through the coil groups W3, W1 and W2, W4 generates two pole magnetic field.

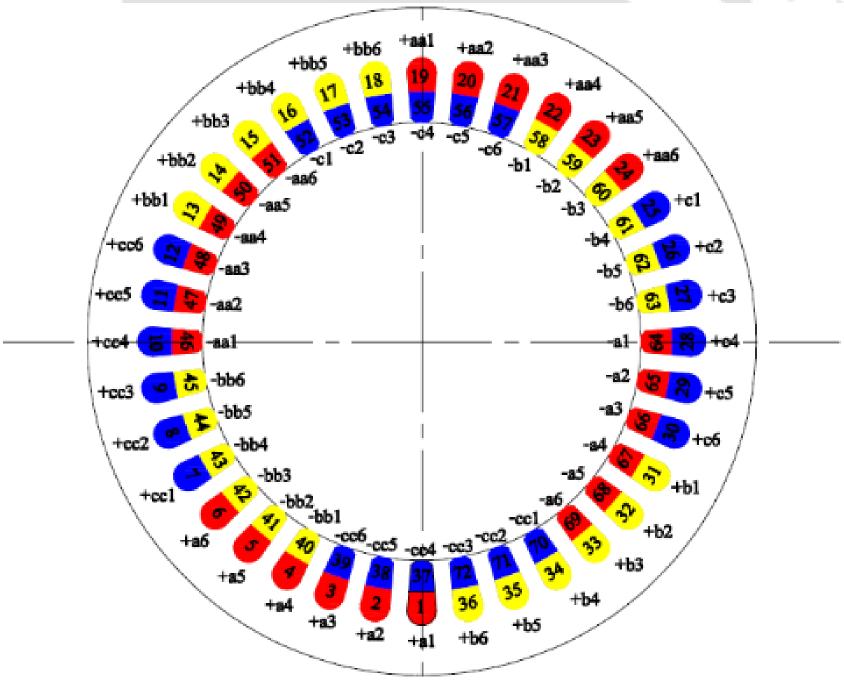

Figure 1.4: Winding diagram of double layer bridge configured winding.

Khoo et al. [6] practically implemented bridge configured winding on a brushless permanent magnet motor and showed its capability to generate controllable forces. However, the problem with the bridge configured winding is that the direct relationship with respect to frequency of force and bridge supply is not known. This is very much essential for either active control of rotor vibration or development of a bearingless motor. In addition to that, one of the major hurdles in understanding of bridge

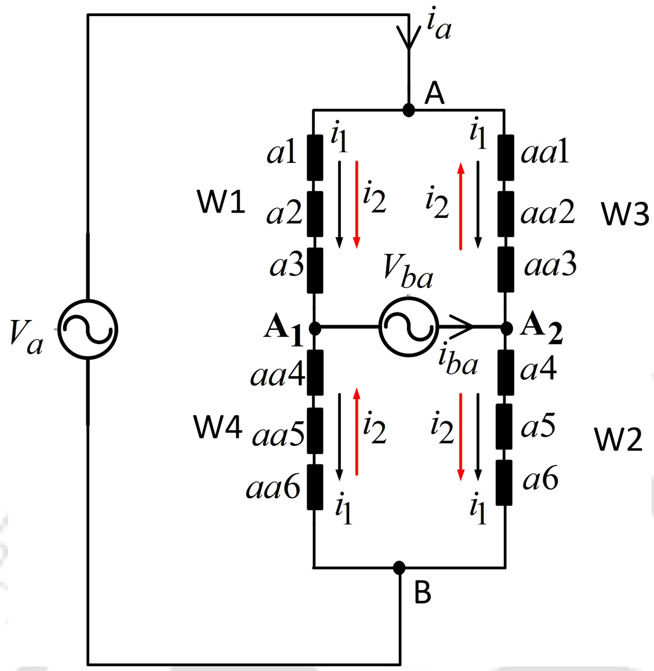

Figure 1.5: Circuit diagram of single phase of a bridge configured winding.

configured electrical machine is the unknown behavior of the machine in its eccentric rotor conditions.

1.2 Motivation

The objectives of this work relate centrally to the more electric engine concept. One of the main features characterise present trends in all rotating machines is the integration of an electrical motor or generator into the overall machine. These machines present great rotordynamic challenges and at the same time they also present great opportunities through the ability to achieve transverse actuation (in two independent directions) without any significant loss. This opportunities can be tapped by developing electrical machines having transverse force producing capability. It can be a great contribution to the scientific community, if these effects can be achieved with low power requirement. Bridge configured winding scheme is one such novel stator winding scheme which can be installed in an electrical machine to produce transverse forces with a low power requirement along with its primary function as a motor or generator. It is paramount to know the nature of the magnetic fields and the method of producing controllable transverse forces in an electrical machine with bridge configured winding.

1.3 Aim of the research

Wear and tear in a rotor bearing system is an obstacle for proper functioning of a high speed electrical machine. This problem can be solved if an electrical machine having the capability of producing controllable transverse force is used. The biggest disadvantage of any such existing machine is that the lateral force generation affects the torque production capability of the machine. The bridge configured winding is a special winding scheme, where lateral force production does not affect the torque generation capability of the machine. However, implementation of bridge configured winding for active vibration control and bearingless application offers many challenges. The work in this thesis aims to address these challenges by setting up the following objectives:

- Study of effect of different eccentricity conditions on UMP generation in parallel stator winding electrical machine.
- Establishment of the relationship between the frequency components of the induced bridge currents with the static, dynamic and mixed eccentricity conditions.
- Development of the method for implementation of current or voltage supply in the bridges to generate transverse forces of selective frequencies in the air gap of the machine.
- Development of a generalized coupled field circuit and rotor model to analyse the effect of bridge supply and effect of different eccentricity conditions.
- Development of an approximate MATLAB/SIMULINK® simulation model for levitation and unbalance vibration control.
- Development of an experimental setup of a 4-pole bridge configured induction machine for the verification of the numerical results and developed bridge supply method .

1.4 Organization of the thesis

The thesis is organized into eight chapters. The brief description of each chapter are as follows

Chapter 1 describes the background of the study along with motivation and aim of the research. It also presents organization of the thesis.

Chapter 2 introduces the fundamentals of unbalanced magnetic pull in an electrical machine. An exhaustive literature review involving unbalanced magnetic pull are discussed in this chapter to understand the state of art in this area.

Chapter 3 discusses the effect of eccentricity on the magnetic field and generation of the unbalanced magnetic pull in electrical machines. These effects are explained for electrical machines with series and bridge configured winding arrangements. A 3.7 kW, four pole machine having 36 slots with a solid rotor is modelled and analysed using COMSOL MULTIPHYSICS® software. The numerical analysis shows the presence of a pulsating 6-pole magnetic field in the air gap of an electric machines with stator winding having parallel branches when the rotor is eccentric. Furthermore, a modified expression of the magnetic field has been used for the calculation of transverse forces acting on the rotor.

Chapter 4 deals with the development of a 2D electromagnetic finite element modelling of a bridge configured induction machine. A finite element code is developed in MATLAB® environment for this purpose. This developed code is capable of accommodating two sets of power supplies, one for the torque production and the other for the transverse force generation. The chapter begins with the discussion of the modelling of the stator electric circuit, rotor electric circuit and mechanical movement modelling of the rotor. Furthermore, the analysis involving the effects of eccentricity conditions on bridge currents and lateral force generation are presented. Relationships of the frequency components of the bridge currents with different eccentricity conditions have been established. Also, a relationship in between the bridge current and force frequency has been presented.

Chapter 5 describes the magneto motive force analysis of an electric machine having bridge configured winding. The generation of different magnetic field components in electric machines with bridge configured winding is explained with the help of magneto motive force analysis for independent excitation of the bridge terminals. A bridge supply sequence has been proposed which can be used for the generation of two pole magnetic field. Furthermore, an analytical relation between the force generated due to interaction of main and bridge supply is presented. The force is calculated using Maxwell stress method [7]. The coefficients of the relationship are calculated using Fourier transform of the magneto motive force distribution.

Chapter 6 presents the coupled rotor model of a bridge configured induction machine. The rotor of the motor has been approximated as a 4 DOF rigid rotor. It describes the study of rotor response in static and dynamic eccentricity conditions along with different bridge supply conditions. The later part of this chapter describes a MATLAB/SIMULINK® model used for demonstration of levitation and harmonic force compensation using PID and convergent control.

Chapter 7 illustrates the development of an experimental setup to investigate the effect of unbalanced magnetic pull in bridge configured winding induction machine. A normal four pole, 36 slots, 3.7 kW induction machine has been re-wound to incorporate bridge configured winding. The machine is also equipped with two pole, four pole and six pole search coils to investigate two pole, four pole and six pole magnetic fields. This setup along with 37 kW bridge configured winding induction machine have been used for the verification of several numerical findings.

Chapter 8 presents the important conclusion of the current research and outlines the directions for future work.

2

Unbalanced Magnetic Pull - A Literature Review

Contents

2.1 Introduction

This chapter presents the literature review of unbalanced magnetic pull (UMP) and its interactions with the mechanical dynamics of the electrical machine. The literature shows that the study related to UMP has started as early as 1899. Literature involving the origin of UMP, methods of UMP calculation, electromechanical interactions and its applications are discussed in this chapter. The study of literature review is divided into the following main sections and they are discussed individually:

- Background of UMP
- Methods to calculate UMP
  - Analytical methods
  - Numerical methods
- Effect of rotor eccentricity on UMP
- Electromechanical interactions
- Bearingless Machines

2.2 Background of unbalanced magnetic pull

The initial work on UMP involves basic calculations of UMP, fundamentals of UMP and its generation. The literature shows that study related to UMP has started as early as 1899. Alexander and Pertsch [8] wrote a review paper on dynamo electric machines. From this paper, it has been found out that Fisher-Hinnen (1899) gave the first formula for UMP for his dynamo design as shown in Equation (2.1).

$$\text{Pull (in dynes)} = \left(\frac{B^2 A}{25 \times 10^6} \times \frac{x}{g\alpha} \right) \tag{2.1}$$

Here, B is the density of flux in the air gap, in lines per sq. cm, A is the cross sectional area of the pole face in sq. cm, x is the rotor displacement, g is the air-gap clearance, α is the ratio of the reluctance of the total magnetic circuit to that of the normal air gap alone. Rosenberg [9] investigated the occurrence and the effect of UMP in electrical machines and derived simple practical formulas. His calculations are based on difference in the flux densities on opposite side of the air gap and developed the equations on graphical basis from the saturation curve. However, Rosenberg could not explain the reason of production of UMP. Later in 1919 Stiel first showed that origin of the UMP is harmonic fields in the air gap. Hildebrand [10] was the first to tabulate all known possible harmonic fields and made following investigations,

- The reason behind generation of pulsating torsional vibration is magnetic fields that has same number of poles but revolving at different speeds.
- The components of magnetic fields having difference of one pole pair leads to generation of unbalanced magnetic pull.
- The components of magnetic fields differing by any number of pole-pairs larger than one, results in deforming the stator and the rotor into a polygon.

Carr [11] proposed to generate different magnetization curve with respect to a varying air gap. This can be used to obtain flux distribution for any given displacement and excitation current. Once the flux density is known the total pull parallel to the axis of the displacement can be calculated as the difference of the pull on both sides of the rotor. Robinson [12] again used saturation curve and considered the effect of saturation, parallel paths in the stator winding and primary reactance. He proposed the formula for the calculation of UMP for a constant displacement of 1/32 inch as

$$\text{Pull} = 2.88e^2\frac{B_g^2}{g}\left[aK_s + (1-a)\,K_R\right]\times 10^{-4} \tag{2.2}$$

Here, B_g is the maximum flux density, g is the air gap length, e is the voltage factor at which maximum pull occurs, to be found from saturation curve, a is the factors for parallel paths, K_s is the factor allowing for the effect of saturation on flux density rise, K_r is the factor allowing for the effect of saturation and primary reactance on the flux density rise. Graybel [13] studied the mechanical driving forces and electromagnetic driving forces acting in an electrical machine independently and in combination. The fundamental component of mechanical driving force arises due to static or dynamic unbalance. The amplitude of vibration can be adjusted by proper balancing of rotor. It has been observed that multiple of rotational frequency component of vibration are present due to imperfection in the mechanical design or presence of dissymmetry in the construction of machine. Among all these components, second harmonic component of vibration is more troublesome. This component of vibration is present due to shafts having portion of non circular area created due to presence of keyways, slightly elliptic bearings or any other mechanical imperfections. Multiple harmonic components of force arises due to electromagnetic interactions as well. Among them, second harmonic component of electromagnetic driving force is important. This driving force acting with mechanically induced second harmonic force leads to beating effect. This effect can be troublesome if the machine has an inherent resonant frequency equal to the double of supply frequency. The beating effect can be eliminated by proper designing of frame in such a way that second harmonic component generated due to mechanical driving forces vanishes. Covo [14] studied the available UMP calculation formula and saw that these are not applicable for machines having eccentricities more than 10 %. It is also seen that an increment in the number of poles leads to increment in average pull for a given eccentricity. However, the magnitude of alternating component of magnetic pull decreases with increase in number of poles. He further improved the available UMP formulations however, rotor skew and rotor bar currents have not been considered. Summers [15] also studied the generation of double supply frequency vibration component in a two pole induction motor. It was found that effect of double supply frequency vibration component is more predominant in a two pole AC machine. This happens because the distance between the poles are comparatively higher than the other configurations. The phenomena of beating effect has also been explained. The beating effect arises due to the interaction of double supply frequency component and second harmonic component of force generated due to mechanical faults which differs by two times the slip frequency. Robinson [16] demonstrated that a line frequency component of vibration is also present with the double supply frequency component of vibration in all AC machines.

2.3 Methods to calculate unbalanced magnetic pull

The literature related to calculation of unbalanced magnetic pull can be divided in two subsections, (i) Analytical approach and (ii) Numerical approach.

2.3.1 Analytical approach

Several authors have studied and derived the unbalanced magnetic pull acting in an electrical machine by analytical approach. For the calculation of unbalanced magnetic pull, the first step is the calculation of magnetic field distribution in the air gap. Most of the authors have used air gap pearmeance approach and few of them used conformal transformation technique for the calculation of magnetic field distribution. Few notable work using air gap permeance approach has been carried out by Jordan et al. [17], Früchtenicht et al. [7], Belmans et al. [18] and Holopainen et al. [19]. The permeance is the measure of magnetic flux passing through the air gap and defined as the inverse of reluctance. For an eccentric rotor, the air gap permeance is calculated with the help of air gap distribution. The air gap distribution in the stator reference frame can be approximated by using trigonometrical relation using small angle approximation. If the variation in airgap length is very small compared to the outer radius of the rotor and the air gap length of a concentric rotor, the variation can be approximated as

$$\delta(\theta, t) = \delta_m(1 - \varepsilon\cos(\theta - \omega_\varepsilon t - \phi_\varepsilon)) \tag{2.3}$$

Here, δ_m is the mean air gap length, ε is the relative eccentricity ($\varepsilon = \frac{e}{R-r}$ where e is eccentricity, R is stator inner radius and r is outer radious of the rotor), ϕ_ε is the phase angle and ω_ε is the whirling frequency. The whirling frequency is zero when the rotor is in static eccentricity condition.

The air gap permeance is inversely proportional to the air gap length. With the help of approximated air gap length, the air gap permeance can be represented in terms of Fourier series as

$$\Lambda(\theta, t) = \frac{1}{\delta(\theta, t)} = \sum_{\lambda=0}^{\infty} \Lambda_\lambda \cos[\lambda(\theta - \omega_\varepsilon t - \varphi_\varepsilon)] \tag{2.4}$$

The Fourier coefficients Λ_λ are,

$$\Lambda_\lambda = \begin{cases} \frac{\mu_0}{\delta_m}\frac{1}{\sqrt{1-\varepsilon^2}}(\lambda = 0) \\ \frac{2\mu_0}{\delta_m}\frac{1}{\sqrt{1-\varepsilon^2}}\left(1 - \frac{1-\sqrt{1-\varepsilon^2}}{\varepsilon}\right)^\lambda(\lambda > 0) \end{cases} \tag{2.5}$$

Further, a sinusoidal distribution of MMF is assumed which upon multiplication with air gap permeance gives magnetic field distribution in the air gap of the electrical machine.

$$UMP = l\int_0^{2\pi} \frac{b^2(\theta, t)}{2\mu_0} r d\theta \tag{2.6}$$

Upon calculation of magnetic field distribution, the unbalanced magnetic field can be calculated by applying Maxwell equation as Equation (2.6) or by calculating magnetic field energy (W_ϵ) as in Equation (2.7) which upon differentiation with respect to eccentricity (ϵ) gives unbalanced magnetic pull as in Equation (2.8).

Here l is the axial length of the rotor, b(θ, t) is the magnetic flux density, r is the outer diameter of the rotor and μ_0 is the permeability of free space.

$$W_\epsilon = \frac{1}{2}\int_0^{2\pi} \frac{b^2(\theta,t)}{\mu_0}\delta(\theta,t)Rld\theta \tag{2.7}$$

$$UMP = \frac{\delta W_\epsilon}{\delta \epsilon} \tag{2.8}$$

The sinusoidal approximation of MMF distribution is a poor approximation for an eccentric rotor motor especially when the stator winding has parallel paths. In these cases, conformal transformation based method can provide better approximation because this technique can be used to study different combination of windings. However, this technique has not been used much in the literature. Swann [20] proposed conformal transformation technique to be used in electrical machine because of its capability to accomodate different winding configurations. Dorrell and Smith [21] presented a detailed modelling approach using conformal transformation by studying various winding configuration in an electrical machine. Basically, in conformal transformation an eccentric rotor - stator configuration (set of two eccentric circles) in Z plane can be transformed to concentric rotor - stator configuration (set of two concentric circles) in T plane. This is achieved by utilizing a simple inversion as

$$\bar{z} = \frac{1}{\bar{t}} \tag{2.9}$$

By finding a proper value of d in Z plane and c in T plane, an eccentric rotor machine represented by circles of radius R_1 and R_2 shown in Figure 2.1(a) can be mapped on the T plane as two concentric circles of radius r_1 and r_2 as shown in Figure 2.1(b). However, this transformation leads to irregular slot pattern in T plane. This technique transforms a machine from magnetically asymmetric to magnetically symmetric but electrically asymmetric, i.e. to a machine which has uniform air gap but non-uniform winding distribution. Hence, any method based on this technique must be capable of accommodating general asymmetrical winding. Further, phase band current in Z plane is obtained using certain impedence matrix and connection matrix. With the known phase band current, the magnetic field distribution can be calculated and unbalanced magnetic pull is computed using Maxwell equation presented in Equation (2.6).

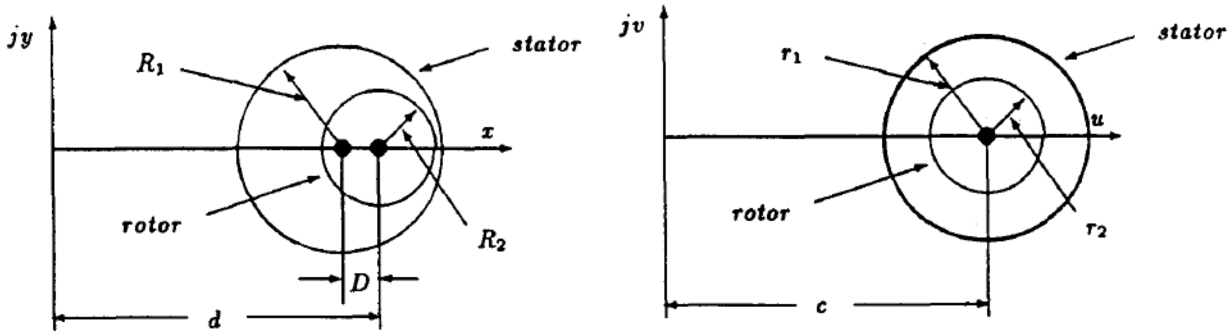

(a) (b)

Figure 2.1: (a) Z- plane, (b) T- plane. [21]

2.3.2 Numerical approach

Considering the limitations in analytical approach of calculations of UMP, the numerical approach for the analysis of electrical machines has become quite popular. The trend is to use finite element method for the simulation of electrical machine due to its flexibility and accuracy. The literature of the numerical approach has been presented in two parts. The first describes the simulation of electrical machines using FE method and later part describes the methods used for the calculation of UMP. Silvester [22, 23] and Hannalla and Macdonald [24] are among the first few authors who applied FEM for the simulation of electrical machines. Vassent et al. [25] used FEM for the analysis of induction machine by applying complex magneto-dynamic formulation considering steady state and sinusoidal power supply. The simulation has been carried out by assuming the presence of single harmonic as the supply frequency in the stator and slip supply frquency in the rotor. This kind of formulation where the harmonics due to the motion such as locked rotor condition or velocity close to the synchronous speed are not important give very accurate results with short-computation time [26–28]. However, when the harmonics problems cannot be neglected, magneto-dynamic formulations fail in those conditions.

In addition to this, certain effects such as harmonics due to the rotor movement and the non-sinusoidal quantities, the end-windings effects, and rotor-bar skew-ness are difficult to include. Vassent et al. [29], Pham et al. [27] and Rodger et al. [28] implemented time stepping scheme with the rotor motion at constant speed in order to take into account the harmonics due to the motion. The finite element field equations are coupled with the circuit equations to incorporate the end-winding effects [30, 31]. The time stepping method is quite useful in the sense that it can be used to calculate all the parameters of the machine. The skewed rotor effect and homopolar flux is not possible to incorporate in a 2D FE model. Tenhunen and Arkkio [32] used 2D multi slice model to incorporate skewed rotor effect. However, it comes at the cost of computational effort. Also, the homo-polar flux is usually neglected in the finite element analysis [33].

In addition to these formulations, there are few formulations in which the transient dynamic behavior of the induction machines is analyzed and reported by Vassent et al., [26] and later by Ho et al., [34]. This transient dynamic analysis is performed by coupling the mechanical motion equation with the coupled field-circuit equation. The basic steps involved in the finite element analysis of a cage induction machine can be summerised as

- Coupling of magnetic field and electrical circuit equations.
- Coupling of magnetic field − electrical circuit equations with mechanical equation.
- Use of Galerkin's method for the discretization of the coupled magnetic field, electrical circuit and mechanical equations.
- Use of numerical technique such as Newton-Raphson algorithm to deal with the non-linearity due to the presence of ferromagnetic materials.

The algebraic details of these procedures has been described in details by Salon et al., [35] and Silvester and Ferrari, [33] in general and by Savov et al., [36] for cage induction motor in particular.

For the calculation of electromagnetic forces acting between the stator and rotor, two methods are very popular, i.e. method based on principle of virtual work [37] and method based on Maxwell stress tensor [38]. The virtual work method has been used by the group of Arkkio extensively to analyse UMP acting in electrical machines [39–41] The Maxwell's stress tensor method is one of the most efficient general methods for the calculation of forces on bodies under the influence of magnetic fields. It leads to expressions that allow the computation of forces on diverse structures such as the rotor of an electric machine. In contrast to the virtual work method which is based on energy, the Maxwell stress tensor method describes the force directly in terms of the magnetic field strength. The methods based on the Maxwell stress tensor have been used by Arkkio, [30] and Savov et al., [36].

The Maxwell stress approach computes the local stress at all points of a boundary surface and then sums the local stresses using a surface integral to find the overall force. In three dimensions the force is a surface integral given by

$$\overrightarrow{F} = \oint_S \sigma_{Maxwell} d\overrightarrow{S} \tag{2.10}$$

Here, $\sigma_{Maxwell}$ is the the magnetic stress tensor, $\overrightarrow{n}$ is the unit normal vector of the integration surface S and $\overrightarrow{B}$ is the magnetic flux density.

$$\overrightarrow{F} = \oint_S \left[\frac{1}{\mu_0} \left(\overrightarrow{B}.\overrightarrow{n} \right) \overrightarrow{B} - \frac{1}{2\mu_0} \left(\overrightarrow{B}.\overrightarrow{B} \right) \overrightarrow{n} \right] dS \tag{2.11}$$

In a 2D model the surface integral is reduced to a line integral along the air gap. The normal σ_{nn} and tangential τ_{tt} components of the Maxwell stress are

$$\sigma_{nn} = \frac{\left(B_n^2 - B_t^2\right)}{2\mu_0} \tag{2.12}$$

$$\tau_{tt} = \frac{2B_n B_t}{2\mu_0} \tag{2.13}$$

Here, B_n and B_t represent radial and tangential components of flux density respectively. If a circle of radius r is taken as the integration path in the air gap of the motor, the forces can be represented as

$$F_x = l \int_0^{2\pi} \left(\sigma_{nn} \cos\theta - \tau_{tt} \sin\theta \right) r d\theta \tag{2.14}$$

$$F_y = l \int_0^{2\pi} \left(\sigma_{nn} \sin\theta + \tau_{tt} \cos\theta \right) r d\theta \tag{2.15}$$

Here, l is the axial length of the machine.

2.4 Effect of eccentric position of rotor

Due to manufacturing tolerances, it is really difficult to manufacture a motor where the rotor is concentric with the stator. This leads to requirement of study related to effects of eccentric position on the behaviour of motor. There are two recent reviews related to eccentric rotor condition in an electrical machine by Frosini and Pennacchi [42] and Salah et al. [43] which covers different aspects of presence of eccentricity in a motor. Effects of eccentric rotor position, from generation of UMP and means to control have been studied by many researchers. The important contribution has been reported by the research groups of Dorrel and Arkkio. The study in the literature is basically focused on modelling various eccentricity conditions, generation of additional magnetic fields and different frequency components of UMP with respect to eccentricity conditions.

A rotor is said to be statically eccentric if the rotor is eccentric in one direction with respect to the center of the stator of an electrical machine. A rotor is said to be dynamically eccentric if the rotor center whirls around the stator center. The electric machine which has both types of the eccentricity is said to be in mixed eccentricity condition. The presence of static and dynamic eccentricity in an electrical machine generates a magnetic field of $p \pm 1$ pole pair, where p is the fundamental component of the magnetic field. Both of the eccentricity condition generates same components of magnetic field however its rotational frequency is different. p and $(p \pm 1)$ pole magnetic field rotates with frequency of f_s Hz in static eccentricity condition whereas, $(p+1)$ pole pair magnetic field rotates with $(f_s + f_r)$ Hz and $p-1$ pole pair of magnetic field rotates with $(f_s - f_r)$ Hz, here f_s and f_r are stator excitation frequency and rotor rotational frequency respectively [39, 44–46]. The magnetic field expression and forces acting on the rotor in an eccentric rotor motor can be expressed as represented by Tenhunen et al. [44] as

$$b(\theta, t) = B_p \left\{ \begin{array}{l} \cos(p\theta - \omega t - \phi_m) + \frac{\varepsilon}{2}\cos((p+1)\theta - (\omega + \omega_\varepsilon)t - (\phi_m + \phi_\varepsilon)) \\ +\frac{\varepsilon}{2}\cos((p-1)\theta - (\omega - \omega_\varepsilon)t - (\phi_m - \phi_\varepsilon)) \end{array} \right\} \tag{2.16}$$

Here, θ is the angular position, ϵ is the relative eccentricity, ϕ_m is the phase angle of magnetizing current, ϕ_ϵ is the phase angle of eccentricity field and ω_ε is the angular frequency of the rotor which can be defined in terms of slip(s), supply frequency(ω), pole pair (p) as $\omega_\varepsilon = (1-s)\frac{\omega}{p}$.

The radial components of force acting on the rotor is calculated along vertical and horizontal directions with respect to the cross-sectional geometry by surface integral over the rotor outer surface as shown in Equation (2.6) and can be represented in complex form as

$$F = \frac{\pi R l}{2\mu_0}\left(B_p B_{p-1} + B_p B_{p+1}\right).\left\{\cos(\theta - \omega_\omega t - \phi_\omega) + \mathrm{j}\sin(\theta - \omega_\omega t - \phi_\omega)\right\} \tag{2.17}$$

Here, R is the outer radius of the rotor, l is the axial length of the rotor, B_p is the fundamental component of magnetic flux density, $B_{p\pm1}$ are the $(p \pm 1)$ pole pair magnetic flux density. Equations (2.16) and (2.17) represent the case of static eccentricity, if $\omega_\varepsilon = 0$, otherwise, it represents dynamic eccentricity condition.

Arkkio [47] studied the effect of common asymmetries such as rotor-cage faults, eccentric rotors and unsuitable number of rotor slots in a squirrel cage induction motor. The study has been carried out on two motor configurations i.e. two pole and four pole motor. The two pole motor has closed rotor slots whereas four pole motor has semi open rotor slots. Also to consider the effects of circulating current two types of stator winding has been used for the simulation, one with series connection and one with parallel connection. The effect of rotor skew and core loss have been neglected. The following findings have been reported,

- When the rotor has a broken rotor bar, it has been found that the force vector rotates with the rotor. The presence of higher harmonics due to stator slotting along with fundamental component of the force varies with time at twice the slip frequency. The higher order harmonics component increases with the increase in the load and in between the no load point and rated point the fundamental component is the dominant component. The parallel winding is able to reduce the UMP and reduction is more in four pole winding compared to two pole winding. The saturation in core tries to make magnetic field distribution symmetric and due to which UMP reduces at high level of saturation.

- A broken end ring produces higher amount of UMP compared to a broken rotor bar. This ratio is 4 in two pole motor and 3 in four pole motor. Parallel path is again able to reduce this force however again reduction is more in four pole machine compared to a two pole machine.

- Both of the eccentricity conditions i.e. static and dynamic eccentricity conditions have been studied. The simulation has been carried out for 20 % of static and dynamic eccentricity with varying load. In the case of static eccentricity condition, the UMP increases steadily in a four pole motor whereas in a two pole motor, the UMP first decreases and then increases with the increase in load. This reduction happens because the two pole motor has closed rotor slots. At low load the iron bridges are non saturated and it allows asymmetric flux to pass which results in flow of circulating currents through the rotor bar and results in reduction in UMP. However, with the increment in load these iron bridges gets saturated and does not allow asymmetric flux to pass which results in increment of UMP. In the case of dynamic eccentricity, both of the motor shows intial decerement of UMP with the load increment and at the load well over the rated power UMP starts to increase. This happens due to the presence of higher harmonics in the air gap field.

- The study shows that if the no of rotor slots are even, then the large local forces in opposite sides cancels each other and net resultant force is zero whereas if the number of slots are odd a net force might occur in the machine.

Dorrell [48] studied and reviewed the various factors affecting the magnetic field asymmetry in the air gap of the motor leading to UMP. An experimental study is performed to study the effect of tooth saturation. The effect of slotting has not been presented because the effect of slotting comes in terms of audible noise and high frequency vibration not the UMP. Parallel paths reduces UMP, whether winding is on the rotor or the stator. The presence of rotor cage and parallel path shows significant effect on the generation of UMP. A cage rotor has many parallel paths, it reduces UMP considerably when compared with the wound rotor configuration. Bradford [49] showed that the cage rotor is able to damp 80 % of UMP when compared to wound rotor in the same machine. Dorell and smith [50] showed that parallel path in stator is less effective than a cage rotor because cage rotor has many parallel paths. However the parallel path in stator winding also reduces the UMP. They also showed that due to parallel connection a backward rotating magnetic field develops in the air gap because of uneven distribution of stator winding currents which also generates twice of supply frequency UMP. Which says that certain parallel connection which is used to damp UMP can also create further problems. Dorrel [48] summarized the behavior of UMP in following conditions,

(i) Transient run-up UMP - As per the literature [51] the most common failure in an induction motor is the bearing failure. Investigation of transient UMP is necessary because it happens several times in motor and can cause severe damage to bearing of the motor. It has been seen by many authors that transient UMP is much higher than the steady state UMP. It has also been seen that in the case of dynamic eccentricity no load UMP is approaching transient UMP.

(ii) Use of parallel path - It has been seen that parallel path in the stator winding is able to reduce UMP in the wound rotor motor. This reduction is more noticeable when cage rotor in dynamic eccentricity case has been used.

(iii) Effect of variable frequency operation - Authors have studied UMP in a cage rotor and two parallel paths in the stator winding. It is observed that the increase in frequency decreases the UMP. This happens because very low current flows at a lower frequency in the rotor cage which reduces the damping effect.

(iv) Effect of tooth saturation - A method has been described to incorporate the tooth saturation. Considering the mmf distribution to be same in the case of saturated and unsaturated conditions, the flux density can be determined. If there is no saturation, then permeability of iron can be considered infinite and MMF at a point in the air gap can be calculated as

$$F(x, y, t) = \frac{b(x, y, t)g(x, y, t)}{\mu_0} \tag{2.18}$$

However, if tooth saturation is considered then there would be a drop of MMF in stator tooth hence, total MMF can be written as

$$F(x, y, t) = \frac{b(x, y, t)g(x, y, t)}{\mu_0} + \frac{2b(x, y, t)l}{\mu_r \mu_0} \tag{2.19}$$

Here, l is the length of the stator tooth and μ_r is the relative permeability. The relative permeability can be obtained with the help of B-H curve of the stator core. An iterative method can be used to obtain the flux density using Equation (2.19) considering the saturation effect of the tooth. It has been observed that tooth saturation reduces UMP. The UMP vibration has been measured by the use of accelerometer fitted at the top of the stator casing.

Debortoli et al. [52] demonstrated the effect of parallel winding on UMP production. He investigated UMP in different winding connections, i.e. series as well as parallel and found that parallel winding connection reduces UMP. In the parallel winding, the stator circuits which is located at the farthest point from the rotor has lower inductance. Hence, a higher amount of current flows in those circuits and it controls UMP even if the rotor is eccentric. These currents are called as circulating current.

The rotor orientation can change axially with respect to length of the motor. Tenhunen [39] modelled and studied all the possible orientations of the rotor, i.e. when the rotor is parallelly eccentric and when the rotor is diagonally eccentric (one end eccentric and both end eccentric) with respect to the stator. Both static and dynamic eccentricity have been considered in these orientations. To study the effect of equalizing current, two machines have been simulated with series and parallel windings having an eccentricity of 10%. The number of turns of the windings have been selected in such a manner that it produces the same flux in both of the windings. The following observations have been made in the static and the dynamic eccentricity conditions with respect to series and parallel winding configurations,

(i) Static eccentricity - The behavior of equalizing currents flowing in the parallel winding at no load has been calculated and it has been shown that, the induced current in one phase is higher than other phases, which faces the minimum and maximum air gap position. It has been seen that after a slip value of 0.01 the UMP starts increasing. The fundamental component of UMP decreases slightly with the increase in load however, other higher harmonic components of vibration increases. Since in both of the winding configuration (series and paralell) rotor cage has been used hence in series connection the equalizing current flows only in the rotor side so UMP is higher in the series connected winding than the parallel winding connection. It has also been seen that at small slip UMP developed in series connected coils are much higher than the parallel winding. This happens due to the closed rotor slot. At small slip, the iron above the rotor bar allows the asymmetric magnetic field to flow and does not induce any circulating current in the rotor bar, whereas when the load is applied, the iron bridge becomes saturated and the field crosses the rotor bar due to which circulating current starts flowing in the rotor bar and in return UMP drops down significantly. In other type of eccentricity, when the rotor is eccentric at only one end diagonally, induced circulating current becomes half compared to parallel case, however the nature of the circulating current remains the same. Since the circulating current arises due to the induced emf in eccentric end only. The UMP decreases in eccentric end and increases in concentric end. Hence, overall there is not much difference in the UMP in series and parallel winding configuration machine in this type of eccentricity condition. In the 3rd type of eccentricity, when the rotor is diagonally eccentric in both sides of the rotor, equal and opposite circulating current is induced in the parallel winding of the stator as well as the rotor cage. Due to that there is no net circulating current flows through the winding and UMP has no effect of the parallel winding.

(ii) Dynamic eccentricity - The highest amount of UMP is generated with the series winding with dynamic eccentricity. In series winding, there is no circulating current in the stator winding as well as no equalizing current in rotor cage as well. It happens because the geometric non symmetry rotates synchronously with the magnetic field. Hence, the UMP reaches to its maximum value. When the motor is in loaded condition, the rotor doesn't rotate synchronously with the magnetic field and hence UMP decreases. However, in the parallel winding connection there is always a circulating current so there is always a drop in UMP compared to series connection.

However, with the increase of load, UMP increases in parallel winding due to the effect of higher harmonics.

Tenhunen et al. [53] used AMB for the generation of eccentric rotor motion as well as for the measurement of forces acting on the rotor. They concluded that the forces in combined cylindrical and conical motion can be obtained by adding the force in cylindrical and conical motion individually. Yang [54] studied the stability regions, when the rotor of a motor is in static and dynamic eccentricity conditions. An analytical method has been used by applying time transfer matrix method to find out the rotor instability zones. Dorrell [55] studied the effect of varying eccentricity along the axial length of the motor and presented a model for the study of UMP in cage induction motor. Both dynamic and static eccentricity have been studied. UMP has been studied by various researchers however, it is difficult to quantify or measure it. Dorrell et al. [56] has proposed a UMP index for the comparative study of UMP for various motors of different sizes. UMP indexes termed as UMP factor and UMP gap-factor have been derived considering different winding layouts, voltage and geometry. These indexes can be used to compare level of UMP in different machines. It has been shown that higher is the value of UMP factor and UMP gap-factor, lower is the UMP. Generally studies have been carried out considering uniform variation of eccentricity along axial length however eccentricity can vary along the axial length depending on non aligned side bearing or bent rotor. UMP gets affected with core saturation and winding. Core saturation attenuates UMP. Parallel paths in the winding such as parallel stator winding and squirrel cage rotor also helps in attenuation of UMP. The presence of parallel paths in stator winding helps in reduction of UMP however, they also generates additional vibrations. Various methods have been adopted for the measurements of UMP such as active magnetic bearing, load cells and piezoelectric force cells. After application of loads, load cell goes through some movement that has to be taken care for the measurements. Due to this fact, piezoelectric cells are a better choice of force measurements, which has a very negligible movement.

2.5 Electromechanical interactions

The literature related to UMP in electrical machine is mostly focused on study related to its effect and modelling. However, the coupling of rotor motion with magnetic forces in an electrical machines bring additional dynamics. There are very few studies related to electromechanical interaction reported in the literature. The term electromechanical interaction means, the combined study considering the rotor equation of motion and UMP generated by the machine. The few notable work related to electromechanical interactions in electrical machines have been discussed in this section [3,7,38,57–62].

Früchtenicht et al. [7] developed an analytical model considering the magnetic forces and rotor equation of motion. As a first step, airgap magnetic field is calculated using airgap permeance approach and subsequently forces generated due to eccentric rotor motion are calculated. The total unbalanced magnetic pull being generated due to the eccentric position of the rotor consists of two rectangular components of forces, whose line of action is perpendicular to each other. One component of force acts along the direction of shortest airgap, whereas the other component of force acts along the perpendicular direction of the shortest airgap. The first component which acts along the shortest airgap can be related to electromagnetic spring constant (k_e) and the another component acting along the perpendicular direction to shortest airgap can be related to electromagnetic damping constant (d_e). These constants k_e and d_e have been calculated by differentiating transverse and tangential components of the forces with respect to eccentricity and rotational speed respectively. The derived formula for stiffness and damping coefficients have been represented in Equations (2.20) and (2.21) respectively.

$$k_e = -\frac{\pi l B_p^2}{4\mu_0}\left[\begin{array}{l} \frac{2R}{\delta_e} - \frac{s_{p+1}^2}{s_{p+1}^2+\beta_{p+1}^2}\cdot\frac{\xi_{p+1}^2\cdot\xi_{\text{Schr}.p+1}^2}{1+\sigma_{gRp+1}}\cdot\left(\frac{R}{\delta_e}-p-1\right)+ \\ -\frac{s_{p-1}^2}{s_{p-1}^2+\beta_{p-1}^2}\cdot\frac{\xi_{p-1}^2\cdot\xi_{\text{Schr}.p-1}^2}{1+\sigma_{gRp-1}}\cdot\left(\frac{R}{\delta_e}+p-1\right)\end{array}\right] \tag{2.20}$$

$$d_e = -\frac{\pi l B_p^2}{4\mu_0\Omega_m}\left[\begin{array}{l} \frac{s_{p+1}\cdot\beta_{p+1}}{s_{p+1}^2+\beta_{p+1}^2}\cdot\frac{\xi_{p+1}^2\cdot\xi_{\text{Schr}.p+1}^2}{1+\sigma_{gRp+1}}\cdot\left(\frac{R}{\delta_e}-p-1\right)+ \\ -\frac{s_{p-1}\cdot\beta_{p-1}}{s_{p-1}^2+\beta_{p-1}^2}\cdot\frac{\xi_{p-1}^2\cdot\xi_{\text{Schr}.p-1}^2}{1+\sigma_{gRp-1}}\cdot\left(\frac{R}{\delta_e}+p-1\right)\end{array}\right] \tag{2.21}$$

Here, $\xi_{\text{Schr}.p\pm1}$ is the skew factors of the eccentricity harmonics, $\sigma_{gRp\pm1}$ is the geometrical leakage coefficients of the eccentricity harmonics, $\xi_{p\pm1}$ is the winding factors of the eccentricity harmonics, β_{p+1} is the resistance-reactance ratios of the rotor mesh, $s_{p\pm1}$ are the eccentricity harmonic fields slip.

Belmans et al. [38, 57] studied the effect of electromagnetic forces by developing a combined analytical model of rotor equation of motion and forces due to the eccentric position of the rotor. The rotor is modeled as a Laval rotor where a disc of mass m is concentrated in the middle of massless shaft having spring constant K_{mech} and damping constant C_{mech}. The effect of forces on crtical speed of the machine have been studied. It has been demonstrated that electromagnetic forces reduces the critical frequency of the motor. The modified natural frequency and damping ratio of the system due to electromagnetic forces can be represented as shown in Equations (2.22) and (2.23) respectively.

$$\omega_c = \sqrt{\left(\frac{K_{mech} - K_{mag}}{m}\right)} \tag{2.22}$$

$$\xi_c = \frac{C_{mech} - C_{mag}}{2\omega_c m} \tag{2.23}$$

Here, K_{mech} is the mechanical spring constant and K_{mag} is the electromagnetically induced spring constant. C_{mech} is the mechanical damping coefficient and C_{mag} is the electromagnetically induced damping coefficients.

One of the important work in the area of electromechanical interaction has been carried out by Arkkio et al. [63] who formulated a parametric force model using numerical simulation when the rotor of the induction motor is having a cylindrical circular whirling motion. The developed model is also verified using experimental measurements. The parametric equations are developed by assuming a second order frequency response function as formulated in Equation (2.24).

$$\begin{aligned} F_C(s) &= K(s)p_c(s) \\ K(s) &= k_0 + \tfrac{k_{p-1}}{s-z_{p-1}} + \tfrac{k_{p+1}}{s-z_{p+1}} \end{aligned} \tag{2.24}$$

Here, F_c is the force acting on the rotor for the displacement p_c, k is the variables proportional to square of the fundamental component of the flux density in the air gap, $z_{p\pm1}$ are the whirling frequencies at which the slips of the two eccentricity harmonics becomes zero. The earlier developed force models do not include the effect of saturation. However, this model includes the effect of saturation in a way that the numerical model which has been used to estimate the parameters of Equation (2.24) is modeled considering the saturation effect. Further this transfer function has been converted to set of differential equations as shown in Equation (2.25) to analyze the transient response of the rotor.

$$\begin{aligned} \dot{q}_{p-1} &= z_{p-1}q_{p-1} + k_{p-1}p_c(t) \\ \dot{q}_{p+1} &= z_{p+1}q_{p+1} + k_{p+1}p_c(t) \\ F_c(t) &= q_{p-1} + q_{p+1} + k_0 p_c(t) \end{aligned} \tag{2.25}$$

The developed parametric model by Arkkio et al. [63] has been used further by Holopainen et al. [58, 59] to analyse rotodynamic instability in an electrical machine through electromechanical interactions by coupling these parametric force equations with a Jeffcott rotor. It was found that the cross-coupled stiffness term is a major source of instability in an electrical machine.

Holopainen et al. [19] formulated a new parametric force equation for squirrel cage induction motor considering cage current harmonics. Further, this parametric force model is coupled to Jeffcott rotor to study the electromechanical interactions [61]. It is found that the electromechanical interaction affects the most when the motor is being operated at first bending critical speed. The parametric force model which includes cage-current harmonics and one equation for the total electromagnetic force is represented as formulated in Equations (2.26),(2.27) and (2.28).

$$\underline{\hat{i}}^r_{p-1,t} + \tau^{-1}_{p-1}\underline{\hat{i}}^r_{p-1} + a_{p-1}\left((\underline{p}^r_{c,t})^* + \mathrm{j}s\omega_S(\underline{p}^r_c)^*\right)\mathrm{e}^{\mathrm{j}(S\omega_S t+\vartheta_{b0})} = 0 \tag{2.26}$$

$$\underline{\hat{i}}^r_{p+1,t} + \tau^{-1}_{p+1}\underline{\hat{i}}^r_{p+1} + a_{p+1}\left(\underline{p}^r_{c,t} + \mathrm{j}s\omega_S\underline{p}^r_c\right)\mathrm{e}^{\mathrm{j}(S\omega_S t+\vartheta_{b0})} = 0 \tag{2.27}$$

$$\underline{F}^r_e(t) = k_e\underline{p}^r_c + c_{p-1}(\underline{\hat{i}}^r_{p-1})^*\mathrm{e}^{\mathrm{j}(S\omega_S t+\vartheta_{b0})} + c_{p+1}(\underline{\hat{i}}^r_{p+1})^*\mathrm{e}^{-\mathrm{j}(S\omega_S t+\vartheta_{b0})} \tag{2.28}$$

Here, $\underline{\hat{i}}^r_{p-1}$ and $\underline{\hat{i}}^r_{p+1}$ are the space vectors of the harmonic components of the cage currents, the circumflex above a symbol refers to the space-vector character, p is the number of pole pairs, the asterix (*) denotes the complex conjugate, ω_s is the electrical supply frequency, s is the slip of the rotor with respect to the fundamental component of the stator field, ϑ is the phase angle of the magnetic-flux-density space-vector at $t = 0$, $\underline{F}^r_e$ is the total electromagnetic force exerted on the rotor, and $a_{p\pm1}$, $\tau_{p\pm1}$, $c_{p\pm1}$ and k_e are the system parameters.

Further, electromechanical studies have been carried out for an inbuilt actuator where control force can be generated by having additional winding in the stator slots. Laiho et al. [3] developed a low order parametric model for an inbuilt actuator for rotor vibration control. The developed model is consist of a rotor equation of motion coupled with actuator force and eccentricity generated force. However, the force generated due to slot harmonics and unipolar flux have not been considered for the analysis. Sinervo and Arkkio [62] developed a coupled model considering the effect of slot harmonics and unipolar flux. The three forces have been coupled with the rotor equation of motion, namely unbalance force, actuator force and magnetic force due to the slot harmonics and unipolar flux.

2.6 Bearingless machines

The idea of development of bearingless machine is based on the generation of asymmetry in the air gap magnetic field through certain stator winding structures. Researchers started working and analyzing various winding structure as a means to suppress unbalanced magnetic pull since 1970 itself [64]. The various winding structure arrangements on the working of electrical machines such as series, parallel and combination of series and parallel connection, combination of series and parallel winding connection with equalizing connections have been investigated. Figure 2.2 represents various winding arrangements used by Ellison and Yang [64] to study the effect of these winding arrangements on unbalanced magnetic pull generation.

Many researchers have used similar combinations of winding arrangements to study their effectiveness on unbalanced magnetic pull. Berman [65] analyzed combination of series and parallel configuration of the stator winding for a four pole three phase induction motor. Each phase of the winding has two parallel branches comprising of three series connected coils and two equalizer connections.

Figure 2.3 shows the one phase of the winding configuration used by Berman. Dorrell and Smith [21] investigated the three different possible connections of a ten pole double layer machine having ten phase bands. As a first possibility, they have considered a simple series connection winding scheme consisting of two loop currents and two driving voltages as shown in Figure 2.4(a). The second connection is that of the phase bands connected in parallel as shown in Figure 2.4(b). The third possible connection considered is a winding pattern having two adjacent phase bands connected in series to form five parallel paths. This pattern also has the option of having or not having equalizer connections as shown in Figure 2.4(c).

The development of bearingless machine is based on the idea proposed by Hermann [66] in 1973. He proposed a magnetic bearing arrangement where forces are generated by the interaction of p and $p \pm 1$ pole pair magnetic fields by using two sets of stator coil arrangements. The development of bearingless machines can be classified in two sections based on the stator coil arrangements as

(i) Development of bearingless machine using dual set of stator winding

(ii) Development of bearingless machine using single set of stator winding

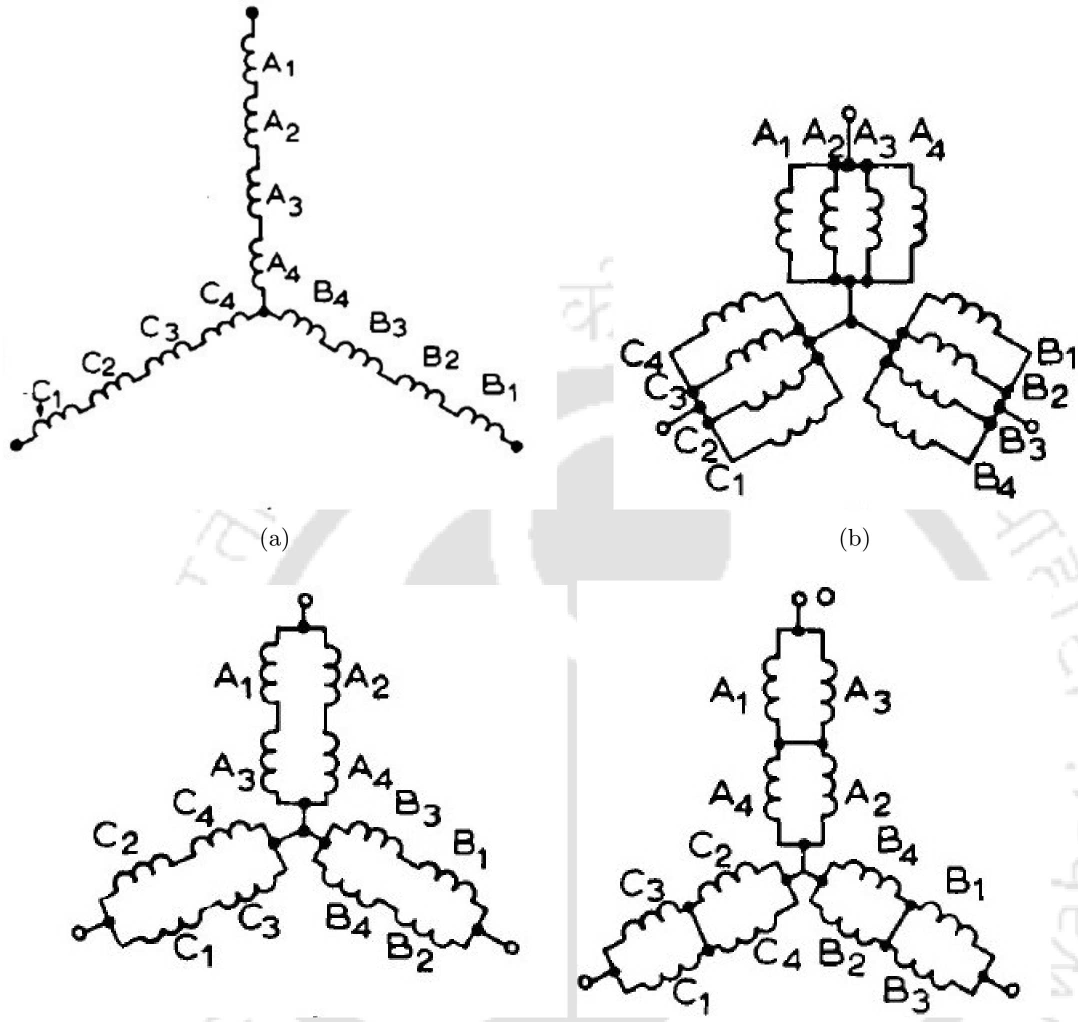

(a) (b) (c) (d)

Figure 2.2: Winding configurations used by Ellison and Yang, (a) series configuration, (b) parallel configuration, (c) combination of series and parallel configuration, (d) combination of series and parallel configuration with equalizing connection [64].

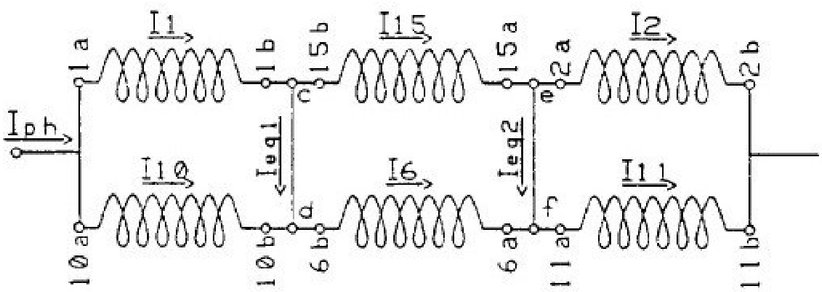

(a)

Figure 2.3: Combination of single phase of series and parallel winding configuration used by Berman [65].

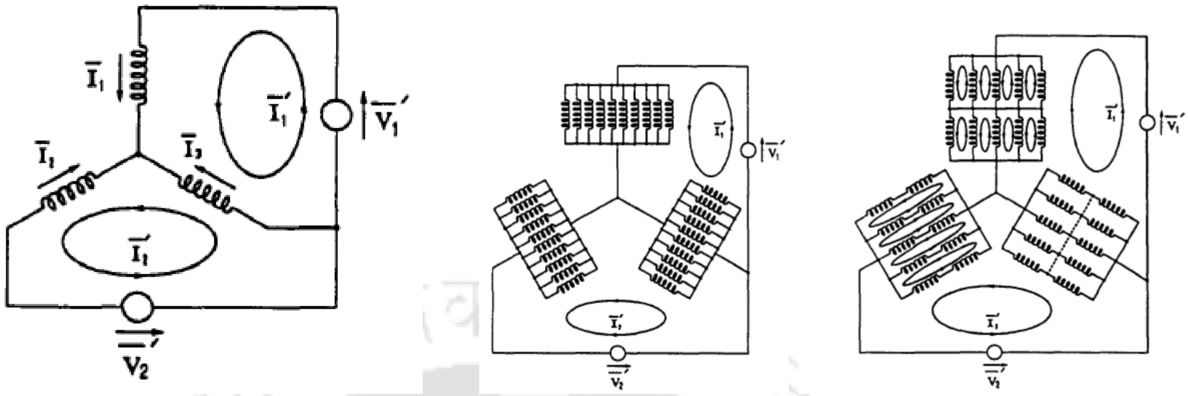

(a) (b) (c)

Figure 2.4: Winding configurations used by Dorrell and Smith, (a) series configuration, (b) parallel configuration, (c) combination of series and parallel configuration [21].

2.6.1 Dual set of stator winding

Most of the research related to bearlingless machines are related to dual set of stator winding configuration.

Figure 2.5(a) shows the magnetic field interaction in a dual set of winding machine. Here, four pole winding is the torque producing winding and two pole winding is responsible for transverse force generation. It can be observed that at the location one, four pole and two pole magnetic fields are having same direction and being added whereas at location three, they are in opposite direction and being substracted. As a result, the magnetic flux density increases at location one and decreases at location three. The increase in magnetic flux density at location one results in transverse force generation at location one. The direction of force generation can be reversed by reversing the direction of supply in two pole stator winding. Figure 2.5(b) represents circuit connection diagram for dual winding configuration. The two sets of coils are wound in the same stator slots and are supplied with two three phase inverters. Chiba et al. [4] implemented dual set of winding scheme in an induction motor. Two phases of four pole and two pole windings have been used, where four pole windng is the torque producing winding and two pole winding is the additional winding to create asymmetry in the magnetic field. A dual set of winding scheme for a cylindrical salient pole motor has been implemented by Chiba et al. [67]. The development of bearingless squirrel cage induction motor brings few additional challenges. A squirrel cage rotor can be seen as both the four pole and the two pole winding connection. The two pole suspension winding current gets induced in the rotor bar which further reduces the radial force as well as introduces a phase delay [68,69]. To deal with the problem of phase lag in radial force generation and unstable operation of radial position of the rotor, several rotor circuits have been investigated and two rotors with two pole and four pole winding has been proposed by Chiba et al. [70]. It has also been demonstrated that the best operation is achieved when the rotor has a four pole winding and the torque producing winding is a four pole winding. However, a design procedure is required for the construction of multi-phase rotor because improper design may lead to increase in secondary resistance which would result in reduction in overall efficiency of the motor [71]. Chiba and Fukao proposed an optimal design technique for the development of multi phase rotor of a bearingless machine having dual stator winding. The group of Chiba also successfully developed a bearingless induction machine having squirrel cage rotor [72,73].

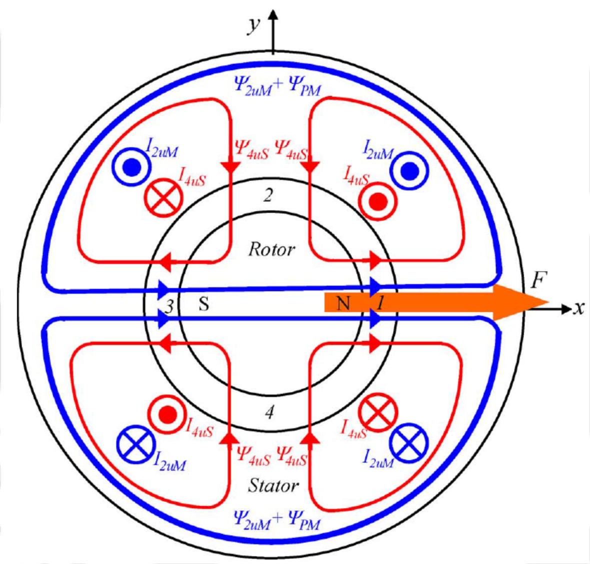

(a)

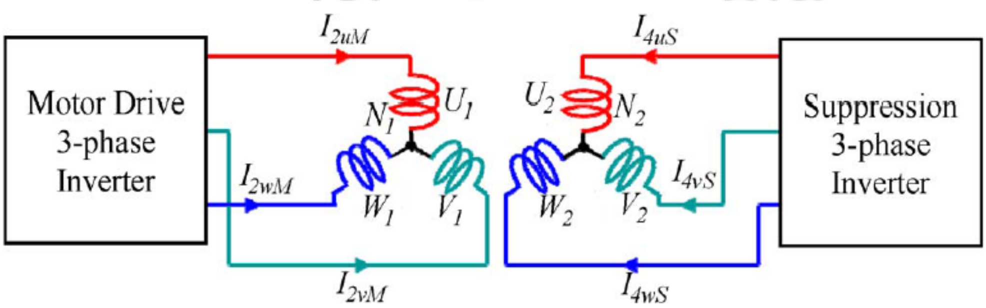

(b)

Figure 2.5: Dual set of winding scheme, (a) Interaction of four pole magnetic field and two pole magnetic field (b) Circuit diagram [74].

2.6.2 Single set of stator winding

The development of dual set of winding connections reduces the torque producing capability of an electrical machine because the same slots are shared by the auxiliary winding to produce the transverse forces. However, a single set of winding can be used for the generation of torque as well as transverse forces without changing the copper quantity in the stator slots. The recent notable works on the development of single set of winding scheme are described in [5, 6, 74–81]. These single set of winding connections can be classified into four groups,

(i) Split winding design, [75–77]

(ii) Middle point current injection design, [74]

(iii) Parallel connection design, [78, 79]

(iv) Bridge configured winding (BCW) design, [5, 6, 79–81]

Figure 2.6 shows the circuit connection of split winding bearingless machine. A three phase stator winding is converted to six phase winding by dividing into six coils meeting at a neutral point. The net resultant force is generated in these kinds of winding connection by independent unbalance current supply in all six phases of the winding by using a six phase inverter [75–77]. i_{um}, i_{vm}, i_{wm} are the main components of phase currents and i_{us}, i_{vs} and i_{ws} are the suspension currents which is used to create asymmetry in the supply.

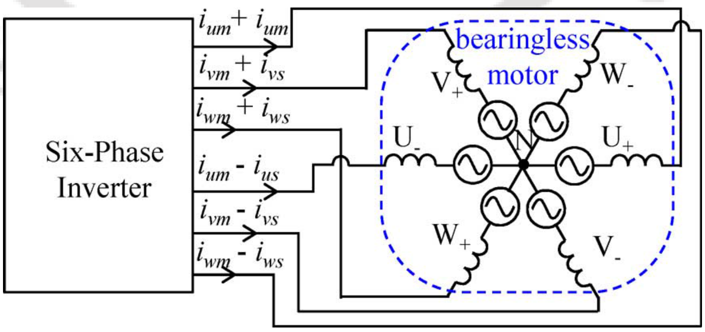

(a)

Figure 2.6: Split winding circuit diagram [78].

Figures 2.7(a) and 2.7(b) show the formation of magnetic field and circuit connection diagram of a middle point current injection winding bearingless machine. In this type of machine, six set of coils are connected in three phase sequence and each phase is consist of two coils connected in series.

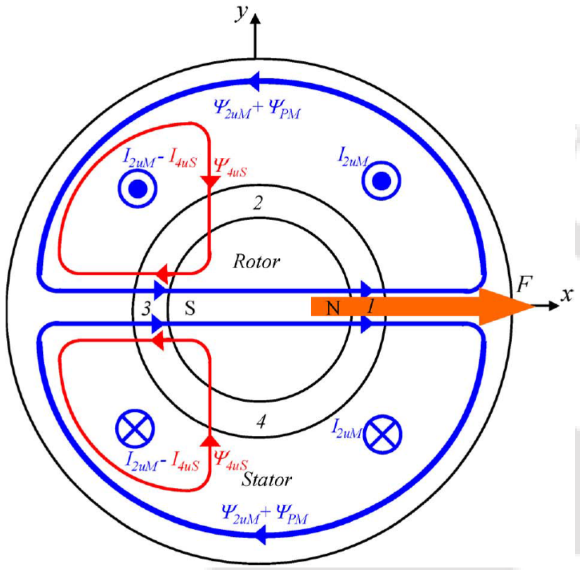

(a)

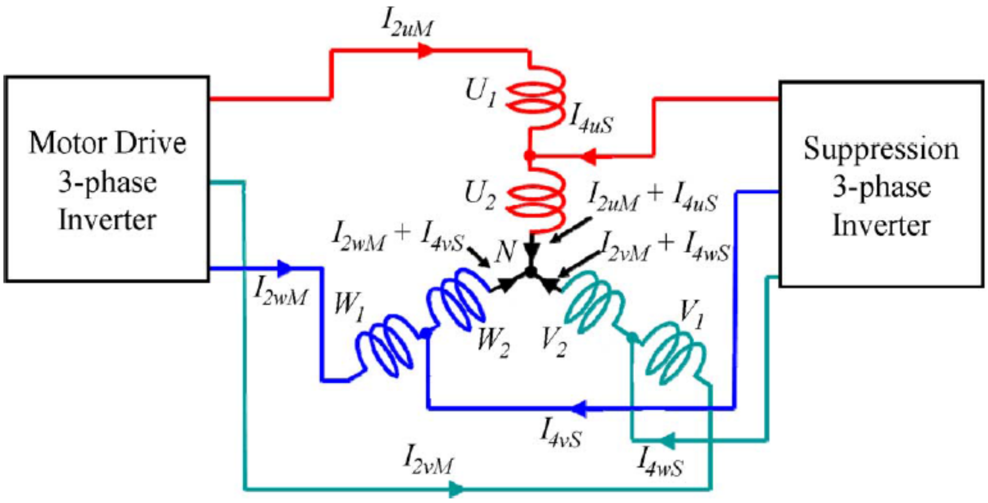

(b)

Figure 2.7: Middle point current injection winding scheme, (a) Interaction of four pole magnetic field and two pole magnetic field, (b) Circuit diagram [74].

Two inverters are used as a power supply where one inverter is used to supply motor driving current in all three phases of the winding and the other inverter connected at the middle point of the series connected coils in each phase of the winding is used to create asymmetry in the air gap which leads to generation of transverse force. Figure 2.7(a) shows the magnetic field generation with respect to these two supply sources. The machine is wound as a two pole machine, the main supply inverter create a two pole magnetic field whereas other inverter (suspension inverter) creates a four pole magnetic field in only one side of the machine. These two components of magnetic field interacts and a radial force is generated. The force direction can be reversed by reversing the current supply direction using the suspension inverter [74].

Figures 2.8(a) and 2.8(b) represent the formation of magnetic field and circuit diagram in a parallel connection winding bearingless machine. In the parallel connection bearingless machines, similar to other configuration, six coils are connected in three phase sequence, where each phase consists of two coil sets. In this configuration two sets of coils in each phases are arranged in parallel spatially. Two sets of inverters are used for the power supply where, one inverter is used for motor current and another one is used to supply suspension current. The main supply inverter is connected at the middle point of the two coil sets in each phase of the winding whereas the suspension inverter is connected at the end terminals. Figure 2.8(a) shows the formation of magnetic field with respect to these two supply sources. The motor is wound as a two pole motor, here a main supply generates a two pole magnetic field and suspension supply generates four pole magnetic field and interaction of these two magnetic fields results in transverse force generation. Similar to other configurations by reversing the sense of supply through the suspension inverter force direction can be reversed [78, 79].

Figure 2.9 represents the circuit diagram of bridge configuration winding. This winding configuration has two parallel paths. The author has exploited the advantage of the parallel path in the winding by adding an additional supply source in between. However, this additional supply source should be isolated from the main supply source. In Figure 2.9, the main supply has been termed as motor supply and bridge supply has been termed as TF (Transverse Force) supply. The main supply is used for the generation of p pole pairs of the magnetic field and the bridge supply is used for the production of $p \pm 1$ pole pairs of the magnetic field [5]. Among these winding configurations, in split and middle point current injection winding scheme a rotational MMF is induced across the suspension terminals whereas no rotational MMF is induced in the parallel winding and the bridge

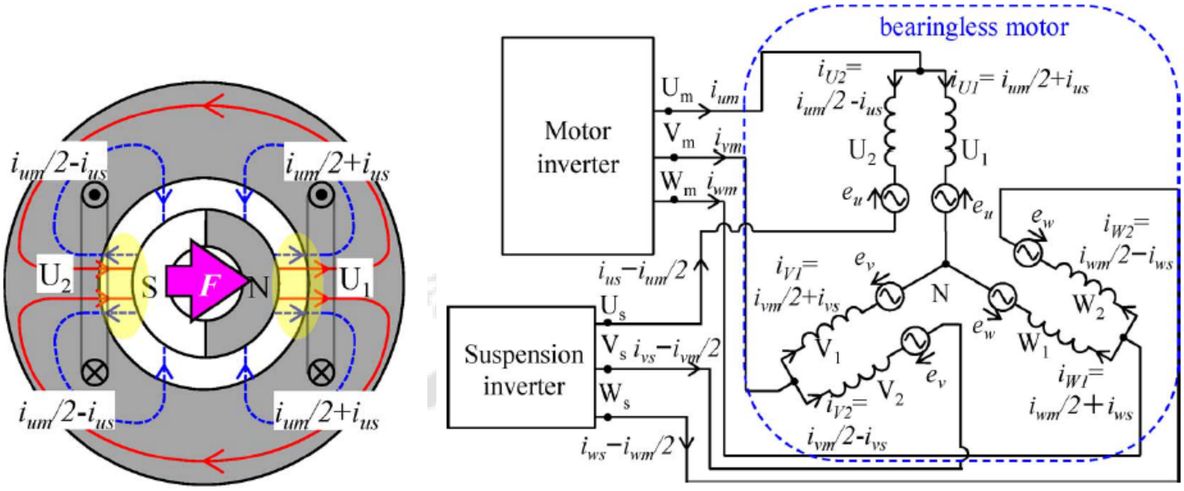

(a) (b)

Figure 2.8: Parallel connection winding scheme, (a) interaction of four pole magnetic field and two pole magnetic field, (b) circuit diagram [78].

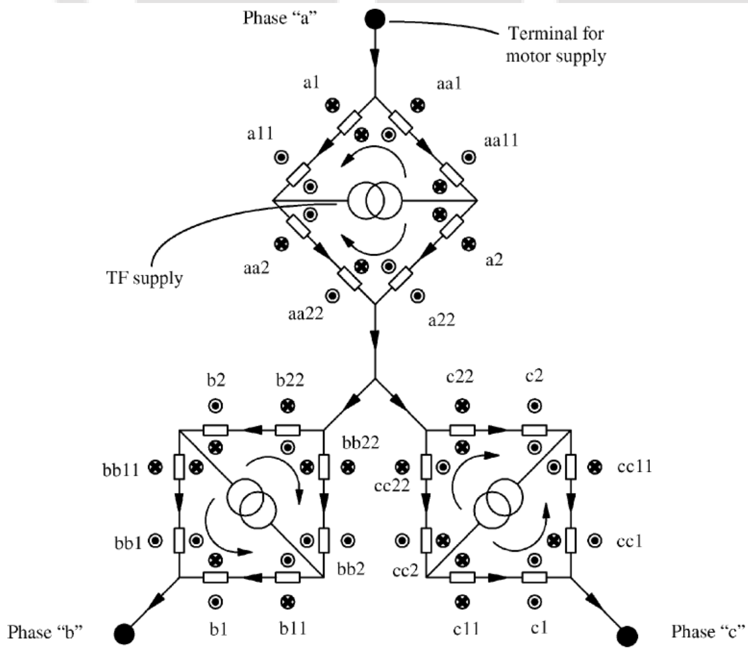

(a)

Figure 2.9: Bridge configuration winding scheme [6].

configured winding [78, 79]. This phenomena provides additional advantage to the parallel and the bridge configured winding scheme where passive vibration control is possible by simply short-circuiting the suspension terminals of the winding connections. The suspension inverter of the parallel winding connection has to carry half of the torque currents and this places bridge configured winding scheme in an advantageous position when the sense of the control requirements of these winding schemes are compared.

2.6.3 Control methods

Generally two types of control methods have been used in the literature for the vibration control or for the development of bearingless machines. The PID controller [4, 67, 68, 72, 82] which does not require any model of the system and an adaptive controller [83–88] which is a model based controller. Chiba et al. [4] developed a bearingless induction motor, where PID controller is used to generate radial force command (F). Based on the feedback measurements the error is amplified and the required force signal is generated by a PID controller as shown in Equation (2.29) .

$$F = k_p e + k_d \dot{e} + k_i \int edt \tag{2.29}$$

Here, k_p is the proportional gain, k_d is the derivative gain and k_i is the integral gain and e is the error signal. Further this force command is converted to current by using a force-current relationship. A force-current relationship is developed by the author by formulating an inductance matrix. The self inductance and the mutual inductances between the two pole and the four pole windings are measured as a function of radial displacement of the rotor. The flux linkage and current relationship can be written as shown in Equation(2.30).

$$\begin{bmatrix} \psi_a \\ \psi_b \\ \psi_\alpha \\ \psi_\beta \end{bmatrix} = \begin{bmatrix} L_4 & 0 & -M\alpha & M\beta \\ 0 & L_4 & M\beta & M\alpha \\ -M\alpha & M\beta & L_2 & 0 \\ M\beta & M\alpha & 0 & L_2 \end{bmatrix} \begin{bmatrix} i_a \\ i_b \\ i_\alpha \\ i_\beta \end{bmatrix} \tag{2.30}$$

Here, L_4 and L_2 are the self inductances of four pole and two pole winding, $M\alpha$ and $M\beta$ are the mutual inductances between four pole and two pole winding, i_a, i_b and i_α, i_β are the instantaneous currents of four pole and two pole windings respectively. The inductance matrix is used to calculate the magnetic energy (W_m) as shown in Equation (2.31) . The radial forces acting on the rotor can be calculated by differentiating magnetic energy with respect to α and β along α and β direction respectively as

$$W_m = i' \times L \times i \tag{2.31}$$

$$\begin{bmatrix} F_\alpha \\ F_\beta \end{bmatrix} = \begin{bmatrix} \frac{\partial W_m}{\partial \alpha} \\ \frac{\partial W_m}{\partial \beta} \end{bmatrix} = MI \begin{bmatrix} -\cos 2\omega t & \sin 2\omega t \\ \sin 2\omega t & \cos 2\omega t \end{bmatrix} \begin{bmatrix} i_a \\ i_\beta \end{bmatrix} \tag{2.32}$$

The similar procedure has been used by the most of the authors for the development of bearingless machines using PID controller [67, 68, 72, 82].

The PID controller doesnot suit well where disturbing forces are having multiple frequency components. For the compensation of disturbance forces which has more than one frequency components, the convergent control algorithm has been found to be very effective. The convergent control technique is a feedforward control method which can deal with the disturbance forces having multiple harmonic excitation components. Burrows and Sahinkaya [86] and Knospe et al. [87, 88] showed that convergent control algorithm can be used in a rotor system to compensate several harmonics disturbances. Tammi [83, 89] used convergent control algorithm for active vibration control of the rotor. It is established that the convergent control algorithm is more effective and simpler compared to other harmonics compensation algorithms such as adaptive FIR filter with LMS algorithm. For multiple sinusoidal signal, the convergent control law can be written as

$$U_{n+1} = \gamma U_n - \alpha g^{-1}(z_k e^{-j\omega kT}) \tag{2.33}$$

Here T is the length of the time step, ω is the frequency of the known disturbance, γ and α are two constants and z_k is the vector of measured signal. In case if there are more than one frequency component of disturbance, then the control law has to be applied in parallel.
The complex multiplier g is a matrix which gives the phase and amplitude of the output as a function of change in amplitude and phase of the control signal. For a particular frequency component ω, it can be obtained from system's transfer function G as

$$g = G(j\omega) = C(j\omega I - A)^{-1}B \tag{2.34}$$

where A, B and C are the matrices of the LTI state-space model.

Laiho et al. [84] implemented convergent control algorithm for vibration suppression in a dual winding induction motor where one set of the winding is used as an inbuilt actuator to suppress the rotor vibration. The low-order linear state space model used as an actuator is identified using finite element simulation data. Sinervo and Arkkio [85] used convergent control technique to suppress rotor vibrations occurring at multiple frequencies in a dual winding two pole induction motor where four pole winding is used as an actuator. Three vibration components are suppressed simultaneously occurring at rotor rotational frequency, magnetic field rotational frequency and double the magnetic field rotational frequency minus the rotor rotational frequency.

2.7 Summary

An exhaustive study of the literature has been carried out to understand the state of the art of UMP. It has been found that all the available analytical and numerical studies mostly revolve around the UMP generation due to the eccentricity present in the machine. Analytical model can calculate UMP very quickly and provide an approximate idea about its magnitude, but it cannot take account of the magnetic saturation, skew effect, effect of slots etc.

There are few studies related to the study of UMP in electrical machine having parallel paths in its stator winding. However, the generation of additional pulsating force in electrical machine having parallel paths in its stator winding requires further investigation.

Several authors have addressed the coupled modelling of magnetic field and electric circuit equations. A few of them have also addressed the coupled modelling of magnetic field, electric circuit and rotordynamics equations. However, in these coupled models, either the bridge configured winding is not addressed or a low dimensional electromagnetic model have been used. So, there is strong need to develop a coupled magnetic field, electric circuit and rotordynamics model for bridge configured winding induction machine with a detailed electrodynamic model.

It has been found that mostly dual set of winding scheme has been used for the development of bearingless machines. However, single set of winding scheme specially bridge configured winding scheme brings additional advantage in terms of controllable transverse force generation. This leads to the requirement of a detailed study of bridge configured winding scheme such that the behaviour of this winding machine can be established in different conditions.

It is also important to develop an analytical model of UMP, generated due to the eccentricity and due to the input bridge currents for a bridge configured induction machine before a detailed numerical study is carried out.

3

Effect of Eccentricity on Magnetic Field

Contents

3.1 Introduction

Bearing faults and eccentricity faults are among the generally available faults which lead to unbalanced magnetic pull generation in an electric machine. An asymmetric air gap magnetic field generates UMP in an electrical machine. There can be many reasons of asymmetry in the air gap magnetic field. In this chapter the asymmetry in the air gap magnetic field due to eccentric rotor case has been analysed.

In the literature it has been shown analytically that in a series winding 2 pole motor, static eccentric position of a rotor generates a magnetic field of f_s Hz, where f_s is the stator coil excitation frequency. In the case of dynamic eccentricity condition an eccentric rotor generates a magnetic field of f_r Hz, where f_r is the rotor whirling frequency [7]. It has also been shown that in a 2 pole series winding motor a pulsating component of UMP is generated along with the constant component of UMP. The pulsating component of UMP arises due to the presence of homopolar flux. However, in a 4 pole series winding connection motor a constant pull acts along the shortest air gap [90]. The effect of parallel path on UMP generation has been studied by few authors mainly by the group of Dorell and Arkkio [21, 50, 90–92]. It has been demonstrated that parallel paths of the winding shifts the direction of the UMP from the shortest air gap direction. In addition, a pulsating force of double supply frequency is generated in a parallel winding and statically eccentric rotor motor. Later, Smith and Dorrell showed analytically that in a statically eccentric rotor, a constant component of UMP is generated due to the interaction of the p and $p \pm 1$ pole pairs of the magnetic field, where p and $p \pm 1$ components of the magnetic field revolves in the same direction and a pulsating component of UMP generates due to the interaction of p and $p \pm 1$ pole pairs of the magnetic field, which revolves in the opposite direction [50]. The generation of the constant and pulsating components of the UMP in a statically eccentric rotor has also been verified by "Dorrell and Smith" through experimental results [92]. Finite Element (FE) analysis of UMP in parallel stator winding connection has been carried out to show the effectiveness of the parallel paths in passive suppression of UMP [90]. It has been shown that due to the presence of static eccentricity a pulsating force of double supply frequency acts on the rotor. Recently, various studies have been carried out to study the effect of different eccentricity conditions in electric motor [43, 46, 53, 93–95]. However, no numerical as well as experimental analysis of eccentricity generated pulsating magnetic field has been carried out to investigate the additional force components in different types of eccentricity conditions. A parallel stator winding helps in passive suppression of UMP. In general, due to the eccentric position of the rotor, the inductance of the parallel paths of the stator winding changes. It results in change in impedance of the parallel path of the stator winding, due to which a potential difference occurs across these parallel paths and a circulating current flows through the parallel paths of the winding which reduces UMP to some extent. Among parallel winding configurations the bridge configured winding is more effective because upon short circuiting the bridge points of the parallel path the potential difference across the parallel path vanishes which leads to effective passive suppression of UMP.

The main objective of this chapter is to analyse the reason behind the generation of additional pulsating component of UMP in a parallel winding electrical machine. For this purpose a comparative study of series and parallel winding electrical machines has been carried in different eccentricity conditions. The behaviour of the air gap magnetic field has been studied to establish the reason behind the generation of the additional component of the UMP. Based on the study additional component of the magnetic field harmonics has been used to derive the force expression for the case of parallel stator winding electrical machine. Also the passive vibration suppression capability of bridge configured winding has been analysed with respect to air gap magnetic field generation.

3.2 Description of series and parallel winding connection

An induction machine with 36 slots have been chosen for the study of effect of eccentricity. In order to compare and investigate the behaviour of the machine, this machine has been simulated using a series and parallel winding configurations. For the series winding connection a single layer and for the parallel winding connection a double layer bridge configured winding scheme have been selected. Figure 3.1(a) and Figure 3.1(b) represent the winding layout of the series winding connection and the parallel winding connection respectively. Figure 3.1(c) and Figure 3.1(d) represent the circuit connection of the series winding connection and the parallel winding connection respectively, whereas Figure 3.1(e) represents the circuit connection of the bridge configured winding (BCW) scheme. The difference between any normal parallel winding scheme and the BCW scheme is that the half of the coil of the parallel side is interchanged. It can be observed in Figure 3.1(e) that the parallel sides of phase A coils $a_4 - a_6$ has been interchanged with coils $aa_4 - aa_6$ as compared to their location in Figure 3.1(d). Similarly, parallel sides of phase B coils $b_4 - b_6$ has been interchanged with coils $bb_4 - bb_6$ and parallel sides of phase C coils $c_4 - c_6$ has been interchanged with coils $cc_4 - cc_6$. When points

$A_1 - A_2, B_1 - B_2$ and $C_1 - C_2$ of Figure 3.1(e) are not connected, it is called bridge OFF condition and when points $A_1 - A_2, B_1 - B_2$ and $C_1 - C_2$ are connected with each other, it is called bridge ON condition. Also, an additional supply source can be added in between these points. This has been addressed in the later chapters. Hereafter, in this chapter, the bridge configured winding in bridge OFF condition has been referred as parallel stator winding.

3.3 Basics of force calculation

Analytical expressions of the eccentricity generated magnetic field in the air gap and the lateral forces due to its interactions have been derived in [7,17,18]. These expressions have been derived for the static and the dynamic eccentricity conditions. The mixed eccentricity condition can be expressed as combination of the static and the dynamic eccentricity conditions. Neglecting the higher harmonic components of the magnetic field, the magnetic field expressions for the static, dynamic and mixed eccentricity conditions can be written as shown in Equations (3.1), (3.2) and (3.3) respectively as,

$$\mathbf{b}_{\mathbf{static}} = \frac{\mu_o A_m r}{p\delta}\cos\left(p\theta - 2\pi f_s t - \phi_m\right) + \frac{\mu_o \varepsilon_s r A_m}{2p\delta}\cos\left(\left(p \pm 1\right)\theta - 2\pi f_s t - \left(\phi_m \pm \phi_s\right)\right) \tag{3.1}$$

$$\mathbf{b}_{\mathbf{dynamic}} = \frac{\mu_o A_m r}{p\delta}\cos\left(p\theta - 2\pi f_s t - \phi_m\right) + \frac{\mu_o \varepsilon_d r A_m}{2p\delta}\cos\left(\left(p \pm 1\right)\theta - 2\pi\left(f_s \pm f_r\right)t - \left(\phi_m \pm \phi_d\right)\right) \tag{3.2}$$

$$\begin{aligned}\mathbf{b}_{\mathbf{mixed}} = \frac{\mu_o A_m r}{p\delta}\cos\left(p\theta - 2\pi f_s t - \phi_m\right) &+ \frac{\mu_o \varepsilon_s r A_m}{2p\delta}\cos\left(\left(p \pm 1\right)\theta - 2\pi f_s t - \left(\phi_m \pm \phi_s\right)\right) \\ &+ \frac{\mu_o \varepsilon_d r A_m}{2p\delta}\cos\left(\left(p \pm 1\right)\theta - 2\pi\left(f_s \pm f_r\right)t - \left(\phi_m \pm \phi_d\right)\right)\end{aligned} \tag{3.3}$$

where f_s is the stator excitation frequency, ϕ_s is the eccentricity angle in static eccentricity condition, ϕ_d is the eccentricity angle at $t = 0$ s in dynamic eccentricity condition, f_r is the rotor rotational frequency, ϵ_s is the static eccentricity, ϵ_d is the dynamic eccentricity, μ_0 is the permeability of the free space, A_m is the amplitude of the main supply current density, p is the pole pair of the main supply fundamental field, ϕ_m is the phase angle of the main supply, r is the rotor radius and δ is the mean air gap length. It can be observed from the magnetic field equations that the air gap magnetic field of the statically eccentric rotor has p, $p-1$ and $p+1$ pole pair magnetic field, which has the same frequency

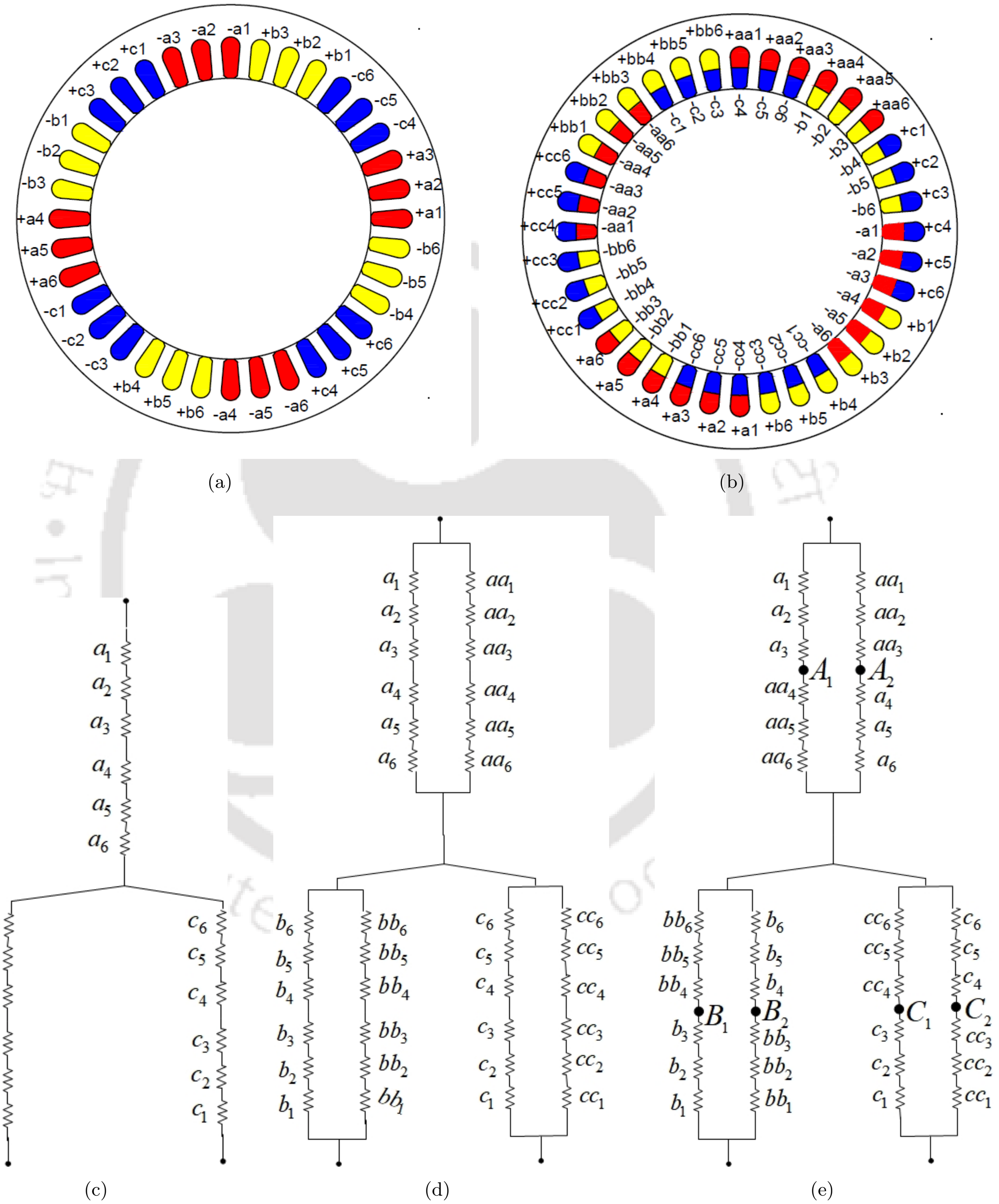

Figure 3.1: Series and parallel winding configuration (a) Series winding; (b) Parallel winding; (c) Series winding circuit; (d) Normal parallel winding circuit; (e) BCW parallel winding circuit.

component as that of the stator supply frequency f_s. The air gap magnetic field of the dynamically eccentric rotor has p, $p-1$ and $p+1$ pole pair magnetic field which has the frequency component of f_s, $f_s - f_r$ and $f_s + f_r$ respectively. The air gap magnetic field in the mixed eccentric rotor condition has p pole pair magnetic field of frequency f_s , $p-1$ pole pair magnetic field of frequency f_s, $f_s - f_r$ and $p+1$ pole pair magnetic field of frequency f_s and $f_s + f_r$. Lateral force acting on the rotor along x-axis for different eccentricity conditions can be calculated using the Maxwell equations by substituting magnetic field expressions in Equation (3.4) for different eccentricity conditions. F_{ss_x}, F_{sd_x} and F_{sm_x} represent the forces acting along x axis in static, dynamic and mixed eccentricity conditions respectively.

$$F_x = rl \int_0^{2\pi} \frac{b^2(\theta,t)}{2\mu_0} \cos(\theta) \tag{3.4}$$

$$F_{ss\_x} = \frac{\mu_0 A_m^2 r^2 l \varepsilon}{4p^2\delta^2} \cos(\phi_s) \tag{3.5}$$

$$F_{sd\_x} = \frac{\mu_0 A_m^2 r^2 l \varepsilon_d}{4p^2\delta^2} \cos(2\pi f_r t + \phi_d) \tag{3.6}$$

$$F_{sm\_x} = \frac{\mu_0 A_m^2 r^2 l \varepsilon_s}{4p^2\delta^2} \cos(\phi_s) + \frac{\mu_0 A_m^2 r^2 l \varepsilon_d}{4p^2\delta^2} \cos(2\pi f_r t + \phi_s) \tag{3.7}$$

Similarly, lateral forces acting on the rotor along y-axis for different eccentricity conditions can be calculated by substituting the magnetic field expression for different eccentricity conditions in Equation (3.8)

$$F_y = rl \int_0^{2\pi} \frac{b^2(\theta,t)}{2\mu_0} \sin(\theta) \tag{3.8}$$

$$F_{ss\_y} = \frac{\mu_0 A_m^2 r^2 l \varepsilon_s}{4p^2\delta^2} \sin(\phi_s) \tag{3.9}$$

$$F_{sd\_y} = \frac{\mu_0 A_m^2 r^2 l \varepsilon_d}{4p^2\delta^2} \sin(2\pi f_r t + \phi_d) \tag{3.10}$$

$$F_{sm\_y} = \frac{\mu_0 A_m^2 r^2 l \varepsilon_s}{4p^2\delta^2} \sin(\phi_s) + \frac{\mu_0 A_m^2 r^2 l \varepsilon_d}{4p^2\delta^2} \sin(2\pi f_r t + \phi_d) \tag{3.11}$$

where F_{ss_y}, F_{sd_y} and F_{sm_y} represent the forces acting along y axis in static, dynamic and mixed eccentricity conditions respectively.

3.4 Numerical simulation of series and parallel stator winding electrical machines

A 2D FE model of a 3.7 kW four pole induction motor having 36 stator slots and with a solid rotor has been modeled for a series and a parallel stator winding connections in COMSOL MULTIPHYSICS® to study the effects of different eccentricity conditions on the air gap magnetic field harmonics and lateral forces acting on the rotor. A solid rotor has been considered for the modelling of the rotor to avoid the rotor bar effects. Triangular elements have been chosen for the discretization of the geometry of the series and the parallel stator winding motor. 52664 triangular elements, 9056 edge elements and 356 vertex elements have been used for the series winding motor whereas 54512 triangular elements, 9236 edge elements and 356 vertex elements have been used for the parallel stator winding motor. Figure 3.2 represents mesh of a 2-D FE model of 36 slot induction motor used in the simulation. Table 3.1 represents the specifications of the machine considered for the numerical modelling. Table 3.1 also represents the specifications of the experimental setup used to verify the numerical model.

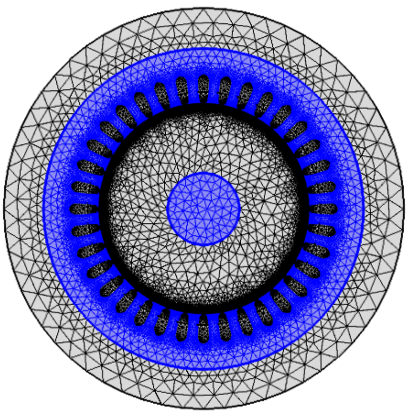

Figure 3.2: Mesh of a 2-D FE model of a 36 slot Induction Machine

3.4.1 Numerical investigation of forces acting on the rotor

The forces acting on the rotor has been calculated for three different eccentricity conditions in the series as well as the parallel stator winding connections. The stator winding excitation frequency (f_s) is 50 Hz and the rotor rotational frequency (f_r) is 25 Hz. Figure 3.3 represents the comparison

Table 3.1: Electrical machine parameters

Numerical Simulation Parameters		
Parameters	Series Winding	Parallel Winding
Connection	Star	Star
Supply Voltage	380 V, 50 Hz	380 V, 50 Hz
Layer	Single Layer	Double Layer
Per Phase DC Resistance	6.8 Ohm	6.8 Ohm
Stator Inner Radius	52.5 mm	52.5 mm
Rotor Outer Radius	51.5 mm	51.5 mm
Static Eccentricity	1/8 mm	1/8 mm
Dynamic Eccentricity	1/8 mm	1/8 mm
Mixed Eccentricity	1/8 mm + 1/8 mm	1/8 mm + 1/8 mm
Rotor speed	25 Hz	25 Hz
Experimental Setup Specifications		
Parameters	Motor I	Motor II
Power	3.7 kW	37 kW
Stator Slots	36	60
Connection	Star	Star
Supply Voltage	240 V, 50 Hz	240 V, 50 Hz
Rotor Bar	26	32
Operating Condition	No load	No load
Air Gap Length	0.5 mm	1.25 mm

of full spectrum FFT of the forces acting on the rotor in the series stator winding connection in all the three eccentricity conditions. It can be observed from Figure 3.3 that in the series stator winding connection motor, in the static eccentricity condition the developed force has a DC component (0 Hz), in the dynamic eccentricity condition the developed force has a 25 Hz (f_r) component, which is the whirling frequency of the rotor, in the mixed eccentricity condition the developed force has the combination of the DC component along with the whirling component 25Hz (f_r) . Figure 3.4 represents the comparison of full spectrum FFT of the forces acting on the rotor in the parallel stator winding connection in all the three eccentricity conditions. It can also be seen in Figure 3.4 that in all the eccentricity conditions, the parallel stator winding connection machine generates an additional frequency component of the force in comparison to the series stator winding connection machine. Additional force components at 100 Hz ($2f_s$), and 125 Hz ($2f_s + f_r$) are generated in the static and the dynamic eccentricity conditions respectively. In the mixed eccentricity condition both of the additional components of force of the static and the dynamic eccentricity are present. The analytical force expressions obtained in Equations (3.5) - (3.7) and (3.9) - (3.11) do not remain valid

Table 3.2: Comparison of the frequency components of force

	Series Winding	Parallel Winding	Analytical Expression
Static Eccentricity	0 Hz	0 Hz, 100 Hz ($2f_s$)	0 Hz
Dynamic Eccnetricity	25 Hz (f_r)	25 Hz (f_r) , 125 Hz ($2f_s + f_r$)	f_r (25 Hz)
Mixed Eccentricity	0 Hz, 25 Hz (f_r)	0 Hz, 25 Hz (f_r), 100 Hz ($2f_s$), 125 Hz ($2f_s + f_r$)	0 Hz, f_r (25 Hz)

for the case of the parallel stator winding motor because it doesn't give all the frequency components of the force obtained through the numerical simulation as shown in Figure 3.4. This happens because magnetic field expressions obtained in Equations (3.1) - (3.3) does not predict all the components of the magnetic field in the case of parallel stator winding connection. Table 3.2 represents the comparison of all the frequency components in the force obtained in different eccentricity conditions in series stator winding, parallel stator winding and from the analytical expression. The air gap magnetic field of the machine with eccentric rotor has been investigated further to know the reason behind this additional force component in case of parallel stator winding. The investigation of the air gap magnetic field has been carried out in section 3.4.2.

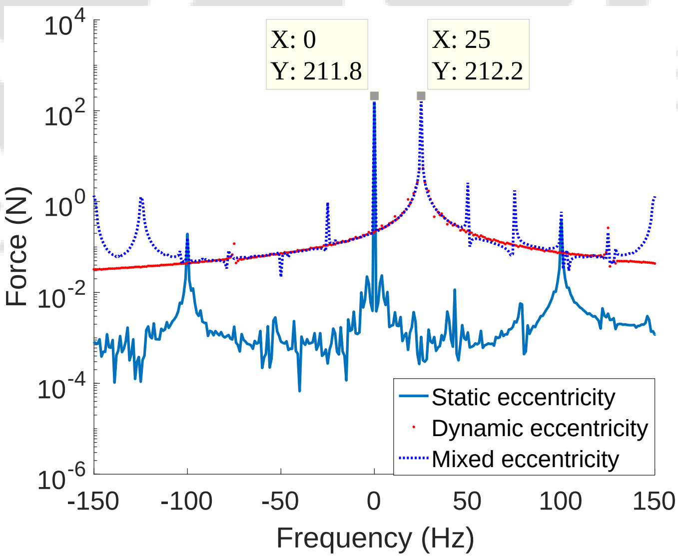

Figure 3.3: Comparison of FFT of forces acting on the rotor in series winding motor in different eccentricity condition.

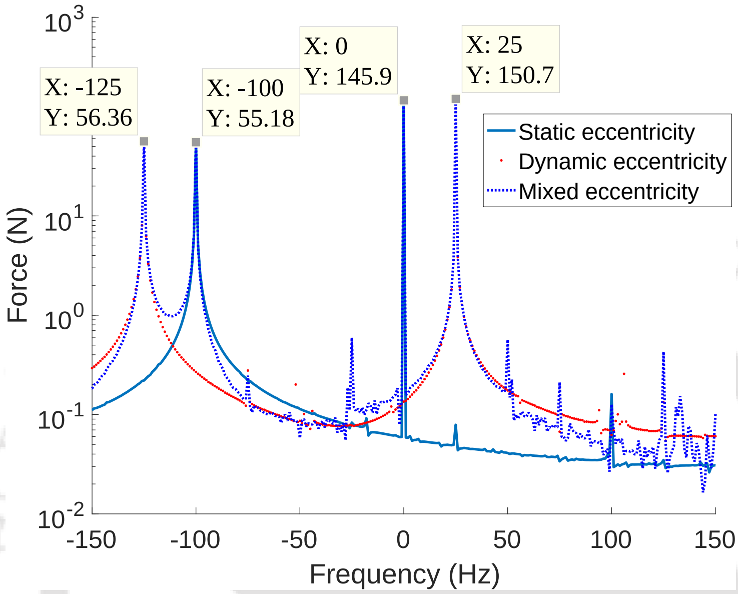

Figure 3.4: Comparison of FFT of forces acting on the rotor in BCW winding motor in different eccentricity conditions when bridges are in OFF condition.

Table 3.3: Comparison of frequency components of the magnetic field

	Series Winding	Parallel Winding	Analytical Expression
Static Eccentricity	50 Hz (f_s)	50 Hz (f_s)	50 Hz (f_s)
Dynamic Eccnetricity	25 Hz ($f_s - f_r$), 50 Hz (f_s), 75 Hz ($f_s + f_r$)	25 Hz ($f_s - f_r$), 50 Hz (f_s), 75 Hz ($f_s + f_r$)	25 Hz ($f_s - f_r$), 50 Hz (f_s), 75 Hz ($f_s + f_r$)
Mixed Eccentricity	25 Hz ($f_s - f_r$), 50 Hz (f_s), 75 Hz ($f_s + f_r$)	25 Hz ($f_s - f_r$), 50 Hz (f_s), 75 Hz ($f_s + f_r$)	25 Hz ($f_s - f_r$), 50 Hz (f_s), 75 Hz ($f_s + f_r$)

3.4.2 Investigation of air gap magnetic field

The investigation of the air gap magnetic field has been carried out in both of the winding connections motor to find out the presence of different components of the magnetic field. The eccentric position of the rotor modulates the magnetic field and generates different harmonic fields in the air gap.

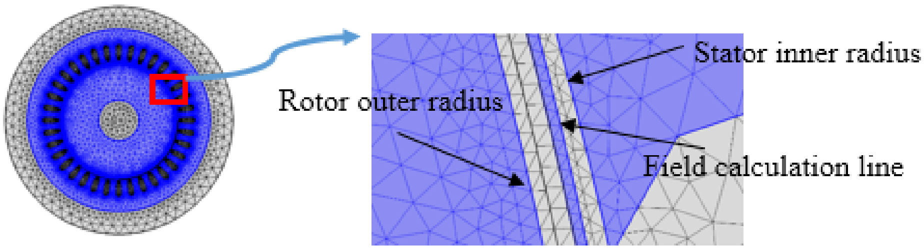

Figure 3.5: Magnetic field calculation line in the air gap.

The air gap of the machine has been divided in four bands to get a uniform meshing. The radial component of the magnetic field in the air gap has been calculated at 2^{10} (1024) nodes along a circle of radius 52.25 mm, shown in Figure 3.5 at each instant of time as

$$\mathbf{B_r} = B_x(\theta, t)\cos(\theta) + B_y(\theta, t)\sin(\theta) \tag{3.12}$$

where B_x and B_y are the components of the magnetic field along x and y direction at the respective nodes. Once the radial magnetic field is calculated at 1024 nodes at each instant of time, the temporal variation and the spatial distribution of the radial magnetic field can be obtained with respect to time. First, the temporal FFT of the radial magnetic field variation at a point (52.25, 0) has been carried out in both of the winding connections with all the eccentricity conditions to see the presence of the frequency component of the magnetic field. Figures 3.6 and 3.7 represent the comparison of the FFT of the magnetic field variation at a point in the case of the series and parallel stator winding connections in different eccentricity conditions respectively. It can be observed that in both of the winding connections, in the static eccentricity condition the air gap magnetic field has only fundamental component of the magnetic field i.e. 50 Hz, whereas in the case of the dynamic as well as the mixed eccentricity conditions, the eccentricity induces a 25 Hz and a 75 Hz components in both, the series as well as parallel connections. The temporal investigation of the magnetic field does not provide

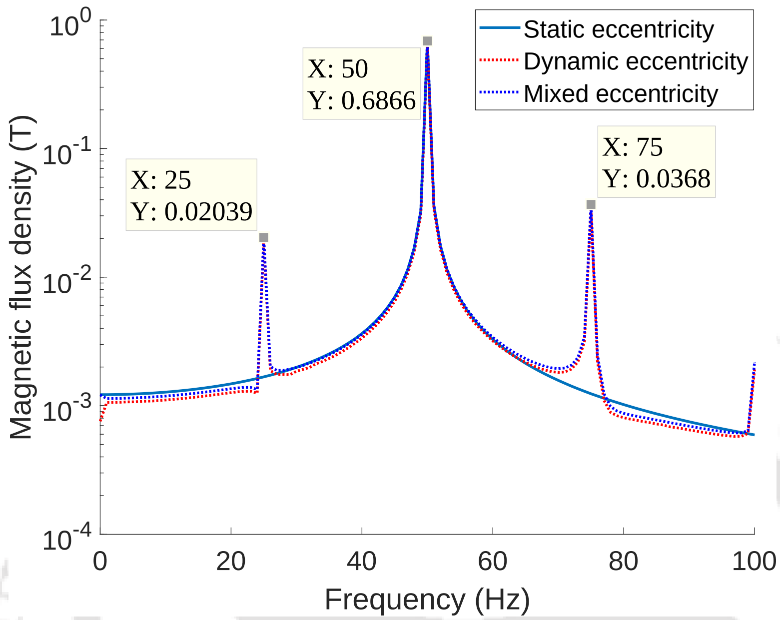

Figure 3.6: Comparison of temporal FFT of the magnetic field at a point in the air gap in series winding machine.

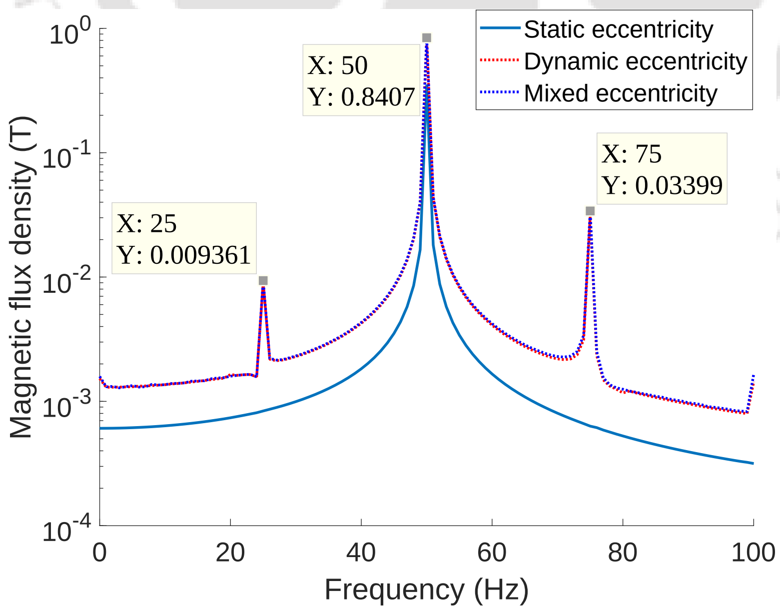

Figure 3.7: Comparison of temporal FFT of the magnetic field at a point in the air gap in BCW winding machine when bridges are in OFF condition.

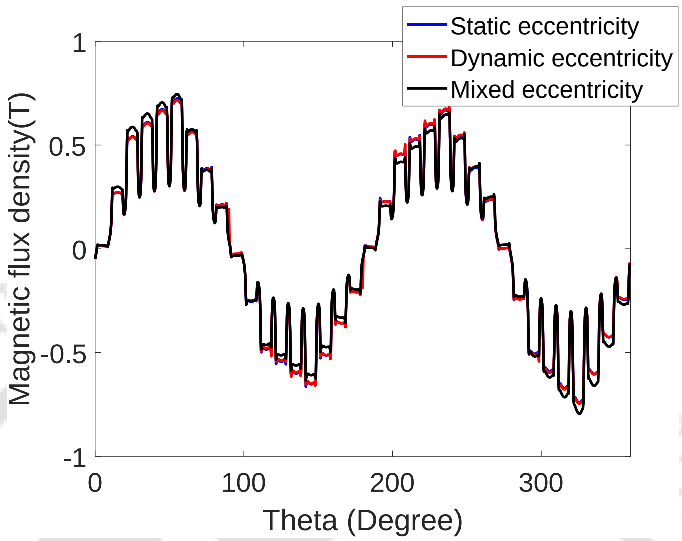

Figure 3.8: Magnetic field distribution in the air gap with series winding connection in different eccentricity condition at a simulation time of 1 s.

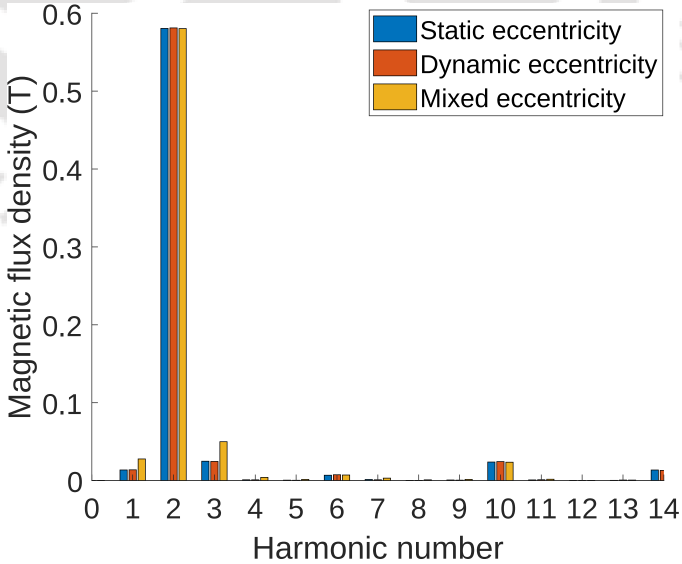

Figure 3.9: Spatial FFT of the magnetic field in the air gap with series winding connection in different eccentricity condition at a simulation time of 1 s.

any information of the presence of any extra frequency component of the force in the parallel stator winding machine because both of the machine show the presence of same frequency components of the magnetic field. Table 3.3 compares the presence of all the frequency components in series and parallel stator winding connection obtained through temporal FFT with analytically obtained magnetic field frequency. It requires further investigation to find out the presence of additional components of the magnetic field. So, for further investigation the spatial distribution of the magnetic field has been studied. The amplitude and phase of the spatial distribution of the fundamental as well as eccentricity induced components of the magnetic field has been investigated.

Figure 3.8 represents the comparison of the spatial distribution of the air gap magnetic field at a particular instant of time in the series stator winding connection in different eccentricity conditions. The spatial FFT has been carried out to see the presence of the harmonic components of the magnetic field. Figure 3.9 represents the harmonic components present in the air gap magnetic field shown in Figure 3.8 . It can be observed that the one pole pair, the two pole pair and the three pole pair magnetic fields are present in the air gap for all the eccentricity conditions. Similar to the series winding connection, the FFT of the spatial distribution of the magnetic field of parallel stator winding has also been carried out. The spatial FFT has been carried out at each instant of time and the amplitude and the phase of the two pole, the four pole and the six pole magnetic field components have been extracted to investigate the behavior of these harmonic components with time in different eccentricity conditions.

3.4.2.1 Static eccentricity

Figure 3.10 represents the variation in the amplitude and the phase of the four pole, the two pole and the six pole magnetic fields with respect to time for the case of the series stator winding connection when the rotor is statically eccentric. It can be observed from Figure 3.10 that the amplitude of the four pole field, the two pole field and the six pole field becomes constant after some time. The phase plots show that the four pole magnetic field, the two pole magnetic field and the six pole magnetic field makes five rotations in 0.1 second, which says that the frequency of rotation of the four pole magnetic field, the two pole magnetic field and the six pole magnetic field is 50 Hz. The same can be observed from the FFT of the magnetic field variation at a point, which shows the presence of a frequency component of 50 Hz as shown in Figure 3.6. The obtained frequency component of these harmonic fields are in line with the analytical expression as shown in Equation (3.1).

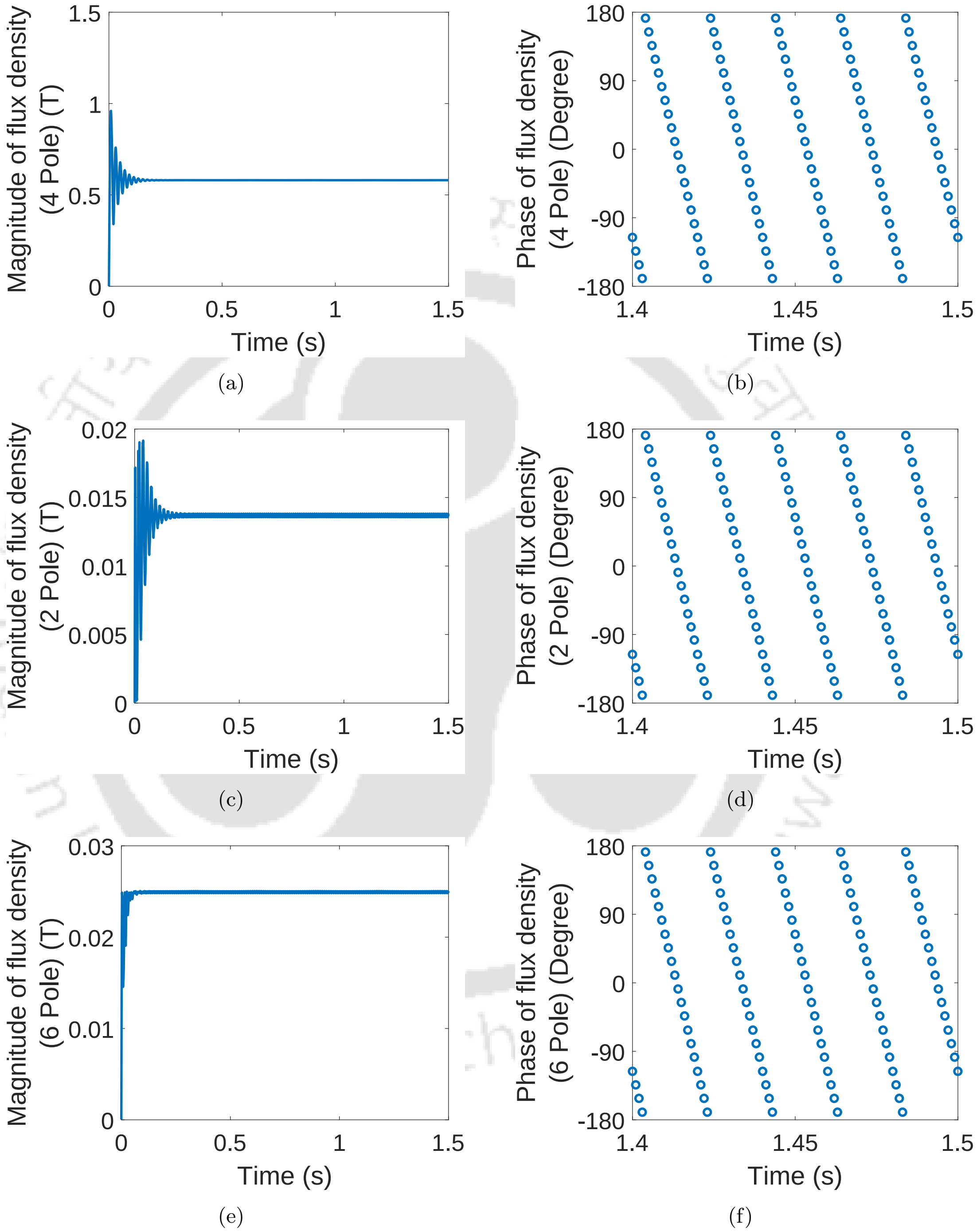

Figure 3.10: Induction motor with series winding when rotor is statically eccentric (a) variation in amplitude of the four pole magnetic field with time (b) variation in phase of the four pole magnetic field with time (c) variation in amplitude of the two pole magnetic field with time (d) variation in phase of the two pole magnetic field with time (e) variation in amplitude of the six pole magnetic field with time (f) variation in phase of the six pole magnetic field with time.

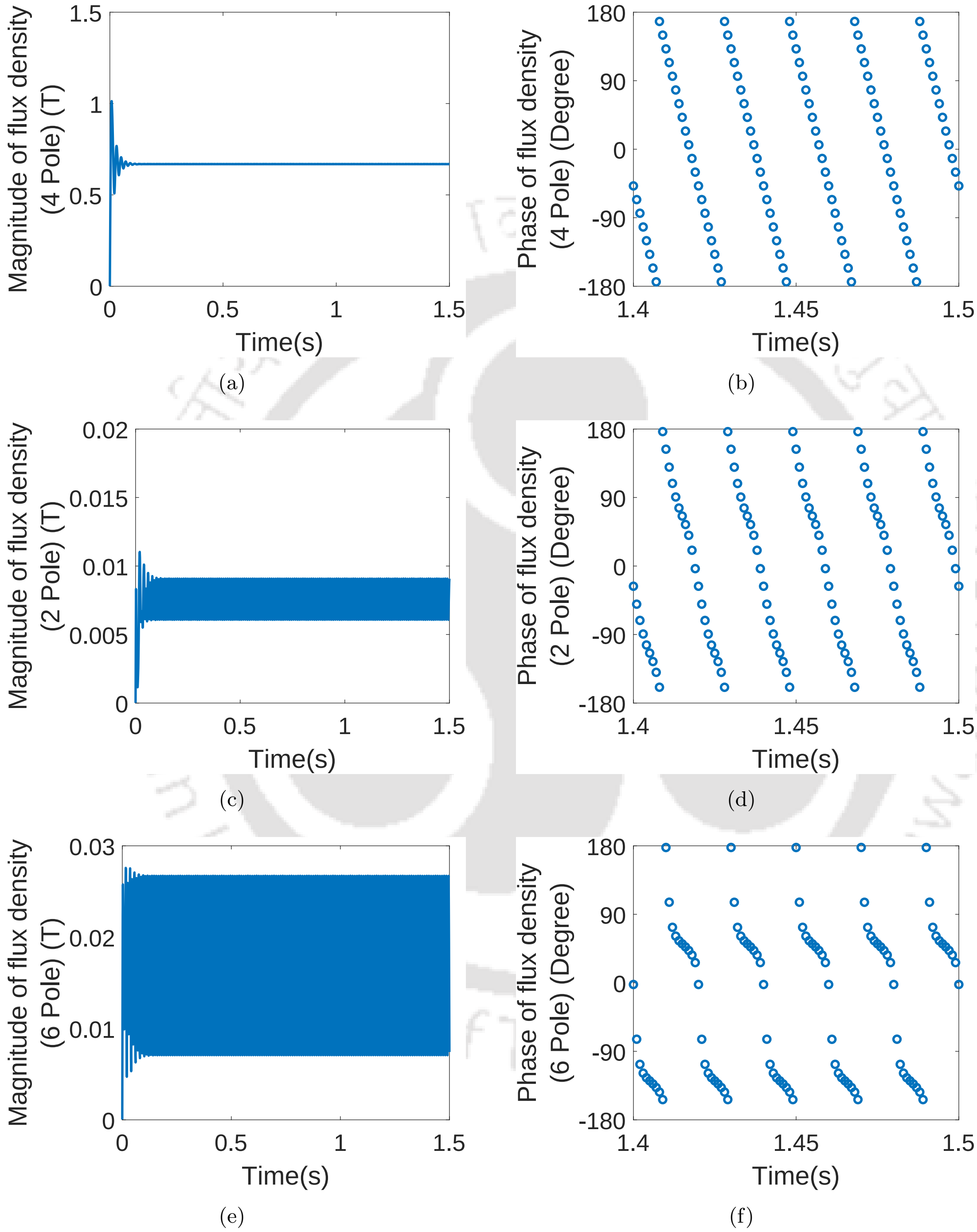

Figure 3.11: Induction motor with BCW winding when rotor is statically eccentric and bridge is OFF (a) variation in amplitude of the four pole magnetic field with time (b) variation in phase of the four pole magnetic field with time (c) variation in amplitude of the two pole magnetic field with time (d) variation in phase of the two pole magnetic field with time (e) variation in amplitude of the six pole magnetic field with time (f) variation in phase of the six pole magnetic field with time.

Figure 3.11 represents the variation in the amplitude and the phase of the four pole, the two pole and the six pole magnetic fields with respect to time for the case of the parallel stator winding connection when the rotor is statically eccentric. It can be observed from Figure 3.11 that the amplitude of the four pole magnetic field becomes constant after some time, however the two pole magnetic field amplitude has small variations with time and the six pole magnetic field amplitude has higher variations with respect to time. The phase plots show that the four pole magnetic field, the two pole magnetic field and the six pole magnetic field makes five rotations in 0.1 second, which says that the frequency of rotation of the four pole magnetic field, the two pole magnetic field and the six pole magnetic field is 50 Hz. The same can be observed from the FFT of the magnetic field variation at a point, which shows the presence of a frequency component of 50 Hz as shown in Figure 3.7. However a small perturbation in the two pole magnetic field phase and a considerable perturbation in the six - pole magnetic field can be observed. This perturbation in the phase of the six pole magnetic field can be seen as the presence of a pulsating component of magnetic field of 50 Hz along with a rotational component of 50 Hz. So, to accommodate this pulsating component of the six pole magnetic field, the magnetic field equation in Equation (3.1) should be modified.

3.4.2.2 Dynamic eccentricity

Figure 3.12 represents the variation in the amplitude and phase of the four pole, two pole and six pole magnetic fields with respect to time for the case of the series stator winding connection when the rotor is dynamically eccentric. It can be observed from Figure 3.12 that the amplitude of the four pole magnetic field becomes constant after sometime, however the two pole magnetic field and six pole magnetic field show small variation in the amplitude with respect to time. The phase plots show that the four pole magnetic field makes ten rotation in 0.2 second, which indicates that the four pole magnetic field rotational frequency is 50 Hz, the two pole magnetic field makes five rotations in 0.2 second which says that the two pole magnetic field rotational frequency is 25 Hz, and the six pole magnetic field makes fifteen rotations in 0.2 second, which says that the six pole magnetic field rotational frequency is 75 Hz. The same can be observed from the FFT of the magnetic field variation at a point, which shows the presence of three frequency components 25Hz, 50 Hz and 75 Hz as shown in Figure 3.6. The obtained frequency components of these harmonic fields are in line with the analytical expression as shown in Equation (3.12).

Figure 3.13 represents the variation in the amplitude and the phase of the four pole, the two pole

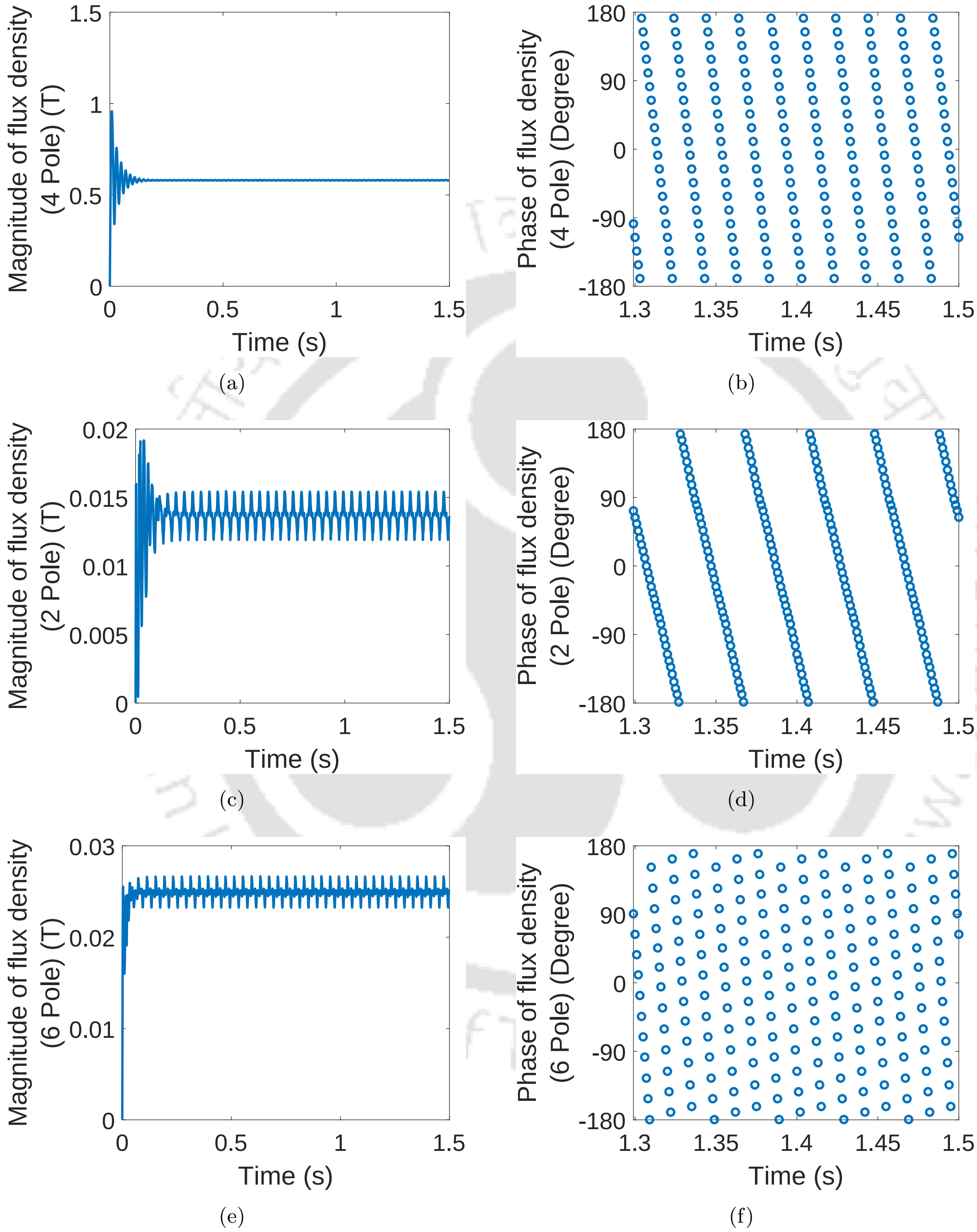

Figure 3.12: Induction motor with series winding when rotor is dynamically eccentric (a) variation in amplitude of the four pole magnetic field with time (b) variation in phase of the four pole magnetic field with time (c) variation in amplitude of the two pole magnetic field with time (d) variation in phase of the two pole magnetic field with time (e) variation in amplitude of the six pole magnetic field with time (f) variation in phase of the six pole magnetic field with time.

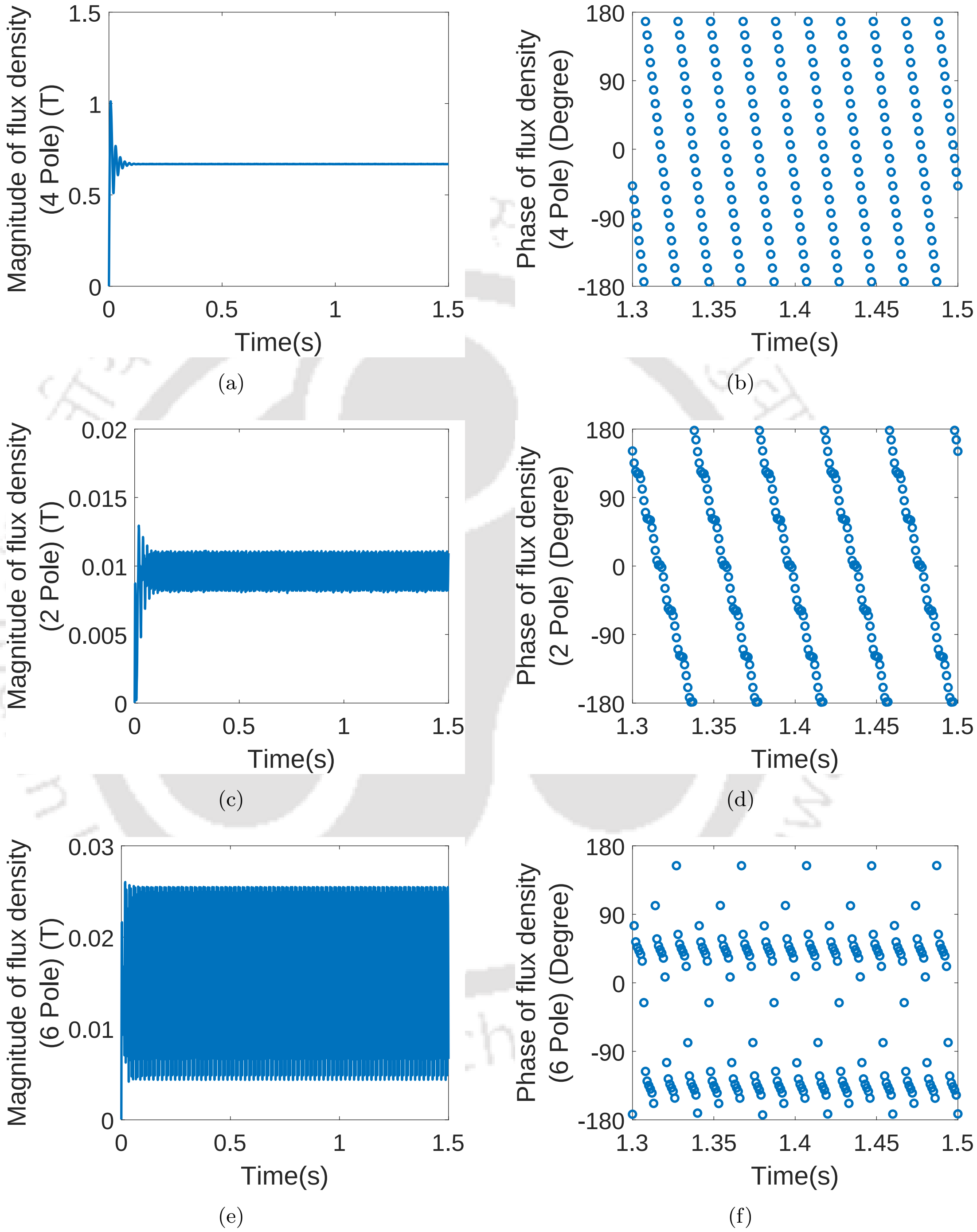

Figure 3.13: Induction motor with BCW winding when rotor is dynamically eccentric and bridge is OFF (a) variation in amplitude of the four pole magnetic field with time (b) variation in phase of the four pole magnetic field with time (c) variation in amplitude of the two pole magnetic field with time (d) variation in phase of the two pole magnetic field with time (e) variation in amplitude of the six pole magnetic field with time (f) variation in phase of the six pole magnetic field with time.

and the six pole magnetic fields with respect to time for the case of the parallel winding connection when the rotor is dynamically eccentric. It can be observed from Figure 3.13 that the amplitude of the four pole magnetic field becomes constant after some time, two pole magnetic field amplitude has a small variation with time and six pole magnetic field amplitude has higher variation with respect to time. The phase plots show that the four pole magnetic field makes ten rotations in 0.2 second which says that the rotational frequency of the four pole magnetic field is 50Hz, the two pole magnetic field makes five rotations in 0.2 second which says that the rotational frequency of the two pole magnetic field is 25 Hz and the six pole magnetic field makes fifteen rotations in 0.2 second, which says that the rotational frequency of the six pole magnetic field is 75 Hz. The same can be observed from the FFT of the magnetic field variation at a point which shows the presence of three frequency components, 25Hz, 50 Hz and 75 Hz as shown in Figure 3.7. However a large perturbation in the phase of the six pole magnetic field indicates the presence of the pulsating magnetic field, which is of same frequency as that of the rotational frequency of the magnetic field. Hence, the magnetic field equation for the dynamic eccentricity condition in Equation (3.2) should be modified with an additional component of pulsating six pole magnetic field.

3.4.2.3 Mixed eccentricity

Figure 3.14 represents the variation in the amplitude and phase of the four pole, two pole and six pole magnetic fields with respect to time for the case of series stator winding connection when the rotor is in the mixed eccentricity condition. It can be observed from Figure 3.14 that the amplitude of the four pole magnetic field becomes constant with time, the two pole magnetic field and the six pole magnetic field show variation in amplitude with respect to time. The phase plot of the four pole magnetic field shows that the four pole magnetic field makes 10 rotations in 0.2 second, which says that the four pole magnetic field rotational frequency is 50 Hz. The phase plot of the two pole magnetic field shows the combination of two different type of rotations, five and ten rotations in 0.2 second which says that the rotational frequency of the two pole magnetic field are 25 Hz and 50 Hz. The phase plot of the six pole magnetic field also shows the combination of two different types of rotations, ten and fifteen rotations in 0.2 second, which says that the rotational frequency of the six pole magnetic field are 50 Hz and 75 Hz. The same can be observed from the FFT of the magnetic field variation at a point which shows the presence of three frequency components, 25Hz, 50 Hz and 75 Hz as shown in Figure 3.6. The obtained frequency component of these harmonic fields are in line

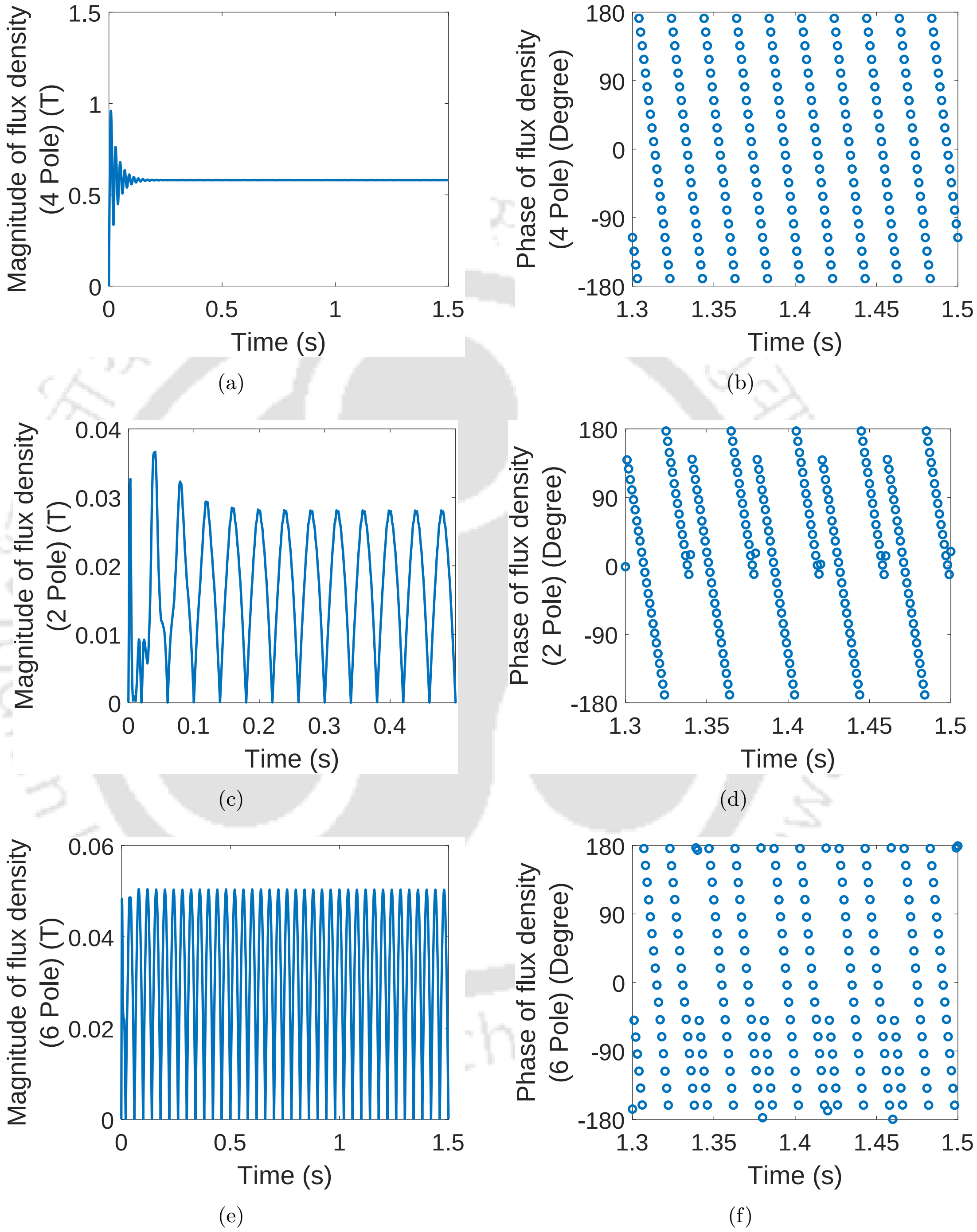

Figure 3.14: Induction motor with series winding when rotor is in mixed eccentric condition (a) variation in amplitude of the four pole magnetic field with time (b) variation in phase of the four pole magnetic field with time (c) variation in amplitude of the two pole magnetic field with time (d) variation in phase of the two pole magnetic field with time (e) variation in amplitude of the six pole magnetic field with time (f) variation in phase of the six pole magnetic field with time.

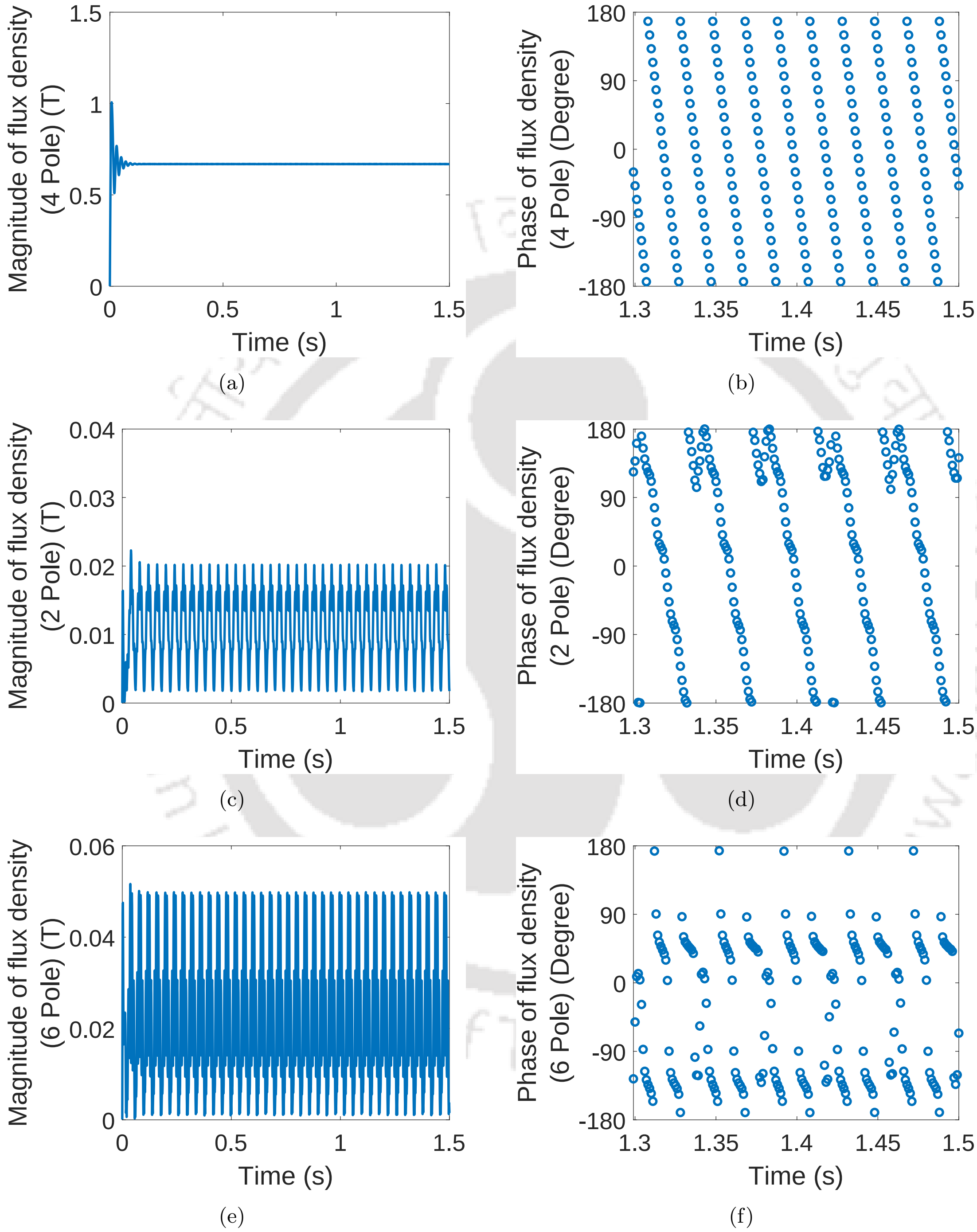

Figure 3.15: Induction motor with BCW winding when rotor is in mixed eccentric condition and bridge is OFF (a) variation in amplitude of the four pole magnetic field with time (b) variation in phase of the four pole magnetic field with time (c) variation in amplitude of the two pole magnetic field with time (d) variation in phase of the two pole magnetic field with time (e) variation in amplitude of the six pole magnetic field with time (f) variation in phase of the six pole magnetic field with time.

with the analytical expression as shown in Equation (3.3).

Figure 3.15 represents the variation in the amplitude and the phase of the four pole, two pole and six pole magnetic fields with respect to time for the case of the parallel winding connection when the rotor is in mixed eccentricity condition. It can be observed from Figure 3.15 that the amplitude of the four pole magnetic fields become constant with time, the two pole magnetic field and the six pole magnetic field show variations in the amplitude with respect to time. The phase plot of the four pole field shows that the four pole magnetic field makes 10 rotations in 0.2 second, which says that the four pole magnetic field rotational frequency is 50 Hz. The phase plot of the two pole magnetic field shows the combination of two different type of rotation, five and ten rotation in 0.2 second, which says that the rotational frequency of the two pole magnetic field are 25 Hz and 50 Hz. However, the phase plot of the six pole magnetic field is a bit complex. It looks like, a combination of ten and fifteen rotations in 0.2 second, however, ten rotation is prominent, which says that the field is rotating with a higher magnitude, 50 Hz component and a smaller magnitude 75 Hz component. Also, a distortion in the phase plot of the six - pole magnetic field demonstrates the presence of the pulsating component of the magnetic field. Hence, the magnetic field equation for the case of the mixed eccentricity condition should be modified with two additional components of six pole pulsating magnetic field of frequency 50 Hz and 75 Hz.

3.5 Modification in analytical expression

It has been seen in numerical investigation of the phase plot of the magnetic field of the parallel stator winding motor that in each eccentricity condition there is an existence of pulsating component of the magnetic field. The pulsating six pole magnetic field has the same frequency component as that of the rotating six pole magnetic field. So, the pulsating six pole magnetic field for the case of the static eccentricity, the dynamic eccentricity and the mixed eccentricity condition can be written as shown in Equations (3.13) - (3.15) respectively which has the same frequency component as that of the rotating six pole magnetic field component as,

$$\mathbf{B_{static}} = B_{3s} cos \left(2\pi f_s t - \phi_{ps}\right) \cos\left(\left(p+1\right)\theta - \phi_{ps}\right) \tag{3.13}$$

$$\mathbf{B_{dynamic}} = B_{3d} cos \left(2\pi (f_s + f_r) t - \phi_{pd}\right) \cos\left(\left(p+1\right)\theta - \phi_{pd}\right) \tag{3.14}$$

$$\mathbf{B_{mixed}} = B_{3s}cos\left(2\pi f_s t - \phi_{ps}\right)\cos\left((p+1) - \phi_{ps}\right) + B_{3d}cos\left(2\pi(f_s + f_r)t - \phi_{pd}\right)\cos\left((p+1) - \phi_{pd}\right) \tag{3.15}$$

where B_{3s}, B_{3d} and ϕ_{ps}, ϕ_{pd} are the amplitude and the phase of the pulsating six pole magnetic field in the case of the static and the dynamic eccentricity conditions respectively. By adding these pulsating magnetic field to (3.1) - (3.3), a modified field equation for the parallel stator winding connection for the case of the static eccentricity, the dynamic eccentricity and the mixed eccentricity condition can be written as shown in Equations (3.16) - (3.18) as,

$$\begin{aligned} \mathbf{b_{st}} &= \frac{\mu_o A_m}{p\delta}\cos\left(p\theta - 2\pi f_s t - \phi_m\right) \\ &+ \frac{\mu_o \varepsilon_s A_m}{2p\delta}\cos\left((p \pm 1)\,\theta - 2\pi f_s t - (\phi_m \pm \phi_s)\right) \\ &+ B_{3s}cos\left(2\pi f_s t - \phi_{ps}\right)\cos\left((p+1)\,\theta - \phi_{ps}\right) \end{aligned} \tag{3.16}$$

$$\begin{aligned} \mathbf{b_{dy}} &= \frac{\mu_o A_m}{p\delta}\cos\left(p\theta - 2\pi f_s t - \phi_m\right) \\ &+ \frac{\mu_o \varepsilon_d A_m}{2p\delta}\cos\left((p \pm 1)\,\theta - 2\pi(f_s \pm f_r)t - (\phi_m \pm \phi_d)\right) \\ &+ B_{3d}cos\left(2\pi(f_s + f_r)t - \phi_{pd}\right)\cos\left((p+1)\,\theta - \phi_{pd}\right) \end{aligned} \tag{3.17}$$

$$\begin{aligned} \mathbf{b_{mi}} &= \frac{\mu_o A_m}{p\delta}\cos\left(p\theta - 2\pi f_s t - \phi_m\right) \\ &+ \frac{\mu_o \varepsilon_s A_m}{2p\delta}\cos\left((p \pm 1)\,\theta - 2\pi f_s t - (\phi_m \pm \phi_s)\right) \\ &+ \frac{\mu_o \varepsilon_d A_m}{2p\delta}\cos\left((p \pm 1)\,\theta - 2\pi(f_s \pm f_r)t - (\phi_m \pm \phi_d)\right) \\ &+ B_{3s}cos\left(2\pi f_s t - \phi_{ps}\right)\cos\left((p+1)\,\theta - \phi_{ps}\right) \\ &+ B_{3d}cos\left(2\pi(f_s + f_r) + t - \phi_{pd}\right)\cos\left((p+1)\,\theta - \phi_{pd}\right) \end{aligned} \tag{3.18}$$

where $\mathbf{b_{st}}, \mathbf{b_{dy}}$ and $\mathbf{b_{mi}}$ are final magnetic field expression in the case of static eccentricity, dynamic eccentricity and mixed eccentricity respectively. Considering these magnetic field and substituting it in Equations (3.4) and (3.8) , the force acting along x and y axis can be written as,

$$F_{ps\_x} = \frac{\mu_0 A_m^2 r^2 l \varepsilon_s \pi}{2p^2\delta^2}\sin(\phi_s) + \frac{\mu_0 A_m r^2 l B_{3s}\pi}{2p\delta}\cos(\phi_m) + \frac{\mu_0 A_m r^2 l B_{3s}\pi}{2p\delta}\cos(2\pi(2f_s)t - 2\phi_s - \phi_m) \tag{3.19}$$

$$F_{pd\_x} = \frac{\mu_0 A_m^2 r^2 l \varepsilon_d \pi}{2p^2\delta^2}\sin(2\pi f_r t + \phi_d) + \frac{\mu_0 A_m r^2 l B_{3d}\pi}{2p\delta}\cos(2\pi f_r t - \phi_m) + \frac{\mu_0 A_m r^2 l B_{3d}\pi}{2p\delta}\cos(2\pi(2f_s + f_r)t - 2\phi_{pd} - \phi_m) \tag{3.20}$$

$$F_{pm\_x} = \frac{\mu_0 A_m^2 r^2 l \varepsilon \pi}{2p^2\delta^2}\sin(\phi_s) + \frac{\mu_0 A_m r^2 l B_s\pi}{2p\delta}\sin(\phi_m) + \frac{\mu_0 A_m r^2 l B_s\pi}{2p\delta}\cos(2\pi(2f_s)t - 2\phi_{ps} - \phi_m) + \frac{\mu_0 A_m^2 r^2 l \varepsilon \pi}{2p^2\delta^2}\cos(2\pi f_r t + \phi_s) + \frac{\mu_0 A_m r^2 l B_d\pi}{2p\delta}\cos(2\pi f_r t - \phi_m) + \frac{\mu_0 A_m r^2 l B_d\pi}{2p\delta}\cos(2\pi(2f_s + f_r)t - 2\phi_{pd} - \phi_m) \tag{3.21}$$

$$F_{ps\_y} = \frac{\mu_0 A_m^2 r^2 l \varepsilon_s \pi}{2p^2\delta^2}\sin(\phi_s) + \frac{\mu_0 A_m r^2 l B_{3s}\pi}{2p\delta}\sin(\phi_m) + \frac{\mu_0 A_m r^2 l B_{3s}\pi}{2p\delta}\sin(2\pi(2f_s)t - 2\phi_s - \phi_m) \tag{3.22}$$

$$F_{pd\_y} = \frac{\mu_0 A_m^2 r^2 l \varepsilon_d \pi}{2p^2\delta^2}\sin(2\pi f_r t + \phi_d) + \frac{\mu_0 A_m r^2 l B_{3d}\pi}{2p\delta}\sin(2\pi f_r t - \phi_m) + \frac{\mu_0 A_m r^2 l B_{3d}\pi}{2p\delta}\sin(2\pi(2f_s + f_r)t - 2\phi_{pd} - \phi_m) \tag{3.23}$$

$$
\begin{aligned}
F_{pm\_y} = &\frac{\mu_0 A_m^2 r^2 l \varepsilon \pi}{2p^2\delta^2}\sin(\phi_s) + \frac{\mu_0 A_m r^2 l B_s \pi}{2p\delta}\sin(\phi_m) \\
&+\frac{\mu_0 A_m r^2 l B_s \pi}{2p\delta}\sin(2\pi(2f_s)t - 2\phi_{ps} - \phi_m) \\
&+\frac{\mu_0 A_m^2 r^2 l \varepsilon \pi}{2p^2\delta^2}\sin(2\pi f_r t + \phi_s) \\
&+\frac{\mu_0 A_m r^2 l B_d \pi}{2p\delta}\sin(2\pi f_r t - \phi_m) \\
&+\frac{\mu_0 A_m r^2 l B_d \pi}{2p\delta}\sin(2\pi(2f_s + f_r)t - 2\phi_{pd} - \phi_m)
\end{aligned} \tag{3.24}
$$

where F_{ps_x}, F_{pd_x} and F_{pm_x} are the forces acting along x direction for the parallel stator winding in the static, dynamic and mixed eccentricity conditions respectively. F_{ps_y}, F_{pd_y} and F_{pm_y} are the forces acting along y direction for the parallel stator winding in the static, the dynamic and the mixed eccentricity condition respectively. It can be seen in Equations (3.19) - (3.24) that the new force expressions have all the frequency components shown in Figure 3.4. F_{ps_x} and F_{ps_y} have DC as well as $2f_s$ component of the force which is 0 Hz and 100 Hz. F_{pd_x} and F_{pd_y} have f_r as well as $2f_s + f_r$ component of the force which is 25 Hz and 125 Hz. F_{pm_x} and F_{pm_y} have DC, $2f_s$, f_r and $2f_s + f_r$ components of the force which is 0 Hz, 25 Hz 100 Hz and 125 Hz.

3.6 Numerical simulation in bridge ON condition

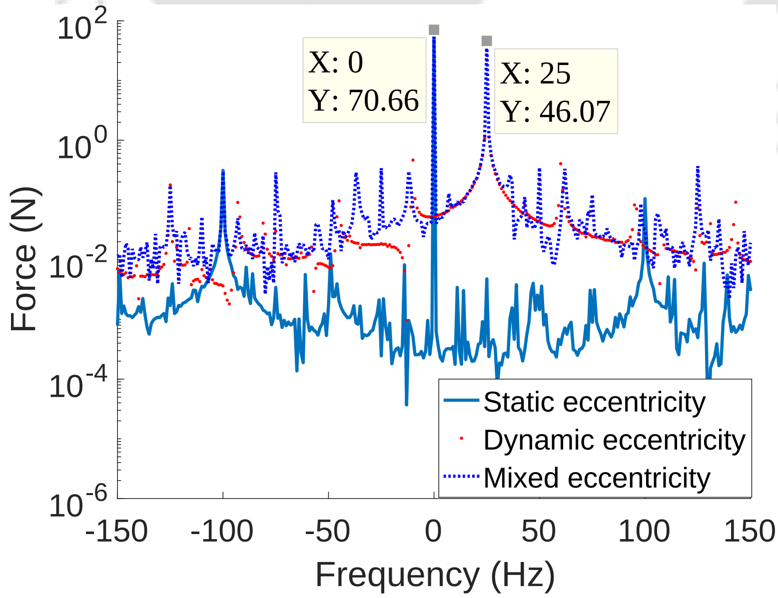

Figure 3.16: Comparison of FFT of forces acting on the rotor in BCW winding motor in different eccentricity conditions when bridges are in ON condition.

Figure 3.16 represents the FFT of the forces acting on the rotor in different eccentricity conditions when bridges of the winding are in ON condition. By comparing Figure 3.4 and Figure 3.16 it can be observed that the bridge ON condition suppresses all the additional components of the forces. The generated UMP has a DC component of force in the static eccentricity condition, 25 Hz component in the dynamic eccentricity condition and a DC and 25 Hz components in the mixed eccentricity condition.

To investigate the reason behind this suppression of additional components of forces, the amplitude and phase of the air gap magnetic fields have been plotted similar to series winding and bridge OFF parallel winding conditions. Figures 3.17 - 3.19 represents the variation in the amplitude and the phase of the four pole, two pole and six pole magnetic fields with respect to time for the case of the static, dynamic and mixed eccentricity conditions respectively when the bridges of the stator winding are in ON condition. It can be seen that amplitude of the two pole, four pole and six pole magnetic field become constant with time. Also phase plot in all the three conditions doesn't show the presence of substantial pulsating component of the magnetic field. Hence it can be concluded that the bridge ON condition suppresses the pulsating components of the magnetic field which in turn suppresses the additional components of the force generated in the parallel stator winding motor.

Table 3.4: Comparison of magnetic field behavior in numerical analysis

Numerical Simulation						
	Series Connection					
	Four - Pole		Two - Pole		Six - Pole	
	Rotation	Pulsation	Rotation	Pulsation	Rotation	Pulsation
Static Eccentricity	5/0.1, 50 Hz	Not Present	5/0.1, 50 Hz	Not Present	5/0.1, 50 Hz	Not Present
Dynamic Eccentricity	10/0.2, 50 Hz	Not Present	5/0.2, 25 Hz	Not Present	15/0.2, 75 Hz	Not Present
Mixed Eccentricity	10/0.2, 50 Hz	Not Present	5/0.2, 25 Hz 10/0.2, 50 Hz	Not Present	10/0.2, 50 Hz 15/0.2, 75 Hz	Not Present
	BCW Connection (Bridge OFF)					
	Four - Pole		Two - Pole		Six - Pole	
	Rotation	Pulsation	Rotation	Pulsation	Rotation	Pulsation
Static Eccentricity	5/0.1, 50 Hz	Not Present	5/0.1, 50 Hz	Very Small	5/0.1, 50 Hz	50 Hz
Dynamic Eccentricity	10/0.2, 50 Hz	Not Present	5/ 0.2, 25 Hz	Very Small	15/0.2, 75 Hz	75 Hz
Mixed Eccentricity	10/0.2, 50 Hz	Not Present	5/0.2, 25 Hz 10/0.2, 50 Hz	Very Small	10/0.2, 50 Hz 15/0.2, 75 Hz	50 Hz, 75 Hz
	BCW Connection (Bridge ON)					
	Four - Pole		Two - Pole		Six - Pole	
	Rotation	Pulsation	Rotation	Pulsation	Rotation	Pulsation
Static Eccentricity	5/0.1, 50 Hz	Not Present	5/0.1, 50 Hz	Not Present	5/0.1, 50 Hz	Not Present
Dynamic Eccentricity	10/0.2, 50 Hz	Not Present	5/0.2, 25 Hz	Not Present	15/0.2, 75 Hz	Not Present
Mixed Eccentricity	10/0.2, 50 Hz	Not Present	5/0.2, 25 Hz	Not Present	10/0.2, 50 Hz 15/0.2, 75 Hz	Not Present

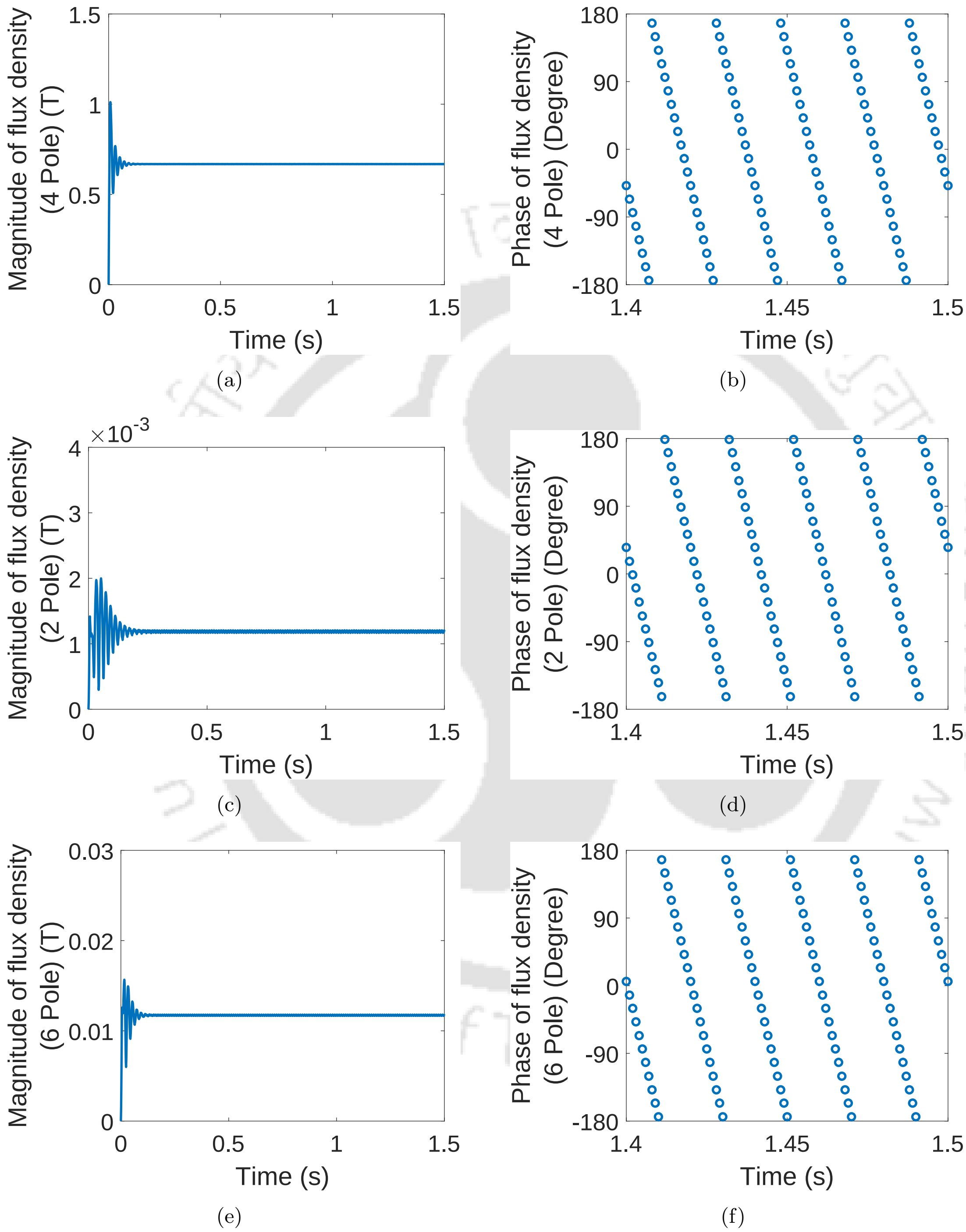

Figure 3.17: Induction motor with BCW winding when rotor is statically eccentric and bridge is ON (a) variation in amplitude of the four pole magnetic field with time (b) variation in phase of the four pole magnetic field with time (c) variation in amplitude of the two pole magnetic field with time (d) variation in phase of the two pole magnetic field with time (e) variation in amplitude of the six pole magnetic field with time (f) variation in phase of the six pole magnetic field with time.

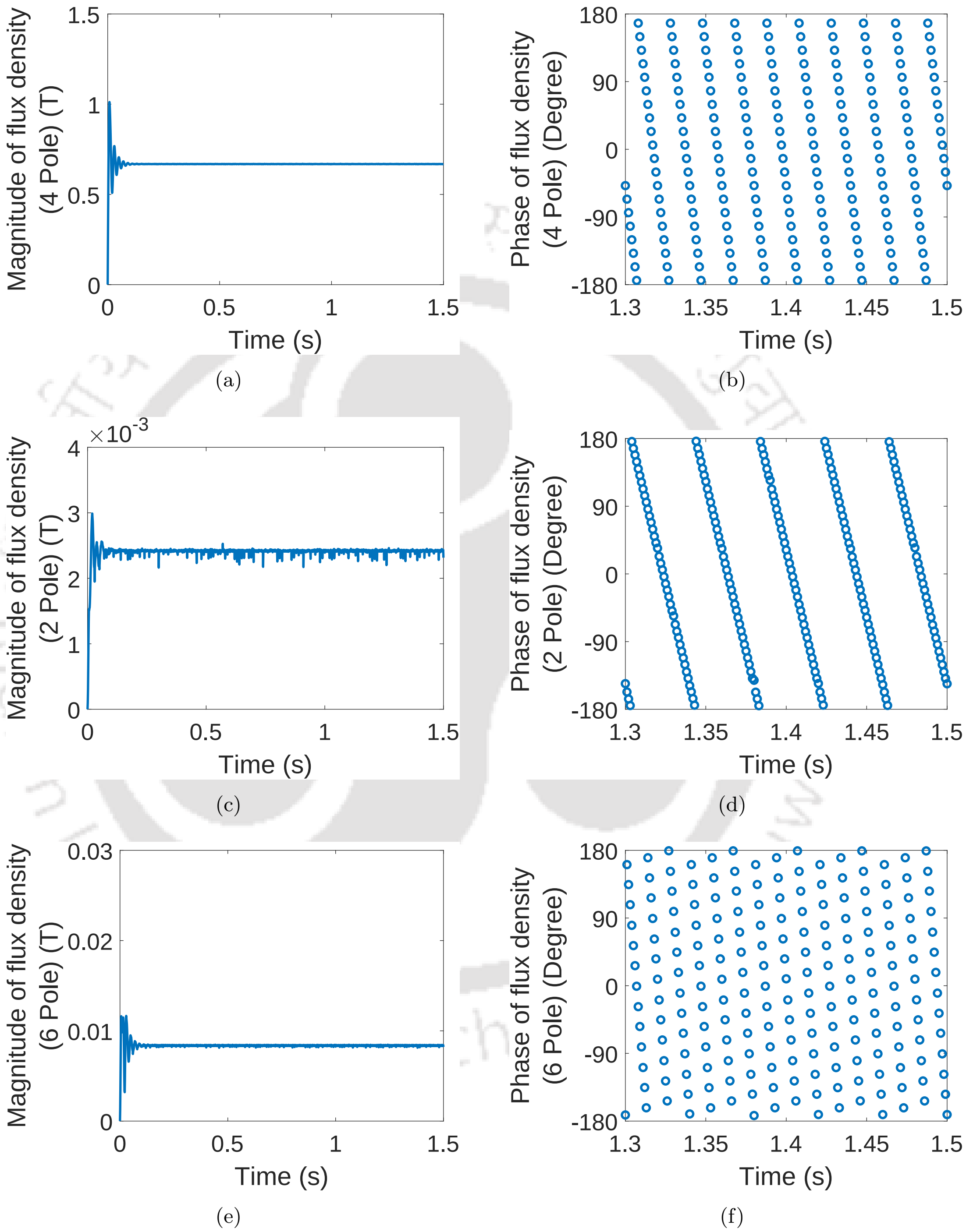

Figure 3.18: Induction motor with BCW winding when rotor is dynamically eccentric and bridge is ON (a) variation in amplitude of the four pole magnetic field with time (b) variation in phase of the four pole magnetic field with time (c) variation in amplitude of the two pole magnetic field with time (d) variation in phase of the two pole magnetic field with time (e) variation in amplitude of the six pole magnetic field with time (f) variation in phase of the six pole magnetic field with time.

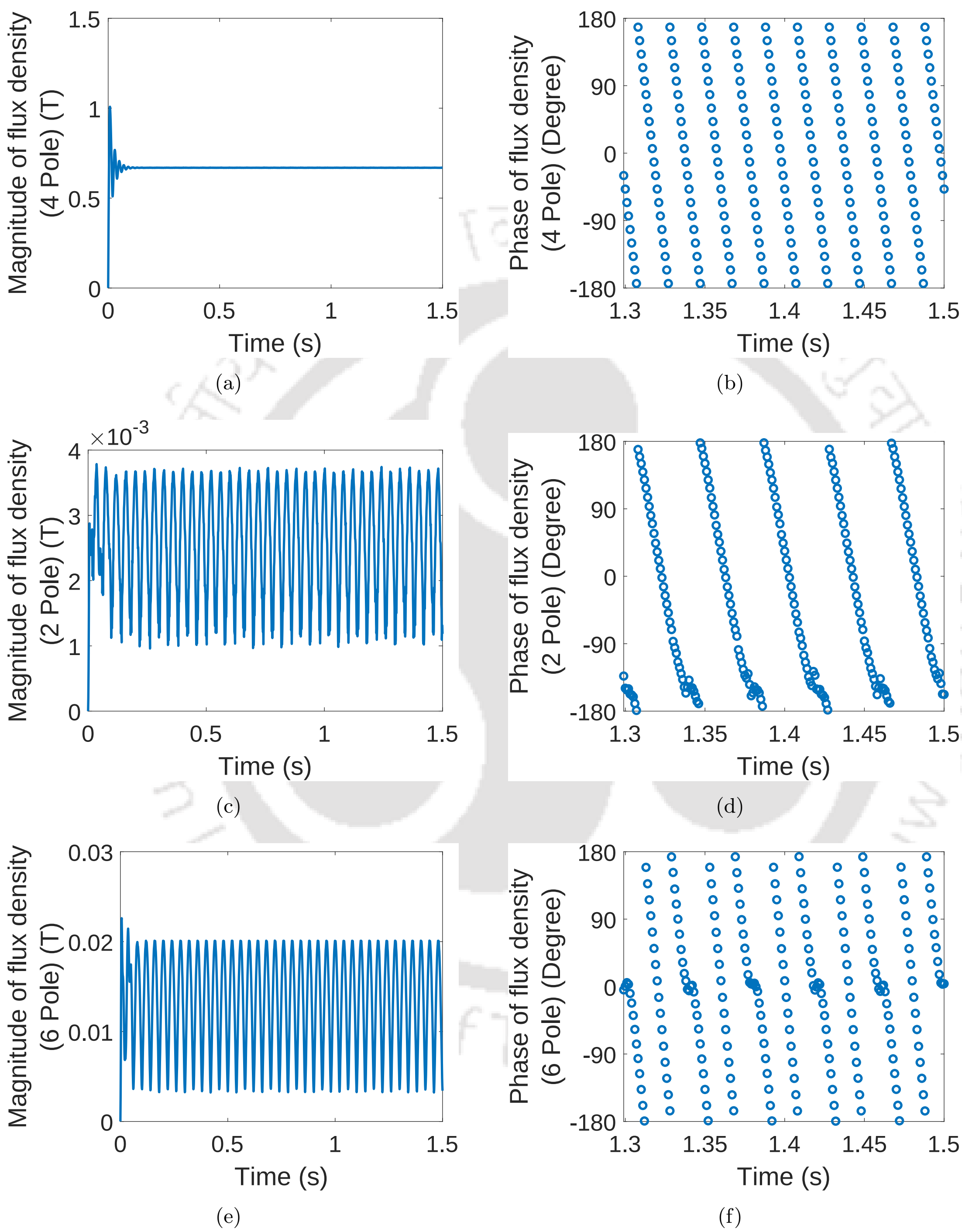

Figure 3.19: Induction motor with BCW winding when rotor is in mixed eccentricity condition and bridge is ON (a) variation in amplitude of the four pole magnetic field with time (b) variation in phase of the four pole magnetic field with time (c) variation in amplitude of the two pole magnetic field with time (d) variation in phase of the two pole magnetic field with time (e) variation in amplitude of the six pole magnetic field with time (f) variation in phase of the six pole magnetic field with time.

3.7 Conclusion

The work presented in this chapter is an investigation of the presence of the eccentricity generated harmonic magnetic field components in the air gap, which is responsible for the lateral force production. It has been demonstrated that the presence of pulsating six pole magnetic field is the reason behind the additional component of the force in a parallel winding connection machine. Based on the numerical investigation a modified magnetic field expressions have been used to calculate the UMP. The analytical force expression calculated using the modified field expressions fits well with the simulation results. The modified force expression can be used for active suppression of the UMP in parallel stator winding machine. In addition to this passive vibration suppression capability of bcw winding scheme in bridge ON condition has also been analysed. It has been established that in bridge ON condition the two pole and the six pole magnetic field pulsation gets eliminated in bridge ON condition.

4

Coupled Field and Circuit Model of an Induction Machine

Contents

4.1 Introduction

In the previous chapter behavior of UMP generation in different eccentricity conditions have been studied by analysing the air gap magnetic field harmonics. Considering the limitation of commercial finite element software, the present work deals with the development of a 2D finite element code of a 36 slot induction machine in MATLAB® environment and further behaviour of bridge currents and UMP have been analysed in different eccentricity conditions. Upon short-circuiting of bridge points, bridge currents flow through the winding, if the rotor of the motor is eccentric with respect to the stator centre.

There are no studies in the literature which demonstrate the effect of the different eccentricity conditions on the bridge currents and generated UMP in an electric machine with bridge configured winding. The finite element (FE) modelling is an efficient modelling technique for the investigation of machine behavior [35,36]. Recently few authors have used finite element modelling for the investigation of unbalanced magnetic pull in different eccentricity conditions and the effect of parallel paths on unbalanced magnetic pull [53, 96, 97]. A few work has been carried out on FE modelling of bridge configured winding to analyse the bridge currents in static eccentricity condition [81]. The developed model does not predict the correct behavior of the bridge currents as well as UMP in the static eccentricity condition. It has been shown that in static eccentricity condition, the bridge currents have $f_s \pm f_r$ frequency components, where f_s is the frequency of the main supply voltage and f_r is the rotor rotational frequency. However, in the static eccentricity condition the bridge current should have only f_s frequency component. It happens because in [81] a transformation matrix has been used for the implementation of bridge configuration winding, which enforces equal bridge currents in all the four legs of a particular phase. This is not a proper modelling of the bridge configuration winding scheme.

The aim of this chapter is to develop a simulation model which can be used to study bridge configured winding for the development of a bearingless machine. Hence, to understand and investigate the actual behavior of the bridge currents and UMP in different eccentricity conditions in bridge configured winding, a FE model of 3.7 kW bridge configured induction machine has been developed. A generalized circuit equation has been used to implement the bridge configuration winding in the FE model. The term generalized circuit means that the same numerical model can be used for the active as well as passive vibration control analysis, i.e when bridge points are short circuited or bridge points are connected with an external isolated supply source. However, the present analysis is based on two conditions, (i) when the bridge points are open (bridge OFF condition) and (ii) when the bridge points are short circuited (bridge ON condition). The analysis for the external supply through the bridge points has not been considered in this chapter. The material nonlinearity has not been considered in the developed FE model. Air gap stitching method has been used for the implementation of rotor rotation, the static, the dynamic and the mixed eccentricity conditions. Considering the complexity in combining rotor transverse motion in commercial softwares, this FE model has been developed in MATLAB® environment. However in this chapter transverse vibration of the rotor has not been coupled with the magnetic field and circuit equation. The coupling of rotor motion has been explained in subsequent chapters.

4.2 Fundamental equations

This work is restricted to 2D field analysis, where the current density ($\vec{J}$) and the magnetic vector potential ($\vec{A}$) are z-directed (parallel to the axial length of the machine) and independent of z,

$$\overrightarrow{J} = J\left(x, y, t\right) \overrightarrow{k} \tag{4.1}$$

$$\overrightarrow{A} = A\left(x, y, t\right) \overrightarrow{k} \tag{4.2}$$

where x and y are the cartesian coordinates, $\overrightarrow{k}$ is the unit vector parallel to the z-axis and t is the time. Since, vectors $\vec{J}$ and $\vec{A}$ have only one component, they can be treated as scalars.

The 2D approximation of field equation in x-y plane can be written as

$$\frac{\partial}{\partial x}\left[\frac{1}{\mu}\frac{\partial A}{\partial x}\right] + \frac{\partial}{\partial y}\left[\frac{1}{\mu}\frac{\partial A}{\partial y}\right] - \sigma\frac{\partial A}{\partial t} - \sigma gradV = 0 \tag{4.3}$$

where $\sigma gradV$ is the source of the excitation. This formulation is based on a squirrel cage induction machine, where two different types of conductors are used. The thick conductors (single conducting area) are used in the rotor and the thin conductors (multi turn coils) are used in the stator winding. The application of electrical continuity equation for the thick and the thin conductors gives $gradV = -U/l$, where U is the applied voltage. Hence, the 2D approximation of the field equation can be written as

$$\frac{\partial}{\partial x}\left[\frac{1}{\mu}\frac{\partial A}{\partial x}\right] + \frac{\partial}{\partial y}\left[\frac{1}{\mu}\frac{\partial A}{\partial y}\right] - \sigma\frac{\partial A}{\partial t} + \sigma\frac{U}{l} = 0 \tag{4.4}$$

we get the circuit equations for the thick and thin conductors by using $E + \frac{\partial A}{\partial t} = -gradV$ and Ohm's law, $J = \sigma E$, as Equations (4.5) and (4.6) respectively.

$$U_r = R_r I_r + R_r \int_{s_r} \sigma \frac{\partial A}{\partial t} ds \tag{4.5}$$

$$U_s = R_s I_s + \frac{nl}{S_s} \int_{S_s} \sigma \frac{\partial A}{\partial t} ds \tag{4.6}$$

The subscripts r and s represent the rotor side and the stator side variables respectively and it has been used consistently in the entire chapter. The combined field equation considering the thick and the thin conductor excitation can be written as [98]

$$\frac{\partial}{\partial x}\left[\frac{1}{\mu}\frac{\partial A}{\partial x}\right] + \frac{\partial}{\partial y}\left[\frac{1}{\mu}\frac{\partial A}{\partial y}\right] - \sigma_r \frac{\partial A}{\partial t} + \frac{n_0}{S_s} I_s + \sigma_r \frac{U_r}{l} = 0 \tag{4.7}$$

where σ_r is the electrical conductivity of the rotor bar, n_0 is the no. of turns in the stator winding, S_s is the c/s area of the stator coil, l is the length of the rotor bar, U_r is the voltage across the rotor bar and μ is the permeability.

4.3 Finite element modelling of BCW electrical machines

In general any electrical machine can be divided into five domains for the purpose of numerical modelling i.e the stator core domain, the stator winding domain, the air gap domain, the rotor core domain and the rotor conductor domain. The Galerkin method has been used for the application of FE discretization in Equations (4.5), (4.6) and (4.7). The elemental matrices have been obtained for the field Equation (4.7) for different domains of the machine. The elemental stiffness matrix for the entire domain, the elemental matrix for the contribution of the induced emf in the field equation due to rotor bar, the elemental matrix for the contribution of the excitation at the stator winding, and the elemental matrix for the contribution of the excitation at the rotor conductor can be represented as Equations (4.8), (4.9), (4.10), and (4.11) respectively.

$$k_c^e = \iint_s \nu \left(\{\mathbf{N}_{,x}\} \lfloor \mathbf{N}_{,x} \rfloor + \{\mathbf{N}_{,y}\} \lfloor \mathbf{N}_{,y} \rfloor\right) dxdy \tag{4.8}$$

$$c_r^e = \iint_s \sigma_r \{\mathbf{N}\} \lfloor \mathbf{N} \rfloor dxdy \tag{4.9}$$

$$p_s^e = \iint_s \frac{n_0}{S_s} \{\mathbf{N}\} dxdy \tag{4.10}$$

$$p_r^e = \iint_s \{\mathbf{N}\} \frac{\sigma_r}{l} dxdy \tag{4.11}$$

The elemental matrix for the rotor circuit equation and the elemental matrix for the stator circuit equation can be represented as Equations (4.12) and (4.13) respectively.

$$q_r^e = R_r \sigma_r \iint_s \{\mathbf{N}\} dx\, dy \tag{4.12}$$

$$q_s^e = \frac{n_0 l}{S_s} \iint_s \{\mathbf{N}\} dx\, dy \tag{4.13}$$

where ν is the magnetic reluctivity ($\nu = \frac{1}{\mu}$) and $\{\mathbf{N}\}$ is a vector of the shape functions. Two types of elements have been used for the FE discretization. Eight noded quadrilateral elements have been used in the stator core, the stator coil, the rotor core and the rotor conductors, whereas six noded triangular elements have been used for the air gap modelling. For eight noded quadrilateral elements, the elemental stiffness matrix, Equation (4.8) can be written in natural coordinate system ($\xi - \eta$) as

$$k_n^e = \int_1^{-1} \int_1^{-1} \nu \{grad\mathbf{N}\} \lfloor grad\mathbf{N} \rfloor |\mathbf{J}| \, d\xi d\eta \tag{4.14}$$

However for six noded quadrilateral elements, the elemental stiffness matrix, Equation (4.8) can be written in natural coordinate system as

$$k_n^e = \int_0^{1} \int_0^{1} \nu \{grad\mathbf{N}\} \lfloor grad\mathbf{N} \rfloor |\mathbf{J}| \, d\xi d\eta \tag{4.15}$$

Similarly for eight noded quadrilateral element, the elemental stiffness matrix, Equations (4.9) -

(4.13) can be written in natural coordinate system as

$$c_r = \int_{1}^{-1}\int_{1}^{-1} \sigma_r \{\mathbf{N}\} \lfloor \mathbf{N} \rfloor |\mathbf{J}| \, d\xi d\eta \tag{4.16}$$

$$p_s = \frac{n_0}{S_s}\int_{1}^{-1}\int_{1}^{-1} \{\mathbf{N}\} |\mathbf{J}| \, d\xi d\eta \tag{4.17}$$

$$p_r = \int_{1}^{-1}\int_{1}^{-1} \frac{\sigma_r}{l} \{\mathbf{N}\} |\mathbf{J}| \, d\xi d\eta \tag{4.18}$$

$$q_s = \frac{n_0 l}{S_s}\int_{1}^{-1}\int_{1}^{-1} \{\mathbf{N}\} |\mathbf{J}| \, d\xi d\eta \tag{4.19}$$

$$q_r = R_r \sigma_r \int_{1}^{-1}\int_{1}^{-1} \{\mathbf{N}\} |\mathbf{J}| \, d\xi d\eta \tag{4.20}$$

After assembling all the elemental matrices the final assembled field equation can be written as Equation (4.21). The assembled rotor and stator circuit equations can be written as Equations (4.22) and (4.23) respectively. The stiffness matrix has the contribution from the entire domain, hence k^e has to be assembled for all the elements in the domain. However, c_r, p_r and q_r are applied to the rotor conductor domains only and p_s and q_s are applied in the stator coil domains.

$$[K]_{n\times n}\{A\}_{n\times 1} + [C_r]_{n\times n}\frac{\partial\{A\}_{n\times 1}}{\partial t} - [P_s]_{n\times z}[T]_{z\times u}\{I_S\}_{u\times 1} + [P_r]_{n\times v}\{U_r\}_{v\times 1} = 0 \tag{4.21}$$

$$[R_r]_{v\times v}\{I_r\}_{v\times 1} + [Q_r]_{v\times n}\frac{d\{A\}_{n\times 1}}{dt} = \{U_r\}_{v\times 1} \tag{4.22}$$

$$[R_s]_{u\times u}\{I_s\}_{u\times 1} + [Q_s]_{u\times n}\frac{d\{A\}_{n\times 1}}{dt} = \{U_s\}_{u\times 1} \tag{4.23}$$

where n represents the number of nodes in the domain, u is the number of stator circuit currents, v is the number of rotor conductors and z represents the number of coil side currents. In our analysis the typical value of n is 29,572. The transformation matrix used for the transformation of phase currents to the coil side currents is $[T]_{z\times u}$.

The BCW scheme has a double layer winding with two parallel paths and one additional source of power supply in each phase of the stator winding. The simulated motor is a 4-pole squirrel cage induction motor which has 36 stator slots and 26 rotor bars. In a conventional 3-phase machine the value of the stator circuit currents would be three. However in our analysis the value of the stator circuit current would depend on whether we use a simple parallel winding connection or a short circuited parallel winding connection with or without a power source. Hence for the inclusion of parallel paths and bridge connections, the field equation (4.21) and the stator circuit equation (4.23) have to be modified. To incorporate the parallel paths of the rotor bars of the squirrel cage along with the end rings, the rotor bar equation (4.22) has to be modified. This has been explained in details in next subsections.

4.3.1 Introduction to BCW winding

Figure 4.1 represents the winding diagram of an induction machine with 36 stator slots and Figure 4.2 represents the coil connection diagram of the winding. Coils $(a1-a3)$, $(aa4-aa6)$ and $(aa1-aa3)$, $(a4-a6)$ form two parallel paths in phase A of the winding. Coils $(b1-b3)$, $(bb4-bb6)$ and $(bb1-bb3)$, $(b4-b6)$ form two parallel paths in phase B of the winding. Coils $(c1-c3)$, $(cc4-cc6)$ and $(cc1-cc3)$, $(c4-c6)$ form two parallel paths in phase C of the winding. For the explanation of the modelling of the circuit, twelve coil groups (W1-W12) have been formed. Coils $(a1-a3)$, $(a4-a6)$, $(aa1-aa3)$, $(aa4-aa6)$, $(b1-b3)$, $(b4-b6)$, $(bb1-bb3)$, $(bb4-bb6)$, $(c1-c3)$, $(c4-c6)$, $(cc1-cc3)$, and $(cc4-cc6)$ has been termed as coil group W1, W2, W3, W4, W5, W6, W7, W8, W9, W10, W11, and W12 respectively.

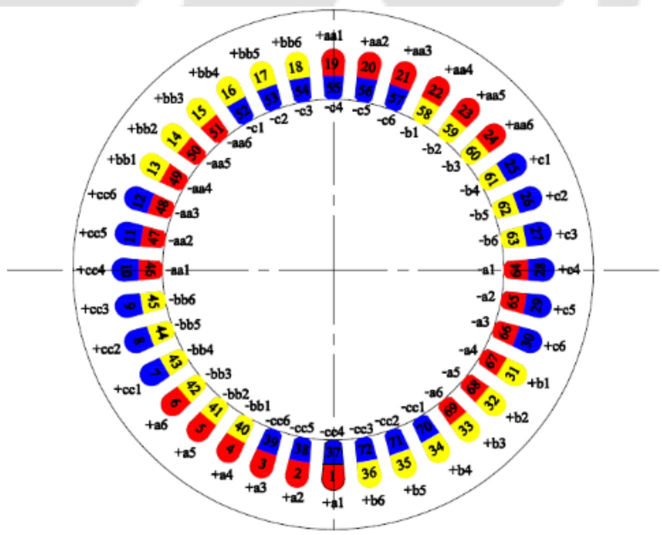

Figure 4.1: Winding diagram of double layer bridge configuration winding.

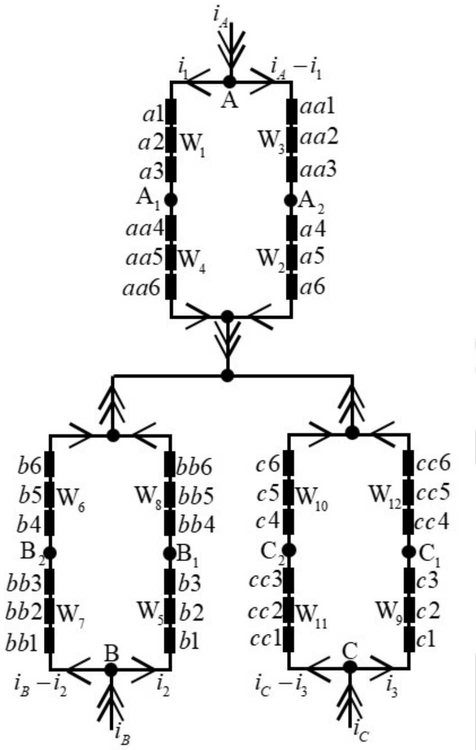

Figure 4.2: Coil connection diagram of the winding.

4.3.2 Stator winding circuit equation when bridges are open (bridge OFF condition)

Figure 4.3 represents the star connected circuit diagram of a bridge configuration wound machine when bridge points are not connected and machine is supplied with a three phase star connected power source. We will refer this connection of the bridge as bridge OFF condition. The two bridge points of phase A are $\mathbf{A_1}$ and $\mathbf{A_2}$, the two bridge points of phase B are $\mathbf{B_1}$ and $\mathbf{B_2}$ and the two bridge points of phase C are $\mathbf{C_1}$ and $\mathbf{C_2}$ respectively. The neutral points of the stator winding and the supply source are $\mathbf{O}$ and $\mathbf{O'}$ respectively. The three phase supply voltages are V_A, V_B, and V_C and the three phase currents of phase A, phase B, and phase C are i_A, i_B, and i_c respectively. The two parallel paths of phase A are $\mathbf{A - A_1 - O}$ and $\mathbf{A - A_2 - O}$ and i_1 and $i_A - i_1$ are the currents flowing in these parallel paths respectively. The two parallel paths of phase B are $\mathbf{B - B_1 - O}$ and $\mathbf{B - B_2 - O}$ and i_2 and $i_B - i_2$ are the currents flowing in these parallel paths respectively. The two parallel paths of phase C are $\mathbf{C - C_1 - O}$ and $\mathbf{C - C_2 - O}$ and i_3 and $i_C - i_3$ are the currents flowing in these parallel paths respectively.

The DC resistance of the each coil group including the end winding resistance is R and the end winding inductance of the each coil group is L_{es}. The Kirchhoff's voltage law (KVL) has been used to

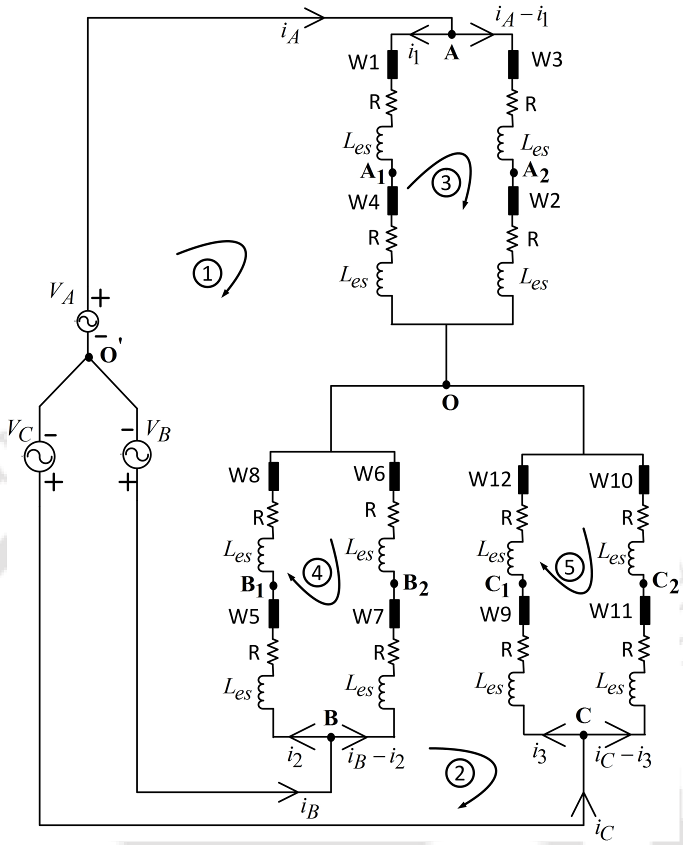

Figure 4.3: Circuit connection when bridges are open.

write the circuit equations. There are five loops in the circuit shown in Figure 4.3. Equations for these five loops have been written as Equations (4.24) - (4.28). In addition to these equations, Equation (4.29) can be written by imposing the Kirchhoff's current law (KCL) about the star point **O** of the winding. By assembling Equation (4.19) for coil group domains W1, W2, ..., W12, matrices Q_1, Q_2, ..., Q_{12} have been obtained respectively.

KVL for loop 1 ($\mathbf{O'AA_1OB_1BO'}$) can be written as

$$[\mathbf{Q}_1 + \mathbf{Q}_4 - \mathbf{Q}_5 - \mathbf{Q}_8]_{1\times n} \frac{d\{\mathbf{A}\}_{n\times 1}}{dt} + 2Ri_1 - 2Ri_2$$
$$+2L_{es}\frac{di_1}{dt} - 2L_{es}\frac{di_2}{dt} = V_B - V_A \tag{4.24}$$

KVL for loop 2 ($\mathbf{O'BB_2OC_1CO'}$) can be written as

$$[\mathbf{Q}_6 + \mathbf{Q}_7 - \mathbf{Q}_9 - \mathbf{Q}_{12}]_{1\times n} \frac{d\{\mathbf{A}\}_{n\times 1}}{dt} + 2R\,(i_B - i_2)$$
$$-2Ri_3 + 2L_{es}\frac{d\,(i_B - i_2)}{dt} - 2L_{es}\frac{di_3}{dt} = V_C - V_B \tag{4.25}$$

KVL for loop 3 (**AA₂OA₁A**) can be written as

$$[\mathbf{Q}_2 + \mathbf{Q}_3 - \mathbf{Q}_1 - \mathbf{Q}_4]_{1\times n}\frac{d\{\mathbf{A}\}_{n\times 1}}{dt} + 2R(i_A - i_1)$$
$$-2Ri_1 + 2L_{es}\frac{d(i_A - i_1)}{dt} - 2L_{es}\frac{di_1}{dt} = 0 \tag{4.26}$$

KVL for loop 4 (**BB₁OB₂B**) can be written as

$$[\mathbf{Q}_5 + \mathbf{Q}_8 - \mathbf{Q}_6 - \mathbf{Q}_7]_{1\times n}\frac{d\{\mathbf{A}\}_{n\times 1}}{dt} - 2R(i_B - i_2)$$
$$+2Ri_2 - 2L_{es}\frac{d(i_B - i_2)}{dt} + 2L_{es}\frac{di_2}{dt} = 0 \tag{4.27}$$

KVL for loop 5 (**CC₁OC₂C**) can be written as

$$[\mathbf{Q}_9 + \mathbf{Q}_{12} - \mathbf{Q}_{10} - \mathbf{Q}_{11}]_{1\times n}\frac{d\{\mathbf{A}\}_{n\times 1}}{dt} - 2R(i_C - i_3)$$
$$+2Ri_3 - 2L_{es}\frac{d(i_C - i_3)}{dt} + 2L_{es}\frac{di_3}{dt} = 0 \tag{4.28}$$

And KCL about point O can be applied as

$$i_A + i_B + i_C = 0 \tag{4.29}$$

Final circuit equation can be represented as

$$[Q]\,\frac{d\{A\}}{dt} + [R]\{I_s\} + [L_{es}]\left\{\frac{dI_s}{dt}\right\} = \{U_s\} \tag{4.30}$$

where $I_s = [i_1\ i_A\ i_2\ i_B\ i_3\ i_C]^\intercal$ and $U_s = [V_A - V_B\ V_B - V_C\ 0\ 0\ 0\ 0]^\intercal$.

4.3.3 Stator winding circuit equation when bridges are closed (bridge ON condition)

Figure 4.4 represents the star connected circuit diagram of a bridge configuration wound machine when the bridge points are closed or connected to a voltage source and the machine is supplied with a three phase star connected power source. We will refer this connection of bridge as bridge ON condition. An eccentric rotor generates a potential difference across the bridge points of the winding due to which, upon connecting these bridge points, a current flows across the bridge points which changes the dynamics of the machine. An isolated controlled voltage source in current control mode can also be connected to these bridge points by which current can be injected in the winding to generate the desired force for bearingless operation or for the purpose of active vibration control. The aim of the present work is to study the effect of eccentric rotor when bridges are open and closed.

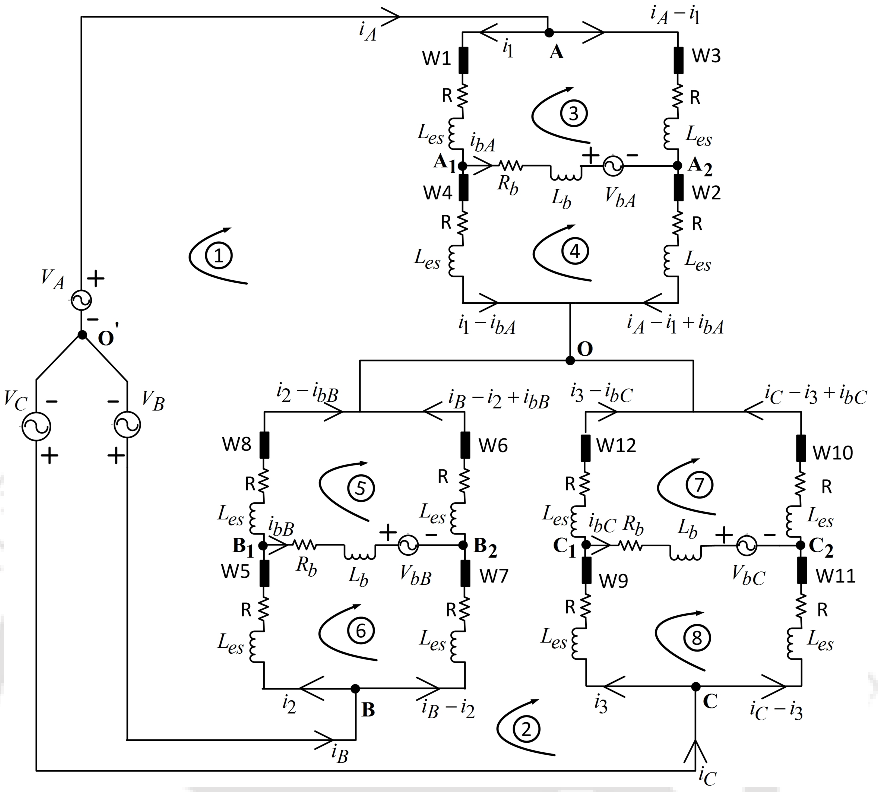

Figure 4.4: Circuit connection when bridges are closed.

However a generalized model has been developed considering a voltage supply across the bridge points. The DC resistance and the inductance of the coil connecting across the bridge points are R_b and L_b respectively. The voltage source connected between the bridge points $\mathbf{A}_1$ and $\mathbf{A}_2$ in phase A of the winding is V_{bA}. The voltage source connected between the bridge points $\mathbf{B}_1$ and $\mathbf{B}_2$ in phase B of the winding is V_{bB}. The voltage source connected between the bridge points $\mathbf{C}_1$ and $\mathbf{C}_2$ in phase C of the winding is V_{bC}. The bridge currents in phase A, phase B, and phase C of the winding are i_{bA}, i_{bB}, and i_{bC} respectively.

The bridge currents in the coil groups are shown in Figure 4.4. Similar to the bridge open condition the Kirchhoff's voltage law has been used to write the circuit equations for eight loops as shown in Equations (4.31) - (4.38) and the Kirchhoff's current law has been applied about the star point **O** as shown in Equation (4.39).

KVL for loop 1 ($\mathbf{O'AA_1OB_1BO'}$) can be written as

$$[Q_1 + Q_4 - Q_5 - Q_8]_{1\times n}\frac{d\{\mathbf{A}\}_{n\times 1}}{dt} + 2Ri_1 - 2Ri_2 \\ -Ri_{bA} + Ri_{bB} + 2L_{es}\frac{di_1}{dt} - 2L_{es}\frac{di_2}{dt} = V_B - V_A \tag{4.31}$$

KVL for loop 2 ($\mathbf{O'BB_2OC_1CO'}$) can be written as

$$[Q_6 + Q_7 - Q_9 - Q_{12}]_{1\times n}\frac{d\{\mathbf{A}\}_{n\times 1}}{dt} - 2Ri_2 - 2Ri_3 \\ +2Ri_B + Ri_{bB} + Ri_{bC} - 2L_{end}\frac{di_2}{dt} \\ -2L_{es}\frac{di_3}{dt} + 2L_{es}\frac{di_B}{dt} = V_C - V_B \tag{4.32}$$

KVL for loop 3 ($\mathbf{AA_2A_1A}$) can be written as

$$[Q_3 - Q_1]_{1\times n}\frac{d\{\mathbf{A}\}_{n\times 1}}{dt} - 2Ri_1 + Ri_A - R_b i_{bA} \\ -2L_{es}\frac{di_1}{dt} + L_{es}\frac{di_A}{dt} = V_{bA} \tag{4.33}$$

KVL for loop 4 ($\mathbf{OA_1A_2O}$) can be written as

$$[Q_2 - Q_4]_{1\times n}\frac{d\{\mathbf{A}\}_{n\times 1}}{dt} - 2Ri_1 + Ri_A + 2Ri_{bA} \\ +R_b i_{bA} - 2L_{es}\frac{di_1}{dt} + L_{end}\frac{di_A}{dt} + L_{es}\frac{di_{bA}}{dt} = V_{bA} \tag{4.34}$$

KVL for loop 5 ($\mathbf{B_1OB_2B_1}$) can be written as

$$[Q_5 - Q_7]_{1\times n}\frac{d\{\mathbf{A}\}_{n\times 1}}{dt} + 2Ri_2 - Ri_B + R_b i_{bB} \\ +2L_{es}\frac{di_2}{dt} - L_{es}\frac{di_B}{dt} = V_{bB} \tag{4.35}$$

KVL for loop 6 ($\mathbf{BB_1B_2B}$) can be written as

$$[Q_8 - Q_6]_{1\times n}\frac{d\{\mathbf{A}\}_{n\times 1}}{dt} + 2Ri_2 - Ri_B - 2Ri_{bB} \\ -R_b i_{bB} + 2L_{end}\frac{di_2}{dt} - L_{es}\frac{di_B}{dt} - 2L_{es}\frac{di_{bB}}{dt} = -V_{bB} \tag{4.36}$$

KVL for loop 7 ($\mathbf{C_1OC_2C_1}$) can be written as

$$[Q_9 - Q_11]_{1\times n}\frac{d\{\mathbf{A}\}_{n\times 1}}{dt} + 2Ri_3 - Ri_C \\ +R_b i_{bC} + 2L_{es}\frac{di_3}{dt} - L_{es}\frac{di_C}{dt} = V_{bC} \tag{4.37}$$

KVL for loop 8 ($\mathbf{CC_1C_2C}$) can be written as

$$[Q_{12} - Q_{10}]_{1\times n} \frac{d\{\mathbf{A}\}_{n\times 1}}{dt} + 2Ri_3 - Ri_C - 2Ri_{bC}$$
$$-R_b i_{bC} + 2L_{es}\frac{di_3}{dt} - L_{end}\frac{di_C}{dt} - 2L_{es}\frac{di_{bC}}{dt} = -V_{bC} \tag{4.38}$$

And Kirchoff's current law about point **O** can be applied as

$$i_A + i_B + i_C = 0 \tag{4.39}$$

Final circuit equation for stator winding can be written as

$$[Q]\,\frac{d\,\{A\}}{dt} + [R]\,\{I_s\} + [L_{es}]\left\{\frac{dI_s}{dt}\right\} = \{U_s\} \tag{4.40}$$

where $I_s = [i_1\ i_A\ i_2\ i_B\ i_3\ i_C\ i_{bA}\ i_{bB}\ i_{bC}]^{\intercal}$ and $U_s = [V_A - V_B\ V_B - V_C\ V_{bA}\ V_{bA}\ -V_{bB}\ V_{bB}\ -V_{bC}\ V_{bC}\ 0]^{\intercal}$. If there is no external supply across the bridge points the supply voltage would be represented as $U_s = [V_A - V_B\ V_B - V_C\ 0\ 0\ 0\ 0\ 0\ 0\ 0]^{\intercal}$.

4.3.4 Rotor bar circuit equation

The Squirrel cage rotor conductors are connected in parallel and short-circuited with each other using the end rings. Figure 4.5 represents the circuit connection of a squirrel cage rotor of an induction machine.

The rotor bar currents, for the rotor bar 1 to rotor bar 26 are I_{b1}, ..., I_{b26} respectively. The end ring

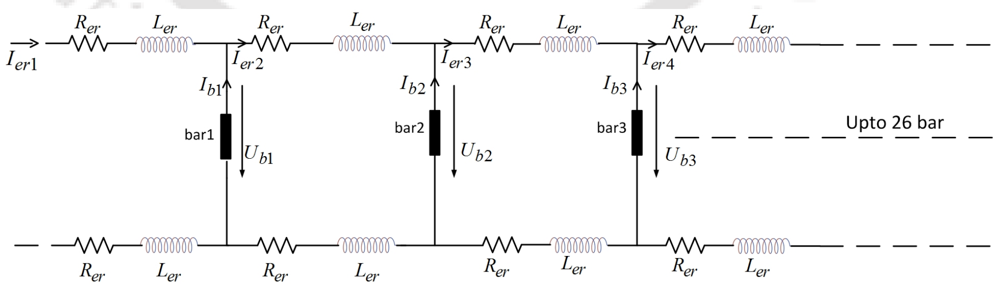

Figure 4.5: Parallel connection of the rotor bar conductors.

effect has been modeled with 26 end resistances (R_{er}) and 26 end inductances (L_{er}). The end ring currents for loop 1 to loop 26 are I_{er1}, ..., I_{er26} respectively. For each individual rotor bar the circuit equation can be written as

$$\begin{aligned} &Q_{r1}\tfrac{dA}{dt} + R_r I_{b1} - U_{b1} = 0 \\ &\vdots \\ &Q_{r26}\tfrac{dA}{dt} + R_r I_{b26} - U_{b26} = 0 \end{aligned} \tag{4.41}$$

where Q_{r1}, ..., Q_{r26} have been obtained by assembling Equation (4.20) for rotor bar 1 to rotor bar 26 respectively. The DC resistance of each rotor bar is R_r and U_{b1}, ..., U_{b26} are the voltage drop across rotor bar 1 to rotor bar 26 respectively. The rotor bar circuit equation, Equation (4.41) can be written in matrix form as

$$[Q_r]\,\frac{d\,\{A\}}{dt} + [R_r]\,\{I_r\} - \{U_r\} = 0 \tag{4.42}$$

The Kirchhoff's voltage law can be used to obtain the circuit equation for each loop as

$$\begin{aligned} &2R_{er}I_{er1} + 2l_{er}\tfrac{dI_{er1}}{dx} - U_{b1} + U_{b26} = 0 \\ &\vdots \\ &2R_{er}I_{er26} + 2l_{er}\tfrac{dI_{er1}}{dx} - U_{b26} + U_{b25} = 0 \end{aligned} \tag{4.43}$$

It can be written in matrix form as

$$2\,[R_{er}]\,\{I_{er}\} + 2\,[L_{er}]\,\frac{d\,\{I_{er}\}}{dt} + [M_2]\,\{U_r\} = 0 \tag{4.44}$$

where $[R_{er}] = \begin{bmatrix} R_{er} & \cdots & 0 \\ \vdots & \ddots & \vdots \\ 0 & \cdots & R_{er} \end{bmatrix}$, $[L_{er}] = \begin{bmatrix} l_{er} & \cdots & 0 \\ \vdots & \ddots & \vdots \\ 0 & \cdots & l_{er} \end{bmatrix}$, $[M_2] = \begin{bmatrix} -1 & 0 & 0 & \cdots & 1 \\ 1 & -1 & 0 & \cdots & 0 \\ \vdots & \vdots & \vdots & \cdots & \vdots \\ 0 & 0 & 0 & \cdots & -1 \end{bmatrix}$, $\{I_{er}\} = \begin{Bmatrix} I_{er1} \\ \vdots \\ I_{er26} \end{Bmatrix}$

.

The connection between the rotor bar currents and the end ring currents can be written as

$$\begin{Bmatrix} I_{b1} \\ I_{b2} \\ \vdots \\ I_{b26} \end{Bmatrix} = \begin{bmatrix} -1 & 1 & 0 & \cdots & 0 \\ 0 & -1 & 1 & \cdots & 0 \\ \vdots & \vdots & \vdots & \cdots & \vdots \\ 1 & 0 & 0 & \cdots & -1 \end{bmatrix} \begin{Bmatrix} I_{er1} \\ I_{er2} \\ \vdots \\ I_{er26} \end{Bmatrix} \tag{4.45}$$

Which can be written in matrix form as

$$\{I_r\} = [M_2]^T \{I_{er}\} \tag{4.46}$$

The final connection equation of the rotor bar and the end ring has been obtained by combining Equations (4.44) and (4.46) as

$$[M_2]^T [M_2] \{U_r\} + 2 [R_{er}] \{I_r\} + 2 [L_{er}] \frac{d \{I_r\}}{dt} = 0 \tag{4.47}$$

4.3.5 Transformation matrix

It can be observed from Equation (4.30) that in the case of bridge open condition there are six current variables available from the circuit equation which includes 3 phase currents and 3 branch currents. In bridge closed condition there are nine current variables available which includes 3 phase currents, 3 branch currents and 3 bridge currents as written in Equation (4.40). A transformation matrix is needed for the coupling of the circuit current in the magnetic field equation as the size of the source distribution matrix, [Ps], in the magnetic field equation, Equation (4.21) is $n \times z$. The value of z is 72 as we have 72 coil sides. The size of source current, I_s in bridge open and bridge closed conditions are 6×1 and 9×1 respectively. Hence transformation matrices of sizes 72×6 and 72×9 are required to couple the circuit currents in the field equation for bridge open and bridge closed condition respectively.

In modelling of the thin coils, three terms have been used, coil sides, full coil and coil group. Each slot of the machine has two layers and consist of two different coil sides, as shown in Figure 4.1. The two-coil sides of a coil are +a1 and -a1. The +ve sign indicates that the current is coming out of the plane and -ve sign indicates that the current is going into the plane. The coil groups W1, W2, W3 and W4 form phase A of the winding, the coil groups W5, W6, W7 and W8 form phase B of the winding and the coil groups W9, W10, W11 and W12 form the phase C of the winding as shown in Figure 4.2. There are 72 coil side currents, 36 full coil currents and 12 coil group currents. There are 6 circuit currents in bridge open condition and 9 circuit currents in bridge closed or bridge supply condition. Figure 4.6 represents the flow chart for conversion of circuit currents to coil side currents. Circuit currents are transformed to coil group currents and coil group currents are transformed to full coil currents and full coil currents are transformed to coil side currents. Conversion of group coil currents to full coil currents and coil side currents has same transformation matrix in bridge open and

Table 4.1: Current transformation group

Bridge Conditions	Coil Side Currents	Coil Currents	Group Coil Current	Circuit Currents
Open	72	36	12	6
Closed	72	36	12	9

bridge supply or bridge closed condition. For the transformation from full coil currents to coils side

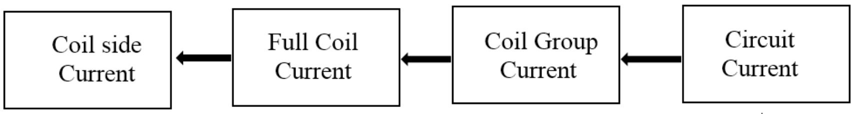

Figure 4.6: Winding arrangement of BCW machine.

currents, the following transformation has been used,

$$\begin{Bmatrix} +i_{a1} \\ -i_{a1} \\ \vdots \\ +i_{cc6} \\ -i_{cc6} \end{Bmatrix} = \begin{bmatrix} 1 & 0 & 0 & \cdots & 0 \\ -1 & 0 & 0 & \cdots & 0 \\ 0 & 0 & 0 & \cdots & 0 \\ \vdots & \vdots & \vdots & \cdots & 1 \\ 0 & 0 & 0 & \cdots & -1 \end{bmatrix} \begin{Bmatrix} i_{a1} \\ \vdots \\ i_{cc6} \end{Bmatrix} \tag{4.48}$$

Which can be written as

$$\{i_{coil\_side}\}_{72\times1} = [T_1]_{72\times36}\{i_{coil}\}_{36\times1} \tag{4.49}$$

Since each coil of the same coil group are connected in series so they must have the same current. For the transformation of phase A coil group currents to phase A full coil currents the following transformation has been used,

$$\begin{Bmatrix} i_{a1} \\ i_{a2} \\ i_{a3} \\ \vdots \\ i_{aa4} \\ i_{aa5} \\ i_{aa6} \end{Bmatrix} = \begin{bmatrix} 1 & 0 & 0 & 0 & \cdots & 0 & 0 \\ 1 & 0 & 0 & 0 & \cdots & 0 & 0 \\ 1 & 0 & 0 & 0 & \cdots & 0 & 0 \\ \vdots & \vdots & \vdots & \vdots & \cdots & \vdots & 0 \\ 0 & 0 & 0 & 0 & 0 & 0 & 1 \\ 0 & 0 & 0 & 0 & 0 & 0 & 1 \\ 0 & 0 & 0 & 0 & 0 & 0 & 1 \end{bmatrix} \begin{Bmatrix} i_{w1} \\ \vdots \\ i_{w12} \end{Bmatrix} \tag{4.50}$$

Similarly, the transformation matrices for two other phases can also be written and can be combined as

$$\{i_{coil}\}_{36\times1} = [T_2]_{36\times12}\{i_{coil\_group}\}_{12\times1} \tag{4.51}$$

For the case of bridge open condition the transformation from circuit currents to coil group current can be achieved as written in Equation (4.52).

$$\begin{Bmatrix} i_{w1} \\ i_{w2} \\ i_{w3} \\ i_{w4} \end{Bmatrix} = \begin{bmatrix} 1 & 0 \\ -1 & 1 \\ -1 & 1 \\ 1 & 0 \end{bmatrix} \begin{Bmatrix} i_1 \\ i_A \end{Bmatrix} \tag{4.52}$$

Similar transformation matrices can be obtained for phase B and phase C. The combined transformation matrix can be written as

$$\{i_{\,coil\_group}\}_{12\times1} = [T_o]_{12\times6}\{i_{circuit}\}_{6\times1} \tag{4.53}$$

In the case of bridge closed and bridge supply condition, the bridge currents pass through the bridge points in each phase. The transformation of circuit currents to coil group currents for phase A can be written as

$$\begin{Bmatrix} i_{w1} \\ i_{w2} \\ i_{w3} \\ i_{w4} \end{Bmatrix} = \begin{bmatrix} 1 & 0 & 0 \\ -1 & 1 & 0 \\ -1 & 1 & 1 \\ 1 & 0 & -1 \end{bmatrix} \begin{Bmatrix} i_1 \\ i_A \\ i_{bA} \end{Bmatrix} \tag{4.54}$$

Similar transformation matrices can be obtained for phase B and phase C. The combined transformation matrix can be written as

$$\{i_{\,coil\_group}\}_{12\times1} = [T_c]_{12\times9}\{i_{circuit}\}_{9\times1} \tag{4.55}$$

So, the final transformation matrix for the bridge open condition can be written as

$$\{i_{coil\_side}\}_{72\times1} = [T_{open}]_{72\times6}\{i_{circuit\_current}\}_{6\times1} \tag{4.56}$$

where $[T_{open}]_{72\times6} = [T_1]_{72\times36}[T_2]_{36\times12}[T_o]_{12\times6}$

Similarly, the final transformation matrix for the bridge closed or bridge supply condition can be written as

$$\{i_{coil\_side}\}_{72\times1} = [T_{closed}]_{72\times9}\{i_{circuit\_current}\}_{9\times1} \tag{4.57}$$

where $[T_{closed}]_{72\times9} = [T_1]_{72\times36}[T_2]_{36\times12}[T_c]_{12\times9}$

The combined discretized final field and circuit equations can be represented as

$$[K]_{n\times n}\{A\}_{n\times1} + [C_r]_{n\times n}\frac{\partial\{A\}_{n\times1}}{\partial t} - [P_s]_{n\times72}[T]_{72\times h}\{I_s\}_{h\times1} + [P_r]_{n\times26}\{U_r\} = 0 \tag{4.58}$$

$$[Q]_{h\times n}\frac{d\{A\}_{n\times1}}{dt} + [R]_{h\times h}\{I_s\}_{h\times1} + [L_{es}]_{h\times h}\left\{\frac{dI_s}{dt}\right\}_{h\times1} = \{U_s\}_{h\times1} \tag{4.59}$$

$$[Q_r]_{26\times n}\frac{d\{A\}_{n\times1}}{dt} + [R_r]_{26\times26}\{I_r\}_{26\times1} - \{U_r\}_{26\times1} = 0 \tag{4.60}$$

$$[M_2]^T_{26\times26}[M_2]_{26\times26}\{U_r\}_{26\times1} + 2[R_{er}]_{26\times26}\{I_r\}_{26\times1} + 2[L_{er}]_{26\times26}\frac{d\{I_r\}_{26\times1}}{dt} = 0 \tag{4.61}$$

where h is 6 in the case of bridge open condition and h is 9 in bridge closed or bridge supply condition.

4.3.6 Time-discretization

The combined field and circuit equations for thick and thin conductors are shown in Equations (4.58) - (4.61). This system of differential equations have been solved using Crank-Nicolson method. The Crank-Nicolson method is a second-order method, which is implicit in time and numerically stable. The time-discretization of Equations (4.58) - (4.61) in matrix form can be written as shown in Equation (4.62). The boundary condition has been applied by forcing the magnetic vector potential (A) to be zero at the outer boundary of the machine.

$$\begin{bmatrix} \left(\begin{matrix} [K]^{t+\Delta t}+ \\ \frac{2}{\Delta t}[C_r] \end{matrix} \right) & [P_s][T] & [\mathbf{0}] & [P_r] \\ \frac{2}{\Delta t}[Q_s] & [R]+\frac{2}{\Delta t}L_{es} & [\mathbf{0}] & [\mathbf{0}] \\ \frac{2}{\Delta t}[Q_r] & [\mathbf{0}] & [R_r] & [T_r] \\ [\mathbf{0}] & [\mathbf{0}] & \begin{matrix} [R]+ \\ \frac{2}{\Delta t}L_{es} \end{matrix} & M_2^T M_2 \end{bmatrix} \{D\}^{t+\Delta t}$$

$$= - \begin{bmatrix} \left(\begin{matrix} [K]^{t+\Delta t} \\ -\frac{2}{\Delta t}[C_r] \end{matrix} \right) & [P_s][T] & [\mathbf{0}] & P_r \\ -\frac{2}{\Delta t}[Q_s] & [R]-\frac{2}{\Delta t}L_{es} & [\mathbf{0}] & [\mathbf{0}] \\ -\frac{2}{\Delta t}[Q_r] & [\mathbf{0}] & [R_r] & [T_r] \\ [\mathbf{0}] & [\mathbf{0}] & \begin{matrix} [R_{er}]- \\ \frac{2}{\Delta t}[L_{er}] \end{matrix} & M_2^T M_2 \end{bmatrix} \{D\}^{t} \tag{4.62}$$

$$+\{S\}^{t+\Delta t}+\{S\}^{t}$$

where $\{S\} = \begin{Bmatrix} \{\mathbf{0}\}_{n\times1} \\ \{U_s\}_{m\times1} \\ \{\mathbf{0}\}_{26\times1} \\ \{\mathbf{0}\}_{26\times1} \end{Bmatrix}$ and $\{D\} = \begin{Bmatrix} \{\mathbf{A}\}_{n\times1} \\ \{I_s\}_{m\times1} \\ \{I_r\}_{26\times1} \\ \{U_r\}_{26\times1} \end{Bmatrix}$

4.3.7 Modelling of rotor eccentricity

To incorporate the rotor movement and the rotor eccentricity, the air gap stitching method has been applied. Figure 4.7 represents the meshed region of the stator and the rotor domains.

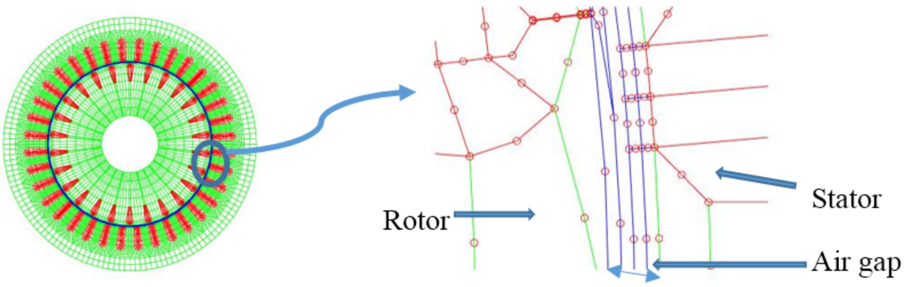

Figure 4.7: Meshed stator and rotor with unmeshed air gap.

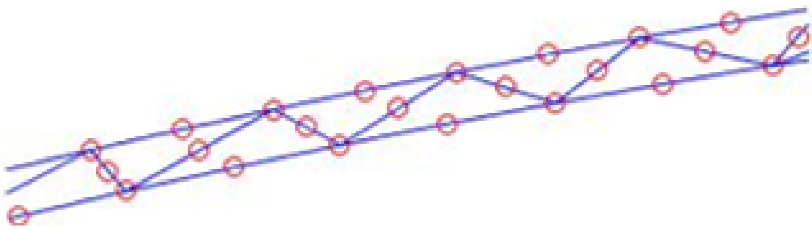

Figure 4.8: Stitching in air gap region.

It can be observed from Figure 4.7 that the air gap region has been divided in four parts. Two parts of the air gap have been modeled with the stator region and one part of the air gap has been modeled with the rotor region. To incorporate the rotation and the eccentricity condition the remaining part of the air gap is stitched using six-noded triangular elements as shown in Figure 4.8. The following algorithm has been used for the stitching of the air gap region. Suppose A, C, E, G, ... are the stator

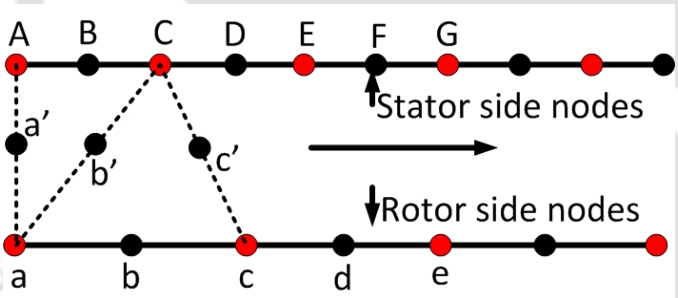

Figure 4.9: Algorithm used for air gap stitching.

side nodes and B, D, F, ... are its mid-side nodes. Similarly, a, c, e, ... are the rotor side nodes and b, d, ... are its mid-side nodes as shown in Figure 4.9. At first any two nodes from the stator side and the rotor side, for example Aa is connected arbitrarily. Now the shorter distance between Ac and aC is chosen to form the first triangle. Considering aC<Ac, △ aAC can be formed. The mid-point of the aC is chosen for the mid-side node of aC. The next triangle is formed by choosing the shorter distance between aE and Cc. In the similar manner the whole domain is stitched. For the incorporation of rotation and eccentricity condition, one portion of the air gap is restitched at each time step.This process is carried out in three steps. First of all rotor portion is rotated about the center point and then its location is shifted as per the eccentricity condition and after that stitching between the rotor side nodes and the stator side nodes is carried out. A rotor is said to be statically eccentric if the rotor centre does not coincide with the stator centre and the rotor rotates about the rotor centre.

The rotor is said to be dynamically eccentric when the rotor centre does not coincide with the stator centre and the rotor rotates about its centre as well as whirls about the stator centre. A rotor is said to have mixed eccentricity if the rotor centre does not coincide with the stator centre and the rotor rotates about its centre as well as whirls about any other point in between the stator centre and the rotor centre.

4.4 Numerical investigation

The coupled field and circuit equation shown in Equation (4.62) has been simulated for two second to calculate the magnetic vector potential at each node, the circuit currents, the rotor bar currents and the voltage across each rotor bar. The magnetic flux density in the air gap has been calculated from the obtained magnetic vector potential using the relationship, $B = \nabla \times A$ and subsequently the transverse forces (F_x, F_y) acting on the rotor have been calculated using the Maxwell stress tensor method as explained in [81]. The calculation of forces has also been explained in Chapter 6. A self developed preprocessor has been used to generate the mesh for the numerical simulation where the stator, rotor and air gap domain has 5760, 3536 and 1025 elements respectively. Time stepping scheme, Crank Nicolson method and MATLAB's inbuilt solver has been used for the simulation.

The results have been generated for two conditions, when (i) bridge connections of the winding are open or bridge OFF condition, (ii) bridge connections of the winding are closed or bridge ON condition. Table 4.2 shows the important parameters of the induction machine used for the simulation. The machine parameters have been calculated using the expressions explained in [99]. The simulation has been carried out for all three types of eccentricity conditions. For the investigation of the static eccentricity condition, the rotor has been shifted by a distance of 1e-4 m along the x-axis which is 10 % of the air gap and the rotor rotates about this point. In case of the dynamic eccentricity the rotor center rotates about the center point of the stator with a whirling radius of 1e-4 m and the rotor also rotates about its own center. Whereas, in the mixed eccentricity condition a static eccentricity of 0.5e-4 m, which is 5% of the air gap, has been given along the x-axis, the rotor center rotates about this point with a whirling radius of 0.5e-4 m and the rotor rotates about its own center as well. The bridge currents and the transverse forces acting on the rotor have been analyzed to study the effect of different eccentricity conditions. The bridge currents, and transverse forces acting on the rotor have been converted to the complex domain to investigate the various modes of the bridge currents

Table 4.2: BCW machine parameters

Parameters	Value
No. of poles	4
No. of stator slots	36
No. of rotor bars	26
Outer dia. of stator	160 mm
Outer dia. of rotor	103 mm
Air gap length	1 mm
Axial length of the motor	135 mm
Resistance per phase	6.8 Ω
End winding inductance	3.94 e-4 A/m
Resistance of each rotor bar	1 e-5 Ω
Rotor end ring resistance	2.49e-6 Ω
Rotor end ring inductance	1.54 E-8 A/m
Supply voltage	37 V, 50 Hz
Slip	0.02

and forces. Three phase bridge currents have been converted from a, b, c to d, q, 0 sequence using Equation (4.63), where d, q represent the orthogonal components of current and 0 is the zero sequence component of the current. The space vector of the bridge currents can be written as $d + jq$. Similarly, transverse forces can be written in complex form as $F_x + jF_y$, where F_x is the force acting along x axis and F_y is the force acting along y axis. A full spectrum Fast Fourier Transform of space vector of bridge currents and transverse forces have been carried out to investigate the relationship between the bridge current modes and force modes. Generally in balanced system zero sequence component of current is negligible, however a substantial amount of zero sequence component of bridge current is present in bridge configured winding. Fast Fourier Transform of zero sequence component of bridge current has also been carried out to know its frequency components.

$$\begin{Bmatrix} d \\ q \\ 0 \end{Bmatrix} = \begin{bmatrix} \cos(0) & \cos\left(-\frac{2\pi}{3}\right) & \cos\left(\frac{2\pi}{3}\right) \\ -\sin(0) & -\sin\left(-\frac{2\pi}{3}\right) & -\sin\left(\frac{2\pi}{3}\right) \\ 0.5 & 0.5 & 0.5 \end{bmatrix} \begin{Bmatrix} a \\ b \\ c \end{Bmatrix} \tag{4.63}$$

Figures 4.10 and 4.11 represent the bridge currents and full spectrum Fast Fourier Transform (FFT) of bridge currents space vector in static eccentricity condition respectively. Figures 4.12 and 4.13 represent zero sequence component of bridge currents in static eccentricity condition and its FFT respectively. Figures 4.14 and 4.15 represent the bridge currents and full spectrum FFT of space vector

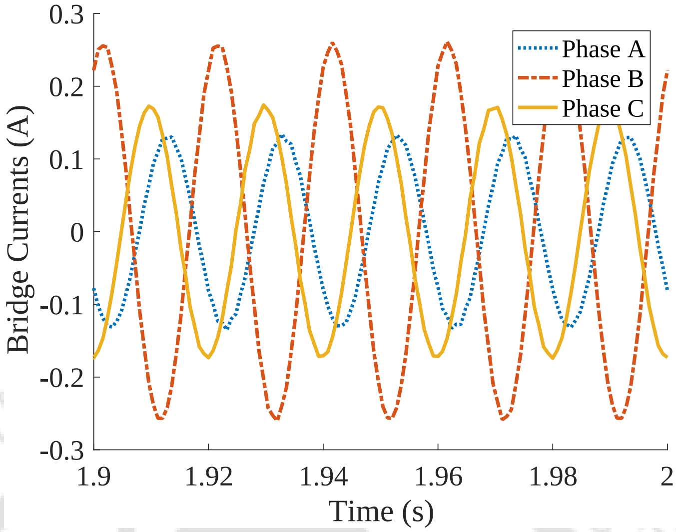

Figure 4.10: Bridge currents in static eccentricity condition.

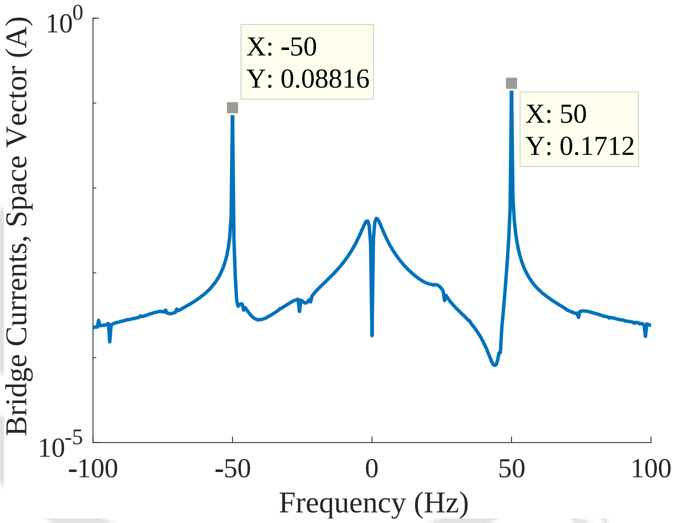

Figure 4.11: Full spectrum FFT of space vector of bridge currents in static eccentricity condition.

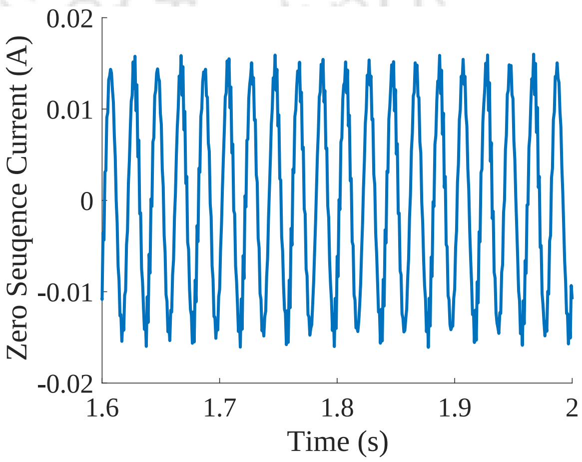

Figure 4.12: Zero sequence component of bridge currents in static eccentricity condition.

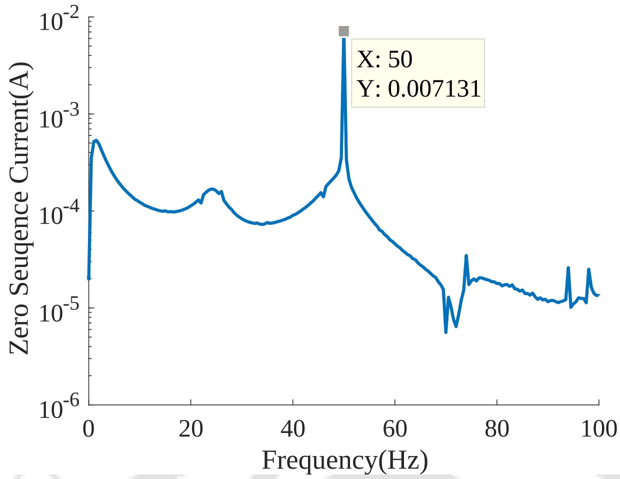

Figure 4.13: FFT of zero sequence of bridge current in static eccentricity condition.

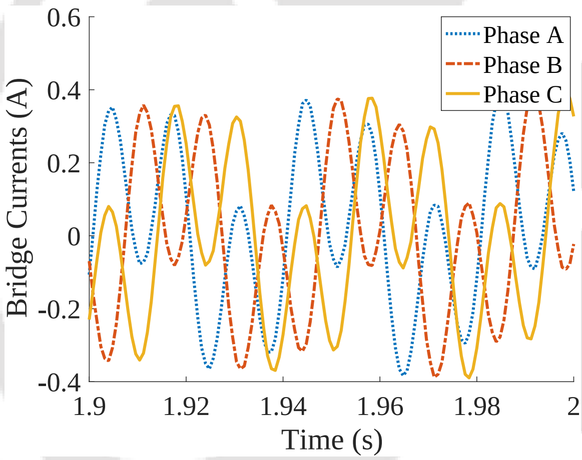

Figure 4.14: Bridge currents in dynamic eccentricity condition.

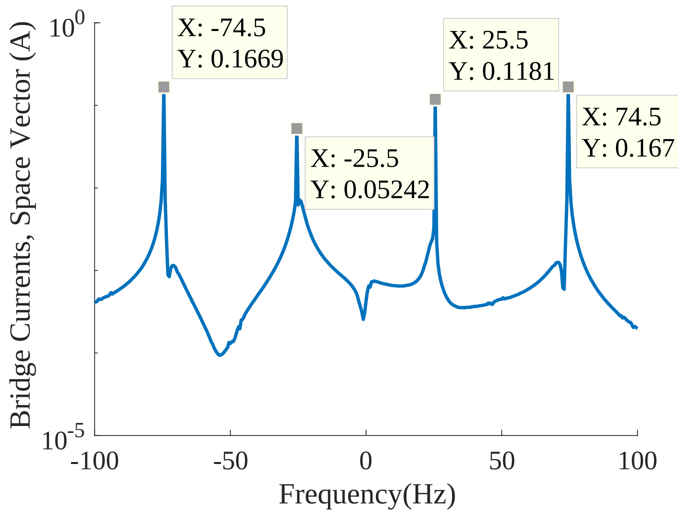

Figure 4.15: Full spectrum FFT of space vector of bridge currents in dynamic eccentricity condition.

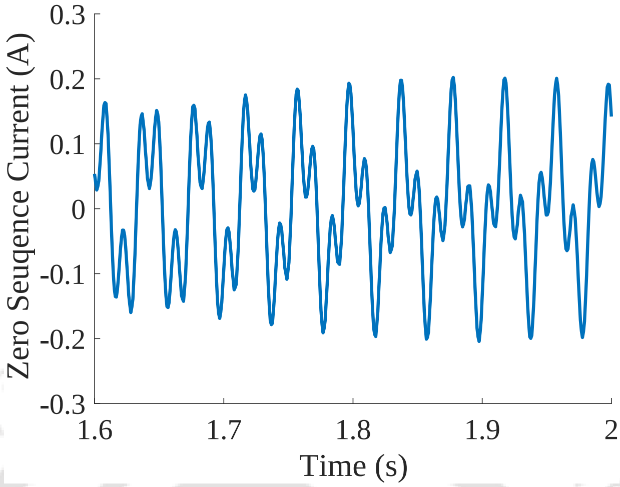

Figure 4.16: Zero sequence component of bridge currents in dynamic eccentricity condition.

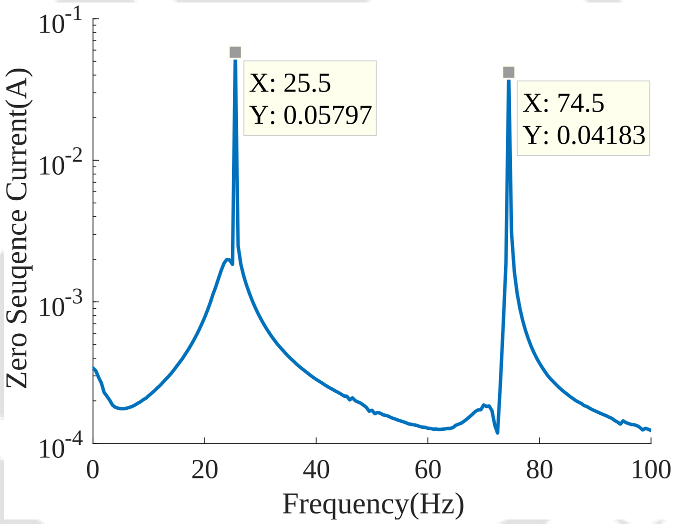

Figure 4.17: FFT of zero sequence of bridge currents in dynamic eccentricity condition.

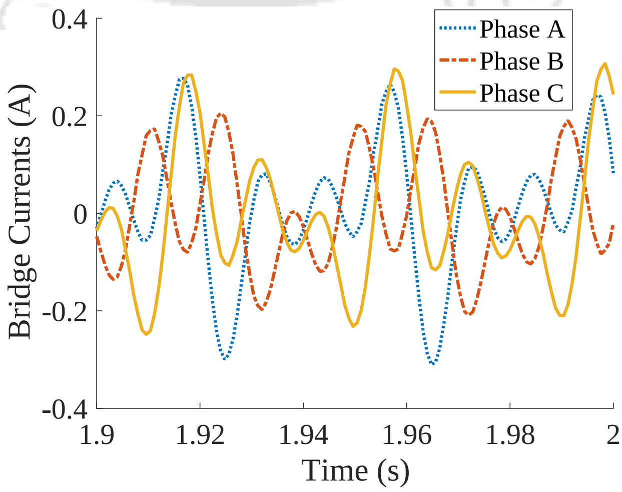

Figure 4.18: Bridge currents in mixed eccentricity condition.

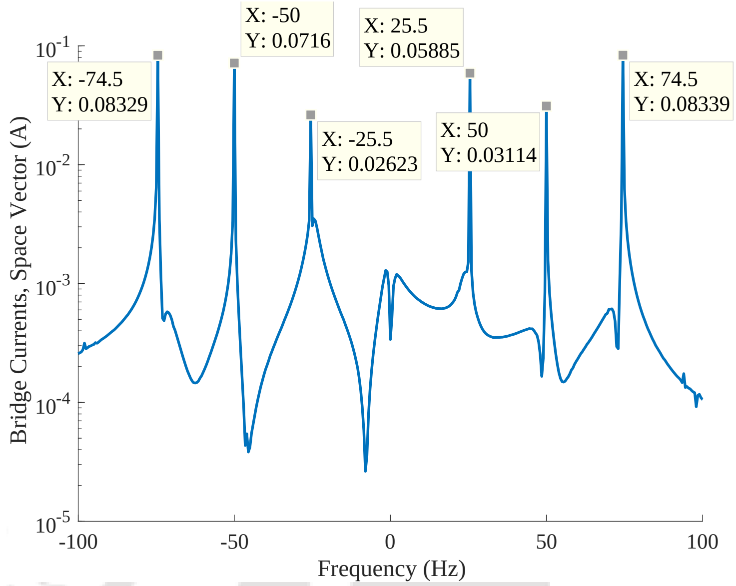

Figure 4.19: Full spectrum FFT of space vector of bridge currents in mixed eccentricity condition.

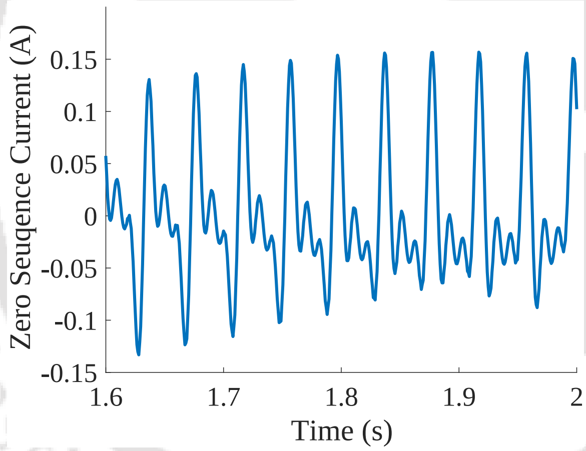

Figure 4.20: Zero sequence component of bridge currents in mixed eccentricity condition.

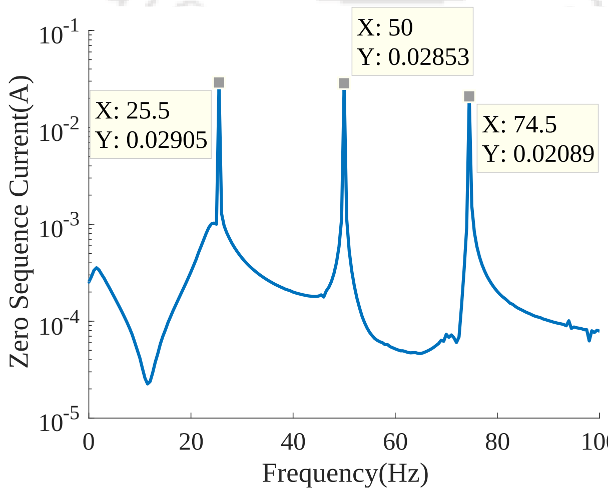

Figure 4.21: FFT of zero sequence bridge currents in mixed eccentricity condition.

of bridge currents in dynamic eccentricity condition respectively. Figures 4.16 and 4.17 represent zero sequence component of bridge currents and its FFT in dynamic eccentricity condition respectively. Figures 4.18 and 4.19 represent bridge currents and full spectrum FFT of space vector of bridge currents in mixed eccentricity condition. Figures 4.20 and 4.21 represent zero sequence component of bridge currents and its FFT in mixed eccentricity condition respectively.

It is a known fact that the eccentric position of a rotor generates $p\pm1$ pole pair magnetic field in the air gap, where p is the fundamental pole pair of the winding. However, these magnetic field components have different angular frequency in different eccentricity conditions. The angular frequency of these components in static and dynamic eccentricity are f_s and $f_s \pm f_r$ respectively [45]. The rotor frequency is given by $f_s(1-s)/p$, where s is the slip. The simulated bridge configured winding is a 4- pole winding, hence eccentric position of the rotor generates 2-pole and 6-pole magnetic fields in the air gap. Based on the above mentioned relationships it can be found that the angular frequency of the 2-pole and 6-pole magnetic fields in the static eccentricity condition is 50 Hz, whereas in dynamic eccentricity condition the angular frequency of 2-pole magnetic field is 25.5 Hz and the angular frequency of 6-pole magnetic field is 74.5 Hz. These magnetic field components create potential difference across the bridge points of the bridge configured winding. When these bridge points are short circuited or in bridge ON condition current flows in the winding which has same frequency components as that of the eccentricity generated magnetic field.

In static eccentricity condition, the space vector of bridge currents have only supply frequency component (f_s) i.e. 50 Hz. In dynamic eccentricity condition the space vector of bridge currents have $f_s \pm f_r$ components i.e. 25.5 Hz and 74.5 Hz. In mixed eccentricity condition the space vector of the bridge currents have combination of the static and dynamic eccentricity components and they are 25.5 Hz, 50 Hz and 74.5 Hz. In all eccentricity conditions the space vector of the bridge currents have both negative and positive mode. A substantial amount of zero sequence component of bridge currents is also present in all the eccentricity conditions, which has the same frequency components as that of the respective space vector of the bridge currents.

Figures 4.22, 4.23 and 4.24 represent the full spectrum FFT of force acting on the rotor in static eccentricity condition, dynamic eccentricity condition and mixed eccentricity condition respectively. The relationship between different bridge current modes and transverse force modes can be written as $\pm f_s \pm f_{bridge}$. Here, f_{bridge} is the frequency component of space vector of bridge currents. It can be

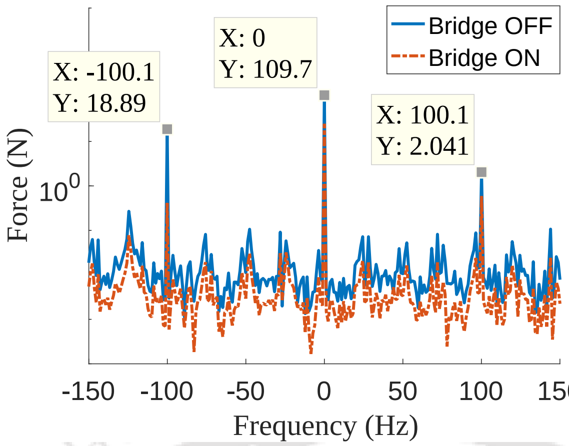

Figure 4.22: Full spectrum FFT of force in static eccentricity condition.

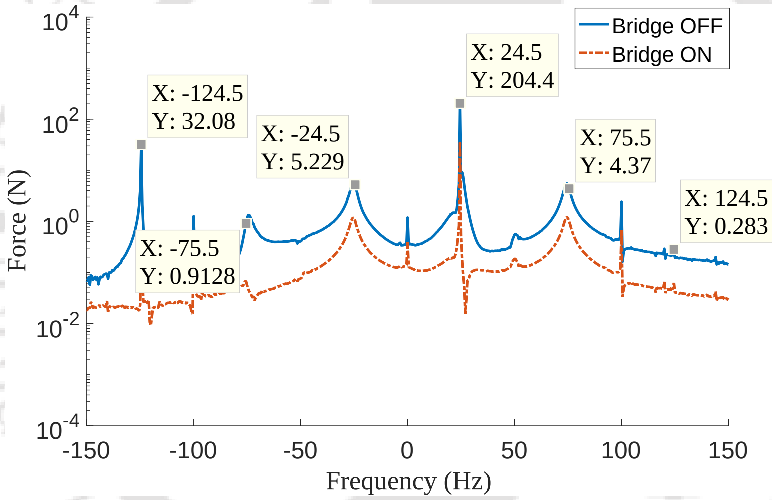

Figure 4.23: Full spectrum FFT of force in dynamic eccentricity condition.

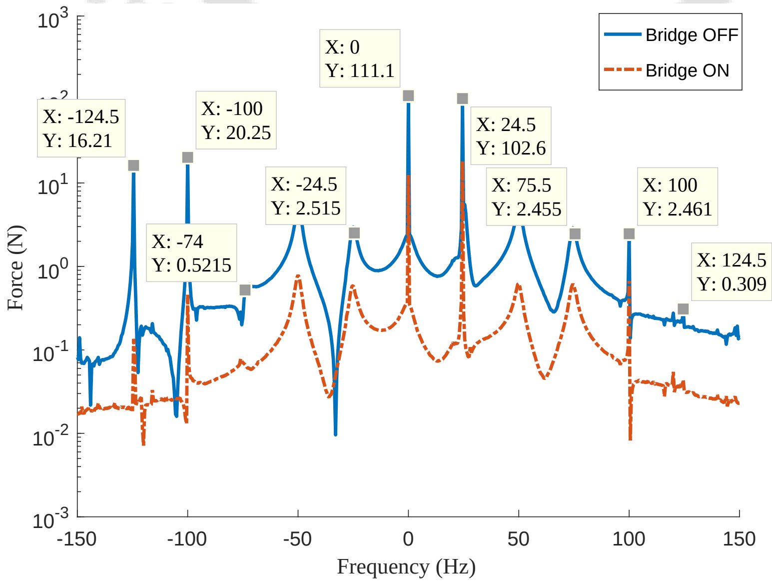

Figure 4.24: Full spectrum FFT of force in mixed eccentricity condition.

observed in Figure 4.22 that in the static eccentricity condition, when bridges are in OFF condition, the forces acting on the rotor has three components, 0 Hz and ± 100 Hz (±50 ± 50), whereas in bridge ON condition the double supply frequency component ($\pm 2f_s$) becomes almost negligible and only the DC component (0 Hz) of the force acts on the rotor. It can be seen in Figure 4.23 that in the dynamic eccentricity condition, when bridges are in OFF condition the force acting on the rotor has six components, ± 24.5 Hz, ± 75.5 Hz and ±124.5 Hz (±50 ± 25.5 and ±50 ± 74.5), whereas in bridge ON condition most of the force component becomes negligibly small and only $+f_r$ (24.5 Hz) component of the force acts on the rotor. In the mixed eccentricity condition all the frequency components of the forces of static and dynamic eccentricity conditions are present. It can be observed in Figure 4.24 that in bridge OFF condition the forces acting on the rotor have 0 Hz, ± 24.5 Hz, ±100 Hz, ± 75.5 Hz and ± 124.5 Hz component whereas in bridge ON condition the forces acting on the rotor has 0 Hz component and $+f_r$ (24.5 Hz) component. Table 4.3 represents the summary of the numerical investigation of bridge currents and UMP.

Table 4.3: Summary of the numerical investigation of bridge currents and UMP

Numerical Simulation						
Type of Eccentricity	Supply Freq.	Slip	Bridge Currents		UMP	
			Space Vector Component	Zero Sequence Component	Bridge OFF	Bridge ON
Static Eccentricity	50 Hz	0.02	±50 Hz	50 Hz	0 Hz, ± 100 Hz	0 Hz
Dynamic Eccentricity	50 Hz	0.02	± 24.5 Hz, ± 74.5 Hz	24.5 Hz, 74.5 Hz	± 24.5Hz, ± 75.5 Hz ± 124.5 Hz	24.5 Hz
Mixed Eccentricity	50 Hz	0.02	0 Hz, ± 24.5 Hz, ± 74.5 Hz	0 Hz, 24.5 Hz, 74.5 Hz	0 Hz, ± 24.5 Hz, ± 75.5 Hz, ± 100 Hz, ± 124.5 Hz	0 Hz, 24.5 Hz

4.5 Conclusion

A FE modelling of a 36 slots 4 pole induction machine with bridge configured winding has been carried out to study the effect of eccentric rotor on the bridge currents and the forces acting on the rotor. This model is able to provide correct behavior of bridge currents and UMP generated due to an eccentric rotor in all types of eccentricity conditions. Various modes of the bridge currents have been analysed by transforming it from a, b, c sequence to $d, q, 0$ sequence. A relationship of bridge current modes with respect to different eccentricity conditions have been established. Also, it has been shown that the zero sequence component of the bridge currents can not be ignored in bridge configured winding. The space vector of bridge currents show the presence of only one frequency component i.e. $\pm f_s$, two frequency components i.e. $\pm(f_s - f_r)$, $\pm(f_s + f_r)$ and three frequency components i.e. $\pm f_s$, $\pm(f_s - f_r)$ and $\pm(f_s + f_r)$ of the bridge currents for the case of the static, dynamic and mixed eccentricity conditions respectively. A relationship with respect to the main supply frequency component (f_s) and bridge currents frequency component (f_{bridge}) has been established. It has been shown that the developed UMP due to the eccentric rotor in bridge OFF condition has $\pm f_s \pm f_{bridge}$ frequency components. It has been also established that bridge currents suppresses all the UMP components other than DC component and $f_s - f_r$ component. It happens because eccentric rotor generates pulsating component of magnetic field which gets suppressed when bridges are in ON condition.

5

Magnetomotive Force Analysis

Contents

5.1 Introduction

The previous chapters deal with bridge configured winding induction machine in different eccentricity conditions. However, the magnetic fields and transverse force due to the bridge supply have not been analysed. A bridge supply through the bridge terminals of a four pole bridge configured winding induction machine generates both two pole and six pole magnetic field harmonics [80]. However, to generate a controllable transverse force only one component of the magnetic field is required. Hence, a further study of BCW winding is important so that the magnetic field generation with respect to the bridge supply can be ascertained. In this chapter, magneto-motive force (MMF) analysis of a bridge configured winding electrical machine having four pole main field has been carried out to establish the generation of the two pole and six pole magnetic fields with respect to the bridge supply conditions.

5.2 MMF analysis of BCW winding

A BCW winding can accommodate two supply sources as it has been discussed in the previous Chapters. The MMF analysis has been carried out to understand the winding configuration with respect to two different supply sources. Figure 5.1 represents circuit diagram and Table 5.1 represents the winding configuration of BCW winding scheme which has been used for the MMF analysis of the bridge configured winding configuration. Points **A, B**, and **C** represent the main supply terminals whereas point **A1-A2**, **B1-B2** and **C1-C2** represent the bride supply terminals.

A three-phase supply can be connected at the main supply terminals **A, B** and **C** to produces a four pole magnetic field (p pole pair of magnetic field) and hence interactions of this field with rotor bar generates a torque and the rotor rotates. Whereas, the bridge points of each phase (**A1 - A2**, **B1 - B2**, and **C1 - C2**) can be excited individually using a supply source which is isolated from the main supply. An isolated supply at the bridge points of the winding creates asymmetry in the magnetic field ($p \pm 1$ pole pair of magnetic field), which generates unbalanced magnetic pull. The MMF analysis has been carried out to investigate the production of different magnetic fields due to these supply sources. Figures 5.2(a) and 5.2(b) represent the MMF axis of a bridge configured winding electrical machine with respect to the main supply and bridge supply respectively. It can be seen that the MMF axes of phase A, Phase B and Phase C of the winding are 120 degree apart when it is analysed with respect to the main supply terminals, whereas MMF axes are 60 degree apart when it is analysed with respect to the bridge supply terminals. It indicates that if the supply direction of Phase B of the bridge supply

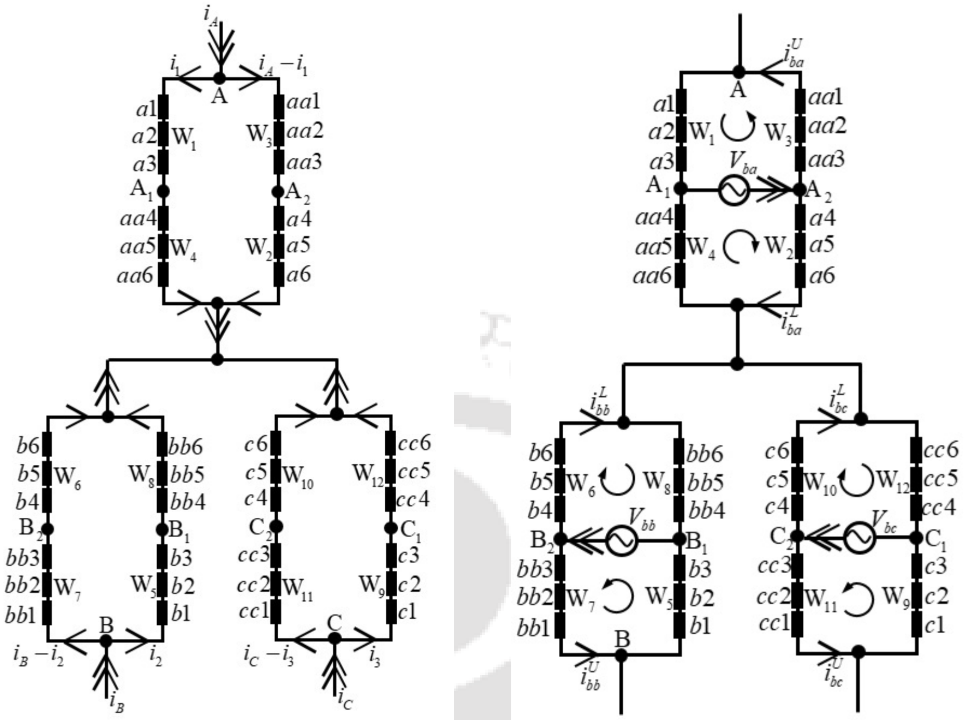

(a) (b)

Figure 5.1: Circuit diagram of BCW winding scheme used for MMF analysis (a) excited using main supply (b) excited using only bridge supply.

is reversed, a rotating magnetic field can be generated.

To verify this phenomena, the MMF distribution has been plotted at a particular time instant, when a sinusoidal current of unit magnitude with a frequency of 50 Hz has been applied in a 36 slot BCW electrical machine in the following four conditions

(i) A three phase supply with respect to the main supply terminals

(ii) A three phase supply with respect to the bridge supply terminals

(iii) A three phase supply with respect to the bridge supply terminals and direction of the supply of phase B is reversed

(iv) A DC supply with respect to the bridge supply terminals and direction of phase B is reversed

Table 5.1 shows the winding distribution which has been considered to plot the MMF distribution in these four conditions. Here, $(a1 - a6)$ and $(aa1 - aa6)$ represents phase A coils, $(b1 - b6)$ and $(bb1 - bb6)$ represents phase B coils, $(c1 - c6)$ and $(cc1 - cc6)$ represents phase C coils. The MMF

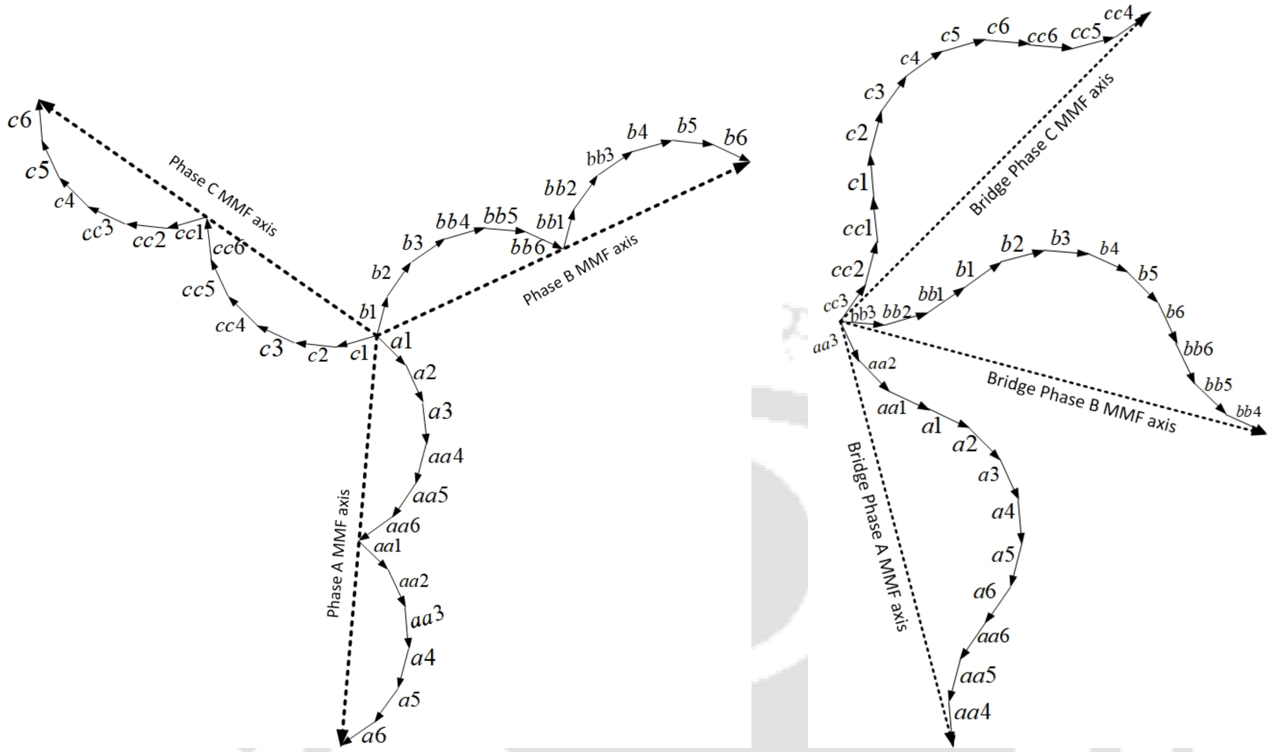

(a) (b)

Figure 5.2: MMF axis with respect to (a) main supply (b) bridge supply.

distribution has been obtained by discrete integration of the distributed current across the slot at each time instant.

The obtained MMF variation with respect to the angular position has been plotted for all the four cases. Here, for the sake of representation, the MMF distribution has been represented at a particular time instant. Figure 5.3(a) represents the MMF distribution, when winding is excited with respect to the main terminals using three phase supply at time, $t = 0.016$ s. It represents the formation of four pole magnetic field for the case when BCW machine is excited with respect to the main terminals. Figure 5.3(b) represents the MMF distribution for the case when BCW machine is excited using normal three phase bridge supply with respect to the bridge terminals at time, $t = 0.016$ s. It demonstrates the presence of additional magnetic field harmonic components along with the two pole magnetic field component. Figure 5.3(c) represents the MMF distribution for the case when BCW machine is excited using bridge supply with respect to bridge terminals with reversal of phase B current at time, $t = 0$ s. It demonstrates the clear formation of two pole magnetic field when the direction of current in phase B of the supply is reversed. Figure 5.3(d) represents the MMF distribution for the case, when phase

B of the bridge supply is reversed and bridge points are excited using a DC supply at time, $t = 0.016$ s. It demonstrates the formation of six pole magnetic field when same phase of supply with reversal of direction of current in phase B of the winding is applied with respect to the bridge terminals. The generation of two pole and six pole magnetic field with respect to different bridge supply conditions have also been verified using finite element model of BCW machine described in Chapter 3. Figure 5.4(a) describes the formation of mixed magnetic field when a three phase supply has been given through the bridge terminals. Figure 5.4(b) describes the formation of two pole magnetic field when phase B of the three phase bridge supply is reversed. Figure 5.4(c) describes the formation of six pole magnetic field when a DC supply is given through the bridge terminals and phase B of the bridge supply is reversed.

Table 5.1: Winding distribution of bridge configured winding

Slot	Deg	Inner	Outer		Slot	Deg	Inner	Outer
1	5	-cc4	+a1		19	185	-c4	+aa1
2	15	-cc5	+a2		20	195	-c5	+aa2
3	25	-cc6	+a3		21	205	-c6	+aa3
4	35	-bb1	+a4		22	215	-b1	+aa4
5	45	-bb2	+a5		23	225	-b2	+aa5
6	55	-bb3	+a6		24	235	-b3	+aa6
7	65	-bb4	+cc1		25	245	-b4	+c1
8	75	-bb5	+cc2		26	255	-b5	+c2
9	85	-bb6	+cc3		27	265	-b6	+c3
10	95	-aa1	+cc4		28	275	-a1	+c4
11	105	-aa2	+cc5		29	285	-a2	+c5
12	115	-aa3	+cc6		30	295	-a3	+c6
13	125	-aa4	+bb1		31	305	-a4	+b1
14	135	-aa5	+bb2		32	315	-a5	+b2
15	145	-aa6	+bb3		33	325	-a6	+b3
16	155	-c1	+bb4		34	335	-cc1	+b4
17	165	-c2	+bb5		35	345	-cc2	+b5
18	175	-c3	+bb6		36	355	-cc3	+b6

5.3 Analytical formulation of force

In order to understand the force production in BCW machine, an analytical expression of force expression has been developed using Fourier coefficients of MMF as a function of the current distribution in the winding as shown in [80]. Each phase of the BCW winding has two parts upper and lower part as shown in Figure 5.1(b). Upon excitation through the bridge points, the current gets divided in

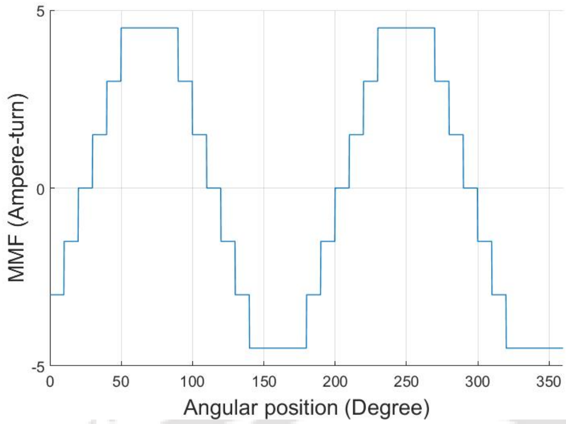

(a)

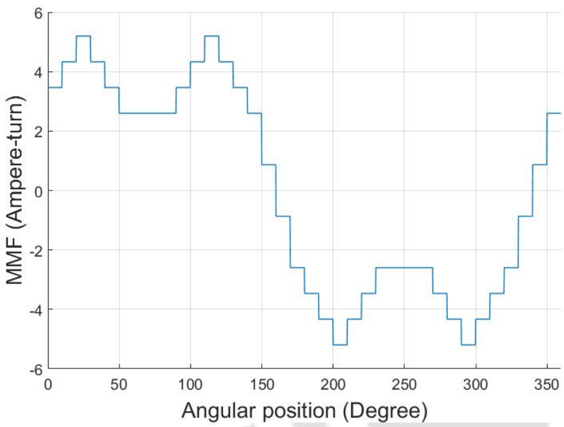

(b)

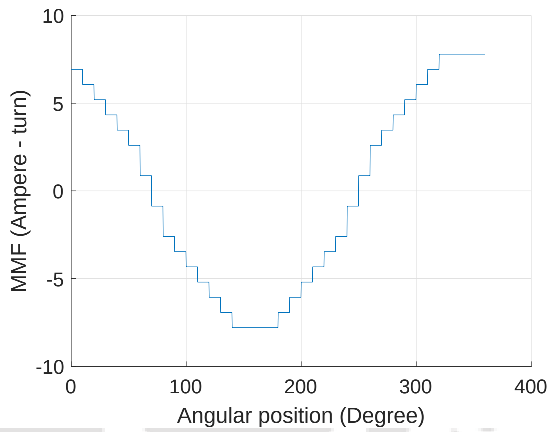

(c)

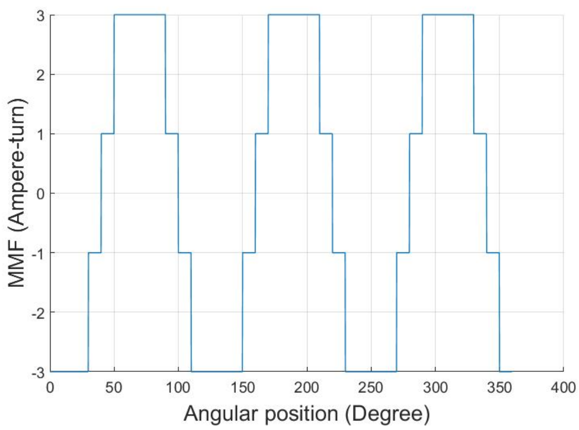

(d)

Figure 5.3: MMF distribution with respect to the angular position at time, $t = 0.016$ s, when (a) three phase current supply has been applied with respect to the the main supply terminals of the winding (b) three phase current supply has been applied with respect to the bridge supply terminals of the winding (c) three phase current supply has been applied with respect to the bridge supply terminals of the winding and direction of phase B supply has been reversed (d) a DC current supply has been applied with respect to the bridge supply terminals of the winding and direction of phase B supply has been reversed.

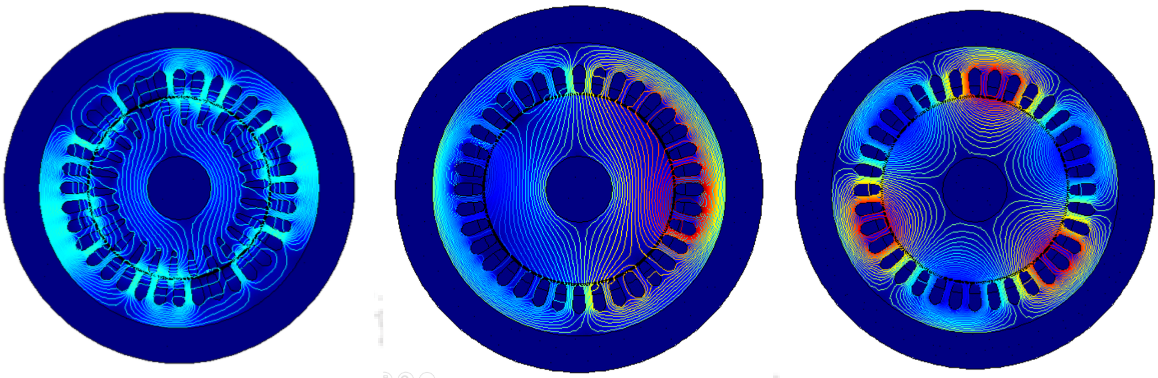

(a) (b) (c)

Figure 5.4: Magnetic field obtained from FE model of BCW induction machine described in Chapter 3 when (a) bridge terminals are supplied by a normal sequence of three phase supply (b) phase B of the three phase bridge supply is reversed (c) a DC supply is given through the bridge terminals and phase B of the bridge supply is reversed.

these two parts. Hence, a DC current of 1 A has been provided in the coils forming upper and lower section of the circuit connection individually. Upon excitation of these upper and lower sections of each phase of the winding, MMF variation has been obtained through the discrete integration. The FFT of the MMF variation has been carried out to separate the 1st harmonics (two pole magnetic field) and 3rd harmonics (six pole magnetic field) components. To know the combined effect of excitation of all the three phases through the bridge points, the obtained components have been added. These excitation currents have been termed as, i_{au}, i_{al} for the phase A bridge currents. i_{bu}, i_{bl} for the phase B bridge currents, i_{cu}, i_{cl} for the phase C bridge currents. The relationship between magnetic field and magnetomotive force can be represented as

$$B = \lambda f_{mm} \tag{5.1}$$

where λ is the air gap permeance and f_{mm} is the magnetomotive force. This can be re-written using Fourier coefficients of 1st and 3rd harmonics of MMF distribution for the case when BCW machine is excited with respect to the bridge terminals as

$$\begin{aligned} B = {} & \frac{\mu_0}{\delta_0} n_0 \,\mathrm{Re}\left[\left(c^a_{1u} e^{-j\theta} + c^a_{3u} e^{-j3\theta}\right) i^U_{ba} + \left(c^a_{1l} e^{-j\theta} + c^a_{3l} e^{-j3\theta}\right) i^L_{ba}\right] \\ & + \frac{\mu_0}{\delta_0} n_0 \,\mathrm{Re}\left[\left(c^b_{1u} e^{-j\theta} + c^b_{3u} e^{-j3\theta}\right) i^U_{bb} + \left(c^b_{1l} e^{-j\theta} + c^b_{3l} e^{-j3\theta}\right) i^L_{bb}\right] \\ & + \frac{\mu_0}{\delta_0} n_0 \,\mathrm{Re}\left[\left(c^c_{1u} e^{-j\theta} + c^c_{3u} e^{-j3\theta}\right) i^U_{bc} + \left(c^c_{1l} e^{-j\theta} + c^c_{3l} e^{-j3\theta}\right) i^L_{bc}\right] \end{aligned} \tag{5.2}$$

This can be rewritten as

$$\begin{aligned} B &= \frac{\mu_0}{\delta_0} n_0 \,\mathrm{Re}\left[\left(c_{1u}^a e^{-j\theta} + c_{3u}^a e^{-j3\theta}\right) i_{ba}^U + \left(c_{1u}^a e^{j\pi/6} e^{-j\theta} + c_{3u}^a e^{j\pi/2} e^{-j3\theta}\right) i_{ba}^L\right] \\ &+ \frac{\mu_0}{\delta_0} n_0 \,\mathrm{Re}\left[\left(c_{1u}^b e^{-j\theta} + c_{3u}^b e^{-j3\theta}\right) i_{bb}^U + \left(c_{1u}^b e^{j\pi/6} e^{-j\theta} + c_{3u}^b e^{j\pi/2} e^{-j3\theta}\right) i_{bb}^L\right] \\ &+ \frac{\mu_0}{\delta_0} n_0 \,\mathrm{Re}\left[\left(c_{1u}^c e^{-j\theta} + c_{3u}^c e^{-j3\theta}\right) i_{bc}^U + \left(c_{1u}^c e^{j\pi/6} e^{-j\theta} + c_{3u}^c e^{j\pi/2} e^{-j3\theta}\right) i_{bc}^L\right] \end{aligned} \tag{5.3}$$

where μ_0 is the permeability of free space, n_0 is number of turns of the coil, δ_0 is the air gap length, $c_{1u}^a, c_{1l}^a, c_{1u}^b, c_{1l}^b, c_{1u}^c, c_{1l}^c, c_{3u}^a, c_{3l}^a, c_{3u}^b, c_{3l}^b, c_{3u}^c$ and c_{3l}^c are the Fourier coefficient of MMF distribution of two pole and six pole magnetic field. Here superscript a, b and c represents phase A, phase B and phase C, subscript l and u represent lower and upper branch of the winding, 1 and 3 represent two pole and six pole respectively. These coefficients have been calculated for two different cases (1) when unit current has been given in all the branches separately (2) when unit current has been given in all the branches separately however direction of supply has been reversed in phase B of the winding. The winding factor for case (1) when unit current has been supplied in all the branches are, $c_{1u}^a = 2.6736e^{j5\pi/6}$, $c_{1u}^b = c_{1u}^a e^{-j\pi/3}$, $c_{1u}^c = c_{1u}^a e^{-j2\pi/3}$, $c_{3u}^a = 0.8199e^{j\pi/2}$, $c_{3u}^b = -c_{3u}^a$, $c_{3u}^c = c_{3u}^a$

whereas, the Winding factor for case (2) when direction of current supply is reversed in the branches of phase B of the winding are, $c_{1u}^a = 2.6736e^{j5\pi/6}, c_{1u}^b = c_{1u}^a e^{-j4\pi/3}, c_{1u}^c = c_{1u}^a e^{-j2\pi/3}, c_{3u}^a = 0.8199e^{j\pi/2}, c_{3u}^b = c_{3u}^a, c_{3u}^c = c_{3u}^a$

The radial magnetic field distribution due to bridge supply is the summation of two pole and six pole magnetic field. In space vector form it can be written as

$$\underline{\hat{B}} = \underline{\hat{B}}_1 + \underline{\hat{B}}_3 \tag{5.4}$$

where these components for the case of normal supply can be written as

$$\underline{\hat{B}}_1 = \frac{\mu_0}{\delta_0} n_0 c_{1u}^a \left(i_{ba}^U + e^{j\pi/6} i_{ba}^L + e^{-j\pi/3} i_{bb}^U + e^{-j\pi/6} i_{bb}^L + e^{-j2\pi/3} i_{bc}^U + e^{-j\pi/2} i_{bc}^L\right) \tag{5.5}$$

$$\underline{\hat{B}}_3 = \frac{\mu_0}{\delta_0} n_0 c_{3u}^a \left(i_{ba}^U + j i_{ba}^L - i_{bb}^U - j i_{bb}^L + i_{bc}^U + j i_{bc}^L\right) \tag{5.6}$$

Whereas these components in the case of reversed phase B supply can be written as

$$\underline{\hat{B}}_1 = \frac{\mu_0}{\delta_0} n_0 c_{1u}^a \left(i_{ba}^U + e^{j\pi/6} i_{ba}^L + e^{-j4\pi/3} i_{bb}^U + e^{-j7\pi/6} i_{bb}^L + e^{-j2\pi/3} i_{bc}^U + e^{-j\pi/2} i_{bc}^L\right) \tag{5.7}$$

$$\underline{\hat{B}}_3 = \frac{\mu_0}{\delta_0} n_0 c_{3u}^a \left(i_{ba}^U + j i_{ba}^L + i_{bb}^U + j i_{bb}^L + i_{bc}^U + j i_{bc}^L\right) \tag{5.8}$$

It can be seen in Equation (5.8) that in the case of three phase bridge supply the sum of $(i_{ba}^U, i_{bb}^U, i_{bc}^U)$ and $(i_{ba}^L, i_{bb}^L, i_{bc}^L)$ would become zero. Which proves that when the direction of phase B of the bridge supply is reversed the six pole magnetic field component would become zero. Similarly it can be observed from Equation (5.7) that the components $(i_{ba}^U, e^{-j4\pi/3} i_{bb}^U, e^{-j2\pi/3} i_{bc}^U)$ and $(e^{j\pi/6} i_{ba}^L, e^{-j7\pi/6} i_{bb}^L, e^{-j\pi/2} i_{bc}^L)$ are 120 degree apart which would lead to generation of rotating two pole magnetic field. The radial forces acting on the rotor of the motor can be calculated using Maxwell stress tensor as [100]

$$f_{bridge} = \int_0^{2\pi} \frac{B^2}{2\mu_0} e^{j\varphi} d\varphi = \frac{\pi d_r l_r}{4\mu_0} \left[\underline{\hat{B}}_1^\star \underline{\hat{B}}_2 + \underline{\hat{B}}_2^\star \underline{\hat{B}}_3\right] \tag{5.9}$$

where $\underline{\hat{B}_2}$ is the space vector of four pole magnetic field generated due to the main supply of the winding, and * denotes conjugate of respective magnetic field. The second term of Equation (5.9) can be eliminated because six pole magnetic field is eliminated if we reverse the direction of supply of phase B of the bridge supply. Using Equations (5.7), (5.8) and (5.9) the force generated in the BCW machine with respect to bridge and main supply for a concentric rotor, can be written as

$$f_{bridge} = \frac{\pi d_r l_r n_0}{4\delta_0} c_{1u}^{a*} \left(i_{ba}^U + e^{j\pi/6} i_{ba}^L + e^{-j4\pi/3} i_{bb}^U + e^{-j7\pi/6} i_{bb}^L + e^{-j2\pi/3} i_{bc}^U - j i_{bc}^L\right)^* \underline{B}_2 e^{jwt} \tag{5.10}$$

If the current components due to bridge supply has $w_1(f_b$ Hz) and $w(f_s$ Hz) is the main supply frequency, a bridge supply would generate a force of frequency $w(f_s) \pm w_1(f_b)$ Hz depending on nature of rotation of the magnetic fields, i.e. if the bridge supply generates a rotating magnetic field in the same direction of the main supply generated magnetic field, the generated force frequency would be $(f_s - f_b)$ Hz and if the bridge supply generates a rotating magnetic field in the reverse direction of the main supply generated magnetic field, the generated force frequency would be $(f_s + f_b)$ Hz .

5.4 Conclusion

This chapter deals with the analysis of bridge configured winding to understand the formation of two pole and six pole magnetic fields, when a supply is given through the bridge terminals in a four pole winding electrical machine. Three supply conditions can be summarized, which can be used for the generation of two pole and six pole magnetic field individually. These supply conditions are,

(i) A three phase bridge supply where direction of supply is reversed for Phase B. This sequence of supply would generate a rotating two pole magnetic field in reverse direction as that of the four pole magnetic field generated due to the three phase supply through the main terminals.

(ii) A three phase bridge supply where direction of supply is reversed for Phase B and phase angles are interchanged for any two phases of the bridge supply. This sequence of supply would generate a rotating two pole magnetic field in same direction as that of the four pole magnetic field generated due to the three phase supply through the main terminals.

(iii) A sinusoidal supply of same magnitude and phase angle or a DC supply through the bridge terminals, where direction of supply of phase B has been reversed would generate a six pole magnetic field. When the supply is sinusoidal in nature, the generated six pole magnetic field would be pulsating, whereas a DC supply would generate a constant six pole magnetic field.

6

Coupled Rotordynamics Modelling

Contents

6.1 Introduction

Vibration control has always been an important aspect of study in rotating machines. A significant amount of reduction in wear and tear can be observed if vibration can be controlled at the source itself. The development of bearingless machines can be a good solution where vibration can be suppressed actively as well as the machine can also be operated at higher speed in the absence of mechanical bearing without any wear and tear. Active magnetic bearing (AMB) can be a good replacement of mechanical bearing, however addition of AMB increases the overall size of the machine. Moreover, unlike AMBs that are external to the machine, an electric machine with controllable UMP can be used in conjunction with mechanical bearings and can exert forces at the centre of mass of the rotor (of the electrical machine). Hence the conversion of an electrical machine to a bearingless machine by generating a radial force in the machine itself solves the purpose.

For the generation of transverse force in an electrical machine the presence of p and $(p+1)$ or $(p-1)$ pole pairs of the magnetic field is essential. Here p is the torque producing and $p \pm 1$ are the auxiliary components of the magnetic field [4]. The general trend is to use the dual set of winding scheme where the main winding is used to generate p pole pair of the magnetic field and the auxiliary winding is used to generate $(p+1)$ or $(p-1)$ pole pair of the magnetic field. The development of dual set of winding connection reduces the torque producing capability of an electrical machine because the same slots are shared by the auxiliary winding to produce the transverse forces. However, single set of winding scheme makes use of full stator slots and the same set of coils can be used for the torque as well as the transverse force generation. There are various types of single set of winding scheme which has been discussed in details in Chapter 2. Among these winding schemes the bridge configured winding bring additional advantage of passive vibration capabilities. However, to make this winding scheme usable a proper bridge supply method has to be developed using which a force of appropriate frequency in required direction can be generated. Considering this need, in Chapter 5 an analytical investigation has been carried out to find out a supply method which can be used to generate a force of appropriate frequency by generating a two pole magnetic field through the bridge supply. Levitation and unbalanced force vibration control requires a transverse force of DC component or a single frequency component which is directly related to the generation of two pole magnetic field in a four pole electrical machine.

In this regard to investigate this further a coupled magnetic field, circuit equation and a rigid rotor equation of motion have been developed to study the vibration and force generation in BCW machine with respect to different bridge supply conditions. The same model has been used for the passive as well as active vibration control analysis, i.e. when the bridge terminals are short-circuited or bridge terminals are connected with an external isolated power source.

The second half of the chapter discusses the development of an approximate MATLAB/SIMULINK® model to demonstrate the control method which can be used for the development of a bearingless machine.

6.2 Coupled magnetic field, electrical circuit and rotordynamic model

A coupled magnetic field, electrical circuit and rotordynamics model has been developed in finite element environment to investigate the generation of force and rotor response in different bridge conditions, i.e. bridge ON, bridge OFF and bridge SUPPLY. The developed model is for a 3.7 kW induction motor with squirrel cage rotor which has 36 stator slots. The circuit diagram implemented in the development of numerical model has been described in Chapter 4 however, for the sake of completeness the circuit connection has been described again. Figure 6.1 represents circuit diagram of a BCW winding scheme implemented for the analysis of 36 slot induction machine. Two types of voltage source isolated from each other can be connected to this winding scheme. One voltage source is the three phase voltage which creates the main field and is called the main supply source and other voltage source is a three single phase voltage source and is called the bridge supply source. terminals **A, B**, and **C** represent the main supply terminals whereas terminal **A1-A2**, **B1-B2** and **C1-C2** represent the bride supply terminals.

A three-phase supply can be connected at the main supply terminals **A, B** and **C** to produces a four pole magnetic field (p pole pairs of the magnetic field) and hence interaction of this field with rotor bar generates a torque and rotor rotates. Whereas, the bridge terminals of each phase (**A1 - A2**, **B1 - B2**, and **C1 - C2**) can be excited individually using a single phase voltage source, isolated from each other and also from the main supply. When the bridge terminals are open, it is referred as bridge OFF condition, when the bridge terminals are connected, it is referred as bridge ON condition and when a voltage source is connected across the bridge, it is referred as bridge SUPPLY condition.

Transverse forces in BCW electrical machines is generated when the rotor is eccentric with respect to the stator center and forces can also be generated by connecting bridge supply through the bridge

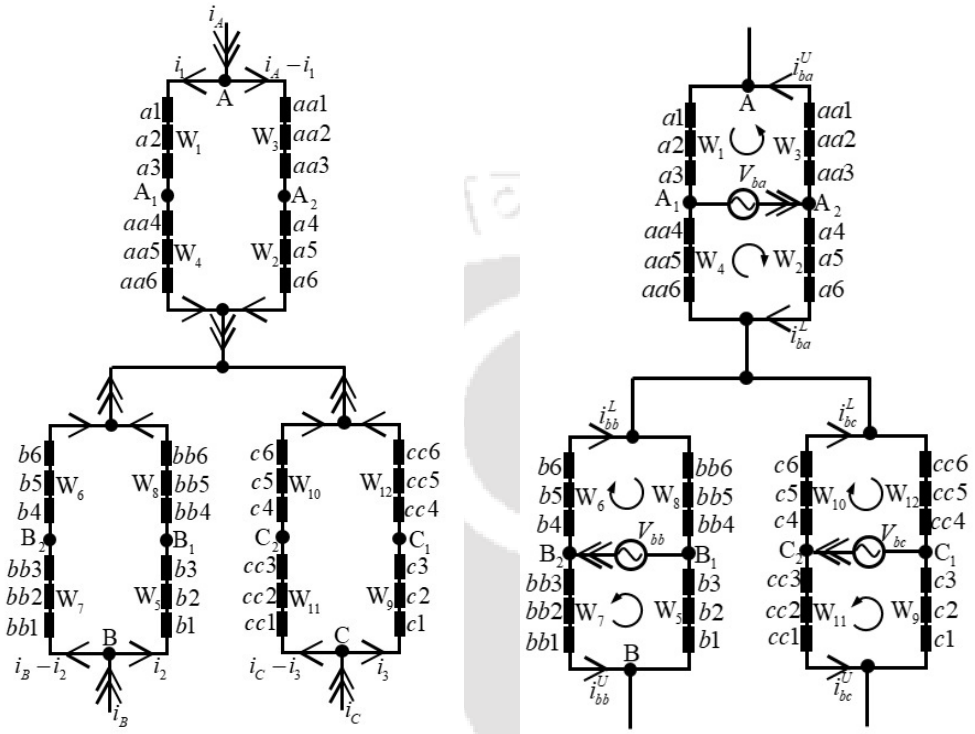

(a) (b)

Figure 6.1: Circuit diagram of BCW winding scheme (a) excited using main supply (b) excited using only bridge supply.

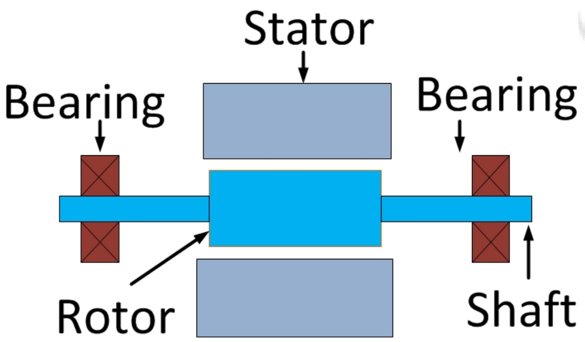

Figure 6.2: Schematic representation of Motor – Rotor system.

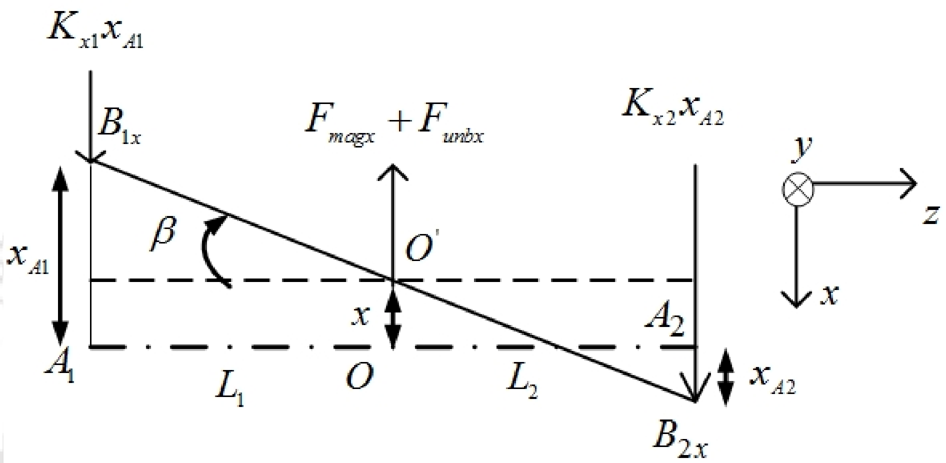

(a)

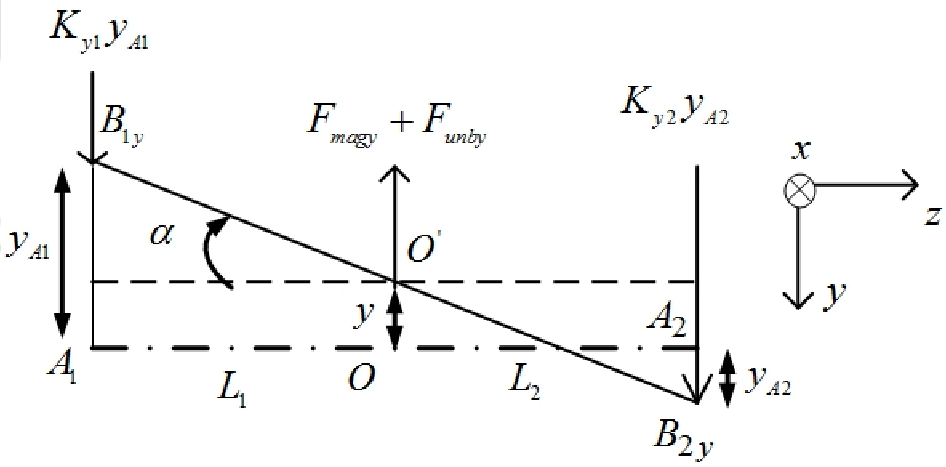

(b)

Figure 6.3: Schematic representation of a rigid rotor motion along (a) $z - x$ axes (b) $z - y$ axes.

terminals while the rotor is concentric with the stator center. The generation of force in an eccentric rotor condition also depends on status of bridge conditions i.e bridge ON or bridge OFF. If bridge is in ON condition it passively suppresses the unbalanced magnetic pull generated due to the eccentric position of the rotor. Figure 6.2 shows schematic representation of an electrical machine consists of bearings, rotor and stator. The rotor and bearing system of the motor has been approximated using a four dof (x, y, α, β) system. Here, x and y are the displacements along x and y axes, α and β are the rotations about x and y axes.

The formulation of coupled magnetic field and circuit equation represented in Chapter 4 has been used for the coupling of the rotor motion with the magnetic field and electric circuit equation of the machine. The magnetic field and electrical circuit equation of BCW induction motor can be represented as shown in Equations (6.1) - (6.4). Equation (6.1) is the field equation for the entire domain of the electrical machine, Equation (6.2) is the stator circuit equation and Equations (6.3) and (6.4) are the rotor circuit equations.

$$[K]_{n\times n}\{A\}_{n\times 1} + [C_r]_{n\times n}\frac{\partial\{A\}_{n\times 1}}{\partial t} - [P_s]_{n\times q}[T]_{q\times m}\{I_S\}_{m\times 1} + [P_r]_{n\times b}\{U_r\} = 0 \tag{6.1}$$

$$[Q]_{h\times n}\frac{d\{A\}_{n\times 1}}{dt} + [R]_{h\times h}\{i_s\}_{h\times 1} + [L_{es}]_{h\times h}\left\{\frac{di_s}{dt}\right\}_{h\times 1} = \{U_s\}_{h\times 1} \tag{6.2}$$

$$[Q_r]_{b\times n}\frac{d\{A\}_{n\times 1}}{dt} + [R_r]_{b\times b}\{I_r\}_{b\times 1} - \{U_r\}_{b\times 1} = 0 \tag{6.3}$$

$$[M_2]^T_{b\times b}[M_2]_{b\times b}\{U_r\}_{b\times 1} + 2[R_{er}]_{b\times b}\{I_r\}_{b\times 1} + 2[L_{er}]_{b\times b}\frac{d\{I_r\}_{b\times 1}}{dt} = 0 \tag{6.4}$$

Here, n is the number of nodes, q is the stator coil sides, b is the number of rotor bar, h is the number of stator currents, which is six in bridge OFF condition and nine in case of bridge ON or bridge supply conditions, $[K]$ is the electromagnetic stiffness matrix, $[C_r]$ represents the contribution of the induced EMF in the field equation due to rotor bar, $[P_s]$ represents the contribution of the excitation at the stator winding, $[P_r]$ is the contribution of the excitation at the rotor conductor, $[Q]$ and $[Q_r]$ are the contribution of the induced EMF in the stator and rotor circuit equations, R is the stator coil resistance matrix, $[L_{es}]$ is the stator end coil inductance matrix, $\{i_s\}$ is the individual stator circuit current vector, $\{I_s\}$ is the stator coil current vector, $\{U_s\}$ is the stator voltage vector, $\{U_r\}$ is the voltage vector across the rotor bar, $\{I_r\}$ is the rotor bar current vector, $[R_{er}]$ and $[L_{er}]$ are the rotor end winding resistance and inductance respectively, $[T]$ is the transformation matrix used for the transformation of circuit current to the coil side currents, $[M_2]$ is the transformation matrix for the conversion of end ring currents to the rotor bar currents. $\{A\}$ is the magnetic vector potential vector. The coupled field and circuit equation is solved for magnetic vector potential (A), stator winding current (i_s), rotor bar current (I_r) and rotor bar voltage (U_r) using Crank - Nicolson method. The Magnetic field is calculated using magnetic vector potential as

$$B = \nabla \times A \tag{6.5}$$

Figure 6.4 shows magnetic fields components at a node in the airgap. The Maxwell's stress method has been used for the calculation of forces at the airgap. Using the normal component (B_n) and tangential component (B_t) of the magnetic fields, the normal (σ_n) and tangential (σ_t) components of the maxwell stress can be calculated as shown in Equations (6.6) and (6.7) respectively. The x and y components of the forces acting on the rotor can be calculated by resolving the stress components along x and y axes and integrating it along a circle of radius r in the airgap using Equations (6.8) and (6.9) respectively. Here, l_r is the axial length of the electrical machine. For the numerical integration Gauss - Quadrature method is used. The magnetic forces acting on the rotor is coupled with the rigid rotor equation of motion as shown in Equation (6.10). Here, m is the mass of the rotor, I $(I_x = I_y = I)$ is the mass moment of inertia of the rotor about x and y axes, I_z is the mass moment of inertia of the rotor about z axis. Ω is the rotor rotational speed, L_1 and L_2 are the distance of the bearing locations from the center of mass of the rotor, (k_{x1}, k_{y1}) and (k_{x2}, k_{y2}) are the bearing stiffness along x and y axes of two mechanical bearings respectively. (F_{magx}, F_{magy}) and (F_{unbx}, F_{unby}) are the magnetic and mass unbalanced forces acting at the centre of mass along x and y axes respectively. Figure 6.3(a) and 6.3(b) represent rotor orientation along $z - x$ and $z - y$ axes respectively. $A_1 - A_2$ is the shaft axis orientation when there is no force acting on the rotor. A_1, A_2 are two bearing locations and O is the center of mass of the rotor. It has been assumed that the unbalance and magnetic forces act at the center of gravity of the rotor. Under the action of forces rotor changes its location and its center of mass moves to a new location O'. Also, the rotor undergoes a rotation about O' along x and y axes by an angle α and β and obtains a new orientation $B_{1y} - B_{2y}$ and $B_{1x} - B_{2x}$ respectively. (x_{A1}, x_{A2}) and (y_{A1}, y_{A2}) are the rotor position with respect to bearing axis along x and y axes respectively.

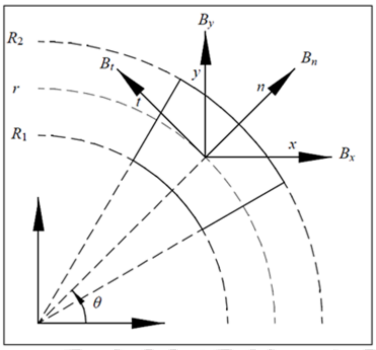

Figure 6.4: Magnetic flux density components at a node at a radius r in the airgap.

Equation (6.10) represents the equation of motion of the rotor with respect to the center of mass of the rotor. Here, $[M]$ is the mass matrix, $[G]$ is the gyroscopic matrix, $[K_m]$ is the bearing stiffness matrix, f_{mag} and f_{unb} are the force vectors representing magnetic and unbalanced mass force acting on the rotor and d is a vector representing rotor displacements.

$$\sigma_n = \frac{\left(B_n^2 - B_t^2\right)}{2\mu_0} \tag{6.6}$$

$$\tau_t = \frac{2B_nB_t}{2\mu_0} \tag{6.7}$$

$$F_{magx} = l_r \int_0^{2\pi} \left(\sigma_n \cos\theta - \tau_t \sin\theta\right) r d\theta \tag{6.8}$$

$$F_{magy} = l_r \int_0^{2\pi} \left(\sigma_n \sin\theta + \tau_t \cos\theta\right) r d\theta \tag{6.9}$$

$$[M]\left\{\ddot{d}\right\} + [G]\left\{\dot{d}\right\} + [K_m]\left\{d\right\} = \left\{f_{mag}\right\} + \left\{f_{unb}\right\} \tag{6.10}$$

Here, $[M] = \begin{bmatrix} m & 0 & 0 & 0 \\ 0 & m & 0 & 0 \\ 0 & 0 & I & 0 \\ 0 & 0 & 0 & I \end{bmatrix}$, $[G] = \begin{bmatrix} 0 & 0 & 0 & 0 \\ 0 & 0 & 0 & 0 \\ 0 & 0 & 0 & -I_z\Omega \\ 0 & 0 & I_z\Omega & 0 \end{bmatrix}$, $\{f_{mag}\} = \begin{Bmatrix} F_{magx} \\ F_{magy} \\ 0 \\ 0 \end{Bmatrix}$,

$$\{f_{unb}\} = \begin{Bmatrix} F_{unbx} \\ F_{unby} \\ 0 \\ 0 \end{Bmatrix}, d = \begin{Bmatrix} x \\ y \\ \alpha \\ \beta \end{Bmatrix},$$

$$\{K\} = \begin{bmatrix} k_{x1} + k_{x2} & 0 & 0 & L_1 k_{x1} - L_2 k_{x2} \\ 0 & k_{y1} + k_{y2} & L_1 k_{y1} - L_2 k_{y2} & 0 \\ 0 & L_1 k_{y1} - L_2 k_{y2} & {L_1}^2 k_{y1} + {L_2}^2 k_{y2} & 0 \\ L_1 k_{x1} - L_2 k_{x2} & 0 & 0 & {L_1}^2 k_{x1} + {L_2}^2 k_{x2} \end{bmatrix}$$

The complete simulation process has been explained using a flowchart shown in Figure 6.5. The input of the simulation are various winding parameters, slip condition (slip) and simulation time (t_f). The simulation is initialized by providing initial values of magnetic vector potential $\{A\}$ at each node, rotor displacement $\{d\}$ and velocity $\left\{\dot{d}\right\}$, stator currents $\{i_s\}$, rotor bar currents $\{I_r\}$ and rotor bar voltages $\{U_b\}$. Based on the requirement of force, a bridge supply along with the main supply can be given to generate transverse force on the rotor of the motor. However, if there is no requirement of lateral force generation, only main supply can be applied. The rotor position is adjusted by using airgap stitching method as explained in Chapter 4. After excitation conditions and rotor positions are defined, the coupled field and circuit equations are solved using Crank - Nicolson method to calculate the magnetic vector potential at each node, stator circuit current, rotor bar current and rotor bar voltage at next time step. The Forces acting on the rotor is calculated by the Maxwell stress tensor method. Once the magnetic force acting on the rotor is known, the mechanical equation of the motion has been solved by using 4th order Runge- Kutta method to calculate the the new position and velocity of the rotor. This process is continued till the final simulation time is achieved.

6.3 Numerical investigation

Simulations have been carried out using the developed coupled numerical model to study the effects of different bridge conditions on the airgap force production. The parameters of the induction machine used for simulation are considered similar to the machine used in Chapter 4. Table 6.1 shows the parameters of the rotor-bearing system.

The following conditions have been investigated,

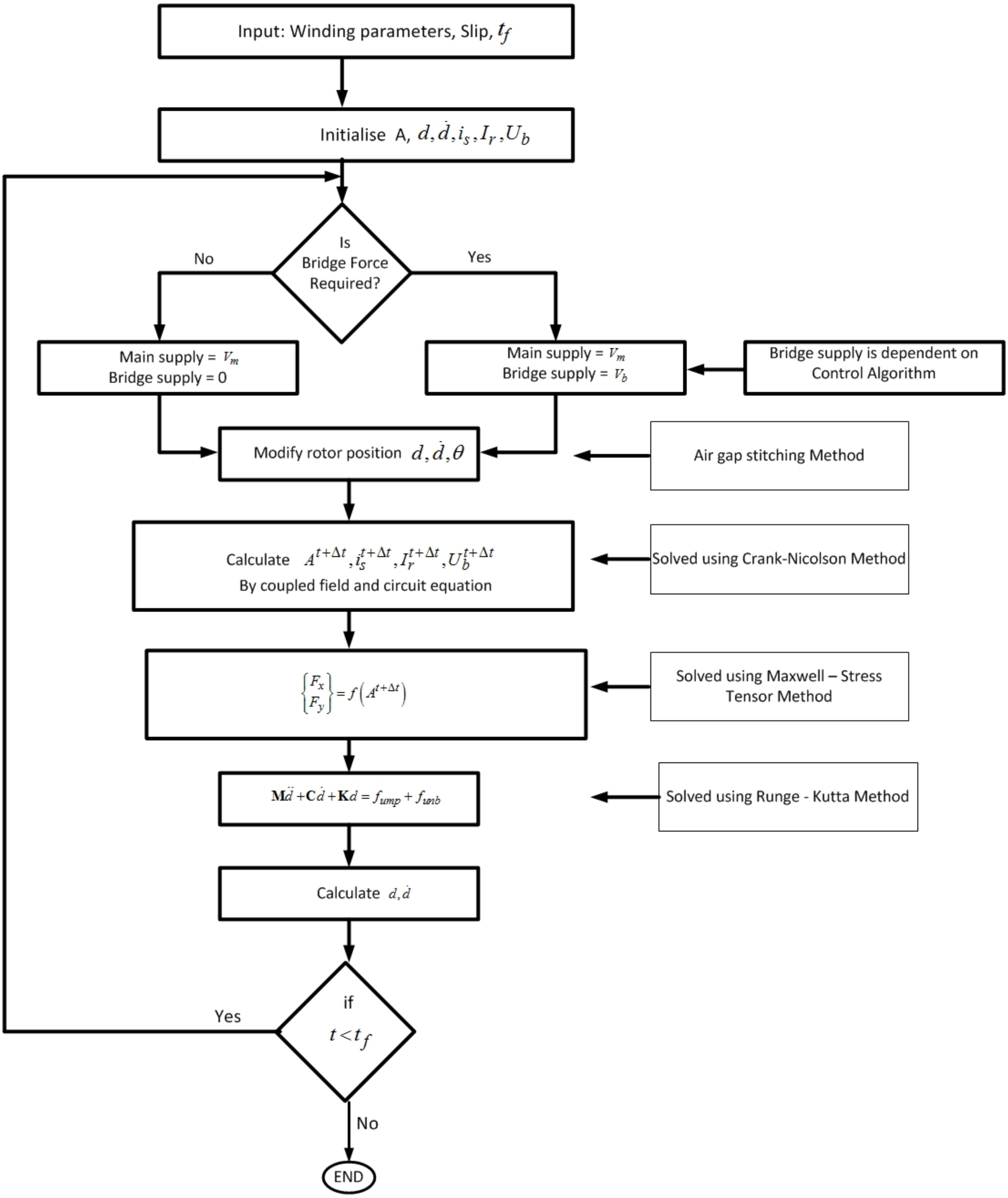

Figure 6.5: Flowchart of simulation.

Table 6.1: Mechanical parameters of the rotor of the induction motor

Parameters	Values
m	10 kg
I	0.0433 kg - m^2
I_z	0.0080 kg - m^2
$L_1 = L_2$	0.1865 m
Mass Unbalance	0.1 kg
Static eccentricity	1e-4 m
Dynamic eccentricity	1e-4 m
$k_{x1} = k_{x2} = k_{y1} = k_{y2}$	1e8 N/m

(i) The effect of statically eccentric rotor in bridge OFF and bridge ON conditions - The rotor has been shifted along x axis by 1e-4 m with respect to the stator center and the rotor is allowed to vibrate about this point with the application of generated magnetic force in bridge OFF and bridge ON conditions.

(ii) The effect of mass unbalance in rotor in bridge OFF and bridge ON conditions - A small unbalance mass of 0.1 kg has been introduced in the rotor at 1e-4 m to generate dynamic eccentricity condition in the machine. The rotor has been allowed to vibrate due to the force generated by the mass unbalance and magnetic pull in bridge OFF and bridge ON conditions.

(iii) The effect of single phase bridge supply - Only one phase of the bridge terminal, i.e phase A of the bridge terminal has been excited to study the force generated and rotor vibrations due to the single phase bridge supply.

(iv) The effect of normal three phase bridge supply - A normal three phase supply has been provided through the bridge terminal in same way as that of the main supply of the winding to study the effect of three phase bridge supply on the transverse force and rotor vibration.

(v) The effect of modified three phase bridge supply - The force generation and rotor vibration has been studied for two conditions; (i) when the bridge supply of the winding generates rotating two pole magnetic field in the same direction as that of the four pole rotating magnetic field generated by the main supply, (ii) when the bridge supply of the winding generates rotating two pole magnetic field in the opposite direction as that of the four pole rotating magnetic field generated by main supply.

(vi) The investigation of the generation of DC component of force which can be used for the development of bearingless machine - In this case generation of DC component of the force has been investigated to establish a relationship with respect to the phase of the bridge supply. This can be used to generate a DC component of the force in any required direction.

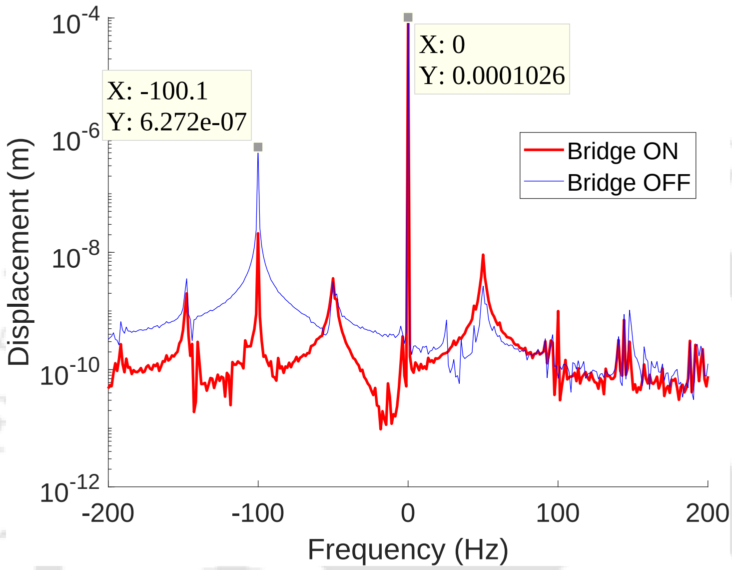

(a)

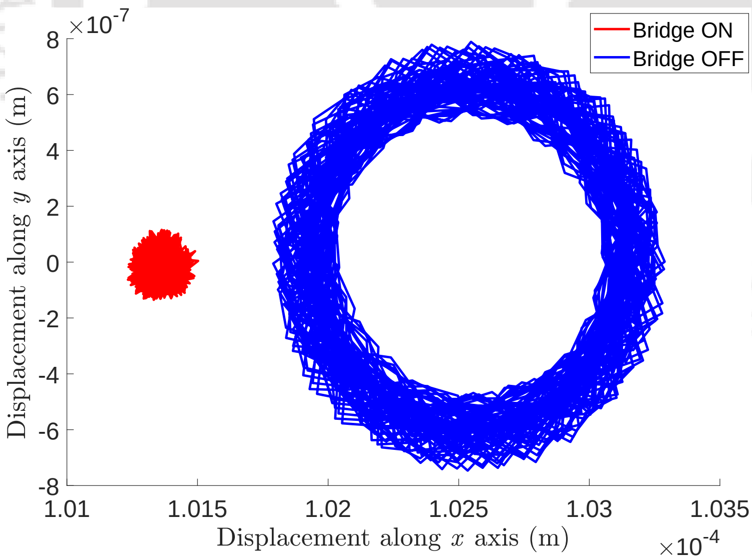

(b)

Figure 6.6: Comparison of (a) full spectrum FFT of rotor response in bridge OFF and bridge ON condition when rotor is in static eccentricity condition (b) rotor orbits in bridge OFF and bridge ON conditions when the rotor is in the static eccentricity condition.

Chapter 4 investigates the effect of different eccentricity conditions on bridge current and force production. It has been shown that in static eccentricity condition two dominant frequency component of the force exists, i.e. 50 Hz(f_s) and 100 Hz ($2f_s$) whereas in the case of dynamic eccentricity the rotor rotational component 24.5 Hz(f_r) and 124.5 Hz($2f_s + f_r$) exist where f_s(50) Hz is the main supply frequency and f_r (24.5 Hz, 2% slip) is the rotor rotational frequency. The similar behavior can be observed in Figure 6.6(a). Figure 6.6(a) shows the Fast Fourier Transform (FFT) of the rotor responses in bridge OFF and bridge ON conditions. It can be seen that bridge ON condition is able to suppress $2f_s$ component of the vibration and only DC component of the force acts on the rotor. Figure 6.6(b) shows the rotor orbits in bridge ON and bridge OFF conditions. It can be seen that in bridge ON condition rotor shifts its position due to which the static eccentricity is reduced.

Figures 6.7(a) and 6.7(b) show the full spectrum FFT of the rotor responses in bridge ON and bridge OFF conditions and rotor orbits in bridge ON and bridge OFF conditions respectively when the rotor is in dynamics eccentricity condition. The dynamic eccentricity has been generated by incorporating a mass unbalance of 0.1 kg at 1e-4 m from the rotor center. It can be seen that the bridge ON condition is able to suppress ($2f_s + f_r$) component of the vibration and only rotational component of the vibration is present which makes the rotor orbit smooth. In order to understand the reduction in force components, the magnetic and the unbalanced force component has been analysed separately. Figures 6.8(a) and 6.8(b) represent comparison of magnetic and unbalanced force in bridge OFF and bridge ON conditions respectively. A slight reduction in unbalanced force and substantial reduction of magnetic force can be observed.

Figures 6.9(a), 6.9(b) and 6.9(c) represent the full spectrum FFT of the force generated, the full spectrum FFT of the rotor responses and comparison of the rotor responses along x and y axes due to the excitation of phase A of the bridge supply respectively. It has been seen that the single phase of bridge supply generates forces of frequencies ($f_s \pm f_b$), i.e 70 Hz and 30 Hz, where f_s (50 Hz) and f_b (20 Hz) are the main supply and bridge supply frequency.

Figures 6.10(a), 6.10(b) and 6.10(c) show the full spectrum FFT of the force generated due to the normal sequence of the bridge supply, the full spectrum FFT of the rotor responses due to the normal sequence of the bridge supply and comparison of the rotor responses along x and y axes due to normal sequence of the bridge supply respectively. It can be observed that similar to the single phase bridge supply, the three phase bridge supply also generates force of frequencies ($f_s \pm f_b$), i.e 70 Hz and 30 Hz. Here, normal sequence of the bridge supply represent similar to the main supply sequence. The three phase main supply voltages are $V_A = 40\cos(2\pi f_s t), V_B = 40\cos(2\pi f_s t - 2\pi/3)$

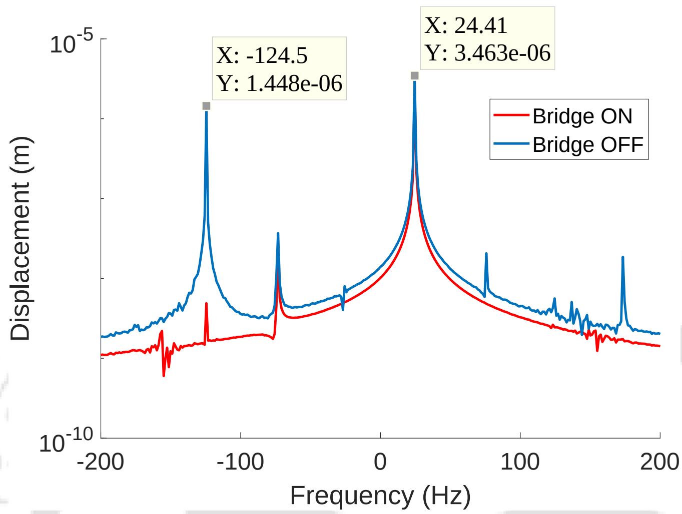

(a)

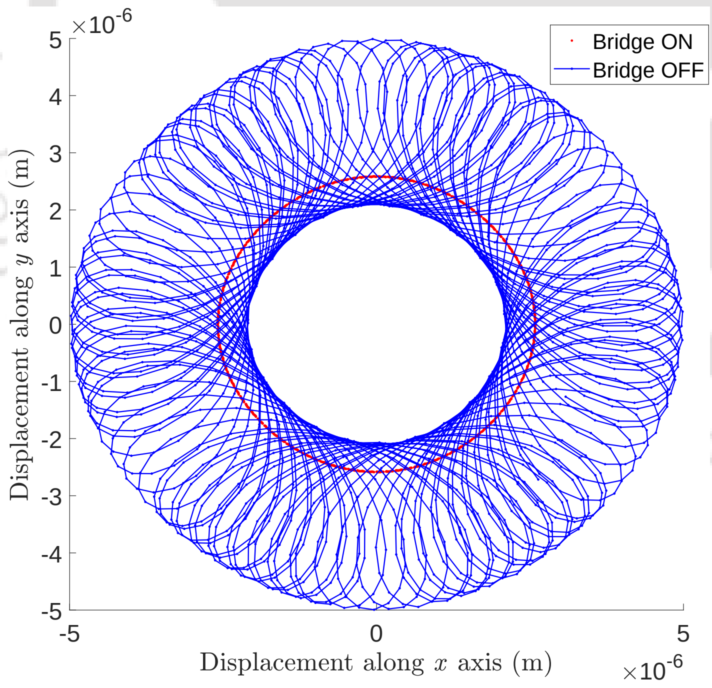

(b)

Figure 6.7: Comparison of (a) full spectrum FFT of rotor response in bridge OFF and bridge ON condition when rotor is in dynamic eccentricity condition (b) rotor orbit in bridge OFF and bridge ON condition when rotor is in dynamic eccentricity condition.

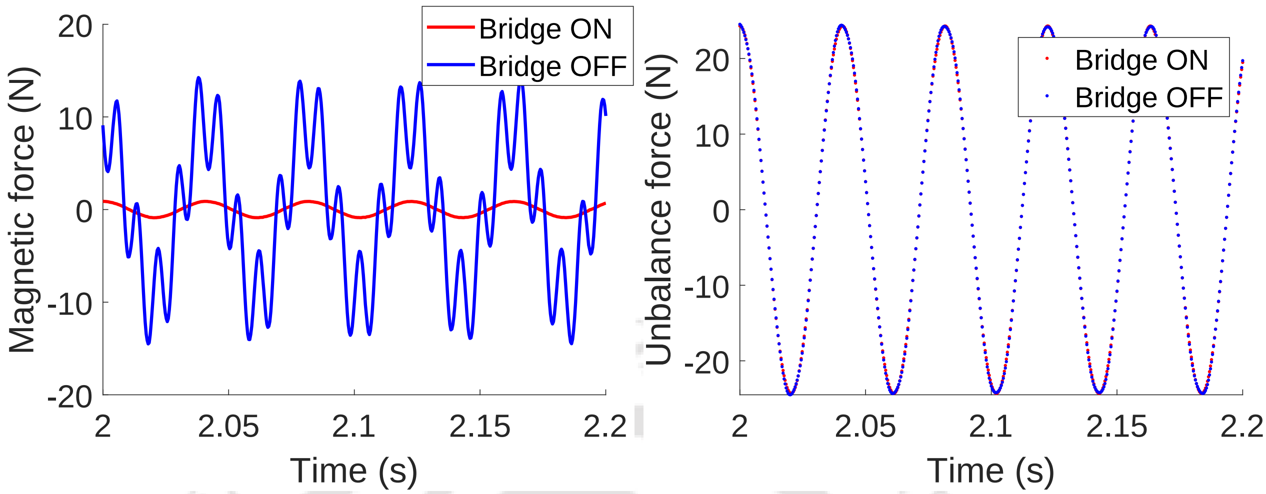

(a) (b)

Figure 6.8: Comparison of (a) magnetic force in bridge OFF and bridge ON conditions when rotor is in dynamic eccentricity condition (b) unbalanced force in bridge OFF and bridge ON conditions when rotor is in dynamic eccentricity condition.

and $V_C = 40\cos(2\pi f_s t - 4\pi/3)$ whereas the normal three phase bridge supply voltages are $V_{A_b} = 20\cos(2\pi f_s t), V_{B_b} = 20\cos(2\pi f_s t - 2\pi/3)$ and $V_{C_b} = 20\cos(2\pi f_s t - 4\pi/3)$.

The generation of transverse forces of desired frequencies have been investigated using the proposed sequence of the bridge supply. Here the term same sequence of bridge supply represents the same sequence of rotation of magnetic field. The same sequence of bridge supply voltages are $V_{A_b} = 20\cos(2\pi f_s t - 4\pi/3), V_{B_b} = -20\cos(2\pi f_s t - 2\pi/3)$ and $V_{C_b} = 20\cos(2\pi f_s t)$. This sequence of supply generates two pole rotating magnetic field which rotates in same direction as that of the four pole rotating magnetic field and generates a force of frequency $f_s - f_b$ i.e 30 Hz, when main supply frequency f_s is 50 Hz and bridge supply frequency f_b is 20 Hz. Figures 6.11(a), 6.11(b) and 6.11(c) represent the full spectrum FFT of the force generated due to the same sequence of the bridge supply, the full spectrum FFT of the rotor responses due to the same sequence of the bridge supply and comparison of the rotor responses along x and y axes due to the same sequence of the bridge supply respectively. It can be seen that due to the interactions of the magnetic field generated due to the main supply and bridge supply produces a force at 30 Hz.

A particular frequency of force can also be generated if the direction of rotation of the four pole magnetic field and two pole magnetic field are opposite. In this case the generated force has $f_s + f_b$ Hz of frequency component. To generate a rotating two pole magnetic field, which rotates in the opposite

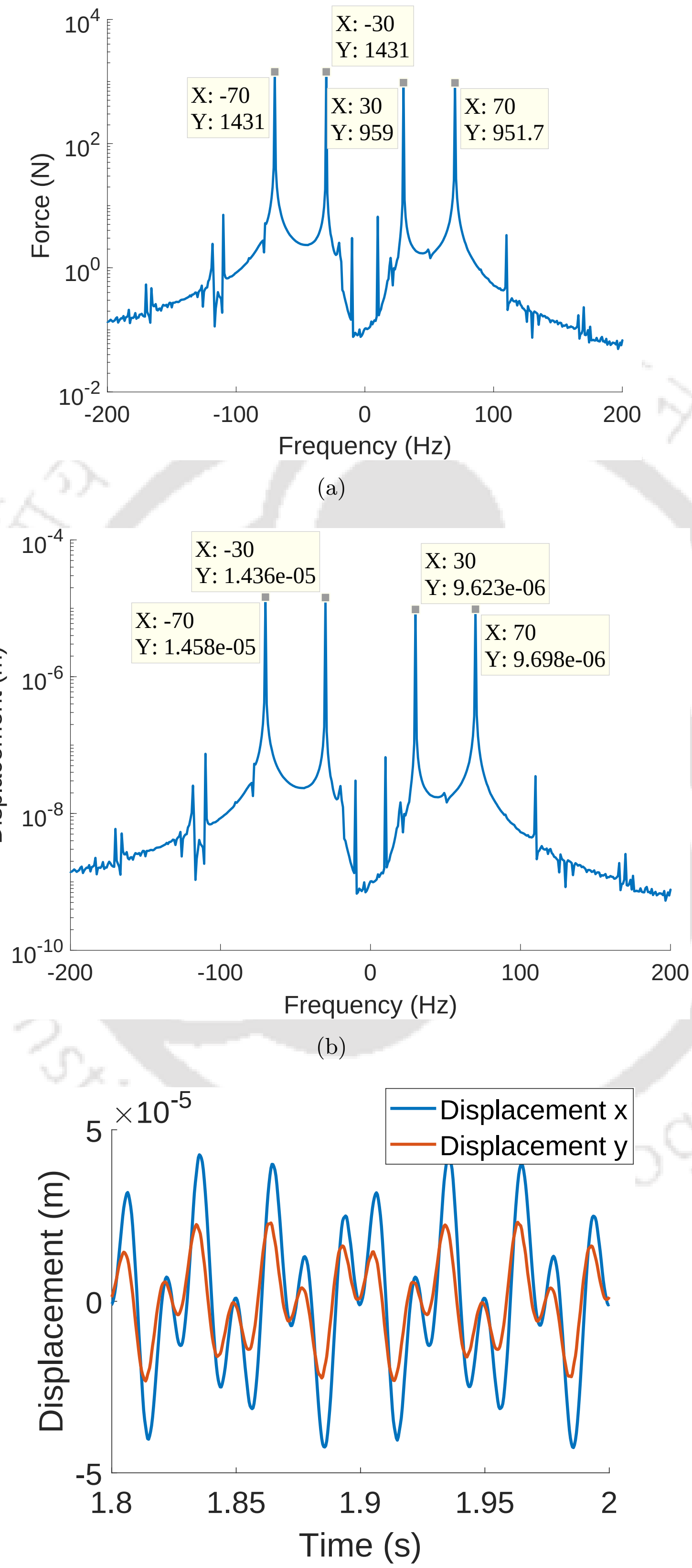

(a) (b) (c)

Figure 6.9: (a) Full spectrum FFT of the transverse force generated due to a single phase of bridge supply at 20 Hz (b) full spectrum FFT of the rotor response when a supply of 20 Hz has been given through the phase A of the bridge terminal (c) Comparison of the rotor responses when a supply of 20 Hz has been given through the phase A of the bridge terminal.

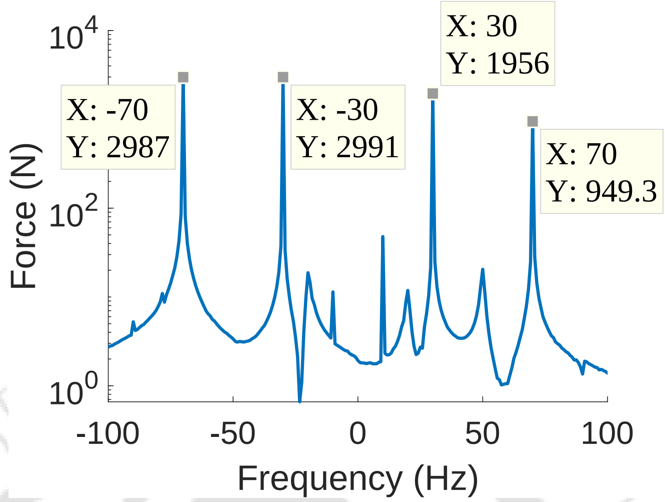

(a)

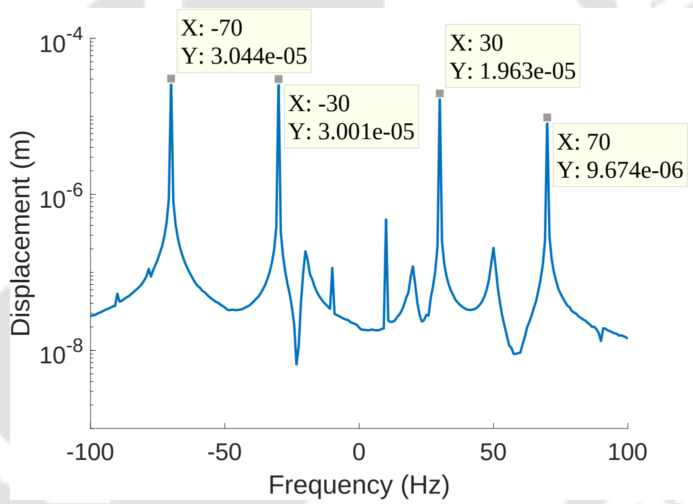

(b)

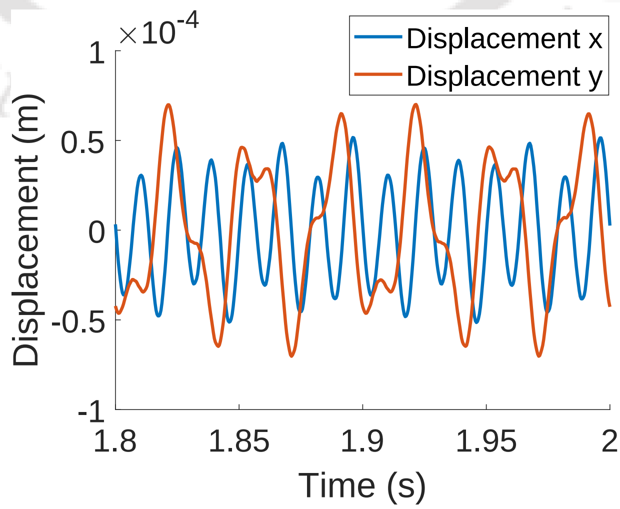

(c)

Figure 6.10: (a) Full spectrum FFT of the transverse force generated due to the normal sequence of bridge supply (b) full spectrum FFT of rotor responses when a normal sequence supply of 20 Hz has been applied through the bridge terminals (c) comparison of rotor responses when a normal sequence supply of 20 Hz has been applied through the bridge terminals.

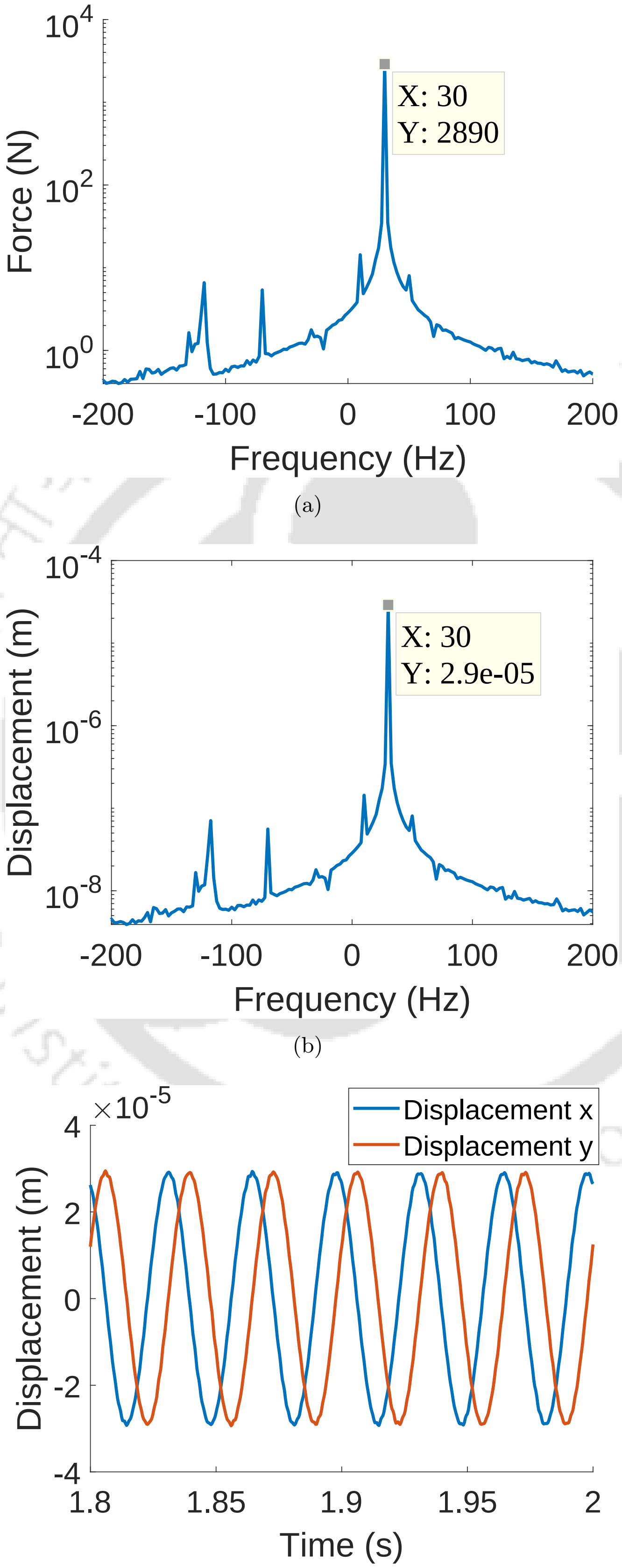

Figure 6.11: (a) Full spectrum FFT of the transverse force generated due to the same sequence of the bridge supply (b) full spectrum FFT of rotor response when a same sequence supply of 20 Hz has been applied through the bridge terminal (c) Comparison of rotor response when a same sequence supply of 20 Hz has been applied through the bridge terminal.

direction as that of the four pole rotating magnetic field the following sequence of the bridge supply has been given to the bridge terminals of the winding, $V_{A_b} = 20\cos(2\pi f_s t), V_{B_b} = -20\cos(2\pi f_s t - 2\pi/3)$ and $V_{C_b} = 20\cos(2\pi f_s t - 4\pi/3)$. This sequence of bridge supply has been referred here as the reverse sequence of the bridge supply. Figures 6.12(a), 6.12(b) and 6.12(c) represent full spectrum FFT of the force generated due to the reverse sequence of the bridge supply, full spectrum FFT of the rotor response due to the reverse sequence of the bridge supply and comparison of the rotor responses along x and y axes due to the reverse sequence of the bridge supply respectively. It can be seen that due to the interactions of the magnetic field generated by the main supply and bridge supply produces a force at 70 Hz.

The generation of DC component of the force is one of the important components of the transverse force because DC component of the force can be used for the purpose of levitation of the rotor of the motor. Since a rotating two pole magnetic field rotating in the same direction as that of the rotating four pole magnetic field generates a force of frequency $f_s - f_b$ Hz, a DC component of the force can be generated by keeping the same sequence bridge supply frequency, same as that of the main supply frequency component. Figures 6.13(a) and 6.13(b) represent the comparison of forces along x and y axes and comparison of the rotor responses along x and y axes when bridges are supplied at 50 Hz equal to the main supply frequency. A number of simulations have been performed at different phases of the bridge supply to establish a relationship between the bridge supply and direction of force generation. A phase angle α has been added in all three phases of the bridge supply which has been varied from 0 deg to 360 deg as, $V_{A_b} = 20\cos(2\pi f_s t + \alpha), V_{B_b} = -20\cos(2\pi f_s t - 4\pi/3 + \alpha)$ and $V_{C_b} = 20\cos(2\pi f_s t - 2\pi/3 + \alpha)$ where $0 \leq \alpha \leq 2\pi$. Figure 6.13(c) represents the variation of forces along x and y axes with respect to the changes in phase (α) of the bridge supply. It can be seen that the variation in the force is sinusoidal. The similar variation has been observed for displacement as well. The direction (phase) of the force and the direction (phase) of the rotor position has been calculated using forces and displacements along x and y axis as, $dir_{force} = \text{angle}(F_x + \text{j}F_y), dir_{disp} = \text{angle}(disp_x + \text{j}disp_y)$. Figures 6.13(d) and 6.13(e) represent the variation in phase of the force and rotor position with respect to the changes in phase of the bridge supply respectively. It can be seen that the force and rotor position changes its direction from -π to +π. This relationship can be used for the levitation or suppression of the rotor vibration and finally in the development of a bearingless machine. The control usually brings some DC stiffness that forces the rotor into a bit different position

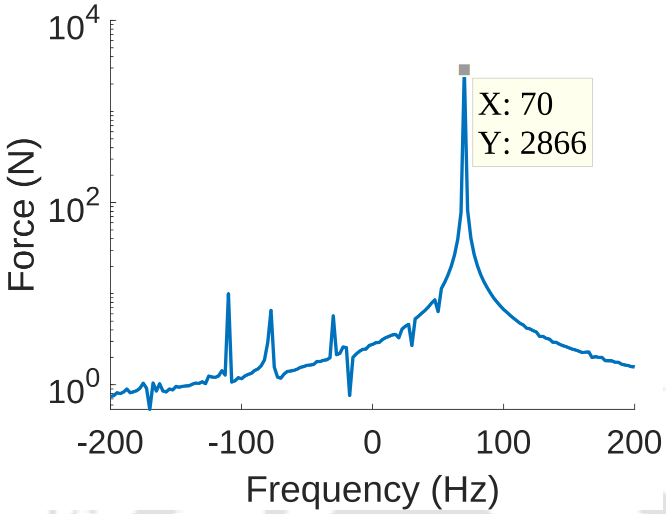

(a)

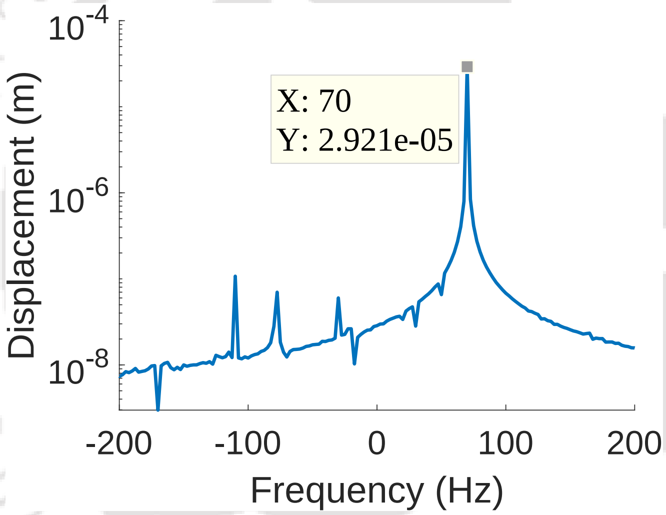

(b)

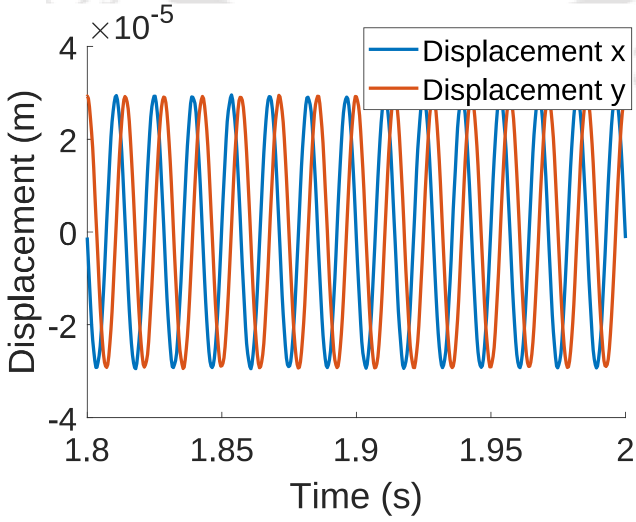

(c)

Figure 6.12: (a) Full spectrum FFT of the transverse forces generated due to the reverse sequence of the bridge supply (b) full spectrum FFT of the rotor responses when a reverse sequence supply of 20 Hz has been applied through the bridge terminals (c) Comparison of the rotor responses when a reverse sequence supply of 20 Hz has been given through the bridge terminals.

than rotating without control.

6.4 Control simulation model

The purpose of this section is to develop an approximate MATLAB/SIMULINK® model to investigate the levitation and vibration control in a bridge configured winding electrical machine. For the development of bearingless machine simulation, it is required to have a force model which can mimic the actuator model of bridge configured electrical machine. The previous section investigate the force production capability in bridge configured winding induction machine. It has been shown that if a proper sequence of bridge supply is followed, then bridge configured winding mimics the behaviour of a dual set of winding configuration. In this section, approximation of analytical force has been used as a replica of electrical machine to simulate the levitation and harmonic force compensation. The magnetic field and the force has been calculated analytically and later two control algorithms, the PID and the Convergent control algorithm has been used to achieve the levitation and harmonic force compensation respectively.

6.4.1 Force expression

For the development of a simulation model, two force expressions are needed viz., (i) force expression of the eccentricity force and (ii) force expression of the actuator force.

6.4.1.1 Eccentricity induced force

The literature says that in static eccentricity condition, the predominant component of force acts along the shortest air gap and is given by Equation (6.11) [7,57].

$$F_{stat} = \frac{\mu_0}{2\delta_m^3}\frac{A_p^2 R^3 l}{p^2}\pi e \tag{6.11}$$

In addition to constant pull, a pulsating force ($F_{pulsating}$) of double supply frequency also acts on the rotor. By neglecting the higher order terms it can be represented as

$$F_{pulsating} = \frac{\mu_0}{2\delta_m}\frac{\pi A_p^2 R^3 l}{p^2}\frac{\epsilon}{(1-\epsilon^2)^{3/2}} cos2(\omega_1 t - \phi_p) \tag{6.12}$$

where δ_m is the mean air gap length, ϵ is the eccentricity ratio and A_p is the amplitude of current

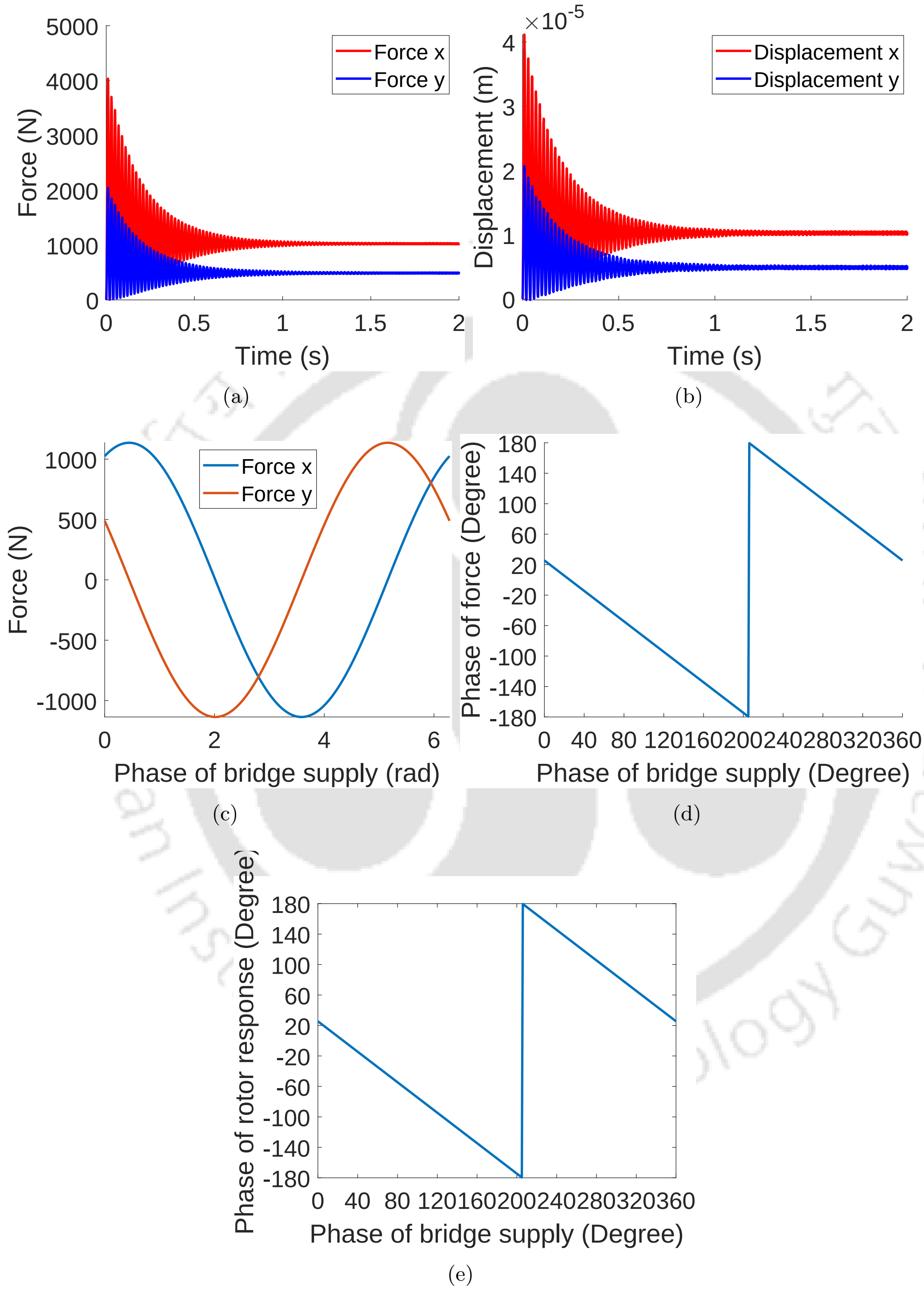

Figure 6.13: (a) Comparison of the forces when a same sequence supply of 50 Hz has been applied through the bridge terminals (b) Comparison of the rotor responses when a same sequence supply of 50 Hz has been applied through the bridge terminals (c) Comparison of the forces when a same sequence supply of 50 Hz has been applied through the bridge terminals with change in phase (d) Variations in phases of the force with respect to the phases of the bridge supply (e) Variations in phase of rotor response with respect to the phases of the bridge supply.

density distribution.

$$A_p = \sqrt{2} n_0 \xi \frac{I_0 \omega_1}{\pi R} \tag{6.13}$$

Here, n_0 is the number of strands used in the stator winding, ξ is the winding factor, ω_1 is the angular supply frequency, R is the outer radius of the rotor, l is the length of the rotor and I_0 is the amplitude of current.

Since the constant pull is dependent on the eccentricity e, the negative magnetic stiffness coefficient K_{mag} can be obtained by differentiating the static force with respect to eccentricity e as

$$K_{mag} = \frac{dF_{stat_x}}{de} = \frac{\mu_0}{2\delta_m^3} \frac{A_p^2 R^3 l}{p^2} \pi \tag{6.14}$$

6.4.1.2 Actuator force

The actuator force can be calculated as an interaction of four pole and two pole magnetic field components. The previous section explains and proves that a two pole magnetic field can be generated by the use of bridge supply through the bridge terminals. Using Maxwell's tensile stress theory the total bridge force or actuator force over the circumference of the rotor in x direction can be calculated as

$$F_{bridge_x} = \int_0^{2\pi} \frac{(b_{pmain} + b_{pbridge})^2}{2\mu_0} cos(\theta) R l d\theta \tag{6.15}$$

where, b_{pmain} is the four pole magnetic flux density due to the main supply and $b_{pbridge}$ is the two pole magnetic flux density due to the bridge supply. The four pole and two pole magnetic fields density can be approximated as sinusoidal distribution [7, 57]as

$$b_{pmain}(\theta, t) = \beta_{pm} cos(p\theta - \omega_1 t - \phi_p) \tag{6.16}$$

$$b_{pbridge}(\theta, t) = \beta_{pb} cos(p_b\theta - \omega_b t - \phi_b) \tag{6.17}$$

Here, $p = 2$ is the fundamental pole pair due to the main supply, $p_b = 1$ is the fundamental pole pair due to the bridge supply, ω_1 and ω_b are the main supply and bridge supply frequency, ϕ_p and ϕ_b are the phase of main supply and bridge supply respectively. The amplitude of main supply flux density (β_{pm}) and bridge supply flux density (β_{pb}) is given by,

$$\beta_p = \frac{\mu_0 A_p R}{\delta_m p} \tag{6.18}$$

$$\beta_{pb} = \frac{\mu_0 A_{pb} R}{\delta_m p_b} \tag{6.19}$$

Here A_{pb} is the amplitude of current density distribution due to the bridge supply,

$$A_{pb} = \sqrt{2} n_0 \xi \frac{I_b \omega_b}{\pi R} \tag{6.20}$$

where n_0 is the number of strands used in stator winding, ξ is the winding factor, ω_b is the angular bridge supply frequency, R is the outer radius of the rotor, l is the length of the rotor and I_b is the amplitude of bridge supply current

Substituting for b_{pmain} and $b_{pbridge}$ in Equation (6.15) we get the actuator force expression along longitudinal (x axis) direction,

$$F_{bridge_x} = \int_0^{2\pi} \frac{1}{2\mu_0} \left[\beta_{pm} cos(p\theta - \omega_1 t - \phi_p) + \beta_{pb} cos(p_b\theta - \omega_b t - \phi_b) \right]^2 cos(\theta) Rl d\theta \tag{6.21}$$

Substituting $p = 2$ for main supply and $p_b = 1$ for bridge supply we get,

$$F_{bridge_x} = \int_0^{2\pi} \frac{1}{2\mu_0} \left\{ 2\beta_{pm}\beta_{pb} Rl cos(2\theta - \omega_1 t - \phi_p) cos(\theta - \omega_b t - \phi_b) cos(\theta) \right\} d\theta \tag{6.22}$$

After integration of Equation (6.22) we get,

$$F_{bridge_x} = \frac{\beta_{pm}\beta_{pb}\pi Rl}{2\mu_0} \left\{ cos\left((\omega_1 - \omega_b)t + (\phi_p - \phi_b) \right) \right\} \tag{6.23}$$

Substituting for β_{pm} and β_{pb} in Equation (6.23) we get the final expression of actuator force (bridge force) along x axis as

$$F_{bridge_x} = \left(\frac{\mu_0 A_p R}{\delta_m P} \right) \left(\frac{\mu_0 A_{pb} R}{\delta_m P_b} \right) \frac{\pi Rl}{2\mu_0} \left\{ cos\left((\omega_1 - \omega_b)t + (\phi_p - \phi_b) \right) \right\} \tag{6.24}$$

Similarly bridge force acting in transverse (along y axis) direction can be written as

$$F_{bridge_y} = \left(\frac{\mu_0 A_p R}{\delta_m P}\right)\left(\frac{\mu_0 A_{pb} R}{\delta_m P_b}\right)\frac{\pi R l}{2\mu_0}\left\{ sin\Bigg((\omega_1 - \omega_b)t + (\phi_p - \phi_b)\Bigg)\right\} \tag{6.25}$$

If the bridge supply frequency is same as that of the main supply frequency, i.e. $\omega_1 = \omega_b$, a constant force in any direction can be generated by managing the phase of the main and bridge supplies. In addition to this the force expression in this case can be approximated as $K_i I_b$ where k_i can be termed as force-current factor.

6.4.2 Rotor model

In line with the objective of development of vibration control and bearingless simulation model, this section deals with the development of rotor bearing system. For the demonstration of disturbing force compensation, a meter long rotor supported by two mechanical bearings at the end has been considered. However, for the demonstration of levitation the rotor is considered to be supported by a mechanical bearing at only one end. Figure 6.14 represents the rotor bearing system considered for levitation control.

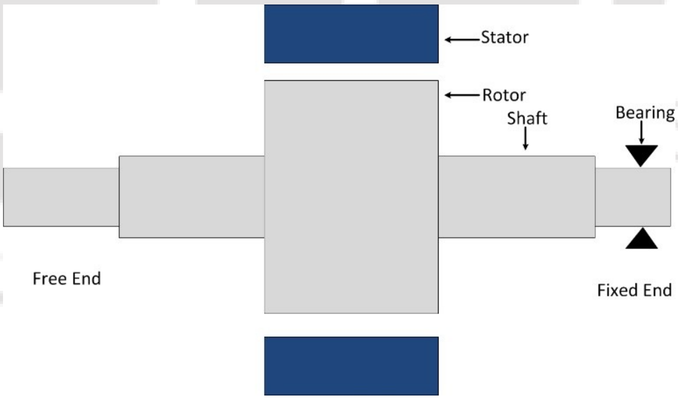

Figure 6.14: Rotor Model.

Keeping the system simple, the rotor of the motor has been modeled using finite element method as a Euler-Bernoulli beam. The rotor has been discretized in 9 elements, 10 nodes. Each node has 4 degree of freedom, among them 1st two are the transverse vibration DOF along x and y direction and last two are angular displacements DOF along x and y axes respectively. The discretized model is represented in Figure 6.15 indicating node number of the discretization. Equation (6.26) represents the equation of motion of the rotor of the motor, where $[M]$ is the mass matrix, $[C]$ is the proportional damping matrix, $[K]$ is the stiffness matrix, f_{unb} is the unbalance force acting on the rotor and f_{bcw} is the sum of all the electromagnetic forces acting on the rotor.

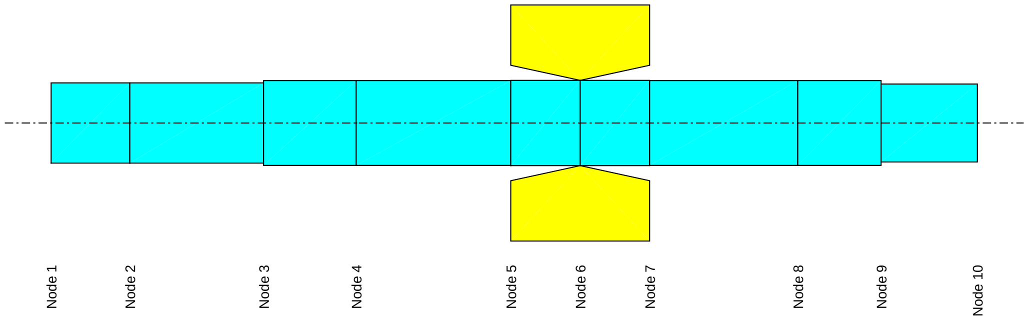

Figure 6.15: Discretized shaft model.

$$[\mathbf{M}]\{\ddot{x}\} + [\mathbf{C}]\{\dot{x}\} + [\mathbf{K}]\{x\} = \{f_{bcw} + f_{unb}\} \tag{6.26}$$

The dynamic reduction has been used to remove the unwanted degree of freedom from the rotor equation of motion. The transverse vibration degree of freedom at each node in x and y direction has to be retained and termed as master degree of freedom (x_m), whereas, angular degree of freedom along x and y axis has to be removed and termed as slave degree of freedom (x_s). To get the transformation matrix of dynamic reduction, Equation (6.26) has been arranged in terms of master and slave degree of freedom as shown in Equation (6.27).f_m is the combined force acting on the rotor.

$$\begin{bmatrix} M_{mm} & M_{ms} \\ M_{sm} & M_{ss} \end{bmatrix} \begin{Bmatrix} \ddot{x}_m \\ \ddot{x}_s \end{Bmatrix} + \begin{bmatrix} C_{mm} & C_{ms} \\ C_{sm} & C_{ss} \end{bmatrix} \begin{Bmatrix} x_m \\ x_s \end{Bmatrix} + \begin{bmatrix} K_{mm} & K_{ms} \\ K_{sm} & K_{ss} \end{bmatrix} \begin{Bmatrix} x_m \\ x_s \end{Bmatrix} = \begin{Bmatrix} f_m \\ 0 \end{Bmatrix} \tag{6.27}$$

Neglecting damping term in Equation (6.27), we get,

$$\begin{bmatrix} M_{mm} & M_{ms} \\ M_{sm} & M_{ss} \end{bmatrix} \begin{Bmatrix} \ddot{x}_m \\ \ddot{x}_s \end{Bmatrix} + \begin{bmatrix} k_{mm} & k_{ms} \\ k_{sm} & k_{ss} \end{bmatrix} \begin{Bmatrix} x_m \\ x_s \end{Bmatrix} = \begin{Bmatrix} f_m \\ 0 \end{Bmatrix} \tag{6.28}$$

Writing it separately in master and slave degree of freedom we get,

$$[M_{mm}]\{\ddot{x}_m\} + [M_{ms}]\{\ddot{x}_s\} + [K_{mm}]\{x_m\} + [K_{ms}]\{x_s\} = \{f_m\} \tag{6.29}$$

$$[M_{sm}]\{\ddot{x}_m\} + [M_{ss}]\{\ddot{x}_s\} + [K_{sm}]\{x_m\} + [K_{ss}]\{x_s\} = 0 \tag{6.30}$$

The dynamic reduction used to be carried out for a range of frequencies component or for a particular frequency component. Considering the reduction for ω, Equation (6.30) can be written as

$$-\omega^2[M_{sm}]\{x_m\} - \omega^2[M_{ss}]\{x_s\} + [K_{sm}]\{x_m\} + [K_{ss}]\{x_s\} = 0 \tag{6.31}$$

$$x_s = A^{-1}Bx_m \tag{6.32}$$

where $A = \left(-\omega^2 M_{ss} + K_{ss}\right)$ and $B = \left(-\omega^2 M_{sm} - K_{sm}\right)$, Equation (6.32) can be used to replace slave degree of freedom by master degree of freedom. Master and slave degree of freedom can be represented with the help of master degree of freedom as Equation (6.33)

$$\begin{Bmatrix} x_m \\ x_s \end{Bmatrix} = Tx_m \tag{6.33}$$

where,

$$T = \begin{Bmatrix} I \\ A^{-1}B \end{Bmatrix}$$

Using Equation (6.33) and pre-multiplying with T in Equation (6.27) we get,

$$\begin{Bmatrix} I \\ A^{-1}B \end{Bmatrix}^T \begin{bmatrix} M_{mm} & M_{ms} \\ M_{sm} & M_{ss} \end{bmatrix} \begin{Bmatrix} I \\ A^{-1}B \end{Bmatrix} \ddot{x}_m + \begin{Bmatrix} I \\ A^{-1}B \end{Bmatrix}^T \begin{bmatrix} C_{mm} & C_{ms} \\ C_{sm} & C_{ss} \end{bmatrix} \begin{Bmatrix} I \\ A^{-1}B \end{Bmatrix} \dot{x}_m + \begin{Bmatrix} I \\ A^{-1}B \end{Bmatrix}^T \begin{bmatrix} K_{mm} & K_{ms} \\ K_{sm} & K_{ss} \end{bmatrix} \begin{Bmatrix} I \\ A^{-1}B \end{Bmatrix} x_m = \begin{Bmatrix} I \\ A^{-1}B \end{Bmatrix}^T \begin{Bmatrix} f_m \\ 0 \end{Bmatrix} \tag{6.34}$$

Equation (6.34) can be represented in short form as

$$[M_{red}]\{\ddot{x}_m\} + [C_{red}]\{\dot{x}_m\} + [K_{red}]\{x_m\} = \{f_m\} \tag{6.35}$$

where,

$$M_{red} = M_{mm} + M_{ms}A^{-1}B + \left(A^{-1}B\right)^T M_{sm} + \left(A^{-1}B\right)^T M_{ss}A^{-1}B$$

$$C_{red} = C_{mm} + C_{ms}A^{-1}B + \left(A^{-1}B\right)^T C_{sm} + \left(A^{-1}B\right)^T C_{ss}A^{-1}B$$

$$K_{red} = K_{mm} + K_{ms}A^{-1}B + \left(A^{-1}B\right)^T K_{sm} + \left(A^{-1}B\right)^T K_{ss}A^{-1}B$$

Equation (6.35) can be represented in state space form as

$$\left\{ \begin{array}{c} \dot{x}_m \\ \ddot{x}_m \end{array} \right\} = \begin{bmatrix} \mathbf{0} & I \\ -\frac{K_{red}}{M_{red}} & -\frac{C_{red}}{M_{red}} \end{bmatrix} \left\{ \begin{array}{c} x_m \\ \dot{x}_m \end{array} \right\} + \left\{ \begin{array}{c} \mathbf{0} \\ M_{red}^{-1} \end{array} \right\} f_m \tag{6.36}$$

Which can be represented as

$$\dot{X} = AX + Bu \tag{6.37}$$

$$Y = CX + Du \tag{6.38}$$

where, A is the state matrix, B is the input matrix, C is the output matrix and D is the state transition matrix.

6.4.3 Control algorithm

In any bearingless machine generally two types of forces are required to be generated and controlled,

- A constant vertical force - for the levitation effect
- Revolving forces - To control revolving unbalanced and magnetic forces

In order to generate and control these two kinds of forces two different control algorithm has been used,

- PID Control - For the control of constant upward force
- Convergent Control - For the compensation of harmonic forces

6.4.3.1 Levitation control

The eccentric motion of the rotor generates two types of forces, a constant force which acts along the shortest air gap (Equation (6.11)) and a pulsating force (Equation (6.12)) which revolves at double the supply frequency. Whereas, with the help of bridge supply of the BCW induction machine a constant as well as a revolving force can be generated, keeping the bridge supply frequency opposite or same to that of the main supply frequency respectively.

For the development of levitation controller, the phenomena of DC component of force generation in an electrical machine is mimicked as an AMB. The force generation by an active bearing magnet(AMB) is represented as

$$f_{AMB} = -K_x X + K_i I \tag{6.39}$$

where K_x is the force - displacement factor, X is the displacement, K_i is the force - current factor and I is the supply current. In the similar way, the actuator force for DC component of force generation, the force − displacement factor can be represented as Equation (6.14) and the force − current factor can be represented by using Equation (6.24) for the case when sense of rotation of magnetic field and its frequency is same when main and bridge terminals are excited through the main and bridge supplies.

6.4.3.2 Convergent control

If the disturbance force acting on the system is of only one particular frequency, it can be controlled easily by generating force of that particular frequency at correct phase. However, if the phase and amplitude of the disturbance force is not predictable, it becomes quite challenging to control it. The convergent control technique can deal with such disturbance forces which has more than one frequency components. The convergent control technique is a very effective feedforward control method to deal with such kind of problems.

For multiple sinusoidal signal, the convergent control law can be written as [83],

$$U_{n+1} = \gamma U_n - \alpha g^{-1}(z_k e^{-j\omega kT}) \tag{6.40}$$

where T is the length of the time step, ω is the frequency of the known disturbance, γ and α are two constants and z_k is the vector of measured signal. In case, if there are more than one frequency components of disturbance, then the control law has to be applied in parallel.

Table 6.2: Simulation parameter

Sl. No	Parameters	Value
1	Mian supply	4 Pole
2	Bridge supply	2 Pole
3	Rotor diameter	0.103 m
4	No. of slot	36
5	No of turns	50
6	Air gap	0.001m
7	Main supply current	10A
8	Bridge supply current	0.15A
9	Proportional Gain	14.6
10	Derivative Gain	0.6
11	Integral Gain	0
12	Alpha	0.01
13	Gamma	0.01
14	Bearing stiffness	1e10 N/m
15	Main supply frequency	50 Hz
16	Bridge supply frequency	50 Hz
17	Rotor weight	10 kg

The complex multiplier g is a matrix which gives the phase and amplitude of the output as a function of change in amplitude and phase of the control signal. For a particular frequency component ω, it can be obtained from system's transfer function G as

$$g = G(j\omega) = C(j\omega I - A)^{-1}B \tag{6.41}$$

where A, B and C are the matrices of the LTI (Linear time invariant) state-space model.

6.4.4 Simulation results

The whole control process has been modeled using MATLAB/SIMULINK®. The simulation parameters have been presented in Table 6.2. Figure 6.16 represents the control block of the simulation model and Figure 6.17 represents the SIMULINK block diagram. Here, convergent control technique is used for the compensation of discrete harmonic components of the rotor vibration. Whereas, PID controller is used as a levitation controller and works on broad band from zero up to the bandwitdth of the actuator [83]. The Reference signal block generates the signal of particular harmonics which is required to be compensated. Based on the reference signal harmonics the convergent control algorithm generates required current which is passed to the actuator. The reference position gives the command to the PID controller which in turn based on error signal passes the required current to the actuator to levitate the rotor.

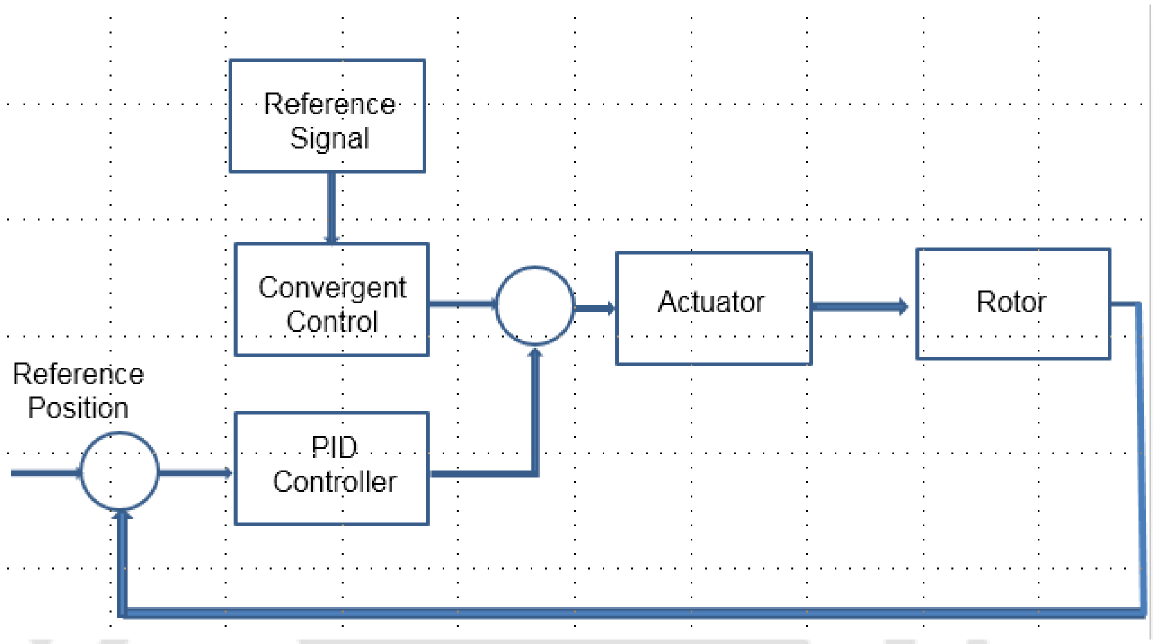

Figure 6.16: Control block diagram.

Three conditions have been simulated,

(i) When an unbalanced force of 0.1 kg is acting on the rotor along with a double supply frequency component of UMP. The both end of the rotor is supported by mechanical bearings. Node 3 and node 9 are the two bearing locations as shown in Figure 6.14. The unbalance has been introduced at a radius of 1e-4 m from the rotor center along x axis.

(ii) When the bearing is removed from one end of the rotor and no other disturbance forces are acting on the rotor. The mechanical bearing at node 3 is removed for the purpose of demonstration of levitation control of the rotor. The assumed air gap length of the motor is 1e-3 m hence the rotor is assumed to be eccentric along y axis by a distance of 1e-3 m.

(iii) When the bearing is removed from one end of the rotor and disturbing forces (Unbalanced force and Double supply frequency component UMP) are acting on the rotor. The mechanical bearing at node 3 is removed and the simulation has been carried out considering the initial position of the rotor eccentric along y axis by a distance of 1e-3 m whereas rotor is assumed to be concentric along x axis. The UMP control due to eccentric rotor position for levitation and disturbance

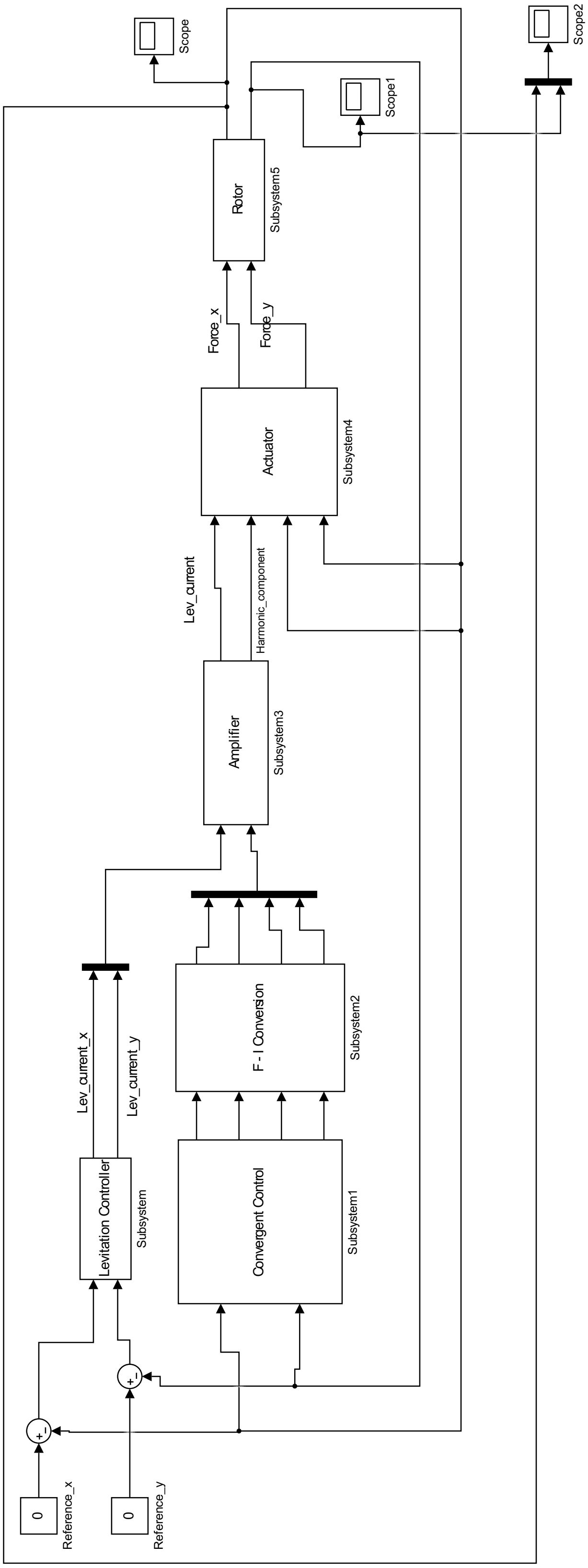

Figure 6.17: SIMULINK block diagram.

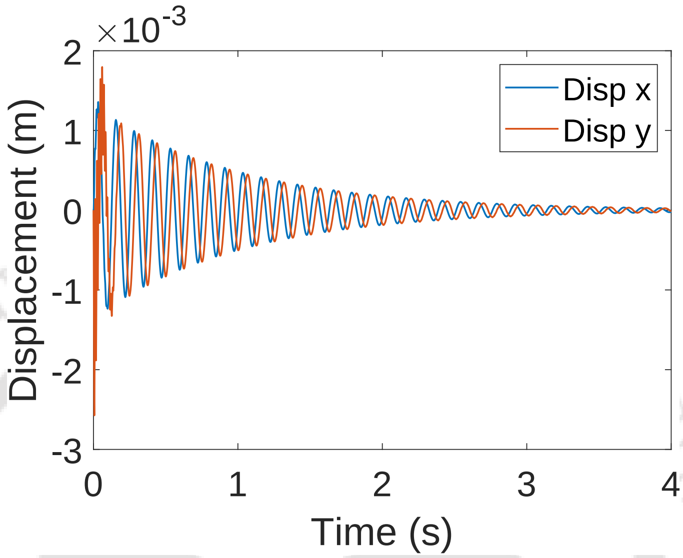

Figure 6.18: Rotor vibration with only harmonic component compensation.

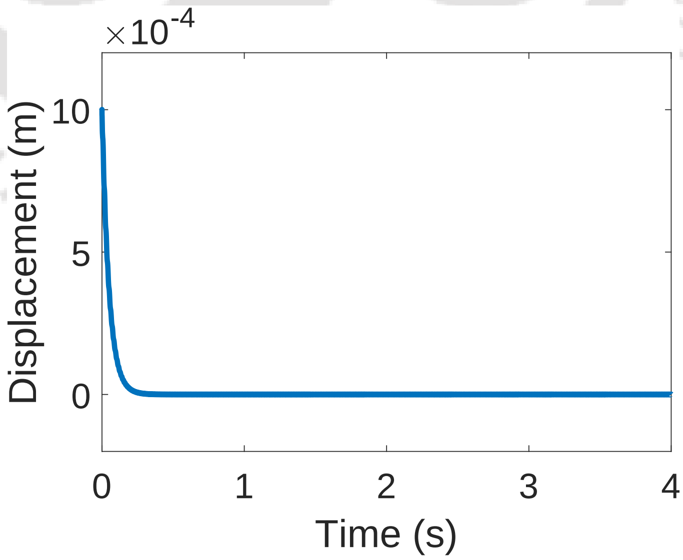

Figure 6.19: Rotor vibration with levitation control.

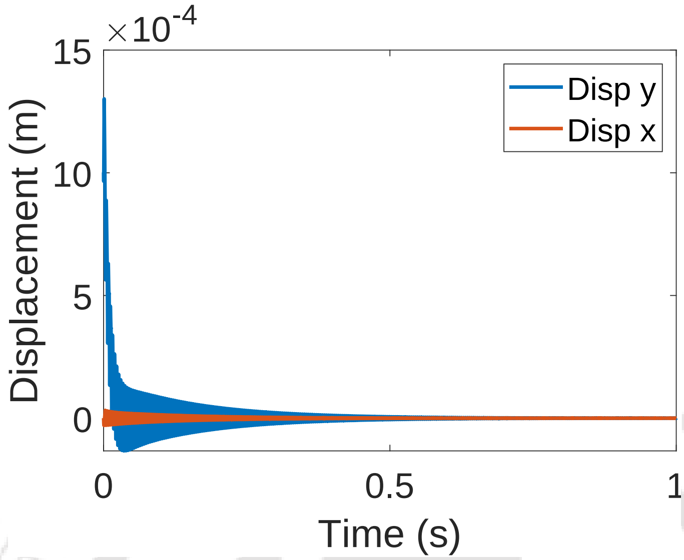

Figure 6.20: Rotor vibration with combined levitation control and harmonic component compensation.

force compensation due to mass unbalance and double supply frequency component force has been demonstrated. The mass unbalance of 0.1 kg is assumed at a radius of 1e-4 m along x axis.

Figure 6.18 represents the rotor vibration with respect to time in x and y direction when only convergent control is applied. In this case two types of forces are acting on the rotor, unbalance force which acts at the rotor spin speed i.e. 50 Hz and unbalanced magnetic pull which acts at double supply frequency, i.e. 100 Hz.

Figure 6.19 represents the rotor vibration with respect to time when only levitation controller is being applied. Considering the air gap of the machine as 0.001 m, an initial condition of 0.001m has been given to the rotor nodes (5, 6 and 7 in Figure 6.14) DOF which falls inside the motor in y direction. It can be observed from Figure 6.19 that PID controller is able to generate the required levitation force to the rotor and rotor oscillates about the rotor center.

Figure 6.20 represents the rotor vibration with respect to time when both levitation and convergent controllers are being applied together. An initial condition of 0.001 m has been given to the rotor nodes (5, 6 and 7 in Figure 6.14) DOF which falls inside the motor in y direction. Also an unbalance force along with double supply frequency component of UMP are acting on the rotor. It can be observed from Figure 6.20 that both of the controller combined together is able to levitate as well as able to compensate the harmonics disturbances acting on the rotor.

6.5 Conclusion

A coupled magnetic field, electrical circuit and rotor equation of motion model has been developed to analyse the rotor vibration and proposed bridge supply methods. In addition a relationship has been demonstrated through the finite element simulation between the bridge supply phase and the direction of generation of force. This can be used for the development of a real time controller for a bearingless machine. Also, an approximate simulation model has been developed in MATLAB/SIMULINK® to demonstrate levitation and vibration control using bridge supply through the bridge terminals of the winding. The developed SIMULINK® model is simple in nature and requires more work to implement it in real world problem.

7

Experimental Investigation

Contents

7.1 Introduction

The previous chapters discuss the analytical and numerical analysis of various aspects of a bridge configured winding (BCW) induction machine. Chapter 3 discusses the numerical analysis of the effects of eccentricity in a rotor of an induction machine on the magnetic fields. Chapter 4 discusses the numerical analysis of the coupled magnetic field and electric circuit equation of a BCW induction machine. Chapter 5 discusses the analytical analysis of the magnetomotive force analysis of a BCW induction machine. Chapter 6 discusses the numerical analysis of the coupled magnetic field, electric circuit and rotordynamic equation of a BCW induction machine. This chapter discusses the experimental verifications of the numerical and analytical findings discussed in the previous chapters. Measurements from two experimental setups have been used for the verification of the numerical findings. The first experimental setup has a 3.7 kW induction machine equipped with bridge configured windings and we will refer this setup as RIG I. This setup has been developed from scratch for the experimental verifications of the numerical and analytical findings of the work presented in this thesis. The details of the development of this experimental setup has been explained in the next section. The second experimental setup has a 37 kW induction machine equipped with bridge configured windings and we will refer this setup as RIG II. RIG II is developed by modifying one existing experimental setup. The rotor of the existing experimental setup has been replaced with a long and slender shaft to make the rotor flexible.

7.2 Development of experimental setup

The main component of the experimental setups (RIG I and RIG II) is the induction machine. The purpose of the development of the experimental setup is to characterize the behavior of bridge configured winding induction machine. The fundamental focus of the study was to investigate the transverse force generation capability of the bridge configured winding induction machine and its effects on the rotordynamics of the rotor system. Hence the shaft of the induction motor has been purposefully chosen as long and slender so that the rotor system become flexible. Hence two experimental setups are developed. RIG I has the inbuilt shaft and in RIG II, the original shaft of the rotor is replaced with a longer shaft. RIG I has an induction machine with 36 slots and it has been rewound with a three phase four pole bridge configured winding configuration. Similarly, RIG II has an induction machine with 60 slots and it has also been rewound with a three phase four pole bridge configured winding configuration. The winding patterns of these two machines are same as that of the winding pattern of the machine used for the numerical investigation discussed in Chapters 4 and 5. It is very important to measure the magnetic fields present in the machine at every instant. Search coils are used to capture the magnetic field present in the machine. Search coils are installed along with the main stator coils during rewinding process. Figures 7.1 and 7.2 show the two experimental setups used for the verification of numerical findings. The main components of RIG I and RIG II are

(i) Induction machine having bridge configured winding.

(ii) Search coils for the measurement of magnetic field.

(iii) Three phase auto transformer and variable frequency drive (VFD) as a main supply source.

(iv) Three single phase programmable AC source as a bridge supply source.

(v) Voltage and current sensors to measure voltage and current in the winding.

(vi) Displacement sensors for the measurement of rotor vibration.

(vii) Data acquisition system for storing and processing of measurement data.

(viii) connectors and battery source for the sensors.

Figure 7.3 shows the schematic representation of the experimental setups. The variable frequency drive (VFD) and three phase auto transformer has been used as a three phase main supply source to the BCW induction machine. The variable frequency drive can be operated upto 100 Hz. The VFD is used as a power supply source for RIG II, whereas three phase transformer is used as a power supply source for RIG I. The VFD is used in RIG II so that the vibration characteristics of the rotor can be studied at variable frequency range because the rotor of the motor is flexible in nature. However, this machine got damaged and very few measurements could be taken on this experimental setup.

For the measurement of voltage across the bridge points of the winding, Voltage transducer LV 20-P and for the measurement of current, current transducer LTS 15-NP has been used. The eddy current sensors, BENTLY Nevada 3300 XL NSv has been used for the measurement of rotor vibrations. 12 V batteries have been used in combination as per the requirement as a power source to these sensors. For the connection of power source to these sensors, 0.25 mm^2 multi strand coils are used. Whereas for the measurements of output signals, RG 55 coaxial cables has been used. All the measurements

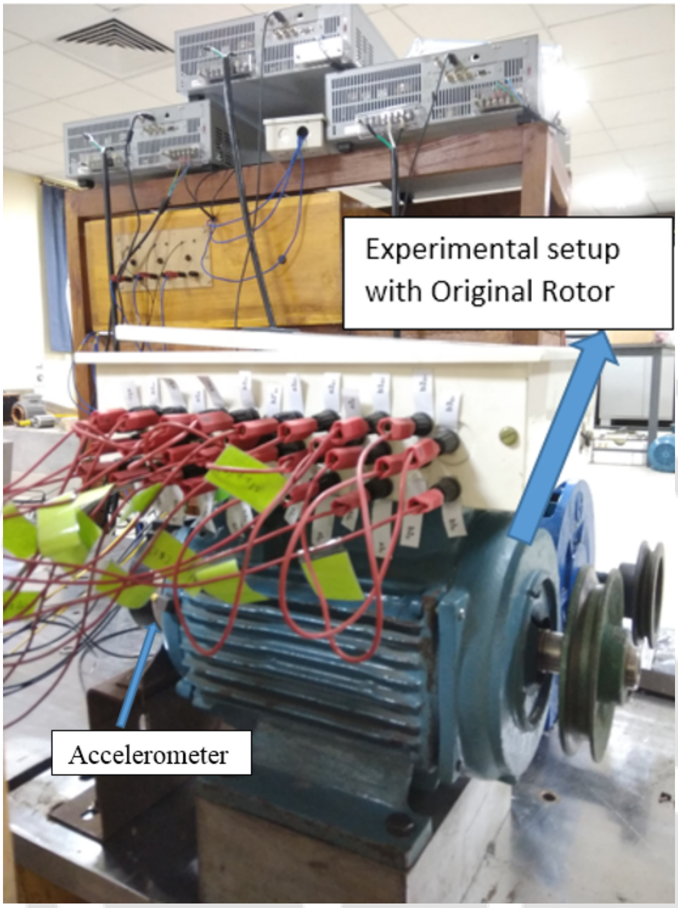

Figure 7.1: RIG I, experimental setup with original rotor.

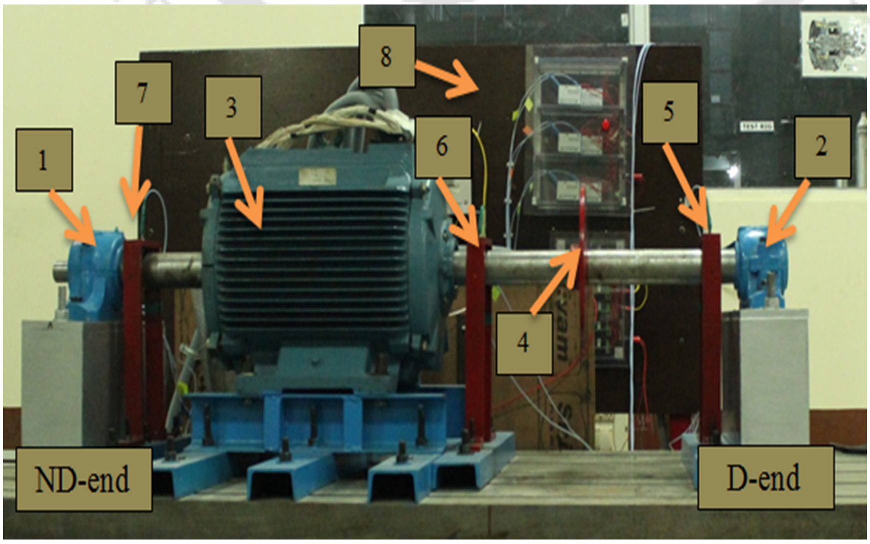

Figure 7.2: RIG II, experimental setup with a long shaft, (1,2) - bearing housing at ND and D end, 3 - test machine, 4 - perforated disc, (5,6,7) - location for the rotor responses, 8 - panel board.

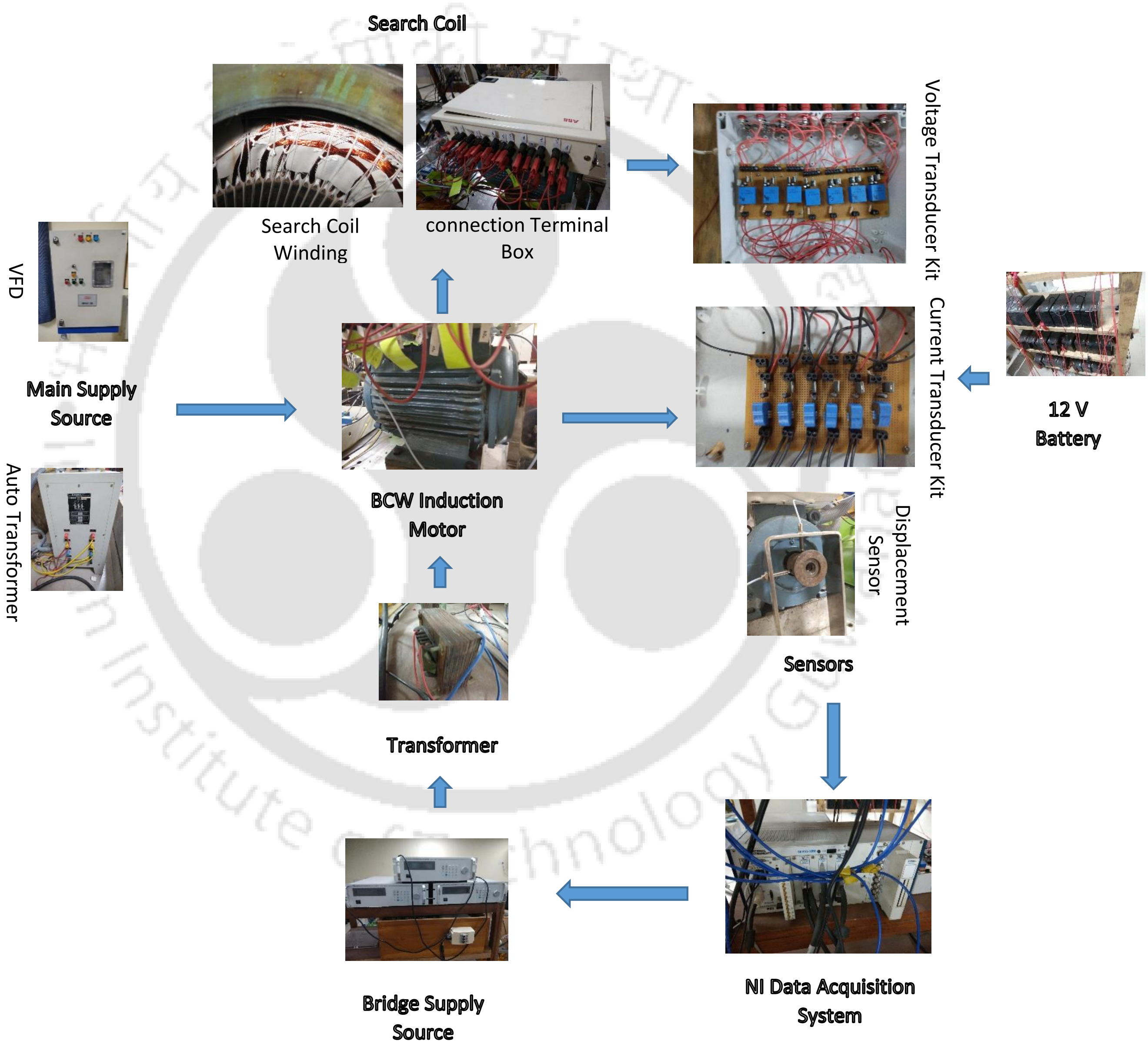

Figure 7.3: Schematic representation of the experimental setup.

has been carried out by NI data acquisition system having NI PXI-1050 chassis and NI PXI-6289, NI PXI 6221 modules. The output signals through the coaxial cables are connected to SCB-68 connector boxes which are connected to PXI modules using SHC68-68-EPM cables. NI LabView software has been used for storing of measured data.

As a bridge supply source, three single phase Chroma programmable AC source (Model 61601) has been used. This source can be used to supply maximum 150 V or 3 A current. As per the requirement of the bridge configured winding, the bridge supply source should be isolated from the main supply source. Hence, for the isolation, the output of these programmable AC sources are connected to bridge terminals of the BCW induction machine through 1:1 transformers. These programmable AC sources are controlled through the NI LabView for the supply of desired bridge voltage of required frequency.

The search coils of two pole, four pole and six pole are required to measure the presence of these harmonic components of the magnetic field, as interaction of these harmonic components of the magnetic field lead to the generation of the transverse force. While rewinding of the machine, two phase of the two pole search coils, three phase of the four pole search coils and two phase of the six pole search coils have been incorporated. Figure 7.4 represents the search coil configuration used in RIG I. The similar configuration has been used in RIG II.

$a1_{2+} - a1_{2-}$ and $b1_{2+} - b1_{2-}$ represent phase A and phase B of the two pole search coil, $a1_{4+} - a1_{4-} - a2_{4+} - a2_{4-}$, $b1_{4+} - b1_{4-} - b2_{4+} - b2_{4-}$ and $b^{'}1_{4+} - b^{'}1_{4-} - b^{'}2_{4+} - b^{'}2_{4-}$ represent phase A, phase B and phase C of the four pole search coil, $a1_{6+} - a1_{6-} - a2_{6+} - a2_{6-} - a3_{6+} - a3_{6-}$ and $b1_{6+} - b1_{6-} - b2_{6+} - b2_{6-} - b3_{6+} - b3_{6-}$ represent phase A and phase B of the six pole search coil respectively. The phase A and the phase B of the two pole and the six pole search coils are at 90 degree electrical angle. However it is not possible to have two phases of the four pole search coils which is 90 degree electrically apart. Hence three phases of the four pole search coils have been used. Phase A and average of phase B and phase C of the four pole search coils are 90 degree electrically apart.

7.3 Experimental investigation of pulsating magnetic field

7.3.1 Analysis

Due to the limitations in the mechanical assembly of the rotor and the stator system, there is an inherent presence of the mixed eccentricity in both of the experimental setups. In an eccentric

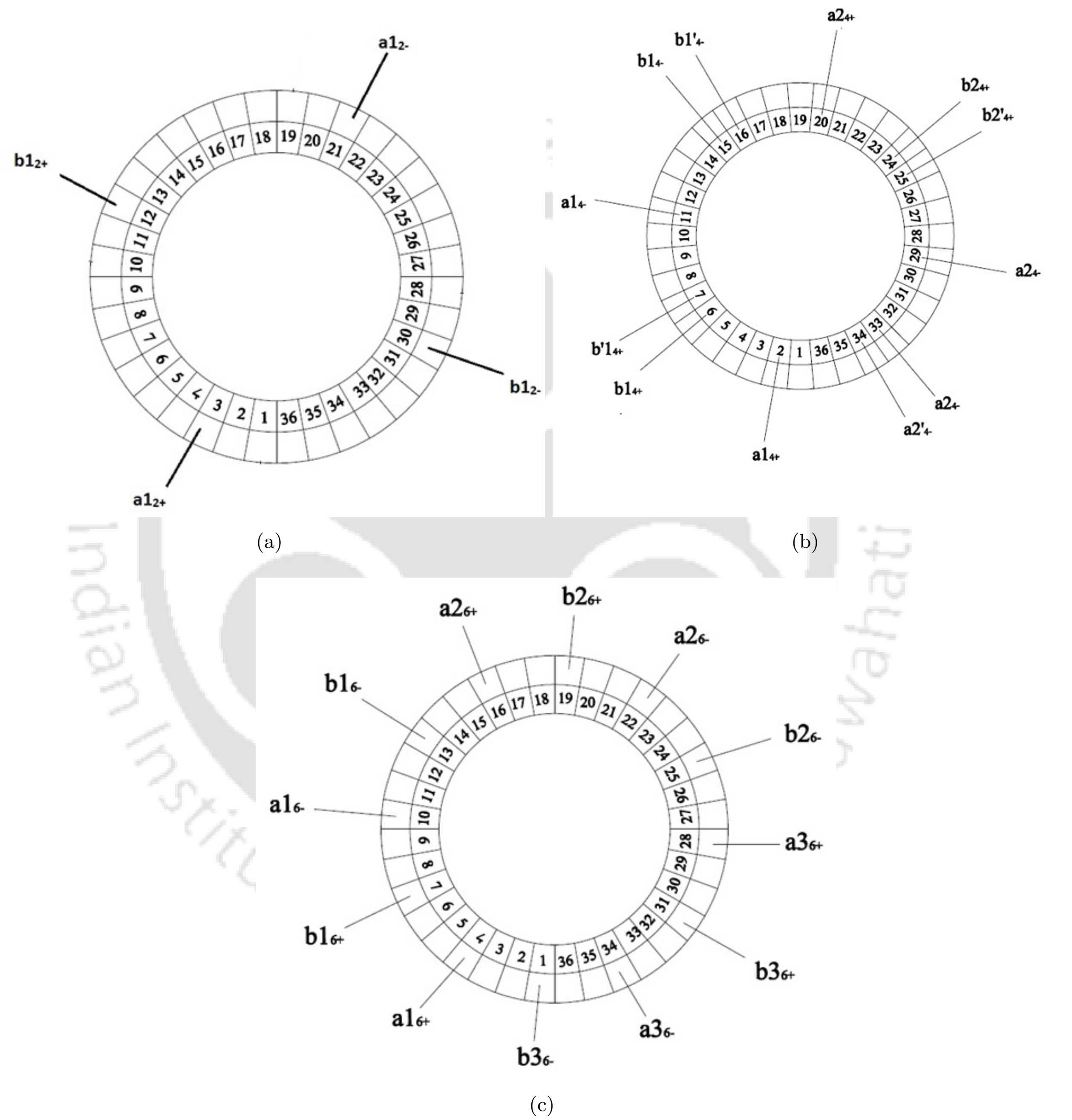

Figure 7.4: Winding configuration of (a) the two pole search coil (b) the four pole search coil and (c) the six pole search coil installed in the induction machine of RIG I

rotor condition, in a four pole electrical machine, the eccentricity would generate two pole and six pole magnetic fields components. As per the numerical investigation presented in Chapter 3, in static eccentricity condition the eccentricity induced two pole and six pole magnetic fields would have 50 Hz frequency component, in dynamic eccentricity condition the eccentricity induced two pole and six pole magnetic fields would have 25 Hz and 75 Hz frequency components respectively, whereas in mixed eccentricity condition the eccentricity induced two pole and six pole magnetic fields would have combination of frequency components generated in static and dynamic eccentricity conditions, i.e., (50 Hz & 25 Hz) for two pole magnetic field and (50 Hz & 75 Hz) for six pole magnetic field. These eccentricity-generated magnetic fields would induce some voltage across the two pole search coils and the six pole search coils. Since the fundamental four pole magnetic field is of 50 Hz, so 50 Hz component due to the four pole magnetic field would also be induced in the two pole and the six pole search coils. Hence, for the analysis of the eccentricity generated magnetic fields, only 25 Hz component of the magnetic field has been investigated for the two pole magnetic field and 75 Hz component of the magnetic field has been investigated for the six pole magnetic field. The induced voltage due the two pole magnetic field in the two pole search coils of 25Hz component and the induced voltage due to the six pole magnetic field in six pole search coils of 75 Hz component has been extracted for the analysis. Whereas, the induced voltage due to the four pole magnetic field in the four pole search coil of 50 Hz component has been extracted for the analysis.

The induced voltage in the six pole search coils, the two pole search coils and the four pole search coils have been measured using the LabView data acquisition system. The sampling frequency of the measurement is 5 kHz. The 75 Hz, 25 Hz and 50 Hz components of the voltage from the six pole, two pole and four pole search coils induced voltage have been separated by fitting the curve as shown in Equations (7.3) - (7.2),

$$V_{2m} = a_1 \cos(2 \times \pi \times 25 \times t) + a_2 sin(2 \times \pi \times 25 \times t) + a_3 t + a_4 \tag{7.1}$$

$$V_{4m} = a_1 \cos(2 \times \pi \times 50 \times t) + a_2 sin(2 \times \pi \times 50 \times t) + a_3 t + a_4 \tag{7.2}$$

$$V_{6m} = a_1 \cos(2 \times \pi \times 75 \times t) + a_2 sin(2 \times \pi \times 75 \times t) + a_3 t + a_4 \tag{7.3}$$

where, V_{2m}, V_{4m} and V_{6m} are the induced voltages in the two pole, the four pole and the six pole search coils respectively. The measurements of induced voltage in search coils have been carried out in both of the experimental setups when bridges are in OFF and ON conditions. A full spectrum FFT of

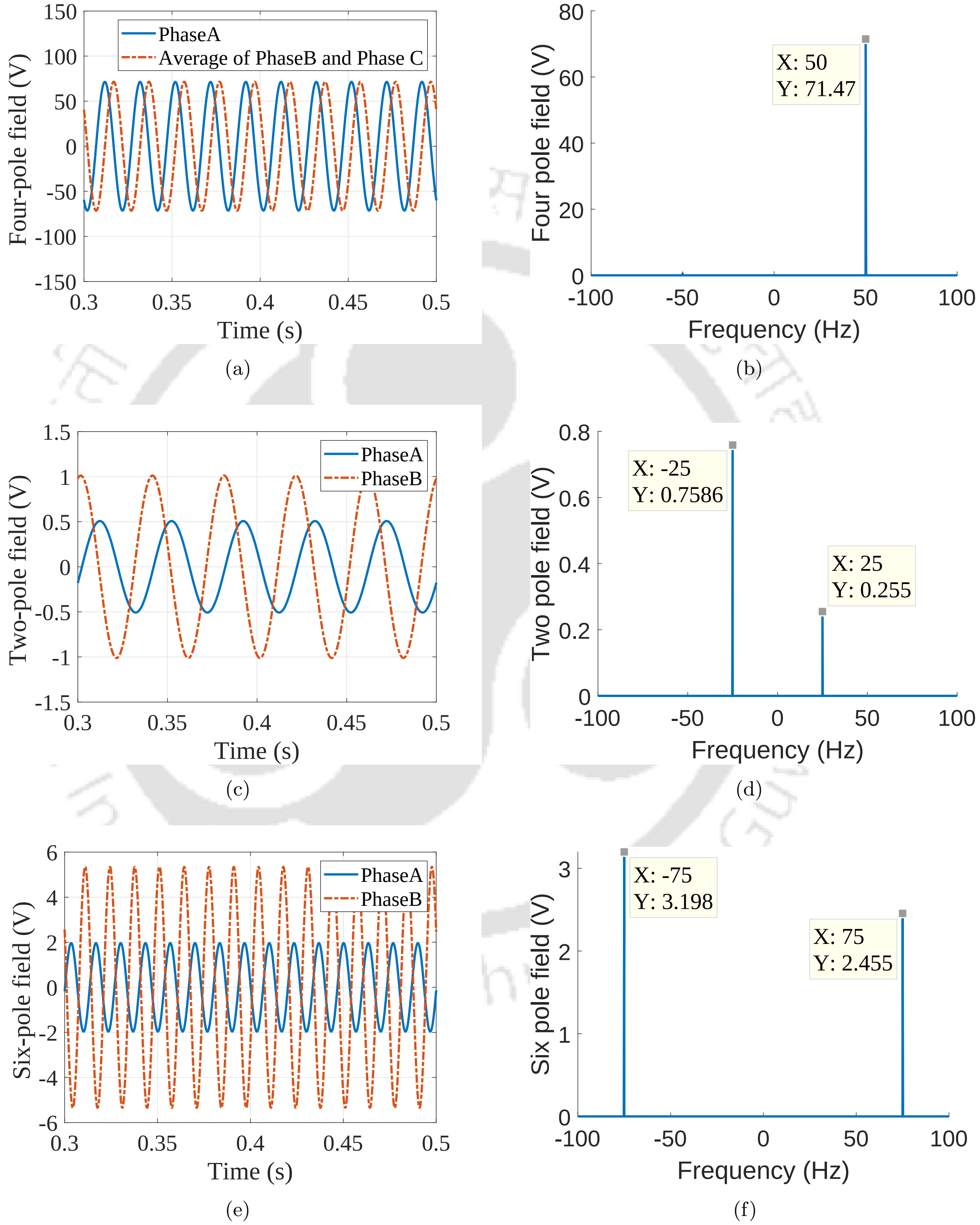

Figure 7.5: Induced voltage in search coils when bridge is in OFF condition in 60 slot induction motor (a) Four pole field (b) FFT of four pole field (c) Two pole field (d) FFT of two pole field (e) Six pole field (f) FFT of six pole field.

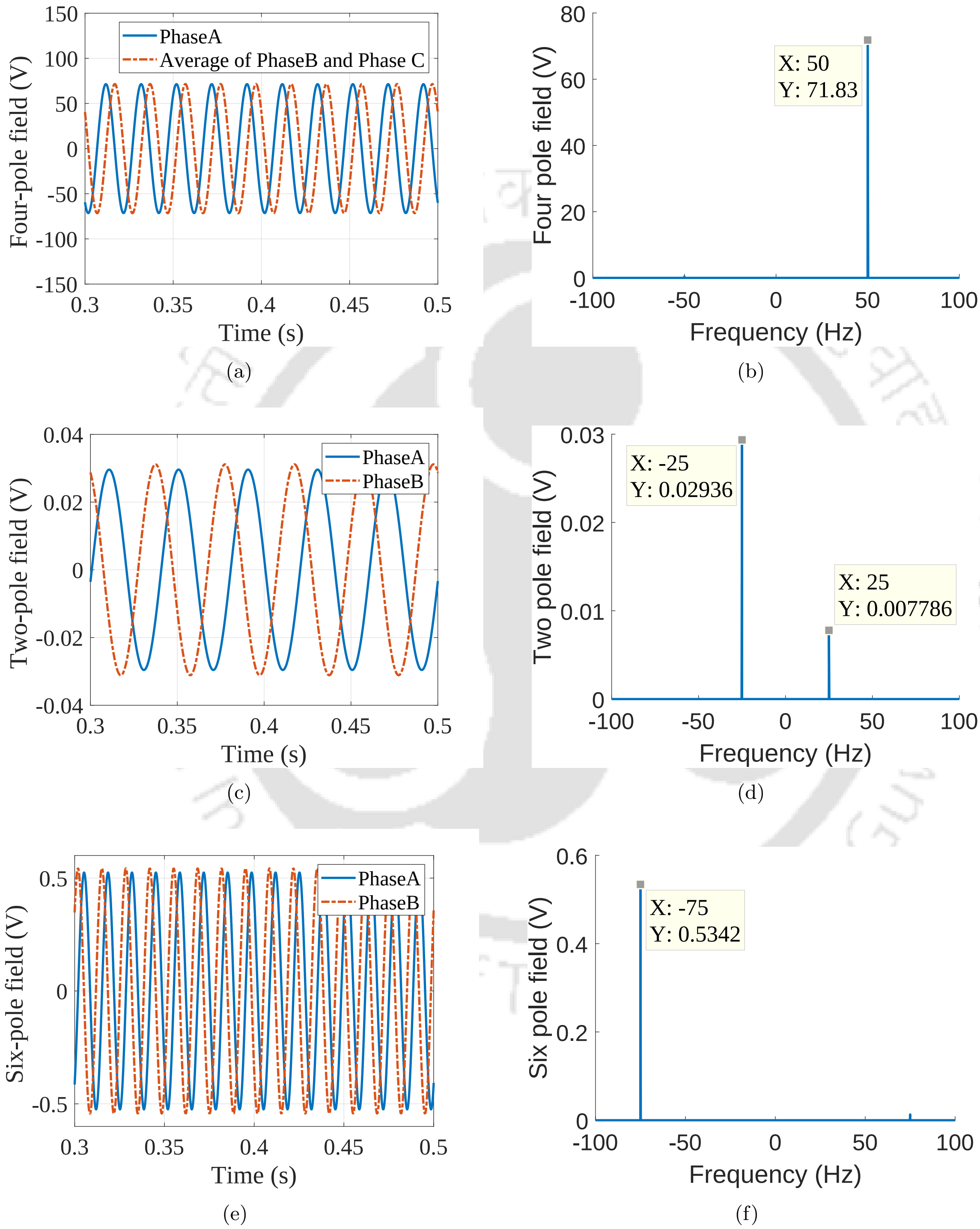

Figure 7.6: Induced voltage in search coils when bridge is in ON condition in the induction machine of RIG II (a) Four pole field (b) FFT of four pole field (c) Two pole field (d) FFT of two pole field (e) Six pole field (f) FFT of six pole field.

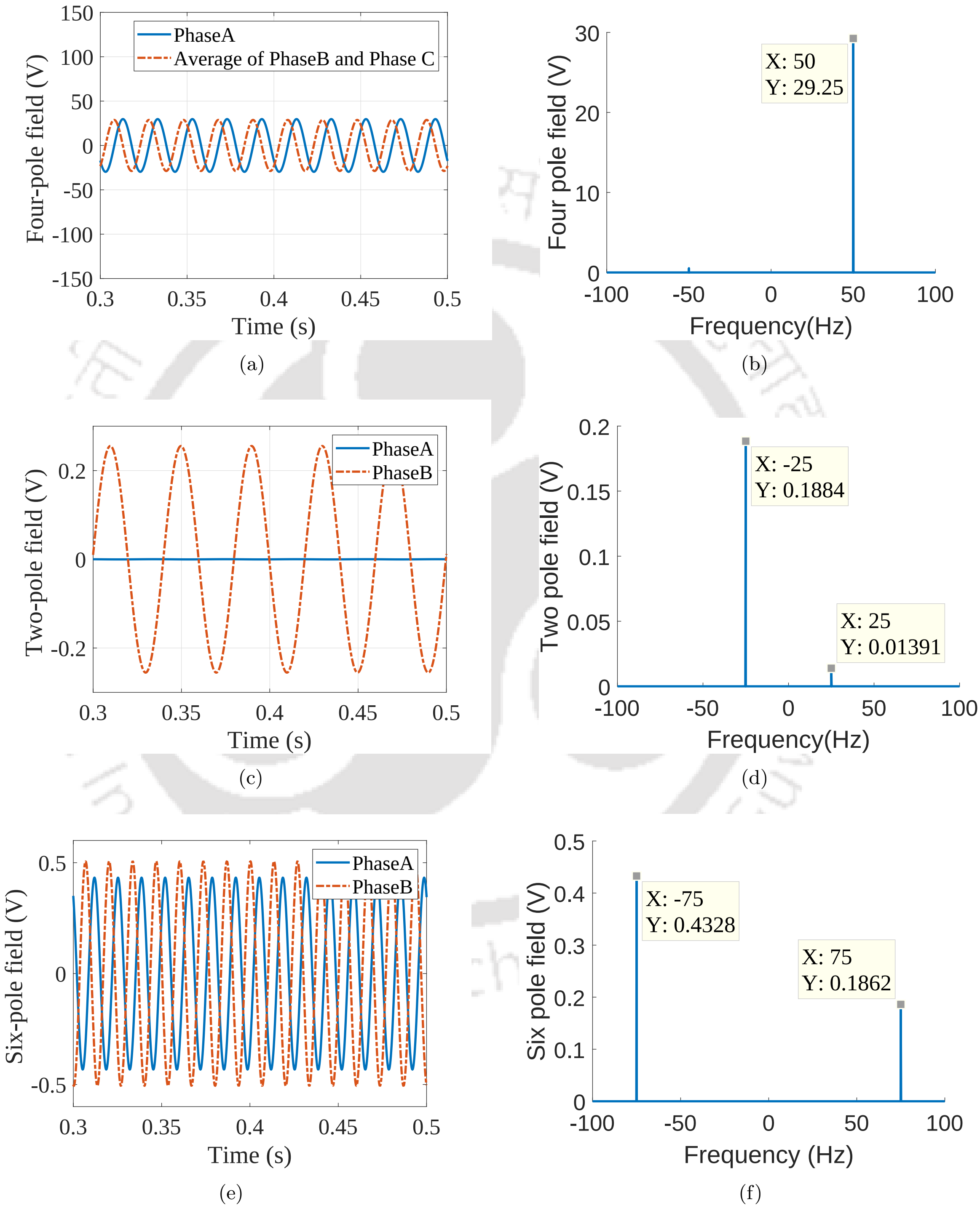

Figure 7.7: Induced voltage in search coils when bridge is in OFF condition in the induction machine of RIG I (a) Four pole field (b) FFT of four pole field (c) Two pole field (d) FFT of two pole field (e) Six pole field (f) FFT of six pole field.

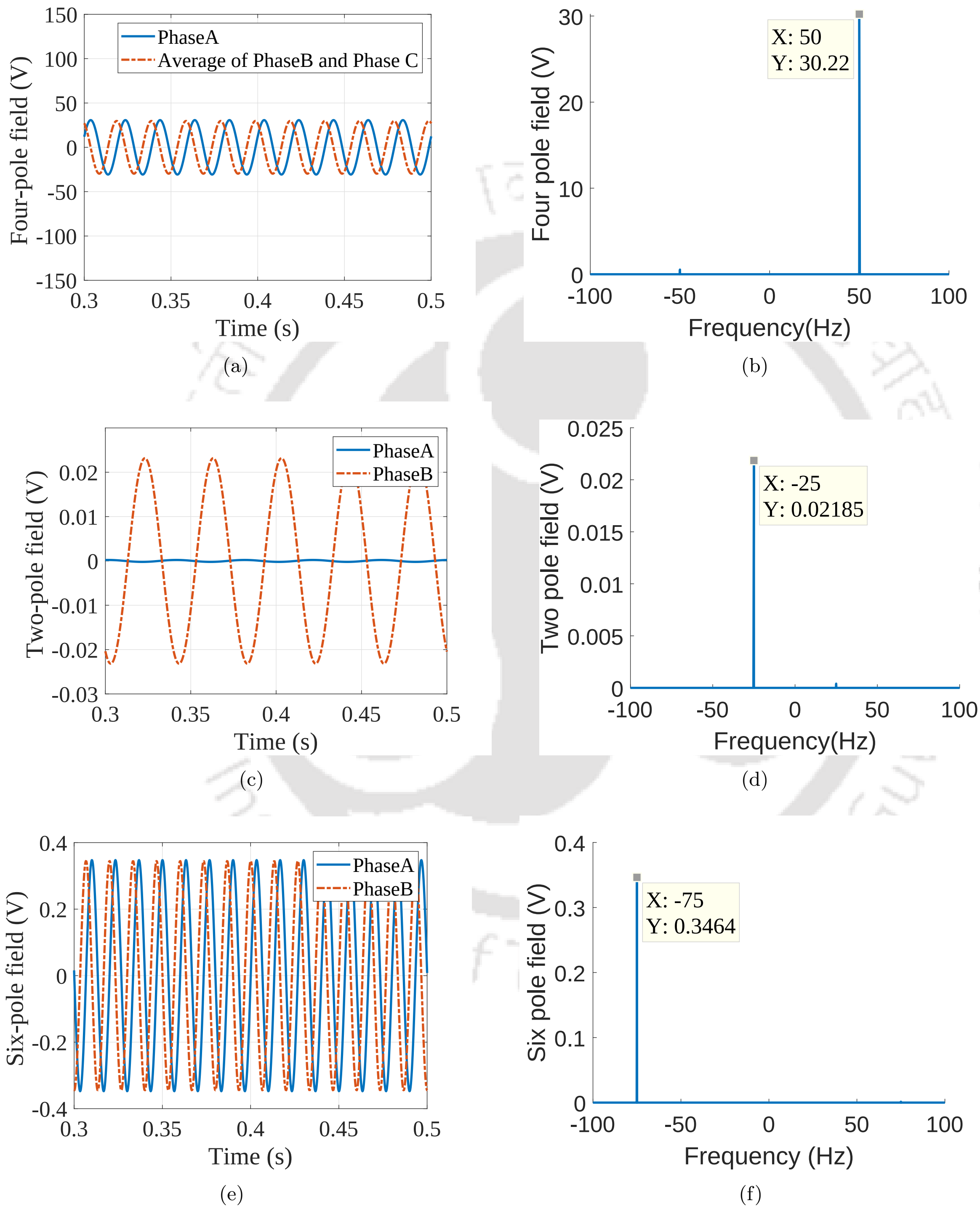

Figure 7.8: Induced voltage in search coils when bridge is in ON condition in the induction machine of RIG I (a) Four pole field (b) FFT of four pole field (c) Two pole field (d) FFT of Two pole field (e) Six pole field (f) FFT of six pole field

the measured voltages have been carried out to see the presence of the pulsating harmonic component in the air gap. To obtain a full spectrum FFT, the measured voltages have been converted in complex form as shown in Equations (7.4) - (7.6)

$$V_4 = V_{a4} + \mathrm{j}(V_{b4} + V_{c4})/2 \tag{7.4}$$

$$V\mathrm{j}_2 = V_{a2} + V_{b2} \tag{7.5}$$

$$V_6 = V_{a6} + \mathrm{j}V_{b6} \tag{7.6}$$

where V_{a4}, V_{b4} and V_{c4} are the extracted 50 Hz component of the voltage from the measured voltages of phase A, phase B and phase C of the four pole search coils respectively, V_{a2} and V_{b2} are the extracted 25 Hz component of the voltage from the measured voltages of phase A and phase B of the two pole search coils, V_{a6} and V_{b6} are the extracted 75 Hz component of the voltage from the measured voltages of phase A and phase B of the six pole search coils respectively.

Figures 7.5 and 7.6 represent the plot of extracted components of induced voltage in search coils and its full spectrum FFT in 60 slot induction machines (RIG II) in bridge OFF and bridge ON conditions respectively. It can be seen in Figure 7.5(b) that FFT of the four pole induced voltage shows the presence of forward rotating four pole magnetic field. FFT of the two pole and six pole induced voltage show the presence of forward as well as backward rotating component of the magnetic field as shown in Figures 7.5(d) and 7.5(f) respectively. It can be understood as the combination of the rotating and pulsating component of the magnetic field. The two pole magnetic field component is quite small and can be ignored. The effect of bridge ON condition can be observed in Figure 7.6. It can be seen that the bridge ON condition has no effect on the four pole magnetic field component. Similar to the bridge OFF condition in bridge ON condition too a forward rotating component of the magnetic field has been observed as shown in Figure 7.6(b). However the bridge ON condition reduces the two pole and the six pole components of the magnetic field as shown in Figures 7.6(d) and 7.6(f) respectively. It makes two pole component of the magnetic field almost negligible and eliminates the pulsating component of the six pole magnetic field.

The same effect has been seen in 36 slot induction machine (RIG I) measurements. It can be seen in Figures 7.7(b) and 7.8(b) that the bridge ON condition has no effect on the four pole magnetic field and a forward rotating magnetic field can be observed. A combination of pulsating and rotating components of six pole magnetic field can be seen in Figure 7.7(f). Similar to RIG II, the

Table 7.1: Comparison of magnetic field behavior in numerical and experimental analysis

Numerical Simulation						
	Series Connection					
	Four - Pole		Two - Pole		Six - Pole	
	Rotation	Pulsation	Rotation	Pulsation	Rotation	Pulsation
Static Eccentricity	5/0.1, 50 Hz	Not Present	5/0.1, 50 Hz	Not Present	5/0.1, 50 Hz	Not Present
Dynamic Eccentricity	10/0.2, 50 Hz	Not Present	5/0.2, 25 Hz	Not Present	15/0.2, 75 Hz	Not Present
Mixed Eccentricity	10/0.2, 50 Hz	Not Present	5/0.2, 25 Hz 10/0.2, 50 Hz	Not Present	10/0.2, 50 Hz 15/0.2, 75 Hz	Not Present
	BCW Connection (Bridge OFF)					
	Four - Pole		Two - Pole		Six - Pole	
	Rotation	Pulsation	Rotation	Pulsation	Rotation	Pulsation
Static Eccentricity	5/0.1, 50 Hz	Not Present	5/0.1, 50 Hz	Very Small	5/0.1, 50 Hz	50 Hz
Dynamic Eccentricity	10/0.2, 50 Hz	Not Present	5/ 0.2, 25 Hz	Very Small	15/0.2, 75 Hz	75 Hz
Mixed Eccentricity	10/0.2, 50 Hz	Not Present	5/0.2, 25 Hz 10/0.2, 50 Hz	Very Small	10/0.2, 50 Hz 15/0.2, 75 Hz	50 Hz, 75 Hz
	BCW Connection (Bridge ON)					
	Four - Pole		Two - Pole		Six - Pole	
	Rotation	Pulsation	Rotation	Pulsation	Rotation	Pulsation
Static Eccentricity	5/0.1, 50 Hz	Not Present	5/0.1, 50 Hz	Not Present	5/0.1, 50 Hz	Not Present
Dynamic Eccentricity	10/0.2, 50 Hz	Not Present	5/0.2, 25 Hz	Not Present	15/0.2, 75 Hz	Not Present
Mixed Eccentricity	10/0.2, 50 Hz	Not Present	5/0.2, 25 Hz	Not Present	10/0.2, 50 Hz 15/0.2, 75 Hz	Not Present
Experimental Investigation						
	BCW Connection (Bridge OFF)					
	Four - Pole		Two - Pole		Six - Pole	
	Rotation	Pulsation	Rotation	Pulsation	Rotation	Pulsation
Motor (60 Slot)	Forward, 50 Hz	Not Present	25 Hz	25 Hz	75 Hz	75 Hz
Motor (36 Slot)	Forward, 50 Hz	Not Present	25 Hz	25 Hz	75 Hz	75 Hz
	BCW Connection (Bridge ON)					
	Four - Pole		Two - Pole		Six - Pole	
	Rotation	Pulsation	Rotation	Pulsation	Rotation	Pulsation
Motor (60 Slot)	Forward, 50 Hz	Not Present	25 Hz	Not Present	75 Hz	Not Present
Motor (36 Slot)	Forward, 50 Hz	Not Present	25 Hz	Not Present	75 Hz	Not Present

bridge ON condition in RIG I reduces the two pole and the six pole magnetic field components and completely eliminates the pulsating component of six pole magnetic field as shown in Figures 7.7(d) and 7.8(f) respectively. A comparison of magnetic field components obtained in the numerical and the experimental investigations have been presented in Table 7.1.

7.3.2 Conclusion

This section investigates the presence of the eccentricity generated harmonic magnetic field components in the air gap. The measurement shows the presence of pulsating 75 Hz, six pole and 25 Hz, two pole components of the magnetic field. However, the presence of the two pole pulsating component of the magnetic field is negligible. This verifies the numerical observation made in Chapter 3 that the presence of pulsating six pole magnetic field is the reason behind the generation of the additional component of the UMP.

In addition to this the passive vibration suppression capability of the BCW winding scheme in bridge ON condition has also been analysed. It has been established that in bridge ON condition, the two pole and the six pole magnetic field components get reduced and it completely eliminates the pulsating component of the six pole and the two pole magnetic fields. This elimination of the pulsating two pole and the six pole components of the magnetic field leads to vibration suppression in bridge ON condition.

7.4 Experimental investigation of eccentricity induced bridge currents and rotor vibrations

7.4.1 Analysis

This section investigates the numerical simulation observations made in Chapter 4. Chapter 4 establishes the relationship of bridge currents frequency components and force frequency components in the static, dynamic and mixed eccentricity conditions. It has been shown that the bridge currents have $\pm f_s$ Hz frequency components in static eccentricity condition, $\pm(f_s - f_r)$ Hz frequency components in dynamic eccentricity condition and combination of these components in mixed eccentricity condition. Also, it has been shown that the frequency components of UMP generated due to an eccentric rotor, is dependent on the frequency components of the induced bridge currents. The generated UMP has $(\pm f_s \pm f_{bridge})$ Hz frequency components. Here, f_s is the main supply frequency, f_r is the rotor rotational frequency and f_{bridge} is the frequency component of bridge current.

The developed experimental setup does not have the facility to change the eccentricity condition of the rotor. However, from the measurements of the bridge currents and rotor vibrations, the type of the eccentricity present in the motor can be guessed by having a comparison with the numerical findings. This also verifies the numerical find in one way.

The bridge currents and vibration patterns have been analysed using both experimental setups (RIG I & RIG II). The induction machine in RIG I uses the original shaft of the machine for the experiment. To capture the vibration signals an accelerometer has been placed on the body of the motor. Whereas, in RIG II, the original shaft of the rotor of the induction machine is replaced with a 1.5 m long shaft to make the rotor system flexible so that more frequency components of the force acting on the rotor can be observed. The eddy current sensors have been used to measure the displacement signals along x (longitudinal direction) and y (transverse direction) axes, which have been placed at location 6 in the experimental setup as shown in Figure 7.2. The measured bridge currents and vibration signals have been analysed further to investigate the effect of eccentricity on it. Similar to the numerical investigation presented in Chapter 4, the measured bridge currents

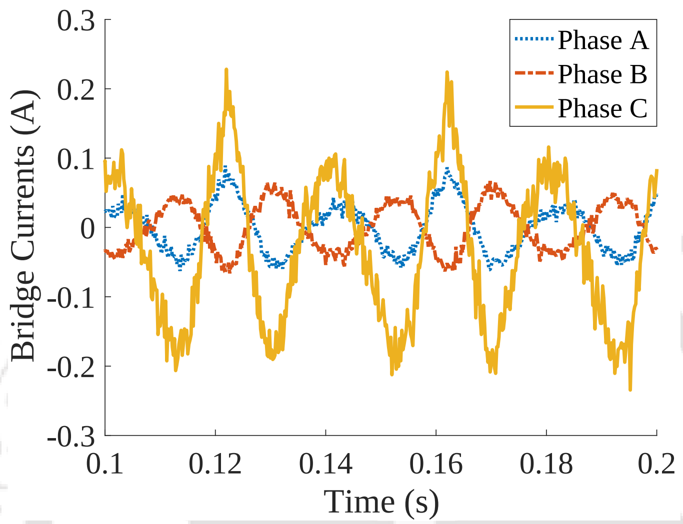

Figure 7.9: Measured bridge currents with the original rotor in RIG I.

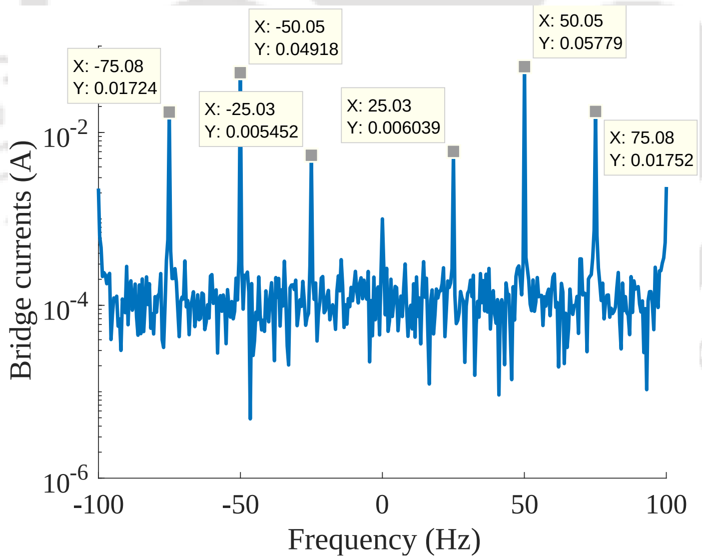

Figure 7.10: Full spectrum FFT of measured bridge currents when the motor has its original shaft in RIG I.

have been converted to space vector as explained in Equation (4.63) and vibration measurements have been converted in complex domain as, $d_x + jd_y$ where d_x and d_y are the rotor displacements along x and y axis respectively. In the case of RIG I, the machine has been supplied using a three phase auto transformer with a rated voltage of 415 V at 50 Hz (f_s). The motor has been operated at no load so the rotor rotational frequency (f_r) is very close to 25 Hz. Since the rotor is a rigid rotor and accelerometer is placed on the body of the motor, the bridge OFF and the bridge ON conditions do not have any effect on the accelerometer signals. The accelerometer data has been presented only for the bridge ON condition. It should be noted that, in bridge OFF condition there would not be any flow of current through the bridge points, so the bridge currents can only be recorded in bridge ON condition. Figure 7.9 shows the bridge currents flowing through the bridge points of the machine and Figure 7.10 shows the full spectrum FFT of space vector of measured bridge currents. The presence

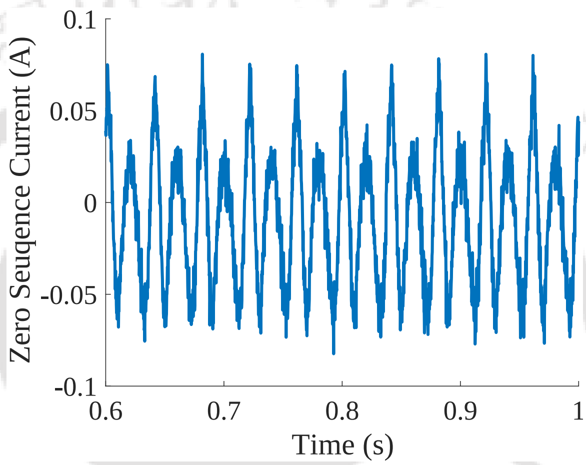

Figure 7.11: Zero sequence bridge currents when the motor has its original shaft (RIG I).

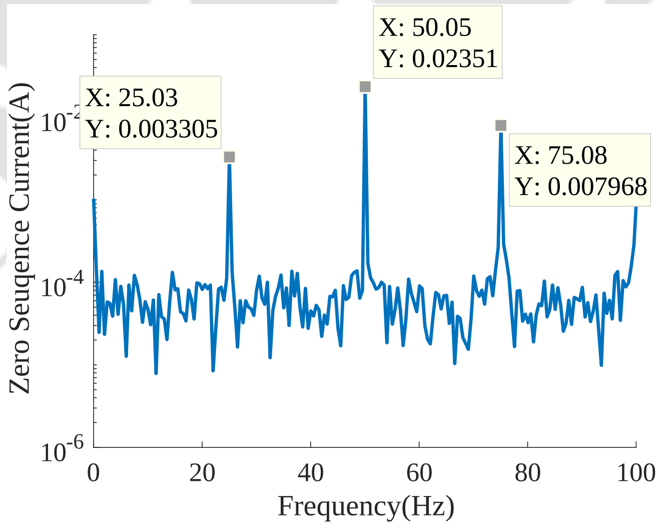

Figure 7.12: FFT of zero sequence bridge currents when the motor has its original shaft (RIG I).

of ± 25 Hz ($f_s - f_r$) and ± 75 Hz ($f_s + f_r$) components in full spectrum FFT of space vector of bridge currents signifies the presence of dynamic eccentricity in the machine whereas the presence of 50 Hz (f_s) component represent the presence of static eccentricity condition in the machine. The presence of all three component of the bridge currents indicates that the machine is being operated in mixed eccentricity condition as shown in numerical investigation. Similar to the numerical investigation zero sequence component is also presented as shown in Figure 7.11. Figure 7.12 represents FFT of zero sequence component of the bridge currents which also signifies the presence of mixed eccentricity condition as all three frequency components are present. The accelerometer data show 0 Hz and 100 Hz components and confirms the presence of static eccentricity. Whereas 25 Hz, 75 Hz and 125 Hz components show the presence of dynamic eccentricity. The presence of these frequency components in combination as shown in Figure 7.13 signifies the presence of mixed eccentricity condition in RIG I. In numerical investigation it has been observed that the bridge currents suppress almost all the frequency components of the UMP other than DC component and $f_s - f_r$ component. Whereas in this experimental setup bridge currents are not sufficient to suppress motor vibration. It might be happening due to the rigid rotor.

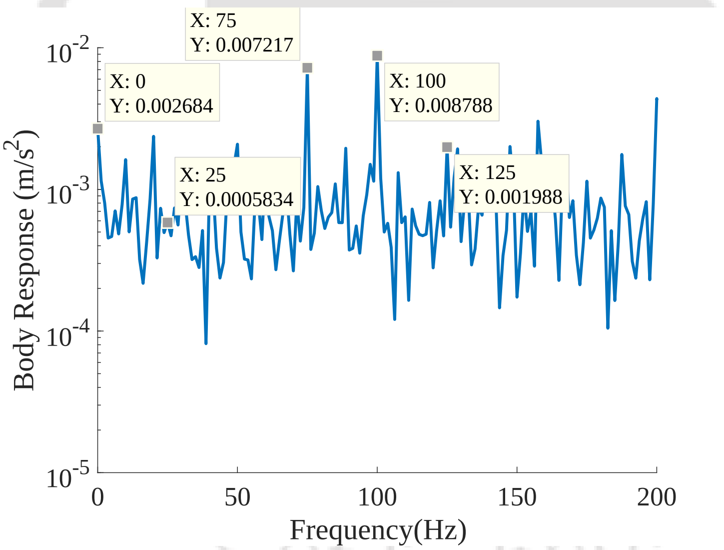

Figure 7.13: FFT of accelerometer data when the motor has its original shaft (RIG I).

So, to investigate further a rotor with a flexible shaft (RIG II) has been used for the experiment as shown in Figure 7.2. Also to have a generalized effect, the rotor vibration has been analyzed at two different supply frequencies i.e. 20 Hz and 30 Hz using a variable frequency drive. 20 Hz and 30 Hz have been chosen as main supply frequencies because the shaft of the motor is flexible and it can not be operated at higher speeds. Again, the motor has been operated at no load condition so for supply frequencies (f_s) 20 Hz and 30 Hz, the rotor rotational frequencies (f_r) are very close to 10 Hz and 15 Hz respectively. Figures 7.14 and 7.15 represent the bridge currents and full spectrum FFT of space vector

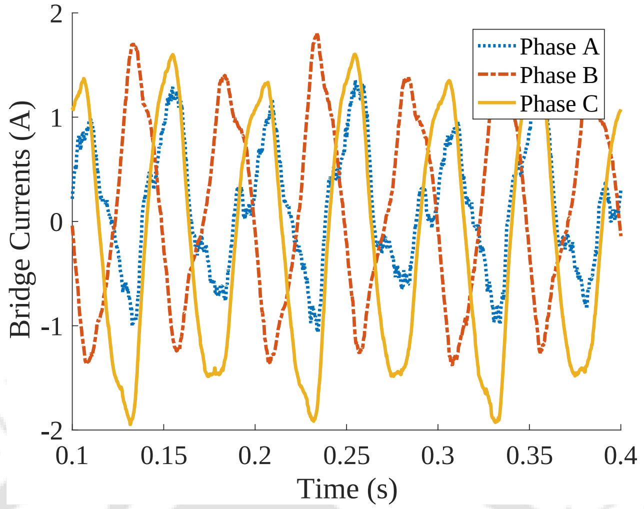

Figure 7.14: Measured bridge currents in experimental setup when the motor has a longer shaft (RIG II).

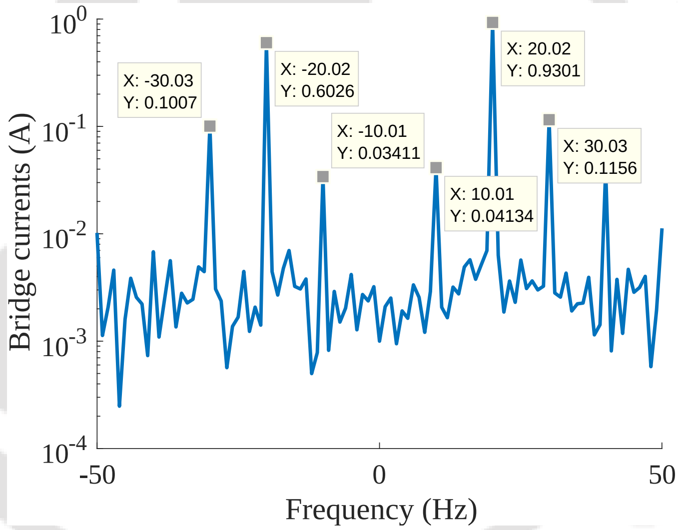

Figure 7.15: Full spectrum FFT of space vector of measured bridge currents when the motor has a longer shaft (RIG II).

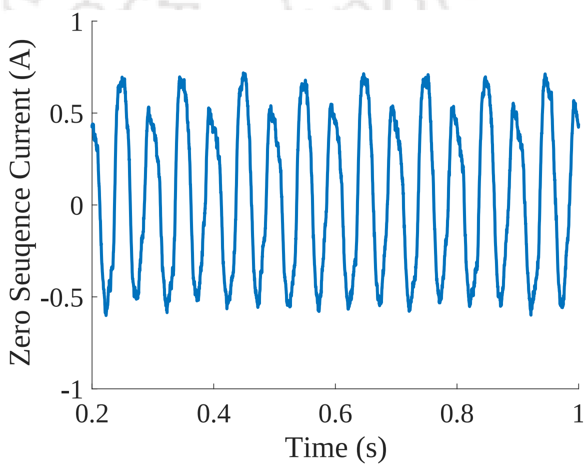

Figure 7.16: Zero sequence bridge currents when the motor has a longer shaft (RIG II).

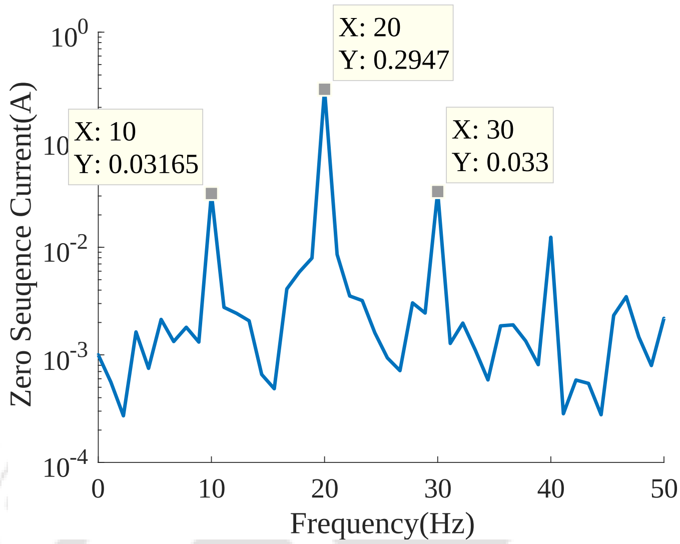

Figure 7.17: FFT of zero sequence bridge currents when the motor has a longer shaft (RIG II).

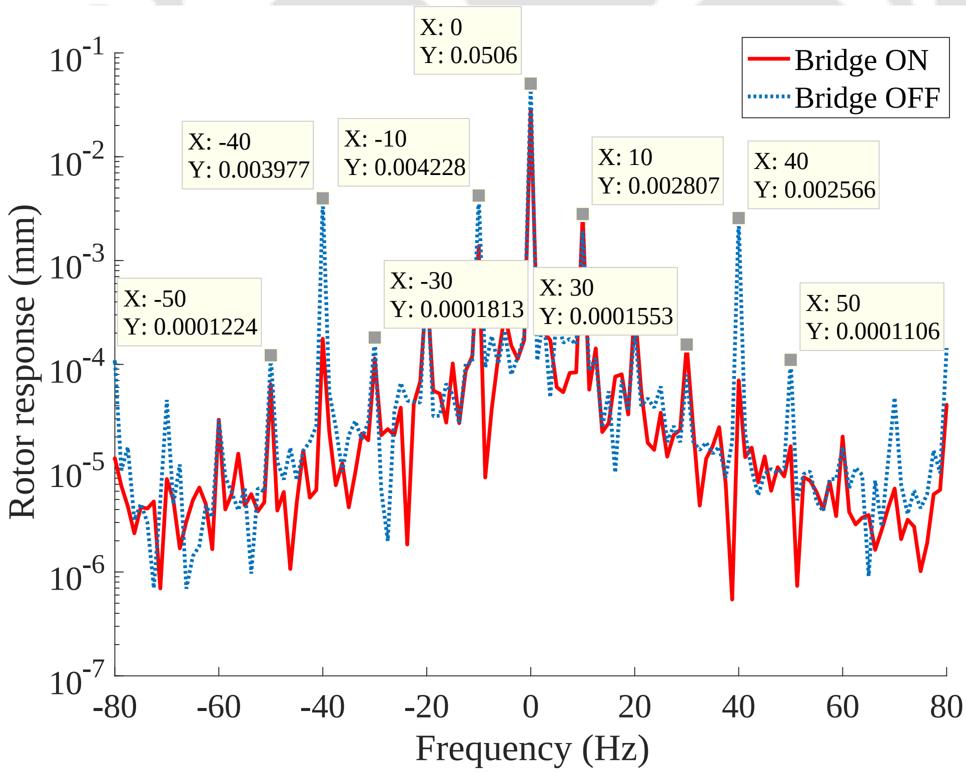

Figure 7.18: Full spectrum FFT of the rotor response when frequency of the main supply is 20 Hz (RIG II).

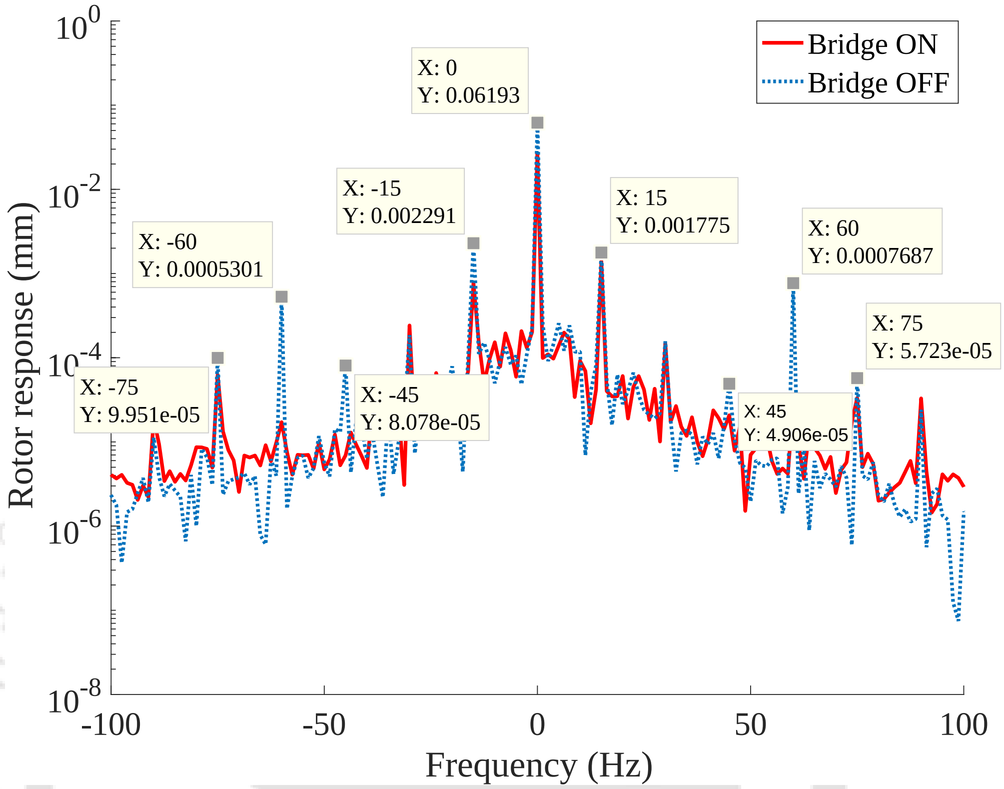

Figure 7.19: Full spectrum FFT of the rotor response when frequency of the main supplyis 30 Hz (RIG II).

of measured bridge currents in longer shaft rotor experimental setup when the main supply frequency is 20 Hz. All three components ±10 Hz $(f_s - f_r)$, ± 20 Hz(f_s) and ± 30 Hz$(f_s + f_r)$ are present which indicates the presence of mixed eccentricity condition in the machine. Figures 7.16 and 7.17 show the zero sequence current and its FFT respectively. FFT plot of zero sequence component of the bridge currents show the presence of all three frequency components. Similar behavior of the bridge currents have been observed when frequency of the main supply is 30 Hz. Figures 7.18 and 7.19 represent the full spectrum FFT of the rotor vibrations measured at location 6 of the RIG II experimental setup as shown in Figure 7.2 when the main supply frequencies are 20 Hz and 30 Hz respectively. It can be observed from Figures 7.18 and 7.19 that the rotor response has all the frequency components as per the relation $\pm f_s \pm f_{bridge}$. f_{bridge} is ±10 Hz, 20 Hz and ±30 Hz when f_s is 20 Hz and f_{bridge} is ±15 Hz, 30 Hz and ±45 Hz when f_s is 30 Hz. The rotor response shows the presence of 0 Hz, ± 10 Hz, ± 30 Hz, ± 40 Hz, and ± 50 Hz frequency components when the bridge are in OFF condition and main supply frequency is 20 Hz. The rotor response shows the presence of 0 Hz, ± 15 Hz, ± 45 Hz, ± 60 Hz, and ± 75 Hz frequency components when bridges are in OFF condition and the main

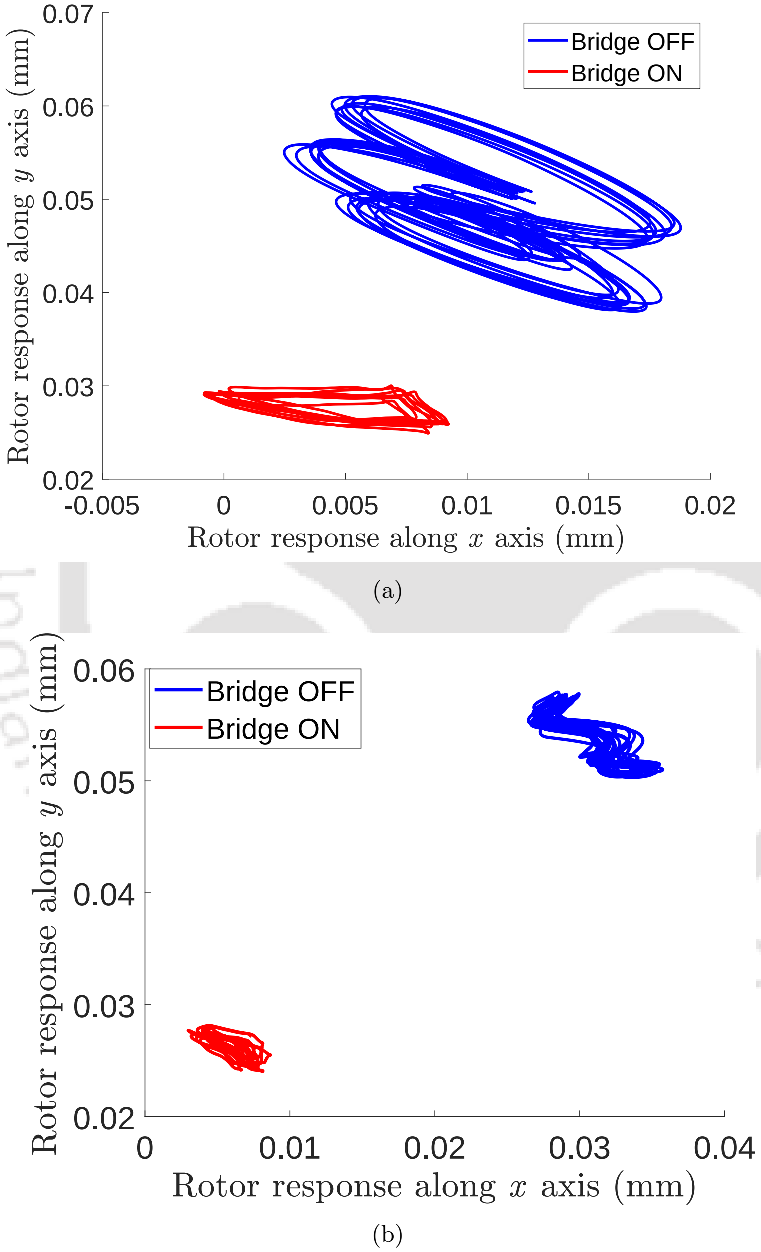

Figure 7.20: Comparison of rotor orbits in bridge OFF and bridge ON condition in Rig II when (a) the main supply frequency is 20 Hz (b) the main supply frequency is 30 Hz.

supply frequency is 30 Hz. Whereas, in bridge ON condition most of the vibration components are suppressed other than the DC component and $f_s - f_r$ component, which is 10 Hz and 15 Hz when the main supply frequency is 20 Hz and 30 Hz respectively.

For completeness, to demonstrate the vibration suppression capability of bridge configured winding, the rotor orbits have been compared in bridge OFF and bridge ON conditions. Figures 7.20(a) and 7.20(b) show the comparison of the rotor orbits in bridge OFF and bridge ON conditions when the main supply frequency is 20 Hz and 30 Hz respectively. It can be observed that the rotor centre is shifted more towards the origin which eventually reduces vibration.

In comparison with the numerical simulation all of the frequency components, be it bridge currents frequency component or vibration measurements frequency component of the experimental results demonstrate the presence of mixed eccentricity condition in the motor. To have a clarity in the interpretation, the simulation and experimental results have been summerised in a table. Table 7.2 presents the comparison of all the bridge currents, UMP and vibration measurement frequency components in all three eccentricity conditions.

Table 7.2: Summary of the numerical and experimental investigation of bridge currents and UMP

Numerical Simulation							
Type of Eccentricity	Supply Freq.	Slip	Bridge Currents			UMP	
			Space Vector Component	Zero Sequence Component		Bridge OFF	Bridge ON
Static Eccentricity	50 Hz	0.02	±50 Hz	50 Hz		0 Hz, ± 100 Hz	0 Hz
Dynamic Eccentricity	50 Hz	0.02	± 24.5 Hz, ± 74.5 Hz	24.5 Hz, 74.5 Hz		± 24.5Hz, ± 75.5 Hz ± 124.5 Hz	24.5 Hz
Mixed Eccentricity	50 Hz	0.02	± 50 Hz, ± 24.5 Hz, ± 74.5 Hz	50 Hz, 24.5 Hz, 74.5 Hz		0 Hz, ± 24.5 Hz, ± 75.5 Hz, ± 100 Hz, ± 124.5 Hz	0 Hz, 24.5 Hz
Experimental Measurements							
Type of Eccentricity	Supply Freq.	Slip	Type of Rotor	Bridge Currents		Motor Body/Rotor Vibration	
				Space Vector Component	Zero Sequence Component	Bridge OFF	Bridge ON
Not Known	50 Hz	No load	Short Rotor	± 25 Hz, ± 50 Hz, ± 75 Hz	25 Hz, 50 Hz, 75 Hz	0 Hz, 25 Hz, 75 Hz, 100 Hz, 125 Hz	0 Hz, 25 Hz, 75 Hz, 100 Hz, 125 Hz
Not Known	20 Hz	No load	Long Rotor	± 10 Hz, ± 20 Hz, ± 30 Hz	10 Hz, 20 Hz, 30 Hz	0 Hz, ± 10 Hz, ± 30 Hz ± 40 Hz, ± 50 Hz	0 Hz, 10 Hz
Not Known	30 Hz	No load	Long Rotor	± 15 Hz, ± 30 Hz, ± 45 Hz	15 Hz, 30 Hz, 45 Hz	± 0 Hz, ± 15 Hz, ± 45 Hz ± 60 Hz, ± 75 Hz	0 Hz, 15 Hz

7.4.2 Conclusion

Similar to the numerical analysis, various modes of the bridge currents have been analysed by transforming it from a, b, c sequence to $d, q, 0$ sequence. A relationship of bridge current modes with respect to different eccentricity conditions have been established. Also, it has been shown that the zero sequence component of the bridge currents can not be ignored in bridge configured winding. The space vector of bridge currents show the presence of three frequency components i.e. $\pm f_s$, $\pm(f_s - f_r)$ and $\pm(f_s + f_r)$ of the bridge currents. The relationship with respect to the main supply frequency component (f_s) and the induced bridge currents frequency component (f_{bridge}) in terms of vibration components have been analysed. It has been shown that the vibration harmonic components in bridge OFF condition has $\pm f_s \pm f_{bridge}$ frequency components. It has been also established that bridge currents suppresses all the UMP components other than DC component and $f_s - f_r$ component. It happens because eccentric rotor generates pulsating component of the magnetic field which gets suppressed when bridges are in ON condition. In comparison with the numerical simulation, experimental behavior of bridge currents and UMP generated vibration show the presence of mixed eccentricity condition in both experimental setups. This behavior of experimental measurements in one way also verifies the capability of the developed code.

7.5 Experimental investigation of the proposed bridge supply method

In this section the effect of bridge supply has been studied in 3.7 kW BCW induction machine of RIG I. Unfortunately the 37 kW experimental setup got damaged, hence only 3.7 kW BCW induction machine has been used for the verification of the proposed bridge supply method in Chapter 5 and effect of various bridge supply conditions discussed in Chapter 6. The accelerometer placed over the body of the motor could not observe the frequency of the force generated due to the bridge supply. Hence, the pulley on the drive end of the shaft has been removed, and the keyway slot on the shaft is covered using a cylindrical sleeve, so that the vibration signals can be observed using displacement sensors. The eddy current displacement sensors are placed to measure the vibration signals of the rotor. Figure 7.21 represents the experimental setup consisting of sleeve on the shaft of the rotor of Rig I.

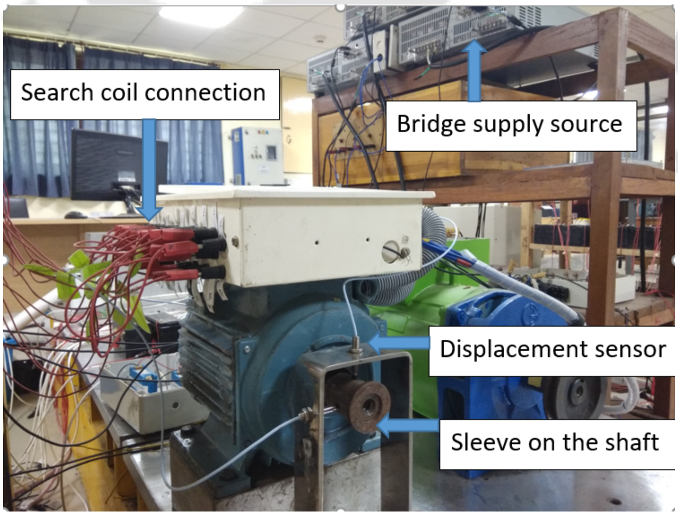

Figure 7.21: Experimental setup with original rotor and a sleeve on the shaft (RIG I).

The analysis of bridge supply has been analysed in two sections. In first section, the generation of the magnetic field components have been studied using the induced voltage in the search coils of the winding and in the second section, the vibration patterns have been analysed in bridge supply conditions.

7.5.1 Analysis of the magnetic field

The induced voltage in the six pole search coils, the two pole search coils and the four pole search coils have been measured using the National Instruments PXI data acquisition system when BCW machine in RIG I has been supplied with respect to bridge points in various ways. The sampling frequency of the measurement is 5kHz. The bridge supply frequency component of the induced voltage from the two pole, four pole and six pole search coils voltage have been separated by fitting the curve as shown in Equations (7.9) - (7.8),

$$V_{2m} = a_1 \cos(2\pi f_b t) + a_2 sin(2\pi f_b t) + a_3 t + a_4 \tag{7.7}$$

$$V_{4m} = a_1 \cos(2\pi f_b t) + a_2 sin(2\pi f_b t) + a_3 t + a_4 \tag{7.8}$$

$$V_{6m} = a_1 \cos(2\pi f_b t) + a_2 sin(2\pi f_b t) + a_3 t + a_4 \tag{7.9}$$

where V_{2m}, V_{4m} and V_{6m} are the induced voltages in the two pole, four pole and six pole search coils respectively and f_b is the frequency of the bridge supply. The measurements of the induced voltages have been carried out when a sinusoidal voltage of amplitude 40 V and frequency 30Hz has been supplied through the bridge points. A full spectrum FFT of the measured voltages has been carried out to see the presence of the harmonic components of the magnetic fields in the airgap. To obtain a full spectrum FFT, the measured voltages have been converted in complex form as shown in Equations (7.10) - (7.12)

$$V_4 = V_{a4} + \mathrm{j}(V_{b4} + V_{c4})/2 \tag{7.10}$$

$$V_2 = V_{a2} + \mathrm{j}V_{b2} \tag{7.11}$$

$$V_6 = V_{a6} + \mathrm{j}V_{b6} \tag{7.12}$$

where V_{a4}, V_{b4} and V_{c4} are the f_b component of the voltage extracted from the measured voltages of phase A, phase B and phase C of four pole search coils respectively, V_{a2} and V_{b2} are the f_b component of the voltage extracted from the measured voltages of phase A and phase B of two pole search coils respectively, V_{a6} and V_{b6} are the f_b component of the voltage extracted from the measured voltages of phase A and phase B of six pole search coils respectively. These induced voltages in search coils have been analysed for three conditions, (i) when bridge points are supplied with a normal three phase supply, (ii) when bridge points are supplied in the same sequence as that of the main supply and (iii) when bridge points are supplied in the reverse sequence as that of the main supply. Figures 7.22, 7.23 and 7.24 represent the full spectrum FFT of 30 Hz component of the induced voltage in all three conditions in four pole search coils, six pole search coils and two pole search coils respectively. It can be observed in Figure 7.22 that in all the supply conditions induced voltage in four pole search coils are negligible which demonstrate that there is no four pole magnetic field generated due to the bridge supply. Figure 7.23(a) demonstrates that a six pole magnetic field is generated in the machine in the case of normal sequence of bridge supply. Figures 7.23(b) and 7.23(c) demonstrate that the induced voltage in the six pole search coils for the case of same sequence of bridge supply and reverse sequence of bridge supply are negligible which indicates that the same and the reverse sequence of bridge supply do not generate six pole magnetic field in the machine.

The analysis of two pole search coils induced voltage is important because the interactions of a rotating two pole magnetic field and a rotating four pole magnetic field leads to a useful component of the transverse force generation. Figure 7.24 (a) shows that a normal sequence of bridge supply generates a pulsating component of two pole magnetic field, i.e. both forward and backward rotating component of the two pole magnetic field is present in the airgap of the machine. Figure 7.24 (b) demonstrates the presence of backward rotating component of the two pole magnetic field when same sequence of bridge supply has been given to the bridge points of the winding. Whereas Figure 7.24 (c) shows the presence of forward rotating component of the two pole magnetic field when reverse sequence of the bridge supply has been applied to the bridge points of the winding.

7.5.2 Analysis of rotor response in different bridge supply conditions

The investigation of rotor responses in different bridge supply conditions have been carried out for four cases, (i) when only one phase of the bridge points are excited, (ii) when the bridge points are excited by normal sequence of the bridge supply, (iii) when the bridge points are excited by the same sequence of the bridge supply as that of the main supply and (iv) when the bridge points are excited by the reverse sequence of the bridge supply as that of the main supply. In all these conditions the main supply frequency (f_s) is 50 Hz.

Figure 7.25(a) shows the comparison of full spectrum FFT of the rotor responses in bridge OFF

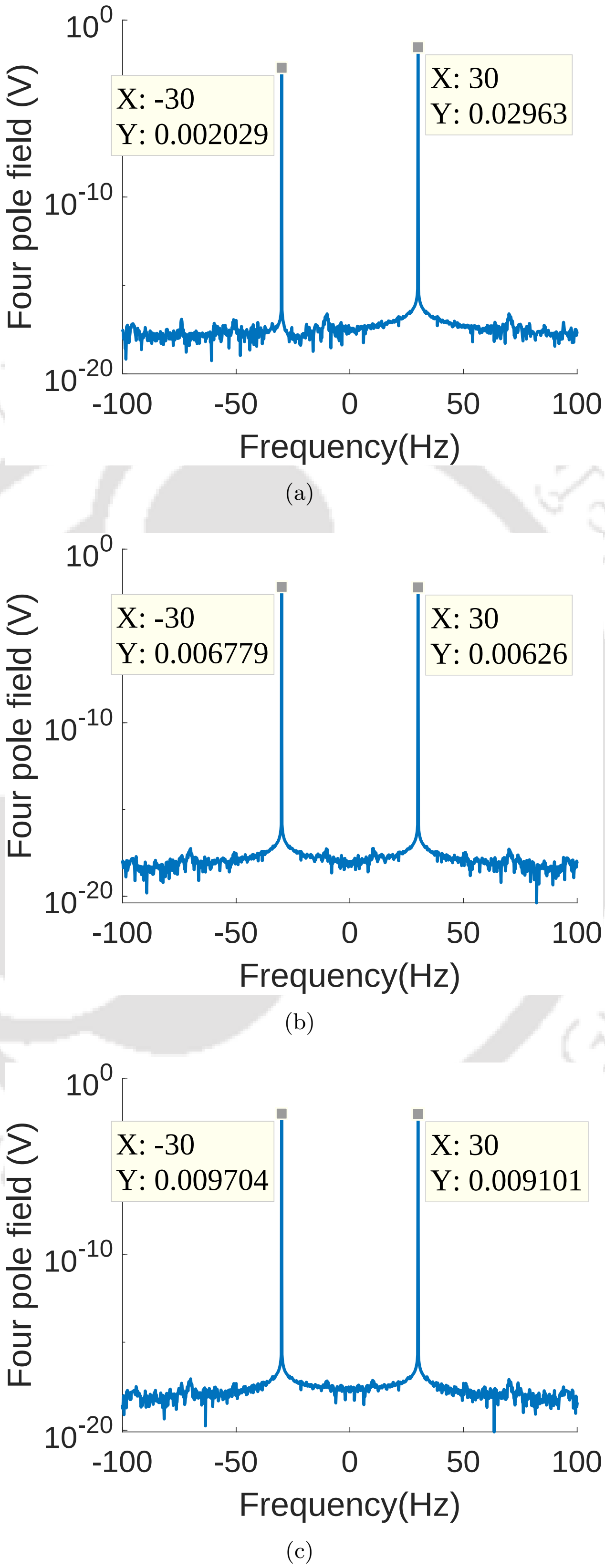

Figure 7.22: FFT of Induced voltage in four pole search coil in RIG I when (a) bridge points are supplied in normal sequence at 30 Hz (b) bridge points are supplied in same sequence at 30 Hz and (c) bridge points are supplied in reverse sequence at 30 Hz.

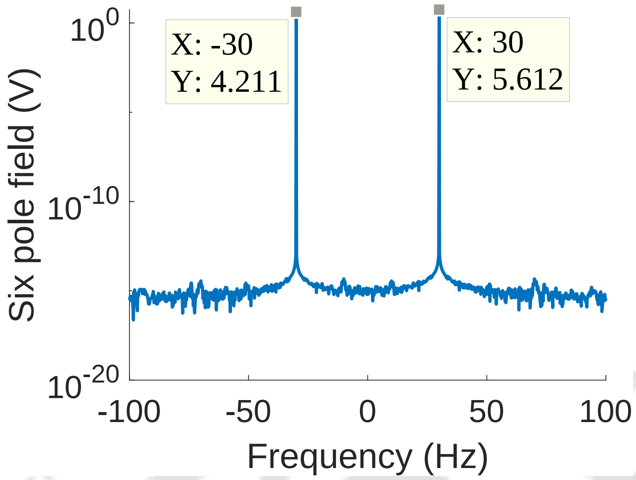

(a)

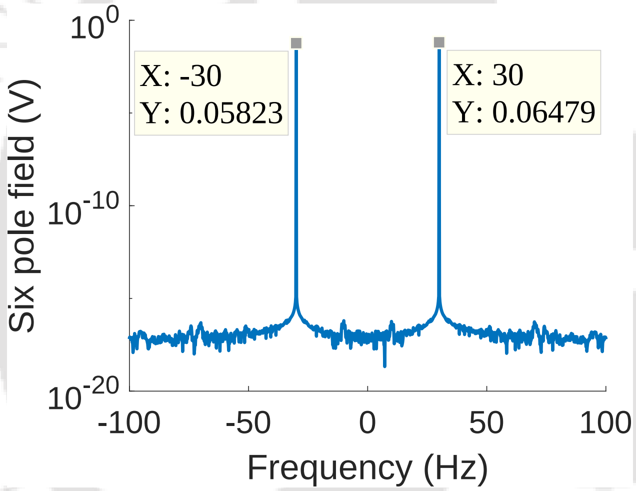

(b)

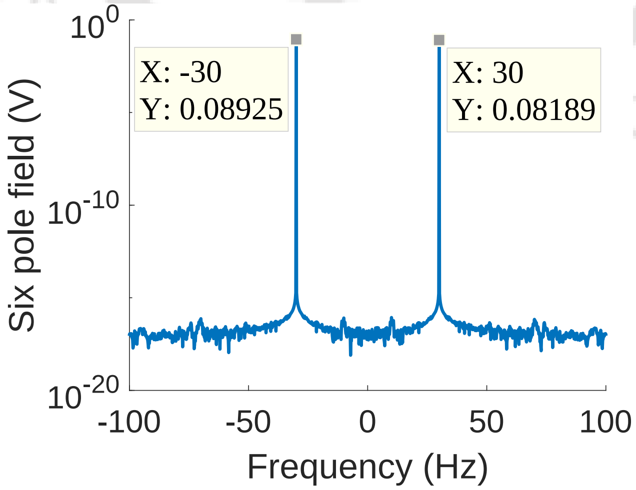

(c)

Figure 7.23: FFT of Induced voltage in six pole search coil in RIG I when (a) bridge points are supplied in normal sequence at 30 Hz (b) bridge points are supplied in same sequence at 30 Hz and (c) bridge points are supplied in reverse sequence at 30 Hz.

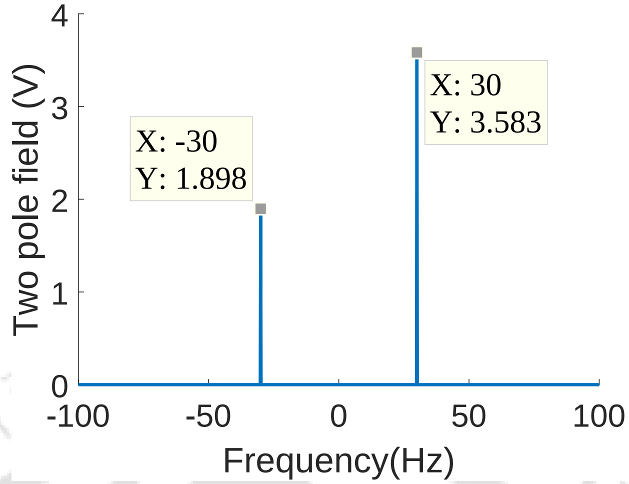

(a)

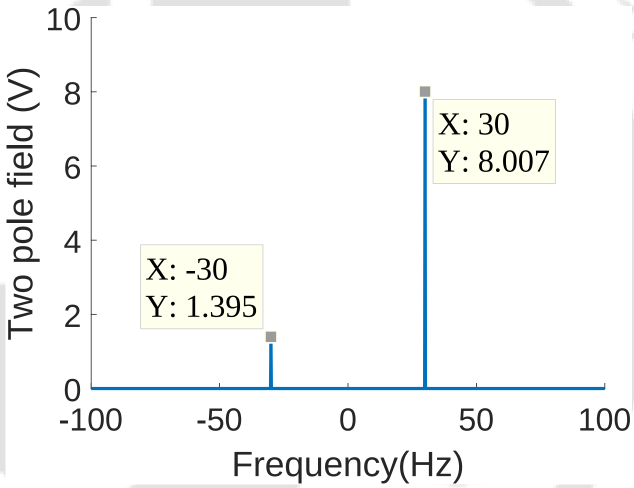

(b)

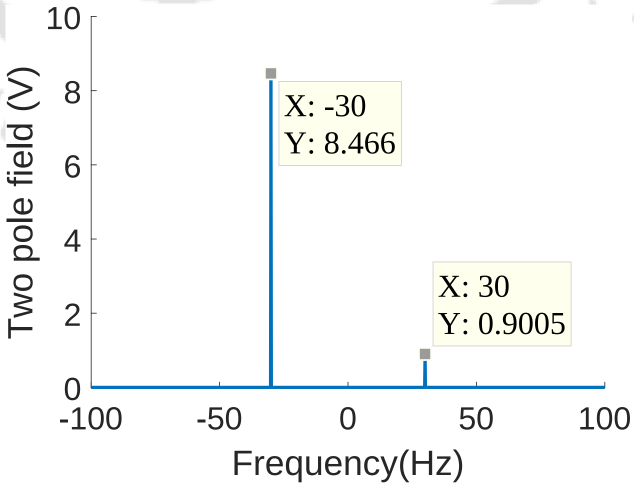

(c)

Figure 7.24: FFT of Induced voltage in two pole search coil in RIG I when (a) bridge points are supplied in normal sequence at 30 Hz (b) bridge points are supplied in same sequence at 30 Hz and (c) bridge points are supplied in reverse sequence at 30 Hz.

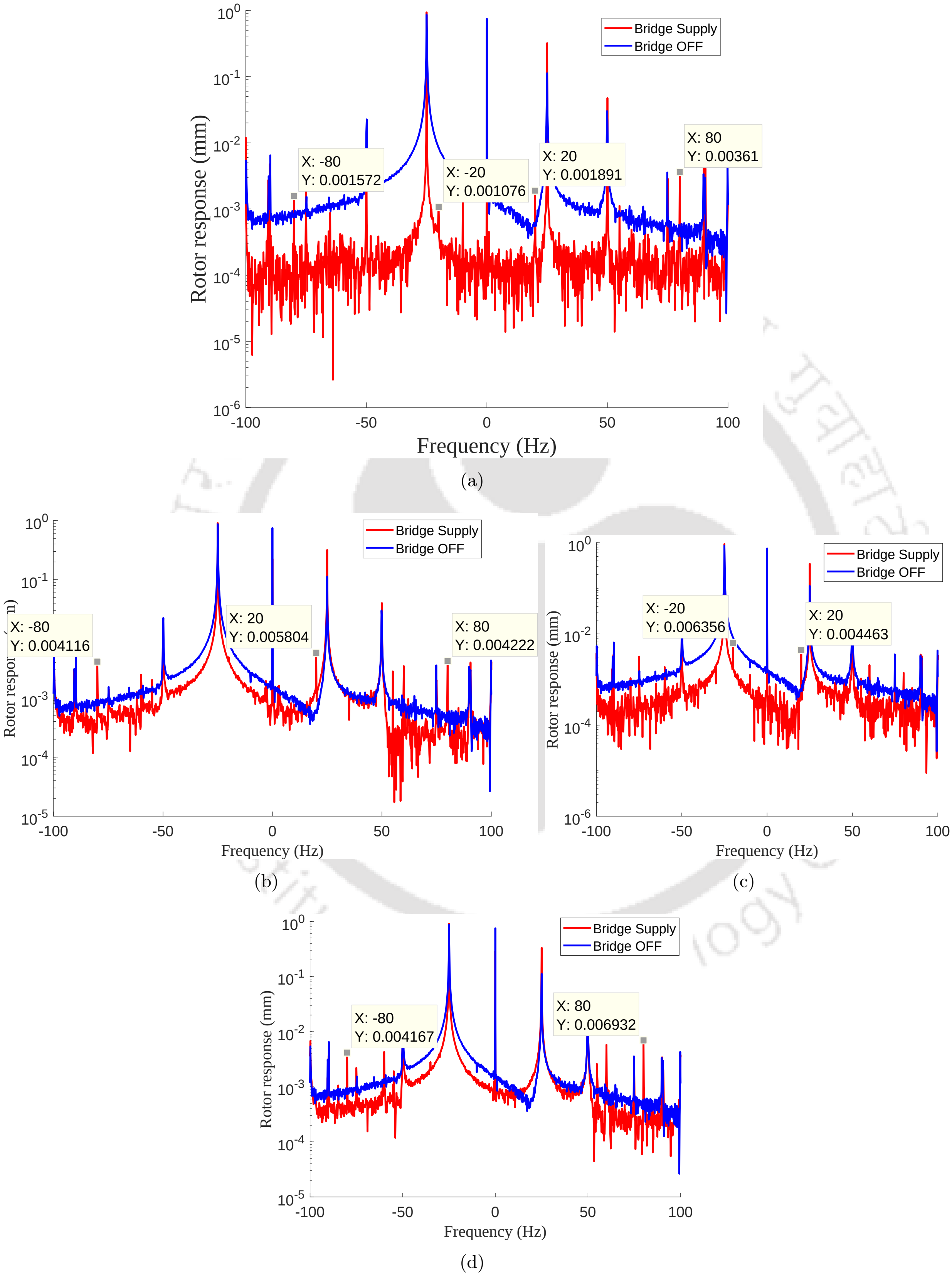

Figure 7.25: Comparison of rotor response FFT with bridge OFF condition in RIG I when (a) a supply of 30 Hz has been given to phase A of the bridge point (b) a supply of 30 Hz has been given to bridge points in normal sequence (c) a supply of 30 Hz has been given to bridge points in same sequence as that of main supply (d) a supply of 30 Hz has been given to bridge points in reverse sequence as that of main supply.

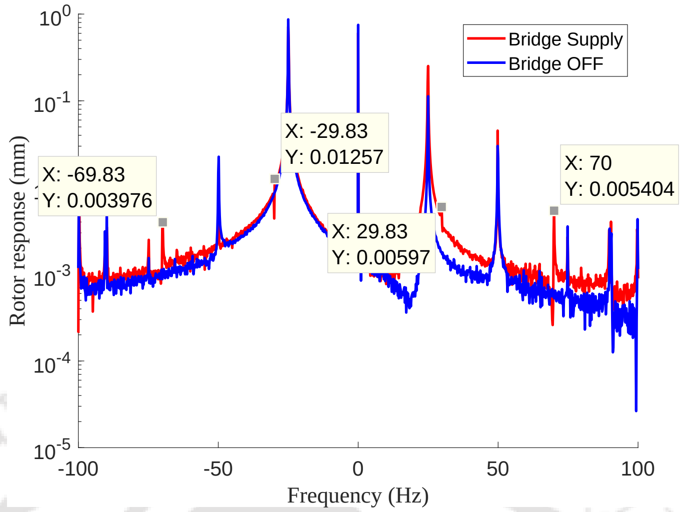

(a)

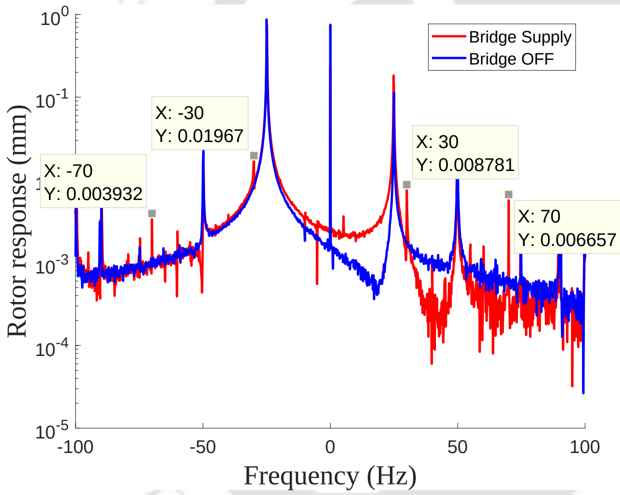

(b)

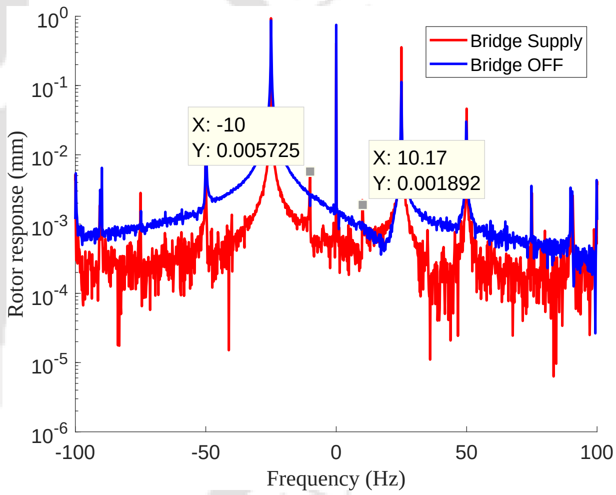

(c)

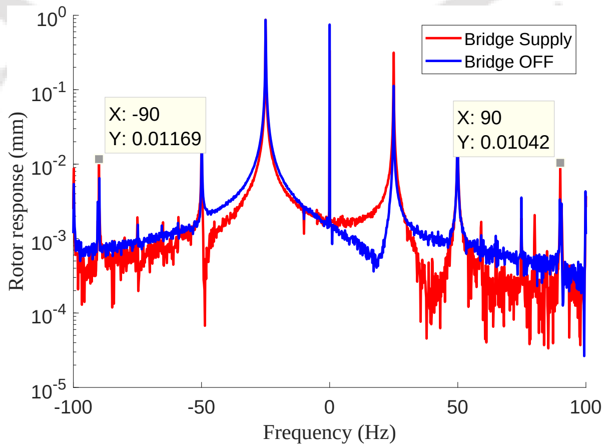

(d)

Figure 7.26: Comparison of the full spectrum FFT of the rotor responses with bridge OFF condition rotor response when (a) a supply of 20 Hz has been applied at the bridge point of phase A (b) a supply of 20 Hz has been applied at the bridge points in normal sequence (c) a supply of 40 Hz has been applied at the bridge points in same sequence as that of the main supply (d) a supply of 40 Hz has been given at the bridge points in reverse sequence as that of the main supply.

and single phase bridge supply condition when a 20 V 30 Hz supply has been applied at the bridge points of phase A. Additional frequency components at $(f_s \pm f_r)$ Hz i.e 80 Hz and 20 Hz can be seen due to the excitation of the single phase of the bridge supply. The same frequency components in rotor response can be observed in Figure 7.25(b) when bridge points are supplied in normal sequence. Figure 7.25(c) shows the comparison of full spectrum FFT of rotor response in bridge OFF condition and when a 40 V 30 Hz same sequence of the bridge supply has been given to the bridge points. It can be seen that $(f_s - f_r)$ Hz i.e 20 Hz of the frequency component is present whereas $(f_s + f_r)$ Hz i.e 80 Hz of the frequency component is not present. Similar behavior can be observed when bridge points are excited in reverse sequence of the bridge supply as that of the main supply. Figure 7.25(d) shows that in reverse sequence of bridge supply $(f_s + f_r)$ Hz i.e 80 Hz of the frequency component is present whereas $(f_s - f_r)$ Hz i.e 20 Hz of frequency component is absent.

The rotor responses have been analysed with respect to few additional frequencies of the bridge supply to establish the general behavior of the rotor responses with respect to bridge supply. Figure 7.26 (a) shows the presence of $(f_s \pm f_r)$ Hz i.e 70 Hz and 30 Hz vibration components, when phase A of the bridge points are excited by 20 V, 20 Hz. Figure 7.26 (b) shows the presence of $(f_s \pm f_r)$ Hz i.e 70 Hz and 30 Hz vibration components, when normal sequence of three phase bridge supply of 20 V, 20 Hz has been applied at the bridge points. Figures 7.26 (c) and 7.26 (d) show the presence of $(f_s - f_r)$ Hz i.e 10 Hz and $(f_s + f_r)$ Hz i.e 90 Hz vibration components, when bridge points are supplied in the same sequence of the bridge supply and reverse sequence of bridge supply of 40 V, 40 Hz respectively. It should be noted that the machine is in mixed eccentricity condition due to manufacturing faults which leads to the presence of other frequency components of the rotor vibration. In addition to this, unevenness in the rotor sleeve, also leads to additional components of the vibration.

7.5.3 Conclusion

A complete analysis of bridge configured winding induction machine has been presented to establish the production of transverse force of a particular frequency component with respect to bridge supply of the winding. It has been demonstrated that a bridge supply of frequency f_b Hz of same sequence as that of the main supply sequence of f_s Hz produces a force of frequency $(f_s - f_b)$ Hz whereas a bridge supply of frequency f_b Hz of reverse sequence as that of the main supply sequence of f_s Hz produces a force of frequency $(f_s + f_b)$ Hz.

8

Conclusion and Future Work

Contents

8.1 Conclusion

Controllable transverse force generation is an important aspect for the rotor vibration control and for the development of bearingless machines. A detailed investigation of the bridge configured winding has been carried out in this thesis. The possible ways for exploiting the bridge configured winding to achieve the objectives of this thesis have been laid out.

8.2 Summary of contribution

Keeping in view the development of bearingless machine using bridge configured winding various aspects of bridge configured winding electrical machine has been analysed in this thesis. The major contributions of this thesis are enumerated below.

- A Finite Element model has been developed using COMSOL MULTIPHYSICS® to analyse the effects of different eccentricity conditions on magnetic fields and forces in series and parallel stator winding electrical machines. The bridge configured winding is a parallel winding and it has been used for the analysis of parallel winding configuration. A solid rotor has been considered for the simulation to omit the effects of rotor bar currents. Both series and parallel winding configurations have been analysed, keeping the frequency of the main supply as 50 Hz and the following observations have been made
  - It has been demonstrated that additional frequency components of the force are present in parallel winding electrical machine when the rotor is in eccentric position. In the static, dynamic and mixed eccentricity conditions the parallel winding configuration has 100 Hz, 125 Hz and (100 Hz & 125 Hz) additional components of UMP respectively.
  - A comparative study of eccentricity generated frequency components of magnetic field have been carried out to understand the effect of eccentricity on the magnetic fields of the air gap in series and bridge configured winding electrical machine. The temporal FFT of the magnetic fields for both series and parallel winding, show the presence of 50 Hz frequency component of the magnetic fields in static eccentricity condition, 25 Hz and 75 Hz frequency components of the magnetic field in case of dynamic eccentricity condition and 25 Hz, 50 Hz and 75 Hz frequency components of the magnetic field in mixed eccentricity condition.

- The generation of the additional frequency components of the forces in different eccentricity conditions have been investigated by analysing the spatial FFT of the air gap magnetic field. It has been concluded that the presence of six pole magnetic field is the reason behind the generation of the additional frequency component of the force in parallel stator winding machines.
- The force expressions have been obtained using Maxwell's stress tensor method for static, dynamic and mixed eccentricity conditions by considering the additional components of the magnetic field. The modified force expressions have all the additional frequency components which have been obtained from the numerical simulation.

• A generalised coupled magnetic field and electrical circuit finite element model of a 3.7 kW induction machine has been developed in MATLAB® environment to accommodate bridge configured winding and rotor circuit equations. This model is simulated in different eccentricity conditions and the following investigations have been carried out,

- The induced bridge phase currents are converted to space vectors and the full spectrum FFT have been obtained to study the presence of different frequency components. The presence of zero sequence component has also been demonstrated.
- A relationship of bridge current modes with respect to different eccentricity conditions have been established. The space vector of bridge currents show the presence of only one frequency component i.e. $\pm f_s$ for the static eccentricity condition, two frequency components i.e. $\pm(f_s - f_r)$, $\pm(f_s + f_r)$ for the dynamic eccentricity condition and three frequency components i.e. $\pm f_s$, $\pm(f_s - f_r)$ and $\pm(f_s + f_r)$ for the mixed eccentricity conditions. Here, f_s is the main supply frequency and f_r is the rotor rotational frequency.
- A relationship with respect to the frequency component of the main supply (f_s) and frequency component of the bridge currents (f_{bridge}) in terms of frequency components of the unbalanced magnetic pull has been established in all three types of eccentricity conditions. It has been shown that the developed UMP due to the eccentric rotor in bridge OFF condition has $\pm f_s \pm f_{bridge}$ frequency components. It has been also established that, bridge currents suppresses all the UMP components other than DC component and $f_s - f_r$ component.

- Magneto motive force (MMF) analysis has been carried out to investigate the effects of main and bridge point excitation of the bridge configured winding.
  - The MMF axes with respect to the bridge supply points of the winding are found to be 60 degrees apart. For the generation of rotating magnetic field the MMF axis must be 120 degree apart.
  - Since the MMF axes are 60 degrees apart, a rotating magnetic field can be generated by reversing the direction of the supply in phase B of the bridge supply.
  - Two supply sequences have been proposed for the generation of rotating two pole magnetic field, when the three phase main supply voltage are $V_A = A_0 \cos(2\pi f_s t), V_B = A_0 \cos(2\pi f_s t - 2\pi/3)$ and $V_C = A_0 \cos(2\pi f_s t - 4\pi/3)$. Similarly, a supply sequence has also been proposed for the generation of six pole pulsating magnetic field.
    (i) The three phase bridge supply voltages sequence of $V_{A_b} = B_0 \cos(2\pi f_s t), V_{B_b} = -B_0 \cos(2\pi f_s t - 2\pi/3)$ would generate a rotating two pole magnetic field, which rotates in the opposite direction of the four pole magnetic field, generated due to the main supply. This sequence of bridge supply is termed as the reverse sequence of bridge supply.
    (ii) The three phase bridge supply voltages sequence of $V_{A_b} = B_0 \cos(2\pi f_s t - 4\pi/3), V_{B_b} = -B_0 \cos(2\pi f_s t - 2\pi/3)$ and $V_{C_b} = B0 \cos(2\pi f_s t)$ would generate a rotating two pole magnetic field which rotates in the same direction of the four pole magnetic field, generated due to the main supply. This sequence of the bridge supply is termed as the same sequence of bridge supply.
    (iii) A single phase of supply through all the phases of the bridge terminals would generate a pulsating six pole magnetic field.
  - A force expression has been presented for the bridge configured winding electrical machine using the Fourier coefficients of the MMF distribution.

- The generalized coupled magnetic field and electric circuit model is further coupled with the rotor equation of motion to simulate the effects of the magnetic forces on the rotor motion. The rotor of the machine has been modelled as a four degree of freedom rigid rotor system. The following investigations have been carried out,

- A static eccentricity condition is simulated when the rotor is eccentric by 1e-4 m along x axis (Longitudinal Direction) with respect to the stator center. The rotor responses show that when the bridge points are short circuited (bridge ON condition) the rotor shifts its position and helps in reduction of rotor vibration.
- A dynamic eccentricity condition is simulated by introducing a mass unbalance in the rotor equation. The effects of bridge OFF and bridge ON conditions on the rotor vibration have been demonstrated for this eccentricity condition.
- The rotor vibration is simulated in different types of bridge supply conditions, such as, single phase bridge supply, normal sequence of the bridge supply and the proposed sequences of the bridge supply. Using the proposed bridge supply sequence, a particular frequency component of the force can be generated which leads to a particular frequency component of rotor vibration.
- it has been demonstrated that the same sequence of the bridge supply generates a force of frequency $f_s - f_b$ Hz where f_s is the frequency of the main supply and f_b is the frequency of the bridge supply. Similarly, the reverse sequence of the bridge supply generates a force with a frequency component of $f_s + f_b$ Hz.
- It has also been demonstrated that by changing the phase of the bridge supply, the direction of the DC component of the transverse force can be changed. A relationship with respect to the change in phase of the bridge supply and the subsequent change in the phase of the produced force and vibration has been presented. This relationship will be useful while developing bearingless electrical machines.

• A simulation model has been developed in MATLAB/ SIMULINK® to demonstrate the vibration control and levitation of the rotor in bridge configured winding machines. A simplified force model has been used to mimic the force generation in a bridge configured winding electrical machine. The DC component of the force has been used for the levitation control and the revolving component of the force has been used to suppress harmonic components of the force. The PID controller and convergent control algorithm has been implemented for the levitation and suppression of harmonic components of the rotor vibration. For the development of levitation model the electrical machine has been modelled as an active magnetic bearing.

- Two experimental setups have been developed to verify the numerical findings. The following objectives have been verified using the experimental measurements
  - Passive vibration capability of bridge configured winding has been demonstrated by short circuiting of bridge terminals of the winding.
  - It has been demonstrated that the generation of pulsating six pole magnetic field in a parallel stator winding electrical machine is the reason behind the generation of additional component of UMP.
  - The relationship in bridge currents frequency with respect to the mixed eccentricity condition shown in numerical simulation has been verified using bridge current measurements.
  - The vibration pattern in mixed eccentricity condition demonstrated in the bridge configured winding in numerical simulation has been verified experimentally.
  - The proposed method of bridge supply to generate two pole magnetic field has been verified using induced voltages in the search coils of the winding.
  - The force generation pattern in proposed bridge supply method has been verified using the measurement of rotor response.

8.3 Future work

Based on the work presented in the thesis the following direction is suggested as possible future work,

- A bearingless machine can be developed using the proposed bridge supply method. The implementation of real time controller is one of the biggest challenge for the development of bearingless machine.
- Similar to a bearingless machines, an active magnetic bearing can also be developed using the same principle of force generation using bridge configured winding.
- It is required to develop an optimized procedure of design of BCW machine for active vibration control or Bearingless applications.
- The measurements of the components of the air gap magnetic field, the response of the rotor, induced voltages in different search coils are related to the vibrations of the stator. However,

the induced voltages in different search coils will be affected by the control currents or voltages in the bridges. The effect of dynamics of the bridge supply on search coil induced voltage for the development of closed loop control requires further investigation.

- The effect of the bridge currents on the losses has not been considered. The currents circulating in the winding will produce more Joule losses and heat, which might results in overheating of the machine if not adequately mitigated. An investigation of the cooling of the machine or its de-rating is also an import aspect of future study.

Bibliography

[1] N. M. Dumitru, "Electromagnetic flux monitoring for detecting faults in electrical machines," Ph.D. dissertation, Helsinki University of Technology; Teknillinen, 2006.

[2] A. Sinervo and A. Arkkio, "Eccentricity related forces in two-pole induction motor with four-pole stator damper winding analyzed using measured rotor orbits," *IEEE Transactions on Magnetics*, vol. 49, no. 6, pp. 3029–3037, June 2013.

[3] A. Laiho, K. Tammi, J. Orivuori, A. Sinervo, K. Zenger, and A. Arkkio, "Electromechanical interaction in eccentric-rotor cage induction machine equipped with a self-bearing force actuator," *Journal of System Design and Dynamics*, vol. 3, no. 4, pp. 519–529, 2009.

[4] A. Chiba, D. T. Power, and M. A. Rahman, "Characteristics of a bearingless induction motor," *IEEE Transactions on Magnetics*, vol. 27, no. 6, pp. 5199–5201, Nov 1991.

[5] W. K. S. Khoo, "Bridge configured winding for polyphase self-bearing machines," *IEEE Transactions on Magnetics*, vol. 41, no. 4, pp. 1289–1295, April 2005.

[6] W. K. S. Khoo, K. Kalita, and S. D. Garvey, "Practical implementation of the bridge configured winding for producing controllable transverse forces in electrical machines," *IEEE Transactions on Magnetics*, vol. 47, no. 6, pp. 1712–1718, June 2011.

[7] J. Früchtenicht, H. Jordan, and H. O. Seinsch, "Exzentrizitätsfelder als ursache von laufinstabilitäten bei asynchronmaschinen," *Archiv für Elektrotechnik*, vol. 65, no. 4, pp. 271–281, Jul 1982.

[8] A. Gray and J. G. Pertsch, "Critical review of the bibliography on unbalanced magnetic pull in dynamo-electric machines," *Proceedings of the American Institute of Electrical Engineers*, vol. 37, no. 9, pp. 1061–1068, Sep. 1918.

[9] E. Rosenberg, "Magnetic pull in electric machines," *Transactions of the American Institute of Electrical Engineers*, vol. XXXVII, no. 2, pp. 1425–1469, July 1918.

[10] L. E. Hildebrand, "Quiet induction motors," *Journal of the A.I.E.E.*, vol. 49, no. 1, pp. 7–11, Jan 1930.

[11] L. H. A. Carr, "Recent progress in induction-motor construction," *Journal of the Institution of Electrical Engineers*, vol. 78, no. 472, pp. 383–391, April 1936.

[12] R. C. Robinson, "The calculation of unbalanced magnetic pull in synchronous and induction motors," *Electrical Engineering*, vol. 62, no. 10, pp. 620–623, Oct 1943.

[13] T. D. Graybeal, "The nature of vibration in electric machinery," *Transactions of the American Institute of Electrical Engineers*, vol. 63, no. 10, pp. 712–718, Oct 1944.

[14] A. Covo, "Unbalanced magnetic pull in induction motors with eccentric rotors [includes discussion]," *Transactions of the American Institute of Electrical Engineers. Part III: Power Apparatus and Systems*, vol. 73, no. 2, pp. 1421–1425, Jan 1954.

[15] E. W. Summers, "Vibration in 2-pole induction motors related to slip frequency [includes discussion]," *Transactions of the American Institute of Electrical Engineers. Part III: Power Apparatus and Systems*, vol. 74, no. 3, pp. 69–72, Jan 1955.

[16] R. C. Robinson, "Line-frequency magnetic vibration of a-c machines," *Transactions of the American Institute of Electrical Engineers. Part III: Power Apparatus and Systems*, vol. 81, no. 3, pp. 675–679, April 1962.

[17] H. Jordan, R. D. Schroeder, and H. O. Seinsch, “Zur berechnung einseitigmagnetischer zugkräfte in drehfeldmaschienen,” *Archiv für Elektrotechnik*, vol. 63, no. 2, pp. 117–124, Mar 1981.

[18] R. Belmans, A. Vandenput, and W. Geysen, “Calculation of the flux density and the unbalanced pull in two pole induction machines,” *Archiv für Elektrotechnik*, vol. 70, no. 3, pp. 151–161, May 1987.

[19] T. P. Holopainen, A. Tenhunen, E. Lantto, and A. Arkkio, “Unbalanced magnetic pull induced by arbitrary eccentric motion of cage rotor in transient operation. Part 1: Analytical model,” *Electrical Engineering*, vol. 88, no. 1, p. 13–24, 2005.

[20] S. A. Swann, “Effect of rotor eccentricity on the magnetic field in the air-gap of a non-salient-pole machine,” *Proceedings of the Institution of Electrical Engineers*, vol. 110, no. 5, pp. 903–915, May 1963.

[21] D. G. Dorrell and A. C. Smith, “Calculation of UMP in induction motors with series or parallel winding connections,” *IEEE Transactions on Energy Conversion*, vol. 9, no. 2, pp. 304–310, June 1994.

[22] P. Silvester and M. V. K. Chari, “Finite element solution of saturable magnetic field problems,” *IEEE Transactions on Power Apparatus and Systems*, vol. PAS-89, no. 7, pp. 1642–1651, Sep. 1970.

[23] P. Silvester, H. S. Cabayan, and B. T. Browne, “Efficient techniques for finite element analysis of electric machines,” *IEEE Transactions on Power Apparatus and Systems*, vol. PAS-92, no. 4, pp. 1274–1281, July 1973.

[24] A. Y. Hannalla and D. C. MacDonald, “Numerical analysis of transient field problems in electrical machines,” *Proceedings of the Institution of Electrical Engineers*, vol. 123, no. 9, pp. 893–898, Sep. 1976.

[25] E. Vassent, G. Meunier, and J. C. Sabonnadier, “Simulation of induction machine operation using complex magnetodynamic finite elements,” *IEEE Transactions on Magnetics*, vol. 25, no. 4, pp. 3064–3066, July 1989.

[26] E. Vassent, G. Meunier, A. Foggia, and G. Reyne, “Simulation of induction machine operation using a step by step finite element method coupled with circuits and mechanical equations,” *IEEE Transactions on Magnetics*, vol. 27, no. 6, pp. 5232–5234, Nov 1991.

[27] T. H. Pham, P. F. Wendling, S. J. Salon, and H. Acikgoz, “Transient finite element analysis for an induction motor with external circuit connections and electromechanical coupling,” *IEEE Transactions on Energy Conversion*, vol. 14, no. 4, pp. 1407–1412, Dec 1999.

[28] D. Rodger, H. C. Lai, R. J. Hill-Cottingham, and P. C. Coles, “Some tricks for modeling rotating electrical machines using finite elements,” *IEEE Transactions on Magnetics*, vol. 40, no. 2, pp. 802–805, March 2004.

[29] E. Vassent, G. Meunier, A. Foggia, and J. C. Sabonnadiere, “Simulation of induction machine operation using a step-by-step finite-element method,” *Journal of Applied Physics*, vol. 67, no. 9, pp. 5809–5811, 1990.

[30] A. Arkkio, “Analysis of induction motors based on the numerical solution of the magnetic field and circuit equations,” Ph.D. dissertation, Helsinki University of Technology, 1987.

[31] E. Vassent, G. Meunier, and A. Foggia, “Simulation of induction machines using complex magnetodynamic finite element method coupled with the circuit equations,” *IEEE Transactions on Magnetics*, vol. 27, no. 5, pp. 4246–4249, Sep. 1991.

[32] A. Tenhunen and A. Arkkio, “Modelling of induction machines with skewed rotor slots,” *IEE Proceedings - Electric Power Applications*, vol. 148, no. 1, pp. 45–50, Jan 2001.

[33] P. P. Silvester and R. L. Ferrari, *Finite Elements for Electrical Engineers.* Cambridge University Press, 1996.

[34] S. L. Ho, H. L. Li, W. N. Fu, and H. C. Wong, “A novel approach to circuit-field-torque coupled time stepping finite element modeling of electric machines,” *IEEE Transactions on Magnetics*, vol. 36, no. 4, pp. 1886–1889, July 2000.

[35] S. Salon, M. DeBortoli, and R. Palma, “Coupling of transient fields, circuits, and motion using finite element analysis,” *Journal of Electromagnetic Waves and Applications*, vol. 4, no. 11, pp. 1077–1106, 1990.

[36] V. N. Savov, Z. D. Georgiev, and E. S. Bogdanov, "Analysis of cage induction motor by means of the finite element method and coupled system of field, circuit and motion equations," *Electrical Engineering*, vol. 80, no. 1, pp. 21–28, 1997.

[37] J. Coulomb, "A methodology for the determination of global electromechanical quantities from a finite element analysis and its application to the evaluation of magnetic forces, torques and stiffness," *IEEE Transactions on Magnetics*, vol. 19, no. 6, pp. 2514–2519, November 1983.

[38] R. Belmans, A. Vandenput, and W. Geysen, "Influence of unbalanced magnetic pull on the radial stability of flexible-shaft induction machines," *IEE Proceedings B - Electric Power Applications*, vol. 134, no. 2, pp. 101–109, March 1987.

[39] A. Tenhunen, "Finite-element calculation of unbalanced magnetic pull and circulating current between parallel windings in induction motor with non-uniform eccentric rotor," *Proceedings of Electromotion'01*, 2001.

[40] A. Tenhunen, T. P. Holopainen, and A. Arkkio, "Effects of saturation on the forces in induction motors with whirling cage rotor," *IEEE Transactions on Magnetics*, vol. 40, no. 2, pp. 766–769, March 2004.

[41] T. P. Holopainen, A. Tenhunen, E. Lantto, and A. Arkkio, "Numerical identification of electromagnetic force parameters for linearized rotordynamic model of cage induction motors," *ASME. J. Vib. Acoust*, vol. 126, no. 3, pp. 384–390, 2004.

[42] L. Frosini and P. Pennacchi, "Detection and modelling of rotor eccentricity in electrical machines: an overview," in *IMechE Event Publications*, Jan. 2004.

[43] A. Salah, Y. Guo, and D. Dorrell, "Monitoring and damping unbalanced magnetic pull due to eccentricity fault in induction machines: A review," in *20th International Conference on Electrical Machines and Systems (ICEMS)*, Aug. 2017, pp. 1–6.

[44] A. Tenhunen, T. P. Holopainen, and A. Arkkio, "Spatial linearity of an unbalanced magnetic pull in induction motors during eccentric rotor motions," *COMPEL - The international journal for computation and mathematics in electrical and electronic engineering*, vol. 22, no. 4, pp. 862–876, . 2003.

[45] O. Vitek, M. Janda, and V. Hajek, "Effects of eccentricity on external magnetic field of induction machine," in *15th IEEE Mediterranean Electrotechnical Conference (Melecon 2010)*, April 2010, pp. 939–943.

[46] D. G. Dorrell, A. Salah, and Y. Guo, "The detection and suppression of unbalanced magnetic pull in wound rotor induction motors using pole-specific search coils and auxiliary windings," *IEEE Transactions on Industry Applications*, vol. 53, no. 3, pp. 2066–2076, May 2017.

[47] A. Arkkio, "Unbalanced magnetic pull in cage induction motors with asymmetry in rotor structures," in *Eighth International Conference on Electrical Machines and Drives*, Sep. 1997, pp. 36–40.

[48] D. G. Dorrell, "Experimental behaviour of unbalanced magnetic pull in 3-phase induction motors with eccentric rotors and the relationship with tooth saturation," *IEEE Transactions on Energy Conversion*, vol. 14, no. 3, pp. 304–309, Sep. 1999.

[49] M. Bradford, "Unbalanced magnetic pull in a 6-pole induction motor," *Proceedings of the Institution of Electrical Engineers*, vol. 115, no. 11, pp. 1619–1627, November 1968.

[50] A. C. Smith and D. G. Dorrell, "Calculation and measurement of unbalanced magnetic pull in cage induction motors with eccentric rotors. I. analytical model," *IEE Proceedings - Electric Power Applications*, vol. 143, no. 3, pp. 193–201, May 1996.

[51] O. V. Thorsen and M. Dalva, "A survey of faults on induction motors in offshore oil industry, petrochemical industry, gas terminals, and oil refineries," *IEEE Transactions on Industry Applications*, vol. 31, no. 5, pp. 1186–1196, Sep. 1995.

[52] M. J. DeBortoli, S. J. Salon, D. W. Burow, and C. J. Slavik, "Effects of rotor eccentricity and parallel windings on induction machine behavior: a study using finite element analysis," *IEEE Transactions on Magnetics*, vol. 29, no. 2, pp. 1676–1682, March 1993.

[53] A. Tenhunen, T. Benedetti, T. P. Holopainen, and A. Arkkio, "Electromagnetic forces in cage induction motors with rotor eccentricity," in *IEEE International Electric Machines and Drives Conference (IEMDC'03)*, vol. 3, June 2003, pp. 1616–1622 vol.3.

[54] B. Yang, Y. Kim, and B.Son, "Instability and imbalance response of large induction motor rotor by unbalanced magnetic pull," *Modal Analysis*, vol. 10, no. 3, pp. 447–460, 2004.

[55] D. G. Dorrell, "Sources and characteristics of unbalanced magnetic pull in 3-phase cage induction motors with axial-varying rotor eccentricity," in *IEEE Energy Conversion Congress and Exposition*, Sep. 2009, pp. 240–247.

[56] D. G. Dorrell, J. K. H. Shek, and M. Hsieh, "The measurement and indexing of unbalanced magnetic pull in electrical machines," in *IEEE Energy Conversion Congress and Exposition (ECCE)*, Sep. 2014, pp. 4827–4834.

[57] R. Belmans, W. Heylen, A. Vandenput, and W. Geysen, "Influence of rotor-bar stiffness on the critical speed of an induction motor with an aluminium squirrel cage," *IEE Proceedings B - Electric Power Applications*, vol. 131, no. 5, pp. 203–208, Sep. 1984.

[58] T. P. Holopainen, A. Tenhunen, and A. Arkkio, "Electromagnetic circulatory forces and rotordynamic instability in electric machines," in *Proceeding of the 6th international conference on rotordynamics*, vol. 1, 2002, pp. 446–463.

[59] T. P. Holopainen, A. Tenhunen, and A. Arkkio, "Electromechanical interaction in rotor vibrations of electric machines," in *Proceedings of the 5th world congress on computational mechanics*, 2002.

[60] D. Guo, F. Chu, and D. Chen, "The unbalanced magnetic pull and its effects on vibration in a three-phase generator with eccentric rotor," *Journal of Sound and Vibration*, vol. 254, no. 2, pp. 297 – 312, 2002.

[61] T. P. Holopainen, A. Tenhunen, and A. Arkkio, "Electromechanical interaction in rotordynamics of cage induction motors," *Journal of Sound and Vibration*, vol. 284, no. 3, pp. 733 – 755, 2005.

[62] A. Sinervo and A. Arkkio, "Including slot harmonics to mechanical model of two-pole induction machine with a force actuator," *Mechanical Systems and Signal Processing*, vol. 32, pp. 282 – 291, 2012, uncertainties in Structural Dynamics.

[63] A. Arkkio, M. Antila, K. Pokki, A. Simon, and E. Lantto, "Electromagnetic force on a whirling cage rotor," *IEE Proceedings - Electric Power Applications*, vol. 147, no. 5, pp. 353–360, Sep. 2000.

[64] A. J. Ellison and S. J. Yang, "Effects of rotor eccentricity on acoustic noise from induction machines," *Proceedings of the Institution of Electrical Engineers*, vol. 118, no. 1, pp. 174–184, January 1971.

[65] M. Berman, "On the reduction of magnetic pull in induction motors with off-centre rotor," in *Conference Record of the IEEE Industry Applications Conference Twenty-Eighth IAS Annual Meeting*, Oct 1993, pp. 343–350 vol.1.

[66] P. K. Hermann, "A radial active magnetic bearing," UK Patent 1 478 868, 1973.

[67] A. Chiba, T. Deido, T. Fukao, and M. A. Rahman, "An analysis of bearingless ac motors," *IEEE Transactions on Energy Conversion*, vol. 9, no. 1, pp. 61–68, March 1994.

[68] S. Nomura, A. Chiba, F. Nakamura, K. Ikeda, T. Fukao, and M. A. Rahman, "A radial position control of induction type bearingless motor considering phase delay caused by the rotor squirrel cage," in *Conference Record of the Power Conversion Conference - Yokohama*, April 1993, pp. 438–443.

[69] M. Ohsawa, S. Mori, and T. Satoh, "Study of induction type bearingless motor," in *Seventh International Symp. on Magnetic Bearings, ETH Zurich*, August 2000, pp. 389–394.

[70] A. Chiba, R. Miyatake, S. Hara, and T. Fukao, "Transfer Characteristics of Radial Force of Induction-type. Bearingless Motors with Four-Pole Rotor Circuits," in *Fifth International Symposium on Magnetic Bearings (ISMB Japan)*, August 1996, pp. 319–325.

[71] A. Chiba and T. Fukao, "Optimal design of rotor circuits in induction type bearingless motors," *IEEE Transactions on Magnetics*, vol. 34, no. 4, pp. 2108–2110, July 1998.

[72] A. Chiba, R. Furuichi, Y. Aikawa, K. Shimada, Y. Takamoto, and T. Fukao, "Stable operation of induction-type bearingless motors under loaded conditions," *IEEE Transactions on Industry Applications*, vol. 33, no. 4, pp. 919–924, July 1997.

[73] T. Hiromi, T. Katou, A. Chiba, M. A. Rahman, and T. Fukao, "A novel magnetic suspension-force compensation in bearingless induction-motor drive with squirrel-cage rotor," *IEEE Transactions on Industry Applications*, vol. 43, no. 1, pp. 66–76, Jan 2007.

[74] A. Chiba, K. Sotome, Y. Iiyama, and M. A. Rahman, "A novel middle-point-current-injection-type bearingless PM synchronous motor for vibration suppression," *IEEE Transactions on Industry Applications*, vol. 47, no. 4, pp. 1700–1706, July 2011.

[75] A. O. Salazar and R. M. Stephan, "A bearingless method for induction machines," *IEEE Transactions on Magnetics*, vol. 29, no. 6, pp. 2965–2967, Nov 1993.

[76] J. M. S. Ferreira, M. Zucca, A. O. Salazar, and L. Donadio, "Analysis of a bearingless machine with divided windings," *IEEE Transactions on Magnetics*, vol. 41, no. 10, pp. 3931–3933, Oct 2005.

[77] H. Zhu, J. Yuan, and J. Jv, "A novel single winding structure and closed loop control of the suspension force vector of bearingless permanent magnet synchronous motors," *Energies*, vol. 9, no. 5, 2016.

[78] R. Oishi, S. Horima, H. Sugimoto, and A. Chiba, "A novel parallel motor winding structure for bearingless motors," *IEEE Transactions on Magnetics*, vol. 49, no. 5, pp. 2287–2290, May 2013.

[79] E. Severson, S. Gandikota, and N. Mohan, "Practical implementation of dual-purpose no-voltage drives for bearingless motors," *IEEE Transactions on Industry Applications*, vol. 52, no. 2, pp. 1509–1518, March 2016.

[80] A. Laiho, K. Kalita, K. Tammi, and S. Garvey, "Dynamics of bridge configured built-in force actuator for vibration control in four-pole cage induction machine," in *18th International congress on sound and vibration*, July 2011.

[81] R. S. Konwar, K. Kalita, A. Banerjee, and W. K. S. Khoo, "Electromagnetic analysis of a bridge configured winding cage induction machine using finite element method," *Progress In Electromagnetics Research B*, vol. 48, pp. 347–373, 2013.

[82] T. Hiromi, T. Katou, A. Chiba, M. A. Rahman, and T. Fukao, "A novel magnetic suspension-force compensation in bearingless induction-motor drive with squirrel-cage rotor," *IEEE Transactions on Industry Applications*, vol. 43, no. 1, pp. 66–76, Jan 2007.

[83] K. Tammi, "Active control of rotor vibrations by two feedforward control algorithms," *Journal of Dynamic Systems, Measurement, and Control*, vol. 131, no. 5, Aug 2009.

[84] A. Laiho, K. Tammi, A. Burakov, A. Arkkio, and K. Zenger, "A built-in force actuator for active control of lateral rotor vibration in cage induction electrical machines," *Journal of Sound and Vibration*, vol. 320, no. 3, pp. 496 – 515, 2009.

[85] A. Sinervo and A. Arkkio, "Rotor radial position control and its effect on the total efficiency of a bearingless induction motor with a cage rotor," *IEEE Transactions on Magnetics*, vol. 50, no. 4, pp. 1–9, April 2014.

[86] C. R. Burrows and M. N. Sahinkaya, "Vibration control of multi-mode rotor-bearing systems," *Proceedings of the Royal Society of London. A. Mathematical and Physical Sciences*, vol. 386, pp. 77–94, 1983.

[87] C. Knospe, R. Hope, S. Tamer, and S. Fedigan, "Robustness of adaptive unbalance control of rotors with magnetic bearings," *Modal Analysis*, vol. 2, no. 1, pp. 33–52, 1996.

[88] C. R. Knospe, S. J. Fedigan, R. W. Hope, and R. D. Williams, "A multitasking dsp implementation of adaptive magnetic bearing control," *IEEE Transactions on Control Systems Technology*, vol. 5, no. 2, pp. 230–238, March 1997.

[89] K. Tammi, "Active control of radial rotor vibrations : identification, feedback, feedforward, and repetitive control methods," G4 Monografiaväitöskirja, Roottorin radiaalivärähtelyjen aktiivinen hallinta, 2007.

[90] A. Burakov and A. Arkkio, "Low-order parametric force model for eccentric-rotor electrical machine with parallel connections in stator winding," *IEE Proceedings - Electric Power Applications*, vol. 153, no. 4, pp. 592–600, July 2006.

[91] D. G. Dorrell, "Calculation of unbalanced magnetic pull in small cage induction motors with skewed rotors and dynamic rotor eccentricity," *IEEE Transactions on Energy Conversion*, vol. 11, no. 3, pp. 483–488, Sep. 1996.

[92] D. G. Dorrell and A. C. Smith, "Calculation and measurement of unbalanced magnetic pull in cage induction motors with eccentric rotors. ii. experimental investigation," *IEE Proceedings - Electric Power Applications*, vol. 143, no. 3, pp. 202–210, May 1996.

[93] Y. Zhou, X. Bao, C. Di, and L. Wang, "Analysis of dynamic unbalanced magnetic pull in induction motor with dynamic eccentricity during starting period," *IEEE Transactions on Magnetics*, vol. 52, no. 7, pp. 1–4, July 2016.

[94] C. Di, X. Bao, H. Wang, Q. Lv, and Y. He, "Modeling and analysis of unbalanced magnetic pull in cage induction motors with curved dynamic eccentricity," *IEEE Transactions on Magnetics*, vol. 51, no. 8, pp. 1–7, Aug 2015.

[95] D. G. Dorrell and O. Kayani, "Measurement and calculation of unbalanced magnetic pull in wound rotor induction machine," *IEEE Transactions on Magnetics*, vol. 50, no. 11, pp. 1–4, Nov 2014.

[96] M. Donát, "Computational modelling of the unbalanced magnetic pull by finite element method," *Procedia Engineering*, vol. 48, pp. 83–89, 2012.

[97] D. G. Dorrell, A. Hermann, and B. B. Jensen, "Analysis of unbalanced magnetic pull in wound rotor induction machines using finite element analysis - transient, motoring and generating modes," in *39th Annual Conference of the IEEE Industrial Electronics Society*, Nov 2013, pp. 7307–7312.

[98] J. P. A. Bastos and N. Sadowski, *Electromagnetic Modeling by Finite Element Methods.* CRC Press, 2003.

[99] S. Kocman, T. Hrubý, P. Pečínka, and A. Neumann, "FEM model of asynchronous motor for analysis of its parameters," in *ELEKTRO*, May 2016, pp. 315–319.

[100] A. Sinervo, T. Jokela, and A. Arkkio, "Controlling rotor vibrations of a two-pole induction machine with unipolar actuator," *IEEE Transactions on Magnetics*, vol. 48, no. 7, pp. 2205–2210, July 2012.

List of Publications

Patent Application

1. **G. Kumar**, K. Kalita, K. Tammi, W.K. Khoo, S.D. Garvey, "Generation of Selective Pole Pair Field and Selective Frequency Transverse Force in Bridge Configured Winding Electrical Machines", Application Number: 201831000913, Priority Date, 09-01-2018..

Journal Publications

- Published Papers:

  1. **G. Kumar**, K. Kalita, K. Tammi, "Analysis of Bridge Currents and UMP of an Induction Machine with Bridge Configured Winding using Coupled Field and Circuit Modeling," *IEEE Transactions on Magnetics*, vol. 54, no. 9, 2018.

- Communicated Manuscripts:

  1. **G. Kumar**, K. Kalita, K. Tammi, P. Kumar, J. Pipuri, A. Banerjee, "Analysis of Pulsating Magnetic Fields in a Parallel Stator Winding Eccentric Rotor Induction Motor," *IEEE Transactions on Magnetics*, **Under Review**.
  2. **G. Kumar**, K. Kalita, K. Tammi, S. Garvey, A. Banerjee, "Dynamics of force generation in bridge configured winding induction machine," *Journal of Sound and Vibration*, **Under Preparation**.

Conference Publications

1. **G. Kumar**, K. Kalita, K. Tammi, "Magnetic Field Harmonics and its Effect on Vibration in Bridge Configuration wound Induction Motor", *21st International Conference on the Computation of Electromagnetic Fields (Compumag 2017)*, Daejeon, South Korea, 18 - 22 June 2017.

2. **G. Kumar**, K. Kalita, "Vibration Control using BCW Induction Motor". *Procedia Engineering*, ELSEVIER, Volume 144, PP. 94–101, 2016.

3. **G. Kumar**, K. Kalita, K. Tammi, "Active Control of Bridge Configured Self-Bearing Motor - A Numerical Study", *Sixth National Symposium on Rotordynamics (NSRD 2019)*, CSIR-National Aerospace Laboratories, Bangalore, 02 - 03 July 2019.

4. **G. Kumar**, K. Kalita, K. Tammi, G. Seamus, "A Coupled Field, Circuit and Rotor Model of a BCW Induction Machine", *Sixth National Symposium on Rotordynamics (NSRD 2019)*, CSIR-National Aerospace Laboratories, Bangalore, 02 - 03 July 2019.